UNIVERSITY OF MILANO-BICOCCA

Faculty of Mathematical, Physical and Natural Sciences
Department of Biotechnology and Biosciences

PhD in Chemical Sciences, Cycle XXVII

Synthesis and characterization of new small-molecule ligands of LPS binding proteins

Carlotta Ciaramelli
760856

Tutor:
Prof. Francesco Peri

Academic Year 2013/2014

Table of contents

Abbreviations

ANS: 1-Anilinonaphthalene-8-Sulfonic Acid

APS: ammonium persulfate

APT: attached proton test

BSA: bovine serum albumine

CD14: cluster of differentiation antigen

CMC: critical micelle concentration

DAMPs: danger (or damage) associated molecular patterns

DCC: dicyclohexylcarbodiimide

DIC: N,N'-Diisopropylcarbodiimide

DIPEA: N,N'-Diisopropylethylamine

DMAP: 4-dimethylaminopyridine

DMF: dimethylformamide

DMP: dimethoxypropane

DMSO: dimethylsulphoxide

DOESY: diffusion ordered spectroscopy

EDC: N-(3-Dimethylaminopropyl)-N'-ethylcarbodiimide hydrochloride

EVOO: extra virgin olive oil

FA: fatty acid

FITC: fluorescein isothiocyanate

*h*CD14: *human* cluster of differentiation antigen

HEK: human embryonic kidney

*h*MD-2: *human* myeloid differentiation 2

HOBt: 1-Hydroxybenzotriazole hydrate

HSQC: Heteronuclear Single Quantum Coherence

IC_{50}: half maximal inhibitory concentration

Ig: immunoglobulin

IM: inner membrane

Kd: dissociation constant

Kdo: 3- deoxy-D-manno-oct-2-ulosonic acid

LBP: lipid Binding Protein

LOS: lipooligosaccharide

LPS: lipopolysaccharide

Lpt: lipopolysaccharide transport

LRR: leucine-rich repeat domain

MAMP: microbe associated molecular patterns

MD-2: myeloid differentiation 2

MTT: thiazolyl blue tetrazolium bromide

NMO: *N*-Methylmorpholine-*N*-Oxide

OM: outer membrane

OVA: ovalbumin

PAMPs: pathogen associated molecular patterns

PBS: Phosphate Buffer Saline

PMB: para methoxybenzylidene

PRR: pattern recognition receptor

RT: room temperature

SDS-PAGE: Sodium Dodecyl Sulphate-PolyAcrylamide Gel Electrophoresis

sH-LptC: LptC (lacking the first 23 amino acids of the transmembrane helix) fused to a N-terminal His$_6$ tag

STD: saturation transfer difference

TBAF: tetra-*n*-butylammonium fluoride

TBS: tert-Butyldimethylsilyl

TEA: trimethylamine

TEMED: N, N, N', N'-tetramethylene-ethylenediamine

TFA: trifluoro acetic acid

THF: tetrahydrofuran

TIR: Toll/Interleukin-1 receptor

TLR: Toll-like receptor

Tris: 2-hydroxymethyl-2-methyl-1,3-propaendiol

Tr-NOESY: transferred NOESY experiments

TsOH: *p*-Toluenesulfonic acid

UDP-GlcNAc: UDP-N-acetylglucosamine

Abstract

The purpose of this work is the design, synthesis and characterization of new small molecules, active as ligands of two different lipopolysaccharide (LPS)-binding proteins. LPS, or bacterial endotoxin, is an amphiphilic macromolecule, ubiquitous on the outer membrane of Gram-negative bacteria. The LPS binding proteins studied during this PhD project belong to two classes: the bacterial proteins of the Lpt transport machinery and the mammalian innate immunity receptor system, including TLR4 receptor and the co-receptors LBP, CD14, MD-2.

Lpt protein complex is responsible for the transport mechanism of LPS from the inner membrane to the cell surface of Gram-negative bacteria, with the protein LptC playing a prominent role. Therefore, the LPS export mechanism is a fundamental step in the LPS biogenesis, representing an ideal target for the development of novel antibiotics against Gram-negative bacteria. Moreover, even though the structures of Lpt proteins have successfully been defined, still very little is known about the mechanism of LPS transport, making the elucidation of the whole process a very challenging research target. In order to study the interaction between LptC and its natural ligand, the LPS, different techniques were used, among which NMR binding studies held an important role. Furthermore, the development of a new fluorescently labelled LPS allowed to perform LPS-LptC interaction studies with fluorescence techniques. In addition, the interaction between LptC and synthetic ligands was analysed: for this purpose, new synthetic small molecules were produced. Specifically, glycolipids and their fluorescently labelled

derivatives were designed and synthesized in order to obtain LptC ligands and, in perspective, potential antibiotics against Gram-negative bacteria.

Toll-like receptor 4 (TLR4), the innate immunity receptor, is responsible for LPS recognition, with the support of other proteins (LBP, CD14 and MD-2), and for the subsequent induction of inflammatory responses. Synthetic small molecules able to modulate the biological activity of innate immunity receptors represent a powerful tool to study the TLR4 receptor system and are of great pharmacological interest as antisepsis and anti-inflammatory agents (antagonists) or as vaccine adjuvants (agonists). Antagonist activity of amino glycolipids (IAXO-102) on TLR4 receptor system was clearly demonstrated by our research group. IAXO-102 was used as a scaffold to develop new derivatives that, while retaining the biological activity of the precursor, presented enhanced characteristics with respect to water solubility, fluorescence and interaction with the hydrophobic binding pocket of the TLR4 receptor complex. In particular, a zwitterionic glycolipid, dimeric molecules and fluorescent probes, used for binding studies, were designed and synthesized. Anionic TLR4 antagonists with a chemical structure similar to lipid X, a biosynthetic precursor of lipid A, were also obtained in our labs. The ability of the new anionic lipid A mimetics to bind the innate immunity co-receptor MD-2 was evaluated through NMR binding experiments. The amphiphilic character of the synthetic TLR4 modulators obtained so far is often associated with low water solubility and poor bioavailability. In this respect, the natural TLR4-active compounds are characterised by better solubility and bioavailability. The chemical modification of these structures is very helpful to modulate their biological activity and to

enhance target specificity. Consequently, the synthesis of new small molecules with chemical structures inspired to natural TLR4 modulators was pursued. In particular, some phenolic compounds from extra virgin olive oil are known for their anti-inflammatory activity, but this activity has never been correlated to a biological activity as TLR4 modulators. Our research group identified some phenolic extracts from olive oils and some of the most abundant phenolic constituents for their activity as TLR4 antagonists. In addition, the synthesis of some analogues of olive oil phenols was performed, in order to obtain new potential TLR4 antagonists, characterised by higher water solubility and reduced toxicity. The TLR4 modulators previously described present antagonist activity, leading to their exploitation as anti-inflammatory or antisepsis agents. On the other side, molecules that can be used as vaccine adjuvants have been produced, performing a conjugation of TLR4 agonist small-molecules to carrier proteins. As a preliminary step, a carboxylated glycoplipid was linked to the protein Ovalbumin, keeping in mind that the final goal of the study is to obtain a new class of potential adjuvants for vaccines against allergies.

In conclusion, the overall aim was the understanding of the biological mechanisms of LPS binding to LptC and to TLR receptor system and the identification of new and more efficient therapeutics against Gram-negative bacteria and all the TLR4 related pathologies. To reach this goal, synthetic small molecules, with different and original chemical structures, were produced to modulate the LptC-LPS and/or TLR4-LPS recognition processes and their interaction with LPS binding proteins was deeply evaluated.

Riassunto

Lo scopo del presente lavoro è la progettazione, la sintesi e la caratterizzazione di nuove molecole, attive come ligandi di due diverse proteine che legano l'LPS (lipopolisaccaride). Gli LPS, o endotossine batteriche, sono macromolecole anfifiliche ubiquitarie sulla membrana esterna dei batteri Gram-negativi. Le proteine che legano gli LPS studiate nel corso di questo progetto appartengono a due categorie: le proteine batteriche di trasporto Lpt e il sistema recettoriale dell'immunità innata nei mammiferi, che comprende il recettore TLR4 ed i co-recettori LBP, CD14, MD-2.

Il complesso proteico Lpt è responsabile del meccanismo di trasporto dell'LPS dalla membrana interna alla superficie cellulare dei batteri Gram-negativi, processo in cui la proteina LptC gioca un ruolo molto importante. Pertanto, il meccanismo di esportazione dell'LPS è uno step fondamentale della sua biogenesi, che rappresenta un target ideale per lo sviluppo di nuovi antibiotici contro i batteri Gram-negativi. Inoltre, anche se le strutture delle proteine Lpt sono state risolte, sono disponibili ancora poche informazioni riguardo il meccanismo di trasporto, rendendo la delucidazione di tale processo un obiettivo molto stimolante.

Al fine di studiare l'interazione tra LptC e il suo ligando naturale, l'LPS, sono state usate diverse tecniche, tra cui gli studi di interazione via NMR hanno avuto un ruolo predominante. Inoltre, lo sviluppo di un nuovo LPS fluorescente ha consentito di effettuare studi di interazione LPS-LptC con tecniche di fluorescenza. In aggiunta, è stata anche investigata l'interazione tra LptC e ligandi sintetici: a questo scopo, sono state

sviluppate nuove molecole sintetiche. In particolare, alcuni glicolipidi e i loro derivati fluorescenti sono stati progettati e sintetizzati per ottenere ligandi di LptC e, in prospettiva, potenziali antibiotici contro i batteri Gram-negativi.

Il Toll-like receptor 4 (TLR4), il recettore dell'immunità innata, è responsabile del riconoscimento dell'LPS, grazie al supporto di altre proteine (LBP, CD14 e MD-2) e della conseguente induzione della risposta infiammatoria. Molecole sintetiche in grado di modulare l'attività biologica dei recettori dell'immunità innata sono un potente strumento per studiare il sistema recettoriale TLR4 e rivestono grande interesse farmacologico come agenti antisepsi e anti-infiammatori (antagonisti) o come adiuvanti vaccinali (agonisti).

L'attività antagonista di ammino-glicolipidi (IAXO-102) sul TLR4 è stata chiaramente dimostrata dal nostro gruppo di ricerca. IAXO-102 è stato utilizzato come scaffold per sviluppare nuovi derivati che, pur mantenendo l'attività biologica del precursore, presentassero caratteristiche migliorate in termini di solubilità in acqua, fluorescenza e interazione con la tasca di legame idrofobica del complesso recettoriale. In particolare, un glicolipide zwitterionico, molecole dimeriche e sonde fluorescenti, utilizzate per studi di interazione, sono stati progettati e sintetizzati.

Inoltre, antagonisti anionici del TLR4 con una struttura chimica simile a lipide X, un precursore sintetico del lipide A, sono stati ottenuti nei nostri laboratori. La capacità dei nuovi mimetici anionici del lipide A di legare il

co-recettore dell'immunità innata MD-2 è stata valutata, tramite esperimenti di interazione via NMR.

Il carattere anfifilico dei modulatori del TLR4 sintetizzati finora è spesso associato ad una bassa solubilità in acqua e a scarsa biodisponibilità. Rispetto a queste caratteristiche, i composti attivi sul TLR4 di origine naturale hanno migliori solubilità e biodisponibilità. La modifica chimica di queste strutture è molto utile per modulare l'attività biologica e per migliorare la specificità nei confronti del target. Di conseguenza, è stata intrapresa la sintesi di nuove molecole con strutture chimiche ispirate ai modulatori naturali del TLR4. In particolare, alcuni composti fenolici contenuti nell'olio extravergine di oliva sono noti per avere un'attività anti-infiammatoria, che però non era mai stata collegata ad un'attività biologica sul TLR4. Il nostro gruppo di ricerca ha recentemente identificato alcuni estratti fenolici da olio di oliva e alcuni dei costituenti fenolici più abbondanti come antagonisti del TLR4. Pertanto, sono stati sintetizzati alcuni analoghi di queste molecole, al fine di ottenere nuovi potenziali antagonisti del TLR4, con una migliore solubilità in acqua ed una ridotta tossicità.

I modulatori del TLR4 descritti precedentemente presentano attività antagonista, portando al loro sfruttamento come agenti anti-infiammatori o antisepsi. D'altra parte, sono anche state prodotte molecole che possano rappresentare potenziali adiuvanti vaccinali, coniugando molecole sintetiche agoniste del TLR4 a proteine carrier. Come lavoro preliminare, un glicolipide carbossilato è stato coniugato all'Ovalbumina, puntando, come fine ultimo, ad ottenere una nuova classe di potenziali adiuvanti per vaccini contro le allergie.

In conclusione, l'obiettivo generale era lo studio dei meccanismi biologici dell'interazione dell'LPS con la proteina LptC e con il complesso recettoriale TLR4 e l'identificazione di nuovi e più efficienti terapeutici contro i batteri Gram-negativi e le patologie correlate. Per raggiungere questo scopo, molecole sintetiche, caratterizzate da strutture chimiche nuove ed originali, sono state prodotte per modulare i processi di riconoscimento LPS/LptC e/o LPS/TLR4 e la loro interazione con le proteine che legano l'LPS è stata approfonditamente valutata.

Chapter 1

Introduction

1.1 Gram-negative bacteria

Bacteria are prokaryotic microorganisms representing the most common human pathogens. All bacterial cells hold a cell envelope or membrane that protects the cytoplasm and it is composed by a wide variety of biological molecules involved in many cellular processes. The cell envelope is made of several layers and, thanks to their different organization, it is possible to distinguish bacteria into two groups: Gram-positives and Gram-negatives, in response to the Gram staining protocol.[1]

In the Gram-negative cell envelope, three principal layers can be distinguished: the outer membrane (OM), the periplasm, and the inner membrane (IM). The outer membrane is oriented towards the outside of the cell and shows a peculiar asymmetrical organization. The inner leaflet is composed of glycerophospholipids and lipoproteins, while the outer leaflet is made of lipopolysaccharides (LPSs). In addition, the outer membrane contains several integral, trans-membrane and outer membrane proteins.

The asymmetrical arrangement of the Gram-negative outer membrane confers various functions to the bacterium: proteins allow the diffusion of compounds across the outer membrane and the LPS component is capable of various chemical arrangements that can influence the bacterium's ability to elude host immune defenses.

The inner membrane, which is in direct contact with the cytoplasm, consists of a phospholipid bilayer, mainly composed of phosphatidyl ethanolamine and phosphatidyl glycerol, decorated with several proteins.
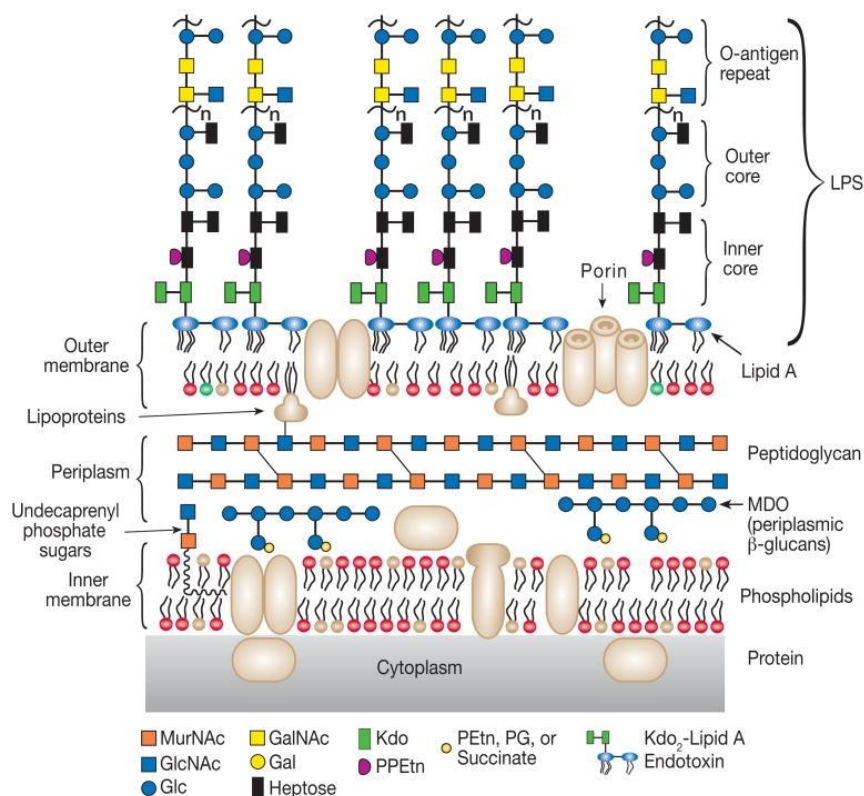
Figure 1.1. Gram-negative cell envelope. Adapted from Raetz, 2002. [2]

The bilayer is arranged with polar heads oriented towards the extracellular face, in order to shield hydrophobic chains from the surrounding polar fluid. Since bacteria lack intracellular organelles that perform a number of essential cellular processes in eukaryotes, such as mitochondria and endoplasmic reticula, many of these functions are performed within the inner membrane in prokaryotic organisms.

The two-membrane system allows for the existence of the periplasm, an aqueous cellular compartment. The periplasm is more viscous than the cytoplasm and it is densely packed with proteins, such as environment-

sensing proteins that determine the bacterial response to environmental signals. The periplasm plays an important role in the survival and activities of the bacterium, acting as a buffer between its interior and the external environment. In the periplasm, a slim peptidoglycan layer is present: peptidoglycan is a biopolymer made up of repeating units of the disaccharide *N*-acetyl-glucosamine and *N*-acetyl-muramic acid, joined with β-(1→4) linkages.[3] The saccharide strands are cross-linked by tetrapeptide side chains. This polymer gives a strong contribution to the cell shape, thanks to its considerable rigidity.

The Gram-positive cell envelope exhibits different characteristics from the Gram-negative one.
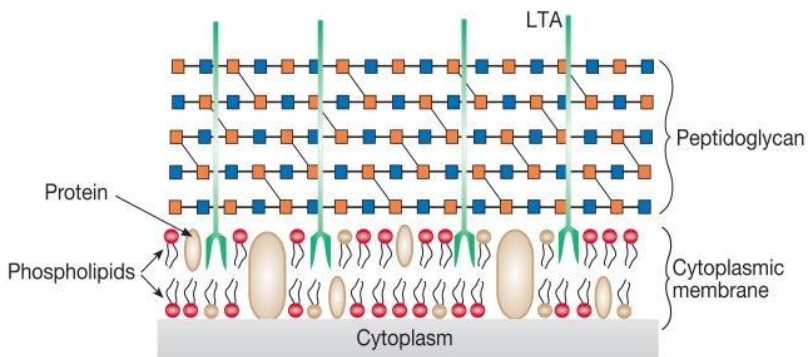
Figure 1.2. Gram-positive cell envelope. Adapted from Raetz, 2002. [2]

First of all, the absence of the outer membrane is noticeable in Gram-positive bacteria, with the consequent absence of lipopolysaccharides. Secondly, the peptidoglycan differs with respect to thickness: the Gram-negative peptidoglycan is only a few nanometers thick, whereas the Gram-positive is characterized by a dense layer of 30–100 nm.[4] In

addition, the peptide cross-links among glycan strands in peptidoglycan show some differences. In fact, the amino acid sequence of the peptide cross-link is: L-Alanine, D-Glutamic acid, Lysine (Gram-positive) or meso-2,6-diaminopimelic (DAP) acid (Gram-negative), D-Alanine. Furthermore, Gram-positive bacteria have peptide stems usually cross-linked through an interpeptide bridge (generally made of glycines), whereas Gram-negative bacteria peptide stems are usually directly cross-linked.

The macromolecules constituting the cell envelope of virulent Gram-positive and Gram-negative bacterial strains are strongly involved in mechanisms of adhesion, colonization and infection of the host. In particular, peptidoglycan for Gram-positive and lipopolysaccharides for Gram-negative bacteria perform the role of antigens, because they are recognized by specific receptors of immune system cells. The focus of this work is on Gram-negative bacteria.

1.2 Lipopolysaccharides

Lipopolysaccharides (LPSs) are amphiphilic macromolecules composed by a polysaccharidic portion and a glycolipidic one. Lipopolysaccharides are ubiquitous molecules in Gram-negative bacteria,[5] where they represent one of the main components of the outer membrane, covering 75% of the external cell surface and conferring its characteristic asymmetry to the outer membrane. They play an essential role in bacterial growth and survival and they are also named bacterial endotoxins.

LPS represents the 3-5% in weight of the whole bacterial cell and its complex structure can be divided into three domains:

- Lipid A, the glycolipid portion
- Core, the oligosaccharide portion
- *O*-Specific Side Chain or *O*-antigen, the polysaccharide portion
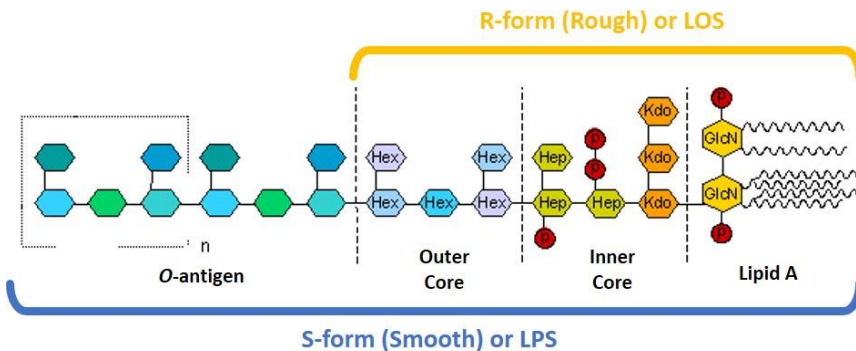
Figure 1.3. Schematic representation of R- and S-type LPS. Adapted from Alexander, 2001. [6]

It is possible to distinguish between Smooth-type LPS and Rough-type LPS, named after the smooth or rough appearance of the bacterial colonies. Smooth-type LPSs (or simply LPSs) are characterised by all the three domains, with the core as a covalent bridge between lipid A and *O*-antigen. On the other hand, Rough-type LPSs, also called lipooligosaccharides (LOSs), lack the *O*-Chain region.

The lipid A is the inner and the most conservative region of LPS.[7] Its long chain acyl moieties are responsible for anchoring LPS to the outer layer of the bacterial outer membrane. Lipid A is composed of 2-amino-2-deoxy-D-glucose (glucosamine, GlcN) disaccharide backbone, with monosaccharides connected by a β-(1→6) glycosidic linkage.
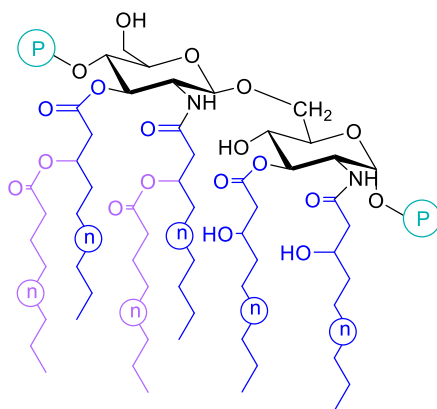
Figure 1.4. General structure of lipid A.

The first glucosamine is called proximal or reducing (GlcN-I) and the second is named distal or non-reducing (GlcN-II). These monosaccharides are generally phosphorylated (GlcN-I at positions 1 and GlcN-II at position

4) and they are both acylated via amide and ester bonds at positions 2 and 3, respectively. These fatty acids (FA), called primary, can be further esterified at their 3-hydroxy group by other fatty acids, called secondary.

However, lipid A has an intrinsic heterogeneity related not only to the nature, number and location of acyl substituents, but also to several variations on the standard structure just described. The number of phosphate groups can vary and they can be substituted by D-Galacturonic acid or L-Arabinosamine; otherwise, phosphate groups can bring substituents, in non-stoichiometric amounts, such as 2-aminoethanol (EtN), 4-deoxy-4-amino-L-arabinopyranose (Ara4N) and 2-aminoethanolposphate (EtNP); these changes on phosphate groups cause the reduction of the negative charge of lipid A, with important biological consequences. [6] Therefore, a bacterial strain produces a family of lipid As.

The two most external regions (core and *O*-antigen) form together the saccharide portion of LPS, which is oriented towards the outside of the cell.

The core, the oligosaccharide region of LPS, is characterized by major *intra*-genus variability compared to the lipid A portion, but it has a low variability within the same bacterial species. It always displays one to three residues of 2-keto-3-deoxy-D-*manno*-octulosonic acid (Kdo). Kdo can be considered a marker for LPSs, because it is a ubiquitous acid monosaccharide found in all bacterial core regions, where it connects the core to the *O*-6 of GlcN-II of lipid A. The core can be virtually divided into two regions: the Inner Core, proximal to lipid A, and the Outer Core, where the *O*-antigen is linked.

The Inner Core is characterized by the presence of peculiar monosaccharides, such as additional Kdo units and heptoses, tipically L-*glycero*-D-*manno*-heptopyranoses (L,D-Hep). The standard structure of the Inner Core is often decorated with non-stoichiometric additions of other sugars, phosphate (P), pyrophosphoethanolamine (PEtN) or phosphorylcholine (PCho) residues that increase the heterogeneity of LPSs. Thus, the Inner Core has an anionic characteristic and it confers rigidity to the membrane, because of the ionic bridges that are formed between different LPS molecules. The major structural diversity of the Outer Core is predictable, since it is a region with more exposure to selective pressures of the host responses and to environmental stresses. It usually contains not only neutral, acid and amino sugars, but also phosphate or pyrophosphate groups, and occasionally non-glycidic substituents, such as amino acid residues.

The functional role of LPS in the bacterial membrane is guaranteed by many factors and the low fluidity state of the hydrocarbon regions of the lipid A, together with the strong lateral interactions between LPS molecules, are the most important features. Indeed, the negatively charged groups - located on lipid A (as phosphates, pyrophosphates, uronic acids) and on the Inner Core from different LPS units – are cross-linked by ionic bridges mediated by divalent cations, such as Ca^{2+} or Mg^{2+}. This arrangement creates a tight net of LPS molecules, which results in hydrophobic substances.

The *O*-antigen is present only in Smooth-type LPSs. It is the most variable domain of LPS: different strains of the same bacterial species can present variations in its structure. The *O*-antigen is generally made of a regular

polysaccharide with an high molecular weight (10.000-60.000 Da) and the repeating unit usually consists of one to five residues with a very large monosaccharide variety (deoxysugars, heptoses, aminosugars, uronic acids), that gives rise to an enormous structural diversity, which can be further increased by several types of non-stoichiometric substituents. In addition, the *O*-antigen is characterized by size heterogeneity, due to the number of repeating units (up to 40), which leads to the typical ladder profile of LPS on SDS-PAGE. The *O*-antigen is also the region of LPS most exposed to the external environment; thus, a variation of its structure can be used from the bacterium to modulate the response to external factors.[8]

The *O*-antigen is an important component of LPS for S-type bacteria, since it has a structural function, protects the cell from external agents, has the role of adhesion to host receptors, and can sometimes present particular structures to mask the bacterium from the immune system of the host. In bacteria that produce R-type LPS these roles are often played by the core.[9]

1.3 LPS biosynthesis and transport

LPS molecules are essential for the survival of most Gram-negative bacteria: they have morphological, protective and adhesion functions, and they are also the target of the host immune system. Consequently, the whole LPS biosynthesis is a crucial event for Gram-negative bacteria.

LPSs are synthesized in the cytoplasm and periplasm; then, they are exported to the outer leaflet of the outer membrane. The transport of LPS is a critical process; in fact, defects in the export mechanism are known to be lethal for the bacterium. The functionality of outer membrane, which is essential for bacterial cell viability and represents the first site of interaction with the host, requires proper assembly of this structure and correct placement of LPS in the outer leaflet of the OM. Therefore, LPS biogenesis represents an ideal target for the development of novel chemicals with antibiotic action against Gram-negative bacteria. [10]

How LPS is synthesized in the cytoplasm and exported to the surface of bacteria has been studied most extensively in *E. coli*. Although the steps along the LPS biosynthetic pathway have been clarified, the precise mechanisms of transport and assembly at the cell surface are still poorly understood.

Briefly, the biosynthesis of LPS goes through the following steps. The synthesis is initiated in the cytoplasm, starting from the small molecule UDP-N-acetylglucosamine (UDP-GlcNAc). A multiplicity of enzymes sequentially works to convert UDP-GlcNAc into disaccharide-1-P, Kdo_2-lipid A, core-lipid A, and culminating in LPS. [11]

The translocation across the inner membrane is performed by the essential ABC transporter MsbA.[12] The final step of LPS biosynthesis takes place at the periplasmic face of the inner membrane, where the lipid A-core moiety is ligated to *O*-antigen (Figure 1.5).[2]
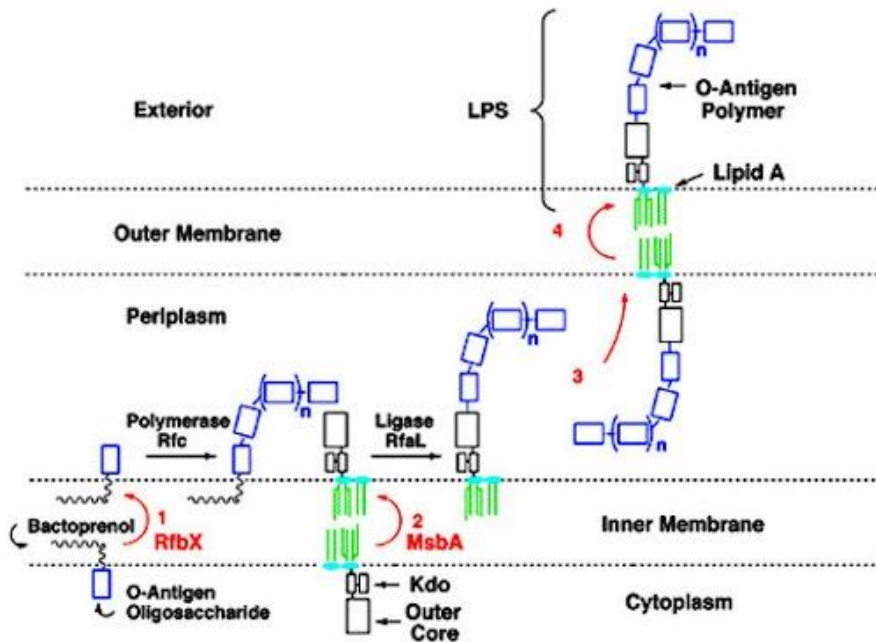
Figure 1.5. Schematic representation of LPS biogenesis.[13] Lipid A-core and the precursor units of *O*-antigen are transported separately to the outer surface of the inner membrane, where they are then attached to each other after the *O*-antigen is polymerized. MsbA initiates lipid A-core transport, and RfbX may do the same for *O*-antigen precursor.

In particular, the first three reactions are catalyzed by soluble enzymes LpxA, LpxC and LpxD, resulting in the addition of two 3-OH fatty acid chains to the 2- and 3-positions of the UDP-GlcNAc, to form UDP-diacyl-GlcN (Figure 1.6).[14]

Next, the UDP-diacyl-GlcN is hydrolyzed by LpxH to form lipid X, a key precursor of lipid A. LpxB condenses lipid X and its precursor UDP-diacyl-GlcN to form disaccharide-1-P.[15] The phosphorylation at 4-position of the disaccharide-1-P is performed by the kinase LpxK and provides the precursor of lipid A, the lipid IVa.[16] Two residues of 2-keto-3-deoxy-D-*manno*-octulosonic acid (Kdo) are incorporated at the 6-position of the lipid IVa by KdtA, using the sugar nucleotide CMP-Kdo as the donor.[17] The resulting Kdo$_2$-lipid IVa undergoes further reactions, catalyzed by LpxL and LpxM to form Kdo$_2$-lipid A. In particular, LpxL adds a secondary lauroyl residue and LpxM adds a myristoyl residue to the distal glucosamine unit.[18]
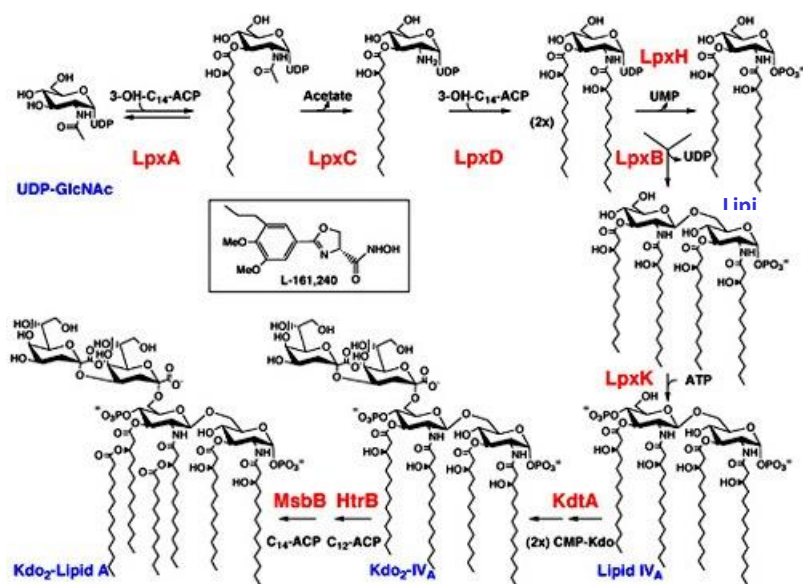
Figure 1.6. Biosynthetic pathway of LPS in *E. coli* K12.[19] The red symbols indicate the relevant structural genes. The blue names refer to the biosynthetic precursors of lipid A (lipid X and lipid IVA) and LPS (Kdo$_2$-Iva and Kdo$_2$-lipid A).

The core oligosaccharides are sequentially assembled on lipid A at the cytoplasmic surface of the inner membrane in a process that involves a number of membrane-associated glycosyltransferases, using nucleotide sugars as donors. The biosynthesis of core oligosaccharides is rapid and efficient, suggesting that the glycosyltransferases work as a coordinated complex. The *O*-antigen, similarly to the core oligosaccharides, is synthesized on the cytoplasmic surface of the inner membrane. Using the sugar nucleotides as donors, the units of *O*-antigen are assembled by glycosyltransferase enzymes on the membrane-bound carrier, the undecaprenyl phosphate.

After the biosynthesis, the core-lipid A is anchored to the inner membrane with its hydrophilic moiety exposed to the cytoplasm and is then flipped across the inner membrane by the essential ABC (ATP Binding Cassette) transporter MsbA, becoming exposed in the periplasm.[12] *In vivo* MsbA displays a remarkable selectivity towards the LPS substrates, being capable to translocate only hexaacylated, but not penta or tetraacylated LPSs. Meanwhile, the transport of the *O*-antigen across the inner membrane and its subsequent polymerization is mediated by at least 3 proteins, Wzx, Wzy and Wzz.[20] Some evidence suggests that these proteins might function by recognizing the first sugar phosphate bound to the undecaprenyl-P. The Wzx flips the *O*-antigen from the cytoplasmic face to the periplasmic face of the inner membrane, while MsbA flips the core-lipid A in the same way. In the periplasmic face of the inner membrane, the *O*-antigen is polymerized by Wzy and Wzz to form *O*-antigen repeating units, which are, in turn, transferred to the core-lipid A by WaaL, resulting in the nascent LPS.

At this point, the biosynthetic process is completed and the newly synthesized LPS is in the periplasm, ready to be exported to the outer leaflet of the outer membrane.

1.3.1 Lpt transport machinery

Export of complete LPS to the cell surface is a pivotal step of LPS biogenesis and it is mediated by the lipopolysaccharide transport (Lpt) machinery. Lpt machinery is composed of seven essential proteins (LptABCDEFG),[21, 22] located in the inner membrane (LptBCFG), in the periplasm (LptA), and in the outer membrane (LptDE). The interaction of all the seven proteins leads to the formation of a transenvelope complex.[23]

The inner membrane ABC transporter LptBFG [25] interacts with the bitopic inner membrane protein LptC.[26] The homologous domains mediate the interactions between the C-terminal region of LptC and the N-terminal region of LptA, and between the C terminus of LptA and the N-terminal region of LptD exposed to the periplasm.[21, 27]

Therefore, the oligomeric structure formed by LptC, LptA and LptD constitutes the protein bridge that connects the inner membrane to the outer membrane.[23] Although the overall architecture of the transenvelope bridge has been defined,[21] the precise mechanism of LPS transport across the periplasm to the outer leaflet of the OM is not yet understood.
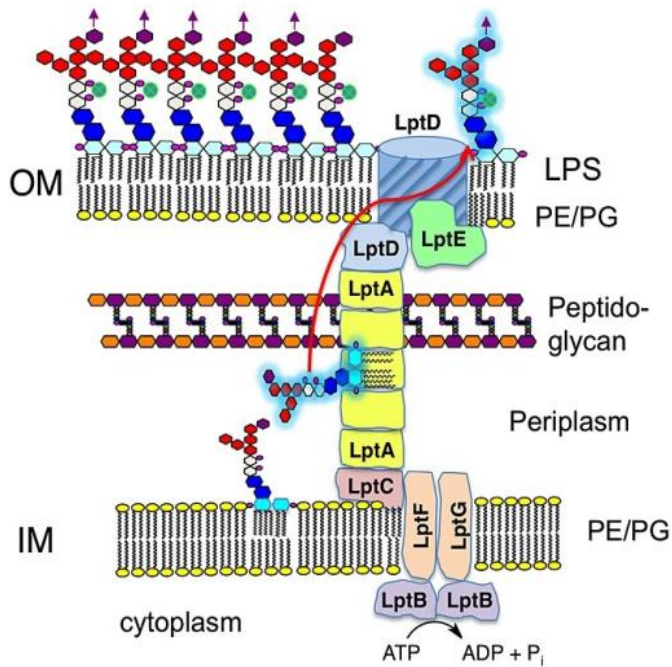
Figure 1.7. Cartoon representation of LPS transport mechanism across the periplasm and outer membrane mediated by Lpt transport machinery.[24]

A model was proposed for the LPS transport mechanism, based on experimental evidence. According to this model, the transport mechanism starts with LPS extraction from the inner membrane by the LptBFG complex, which transfers the molecule to the periplasmic domain of membrane-bound LptC. Then, LptC transfers LPS to LptA. At least two energy-dependent steps are involved in LPS transport: extraction from the inner membrane to the periplasmic domain of membrane-bound LptC, and transfer of LPS from LptC to LptA.[28, 29]

LptA and LptC belong to the same OstA superfamily, like the N-terminal periplasmic domain of LptD, which is recently demonstrated to be essential for LptD function *in vivo*.[23]

The experimental evidence that supports this model is reported. Both LptA[30] and LptC[31] bind to LPS, as demonstrated by qualitative *in vitro* assay. Interestingly, LptA can displace LPS from LptC *in vitro* (but not *vice versa*). This is consistent with their location in the protein bridge and the unidirectional LPS export pathway.

The crystal structure of LptA has been solved both in the presence and in absence of LPS. LptA is a small protein made of 185 amino acids.[30] LptA presents a novel fold consisting of 16 antiparallel β-strands folded resembling a semiclosed β-jellyroll; the structure is not completely symmetrical and it opens slightly at the N- and C-termini. In the presence of LPS, LptA associates in a head-to-tail fashion forming fibrils containing a hydrophobic groove. According to the hypotesis that LptA physically connects IM and OM, the interior cavity of LptA fibers could accommodate LPS.[32] LptC is a bitopic protein possessing only one transmembrane domain.[33] The recently solved crystal structure of LptC revealed a fold similar to that of LptA, with 15 antiparallel β-strands. [31]

(Top View)   (Side View, N-terminus)
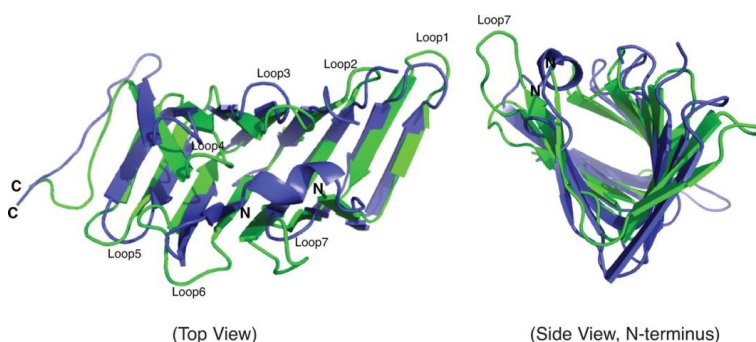
Figure 1.8. Structural comparison of LptA and His6-LptC (24 −191). Ribbon diagrams of LptA (blue; 2.15 Å) (Protein Data Bank accession code: 2R19) and His$_6$ − LptC (24 − 191) (green; 2.2 Å) are superimposed.[31]

Thus, the crystal structures of LptA[32] and of the periplasmic domain of LptC[31] revealed that the two proteins present a very similar β-jellyroll fold, although they do not share significant sequence similarity. LptA and LptC possess hydrophobic residues, forming a hydrophobic core along the proteins, potentially serving as an LPS-binding site.

Very recently, the mechanism of transport of the LPS molecule has been investigated *in vivo* and *in vitro*, by crosslinking the LPS ligand to the different components of the Lpt machinery. Specifically, four residues in LptC and five in LptA were found to interact with LPS *in vivo*. LptC residues directly involved in LPS binding are Thr47, Phe78, Ala172, and Tyr182, located almost exclusively inside the β-jellyroll structure, thus suggesting that LPS binds inside these proteins and transits through the periplasm bound to the cavity of the conserved β -jellyroll fold. [28] However, despite the increasing information obtained on LptC–LPS and LptA–LPS interactions, no quantitative measurements of binding have been performed.

1.4 Innate immunity

The immune system is a versatile defence system that protects organisms from invading pathogenic microorganisms and cancer. Immunity has both a less specific component and a more specific one. The innate immune system, which represents the non-specific immunity, is the first line of defense against invading microorganisms in vertebrates and the only line of defense in invertebrates and plants.[34] Most apparatuses of innate immunity are already present before the beginning of infection and constitute a set of disease-resistance mechanisms that recognize classes of molecules, characteristic of frequently encountered pathogens.

On the contrary, the adaptive immune system, which is the more specific component of immunity, is characterized by highly specialized cells that process and eliminate the hosts, affording protection against re-exposure to the same pathogen.

Innate immunity provides the first line of defence during the critical period after the host's exposure to a pathogen, because adaptive immunity requires some time to trigger its responses. Usually, in a healthy individual, the defence mechanisms of innate immunity are able to clear most of the microorganisms encountered in a few days, before they activate the adaptive immune system. [35] The receptors of innate and adaptive immunity are different and act in a different way.

The receptors of innate immunity recognize broad structural motifs that are highly conserved within microbial species, but are generally absent in the host. The adaptive immunity receptors recognize details of molecular

structure and can discriminate with extreme specificity between antigens featuring only slight structural differences.

LPS can stimulate the innate immune system through its most conserved region (lipid A) and the adaptive immune system through its most exposed region (*O*-antigen or core). The focus of this work is on innate immunity.

1.4.1 PRR and TLR

The strategy of the innate immune recognition is based on the detection of particular overall molecular patterns, called PAMPs (Pathogen-Associated Molecular Patterns), through specific receptors, called Pattern-Recognition Receptors (PRRs). The PAMPs recognized by this type of receptors include combinations of sugars, certain proteins, particular lipid-bearing molecules, and some nucleic acid motifs. Lipoproteins, peptidoglycan, lipoteichoic acids and lipid A of LPS, which constitute the invariant pattern in all Gram-negative bacteria, represent some of the most important PAMPs.

Toll-like receptors (TLR*s*) represent a family of PRR and play a key role in the innate immune system. They are non-catalytic receptors that recognize structurally conserved molecules derived from microbes, consequently activating immune cell responses. TLR*s* appear to be the most widespread and ubiquitous components of the immune system.

Indeed, TLRs are present in vertebrates as well as in invertebrates, and they also represent the host defence against infection in plants. It has

been estimated that most mammalian species have between ten and fifteen types of Toll-like receptors and thirteen TLRs (named TLR1 to TLR13) have been identified both in humans and mice (figure 1.9).[36]
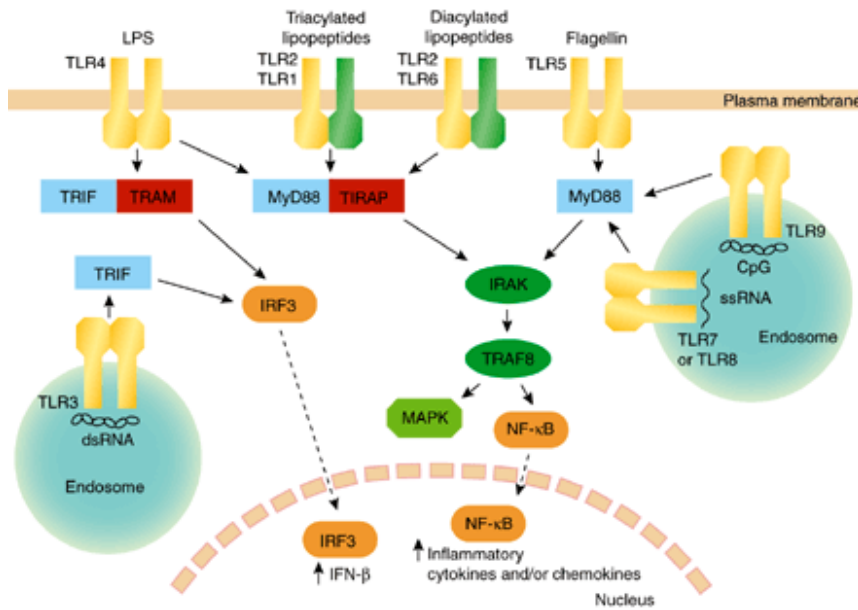
Figure 1.9. Locations, targets and signaling pathways of some TLR*s*. They are present either on the cell membrane or in intracellular compartments and bind to a broad variety of microbes or microbial products. [37]

From a structural point of view, all TLRs are characterized by two conservative regions: the extracellular leucine-rich repeat (LRR) domain and the TIR (Toll/Interleukine-I Receptor) domain, which is the protein–protein interaction module.[38]

1.4.2 Toll-like Receptor 4 (TLR4)

Toll-like Receptor 4 (TLR4) selectively recognizes bacterial lipopolysaccharide (LPS), providing an effective response against Gram-negative bacteria that eludes the physical and anatomic barriers of the organism. TLR4 can also be activated by some endogenous factors.

TLR4 plays a crucial role in immune and inflammatory responses, since it is involved in three important functions. First, it has a sensory function, since the LPS recognition by TLR4 informs innate immunity cells that Gram-negative bacteria are present inside the organism. Second, TLR4 has an effector function, because it initiates recruitment of inflammatory cells to the site of infection and activates them to induce antibacterial functions. Third, TLR4 regulates the adaptive responses; in fact, the TLR4-mediated innate response to a pathogen can be decisive in determining both the nature and the magnitude of the adaptive response.[39]

From a structural point of view, the TLR4 is a single-spanning transmembrane protein containing 799 aminoacids, localized on the cell surface. As for many TLRs, it is composed of an extracellular leucine-rich repeat (LRR) domain and an intracellular TIR (Toll/Interleukine-I Receptor) domain. [40]

Toll-like Receptor 4 is responsible for the activation of the host defence system and the triggering of pro-inflammatory processes. This aim is achieved by the coordinate and sequential action of four endotoxin-binding proteins: the LPS binding protein (LBP), the cluster differentiation antigen 14 (CD14), the myeloid differentiation protein (MD-2) and the TLR4 itself.
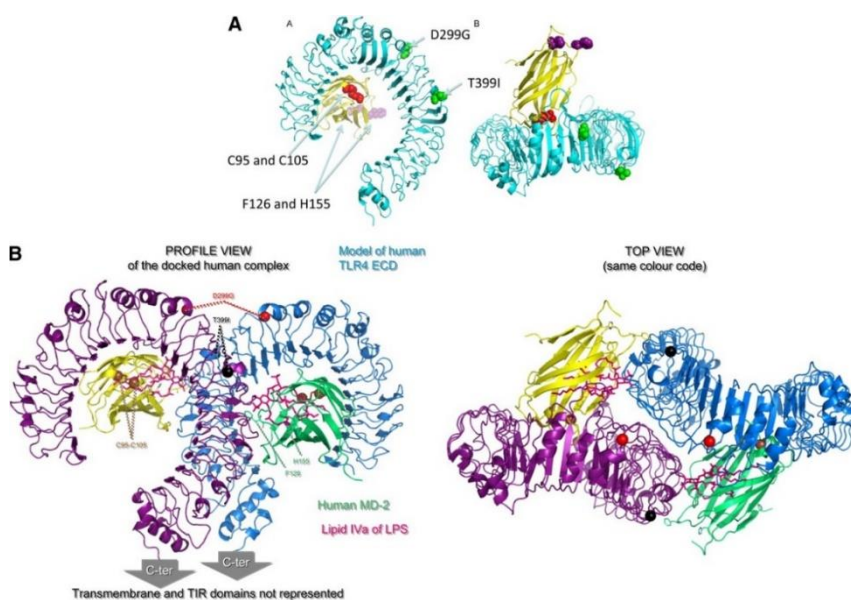
Figure 1.10. Structure of TLR4.MD-2 complex. **A)** Structure of human TLR4 (turquoise) bound to MD-2 (yellow) from crystal structure. **B)** A model of ligand activation of TLR4.MD-2 (lateral and top views). The two TLR4 molecules are represented in purple and turquoise and the two MD-2 molecules in yellow and green.[41]

This sequential process starts with the binding of LBP to LPS aggregates (Figure 1.11). When LBP interacts with endotoxin-rich bacterial membranes or endotoxin aggregates, it catalyses extraction and transfer of LPS monomers to CD14, that protects the acyl chains of the lipid A from the solvent, and forms a complex which is stable in solution in the monomeric form. Then, CD14 transfers LPS monomers to MD-2, which is the TLR4 co-receptor. Hence, the process ends with the formation of the activated (TLR4.MD-2.LPS)$_2$ complex, that has a pivotal role in starting the inflammatory cascade. In fact, the receptor dimerization leads to the recruitment of adapter proteins to the intracellular TIR domain of TLR4, initiating the intracellular signal cascade that culminates in the

translocation of transcription factors to the nucleus and the biosynthesis of cytokines.
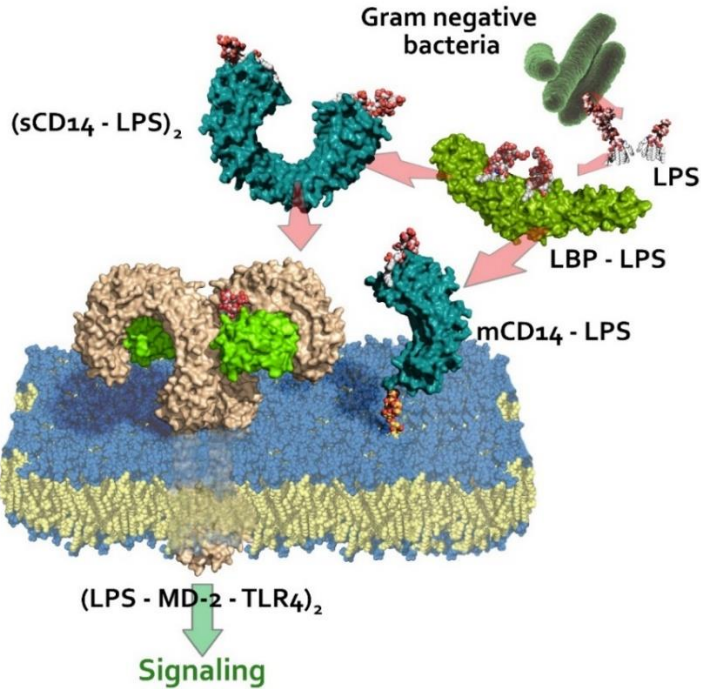
Figure 1.11. TLR4–associated proteins that are involved in LPS sensing. From: Cighetti, 2014.[42]

TLR4 is unique among the TLRs in triggering two distinct signal/transduction pathways (Figure 1.12). One is the MyD88 (Myeloid Differentiating primary response gene88)-dependent pathway, which leads to the activation of transcription factors Nuclear Factor Kappa B (NF-κB) and Activator Protein 1 (AP-1). The second route is the MyD88-independent pathway, based on the TRIF and TRAM effectors, leading to the activation of the Interferon Regulating Factor 3 (IRF-3). The activation

of NF-κB, AP-1 or IRF-3 leads to the expression of several inflammatory mediators (cytokines, chemokines or co-stimulatory molecules).[43]
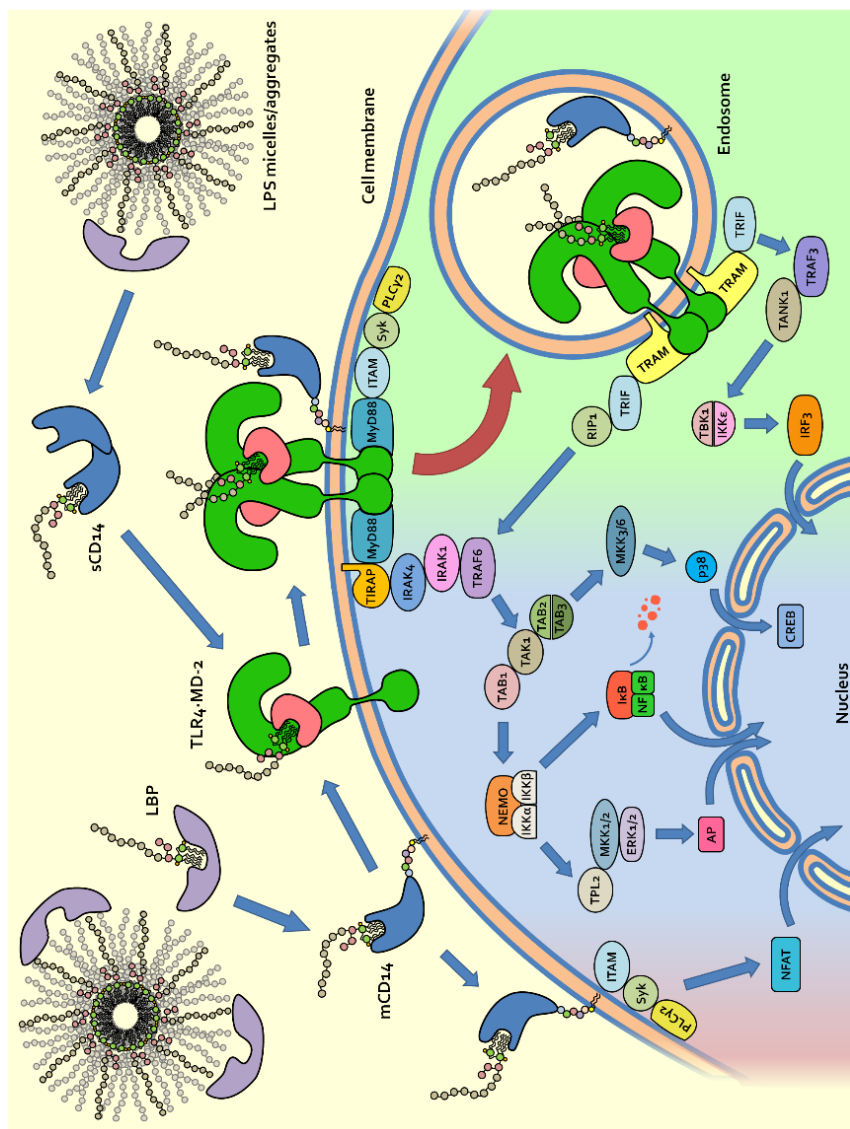
Figure 1.12. The complex signaling pathway of TLR4. Shades indicate the three separate pathways. Red shade: CD14 signal pathway; Blue shade: MyD88-depemdent pathway; Green shade: MyD88-independent pathway. From: Cighetti, 2014. [42]

Crystal structures of the human and murine (TLR4.MD-2.LPS)$_2$ complexes reveal that five of six acyl chains of *E. coli* lipid A moiety enter the hydrophobic binding pocket of the MD-2 bound to TLR4. It is clear from X-ray structures that the sixth acyl chain stays on the rim of the cavity and binds to a second TLR4 molecule that is also part of a TLR4.MD-2.LPS complex.[44, 45]

However, recently published NMR studies indicate that protrusion of one of the six fatty acyl chains of endotoxin bound to MD-2 precedes interaction with TLR4 when endotoxin is bound to MD-2. According to NMR data, the presence of a protruding fatty acyl chain is not necessarily a distinguishing feature of TLR4-activating LPS.MD-2 complexes and it is, therefore, not sufficient for driving TLR4 activation.[46]

While lipid A from *E. coli* is considered the typical chemical structure associated with endotoxic properties, a variety of natural lipid A variants exists, due to modifications in the number and disposition of FA chains and other covalent modifications that impact pathogenesis, bacterial physiology, and bacterial interactions with the host immune system.[47]

1.4.2.1 LBP

From a structural point of view, human LPS binding protein (LBP) is a 58-60 kDa serum glycoprotein, consisting of 452 residues in the mature protein without the signal sequence. It has been proved that the tip of the N-terminal domain of LBP contains a cluster of cationic residues, which are essential for the LPS binding and signalling.

The phospholipid-binding site of LBP seems a suitable site for binding of the lipid A moiety. However, the size of the binding pocket is far too small to accommodate the acyl chains of the typical lipid A and the distance between the cationic and hydrophobic site is too large to allow the interaction of the lipid A molecule with both sites. [48] Therefore, the location of the lipid A-binding site on LBP is not quite clear until now.

The LPS that is embedded in the bacterial membrane has by itself weak immunostimulatory activity, since it is tightly packed. Consequently, the role of LPB in LPS extraction is crucial to get the TLR4 signalling pathway starting.

1.4.2.2 CD14

The protein CD14 is present in two forms: a membrane protein, when it is expressed on the surface of monocytes and granulocytes as a glycosylphosphatidylinositol (GPI)-anchored glycoprotein, or in soluble form in the serum.

The monomeric subunit of CD14 has a curved structure with a concave surface made of a large β-sheet with the repetition of LRR motifs: it generates a pocket that seems to be crucial for ligand binding (Figure 1.13). The most important characteristic of CD14 structure is the N-terminal hydrophobic pocket.[49]
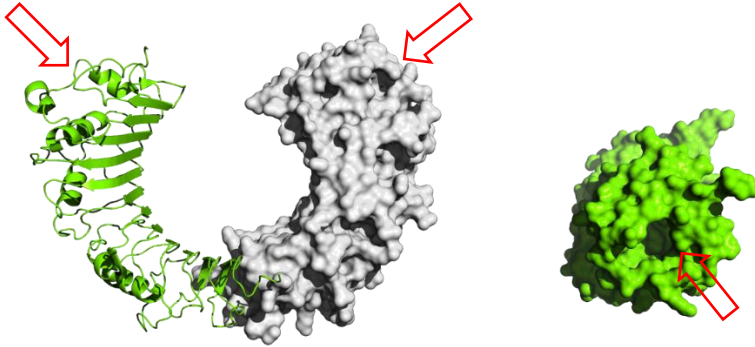
Figure 1.13. Structure of CD14, presented as a dimer (side view, one chain shown as green cartoons, the other as white surface) and as a monomer (top view, green surface). The position of the N-terminal hydrophobic pocket is indicated by red arrows. Adapted from Cighetti, 2014. [42]

The main function of CD14 has long been considered to enhance local LPS concentration, in order to increase the sensitivity of the TLR4 complex with respect to the endotoxin. In fact, CD14 is essential for the activation of TLR4.MD-2 complex when LPS concentration is low and when S-LPS is present, while TLR4 can be activated also in the absence of CD14, when R-LPS and highly concentrated LPS are used.

Nevertheless, it has recently been demonstrated that CD14 also controls a signal pathway on its own, resulting in NFAT transcription factor activation and in the production of IL-2 (Figure 1.12). [50] This pathway causes CD14 internalization from the cell membrane to internal compartments. CD14 also plays a fundamental role in TLR4.MD-2 internalization after LPS binding.[51]

1.4.2.3 MD-2

The protein MD-2 (Myeloid Differentiation factor 2), also known as Lymphocyte antigen 96 (LY96), consists of 160 aminoacids (18.4 kDa). MD-2 presents a β-cup fold structure, composed of two antiparallel β-sheets forming a large hydrophobic pocket for ligand binding.[45] The monomeric form of MD-2 binds to one LPS monomer.[52]

MD-2 binds to the ectodomain of TLR4 and is essential for LPS signalling, since no physiological role of TLR4 in the absence of MD-2 has been demonstrated. [53] MD-2 is the last LPS binding protein before the signal transduction across the cell membrane. It governs the response to different chemotypes of LPS, and its ligand specificity differs between the species. MD-2 also acts as a chaperone for TLR4, supporting its proper glycosylation and cell trafficking.[48] The majority of synthetic TLR4 agonists and antagonists are MD-2 ligands, so that MD-2 is considered the principal target for the pharmaceutical intervention on innate response to LPS. [41]

1.4.3 Deregulated TLR4 pathway activation

The described activation of TLR4 pathway and the subsequent intracellular signalling, in response to bacterial endotoxins, result in the triggering of pro-inflammatory processes necessary for optimal host immune responses to invading Gram-negative bacteria. However, excessively potent and deregulated TLR4 activation and signalling cause severe syndromes such as septic shock, associated with a high mortality. Septic shock occurs when bacteria or their products reach high enough

levels in the bloodstream to trigger complement activation, cytokine release and the coagulation cascade in many parts of the body, so that the immune system is not able to confine the inflammatory response to certain areas of the body. Treatment is most likely to be effective if it is started early in the infection, but diagnosis of septic shock in its early stages is not straightforward, because the early symptoms of shock (fever, hypotension, and tachycardia) are nonspecific. In addition, the transition from the early stages to multiple-organ failure can occur with frightening rapidity. Even if bacteria are the microorganisms most frequently implicated in septic shock, many different species of Gram-positive and Gram-negative bacteria can cause shock and no single antibiotic is effective against all of these bacterial pathogens.[54]

Consequently, targeting the activation of TLR4 by LPS is the key point in developing drugs active against septic shock. The inhibition of TLR4 stimulation by endogenous factors could be used to contrast a wide range of inflammatory and autoimmune disorders associated with the release of reactive oxygen or nitrogen species (ROS/RNS) and inflammatory cytokines induced by DAMPs. TLR4 is an emerging molecular target related to an impressively broad spectrum of disorders, including asthma, cardiovascular disorders, diabetes, obesity, metabolic syndromes, autoimmune disorders, neuroinflammatory disorders, neuropathic pain, CNS disorders such as amyotrophic lateral sclerosis (ALS) and Alzheimer disease (AD), psychiatric diseases, skin inflammations (dermatitis), psoriasis, and some tumours. Since the majority of these pathologies still lack specific pharmacological treatment, small molecules, active in inhibiting TLR4 activation, generate increasing interest.[55]

1.5 TLR4 modulators: antagonism and agonism

A general classification for TLR4 modulators is based on the effect they have on the activation of the TLR4 pathway. They can act as antagonists, when they are able to inhibit the LPS-triggered TLR4 activation, or as agonists, when they stimulate the activation of TLR4 pathway. Molecules able to modulate the activation of TLR4 pathway can interact with one or more receptors or co-receptors of the pathway, interfering at different stages of the signalling.

The greatest effort has been made to obtain TLR4 antagonists, in order to treat septic shock and potentially all the pathologies related to the deregulated activation of TLR4 pathway, described in the previous section. A second reason of interest for the discovery of TLR4 ligands is the development of new agonists that could be employed as vaccine adjuvants: molecules that elicit a controlled immune response.[56, 57]

Recently, scientific research on TLR4 receptor system led to the discovery of an impressive number of TLR4 ligands and modulators. Many of them come from medicinal chemistry, as they are synthesized with the specific purpose of being TLR4 agonists or antagonists. In particular, most of them are lipid A mimetics.

However, especially in the very last years, a surprisingly vast number of molecules of natural origin, mostly coming from plants, have been identified to be able to bind TLR4 or its co-receptors. [55]
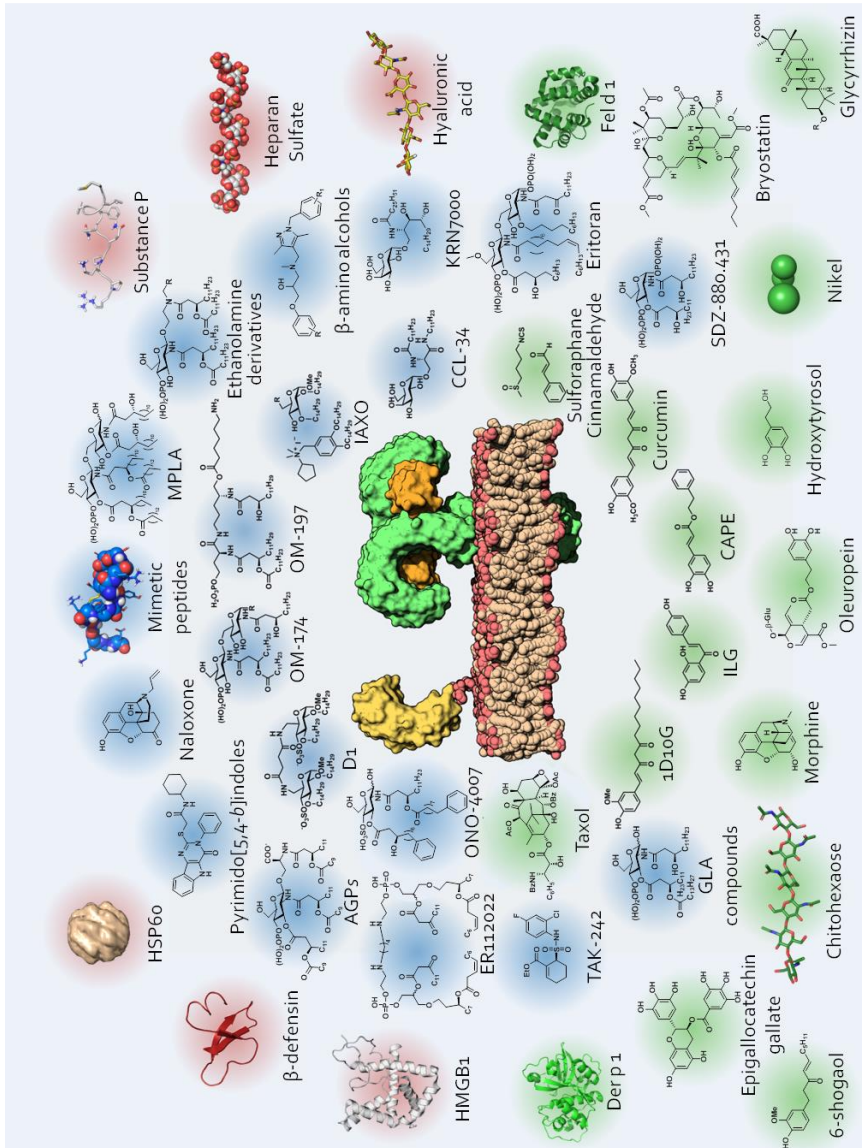
Figure 1.14. Some of known TLR4 modulators. Blue shade: synthetic ligands. Green shade: natural ligands. Red shade: endogenous ligands. From: Cighetti, 2014.[42]

When a potential TLR4 modulator is designed, many considerations have to be taken into account to predict its activity as agonist or antagonist.

45

In particular, it is known that the structure–activity relationship (SAR) of lipid A-like TLR4 modulators is guided by two tightly related factors: the 3D shape of aggregates in solution and the orientation of the small molecule in CD14 and MD-2.TLR4 binding sites. The first factor probably influences the early steps of LPS molecular recognition, where LBP interacts with LPS aggregates and catalyse the extraction of LPS monomers. The second factor is related to the LPS transfer from LBP to CD14 and from CD14 to MD-2.TLR4 immediately before the formation of the (LPS.MD-2.TLR4)$_2$ complex.[58]

To deeply understand the influence the 3D shape of modulator aggregates in solution has on biological activity it is first necessary to explain the relation between the natural ligand (LPS) bioactivity and its molecular and intramolecular conformation.
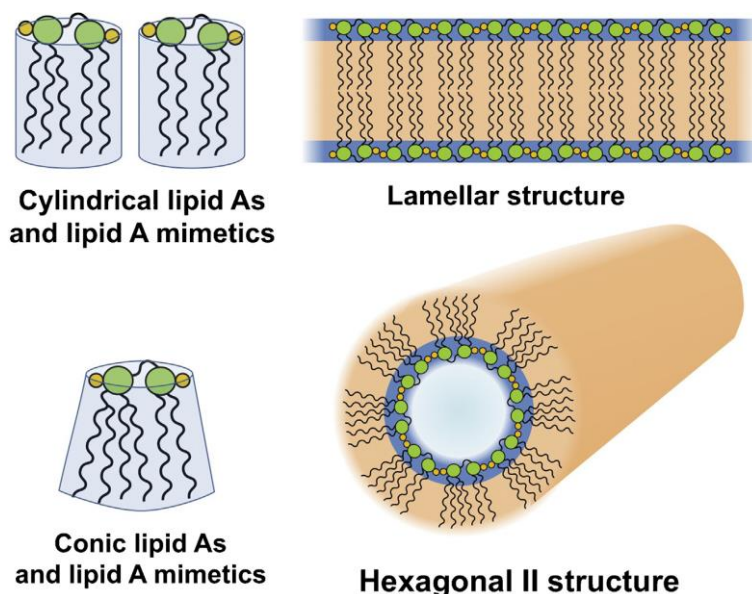

Figure 1.15. Relationship between lipid A chemical structures and 3D aggregate structures. [59]

Different types of lipid A assume the minimum energy conformations, related to the angle (tilt angle) formed between the di-glucosamine backbone and FA chains, which are packed almost parallel to each other.[60] For *E. coli*-type lipid A, this angle was found to be >50°, resulting in a conical molecular shape. Species with a tilt angle <25°, such as Lipid IVa, show a cylindrical shape.

The amphiphilic nature of LPS causes the formation of very stable supramolecular aggregates in micelles, with very low Critical Micelle Concentration (CMC) values estimated in the pM range.[61] The shape of these aggregates depends on the molecular conformation of the lipid A, varying from lamellar for cylindrical lipid A, to cubic or inverted hexagonal II for the conical ones (Figure 1.15). Some important correlations between the lipid A supramolecular structures and biological effects have been found[59]: lipid A giving rise to lamellar aggregates can be active as LPS antagonists, inhibiting cytokine production in response to LPS stimulus, while those assuming cubic or hexagonal II structures are highly active as agonists.[60] Interestingly, the concept of correlation between the structure of aggregates and the biological activity can be applied also to some synthetic lipid A mimetics.

The TLR4.MD-2 heterodimer has complex ligand specificity, so that minor changes in synthetic derivatives structure can dramatically change their activity and induce a switch between agonist and antagonist activity. Thus, by varying the ratio between the volume of lipophilic (FA) and hydrophilic (sugar-phosphate) portions of lipid A, it is possible to switch from an antagonist (related to a cylindrical shape of the molecule) to an agonist activity (conical shape). This rational has so far guided the

successful development of both TLR4 agonists and antagonists, based on anionic amphiphiles structures mimicking lipid A or its precursor, the lipid X. In particular, variations of fatty acid (FA) acyl chains of lipid A with respect to the standard *E. coli* lipid A, through the removal of two or more acyl chains, give rise to the so-called underacylated lipid A variants. These natural or synthetic lipid A variants can block or inhibit the TLR4 activation, acting as antagonists (Figure 1.16).
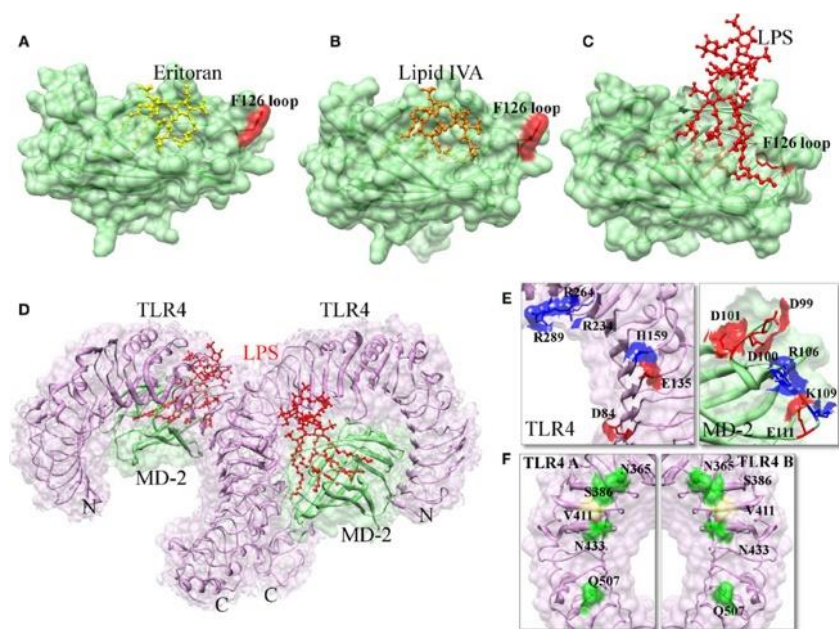
Figure 1.16. The interactions of agonist and antagonistic ligands in TLR4–MD-2 complex**. A)** When TLR4.MD-2 binds to Eritoran, the F126 loop is exposed to the solvent area. **B)** When MD-2 binds to lipid IVA, the F126 loop is exposed to the solvent area. **C)** When TLR4.MD-2 binds to LPS, the F126 loop forms hydrophobic interactions with lipid chains and the second TLR4, as well as TLR4 dimerization to occur. **D)** Structure of TLR4.MD-2.LPS complex, front view. **E)** TLR4–MD-2 dimer interface formed by electrostatic interactions. Positive and negative charged residues are marked in blue and red color, respectively. **F)** TLR4 homodimer interface. Hydrophilic and hydrophobic residues are colored in green and khaki, respectively.[62]

Some fundamental structural aspects of the TLR4 dimerization process and the molecular basis of TLR4 agonism and antagonism have been elucidated, thanks to the structure determination of the (TLR4.MD-2.LPS)$_2$ complex[63] crystals and the crystallographic data of MD-2 bound to TLR4 antagonists lipid IVa[44] and Eritoran (E5564), both further analysed in the next paragraph.[53]

However, the extremely wide variety of chemical structures of TLR4-active compounds, especially in the case of natural compounds, is intriguing and difficult to be rationalised (Figure 1.14). In conclusion, the common effect is the inhibition of the formation of the activated TLR4.MD-2.LPS homodimer, even though these compounds should target TLR4 and/or MD-2 and CD14 in a different way.[64]
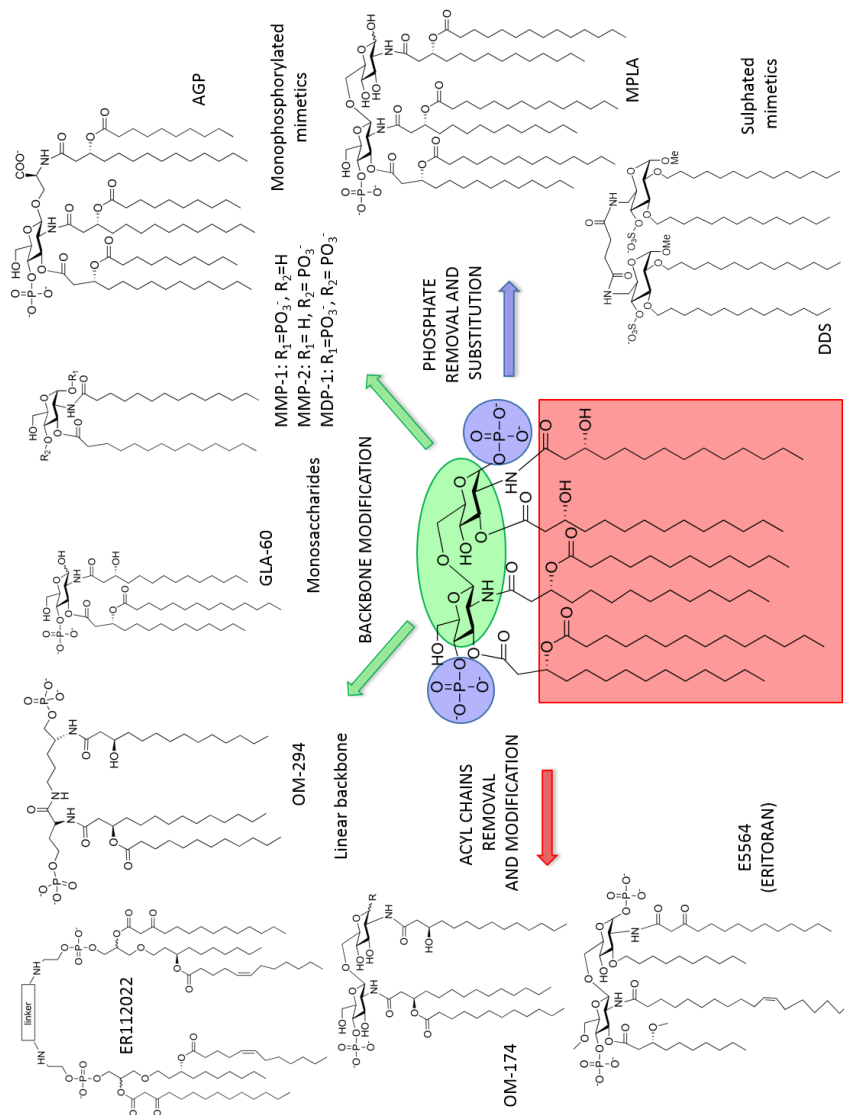
1.5.1 Synthetic TLR4 modulators

Great synthetic effort has been produced through the years to obtain different TLR4-active compounds. Here some of the most representative synthetic TLR4 modulators are presented, divided into two categories: the anionic amphiphiles and the cationic amphiphiles.

1.5.1.1 Anionic amphiphiles

As introduced in the previous paragraph, the most well-established approach to design and synthesize TLR4-active compounds consists in the structural modification of the natural ligand, the lipid A (Figure 1.17).

Different strategies can be applied: varying nature, position and length of FA acyl chains; reducing the number of phosphate groups; applying modifications on the saccharidic backbone.[58]

Figure 1.17. Some anionic TLR4 modulators (agonists and antagonists) obtained by chemical elaboration of *E. coli* lipid A structure. Adapted from Peri, 2014.[55]

The TLR4 modulators obtained using this approach are generally anionic amphiphiles.

Eritoran (Figure 1.17), bearing four acyl chains of different length and nature, is the most representative member of this class of compounds. The antagonist mechanism of Eritoran is based on the capacity of this molecule to insert into the hydrophobic MD-2 binding cavity and occupy MD-2, without promoting the formation of MD-2.TLR4 heterodimer.[41] Antagonist activity is shared by other underacylated lipid A variants with four fatty acid (FA) chains, such as the biosynthetic precursor lipid IVa (Figure 1.6).

An example of non-classical lipid A mimetic is DDS, composed of four ether chains and two sulfate groups, linked to a core of two α-D-glucopyranoside units, bridged through a (C6−C6') succinic diamide linker. The sulfate groups, in anionic form at neutral pH, are bioisosteres of lipid A phosphates. In contrast to natural lipid A, in this compound four linear ether chains ($C_{14}H_{29}$) replace the acyl esters ($COC_{13}H_{27}$ or $COC_{11}H_{23}$) of *E. coli* lipid A and DDS presents a C2 symmetry, with 2-fold rotational symmetry. Compound DDS inhibits in a dose-dependent manner the LPS-stimulated TLR4 activation in HEK-293 cells: HEK-TLR4 cells express human TLR4 and are supplemented with soluble MD-2, LBP, and CD14.[65]

Recently, three anionic lipid X mimetics were synthesized by a convergent strategy from glucosamine, introducing one or two phosphate groups in C-1 and C-4, and two linear C14 acyl chains in C-2 and C-3 positions (Figure 1.17).[66] These mimetics represent a further simplification of lipid X (Figure 1.6). MDP-1, with two phosphates resulted strongly active in inhibiting in

a dose-dependent way the LPS-stimulated TLR4 activation. Detailed results regarding MDP-1 will be presented in paragraph 2.2.2.

Monophosphoryl lipid As (MPLA) and aminoalkylglucosaminide 4-phosphates (AGPs) are the most representative anionic TLR4 agonists. In these compounds, the dephosphorylation or the replacement of the reducing end sugar of lipid A with an amino acid allows to obtain nontoxic TLR4 stimulants with agonist action. A mild TLR4 stimulation is a way to potentiate the intensity and duration of antibody production and immunity response to antigens. Synthetic low toxicity TLR4 agonists are used as vaccine adjuvants and for cancer immunotherapy.[57]

1.5.1.2 Cationic amphiphiles

In the case of cationic amphiphiles, the rules for the rational design of TLR4 modulators are still lacking, and the success in the development of agonists and antagonists mainly relies on a trial-and-error experimental approach.

Amphiphilic polyamines modulate TLR4 activation, acting at different levels of the signalling pathway.[67] The first level of action is based on the formation of stable aggregates with LPS molecules. The anionic amphiphilic nature of LPS enables ionic interaction with positively charged molecules, which can act as "LPS sequestrant", neutralizing its toxicity (antagonists), as described for decapeptide Polymyxin B (Figure 1.18).
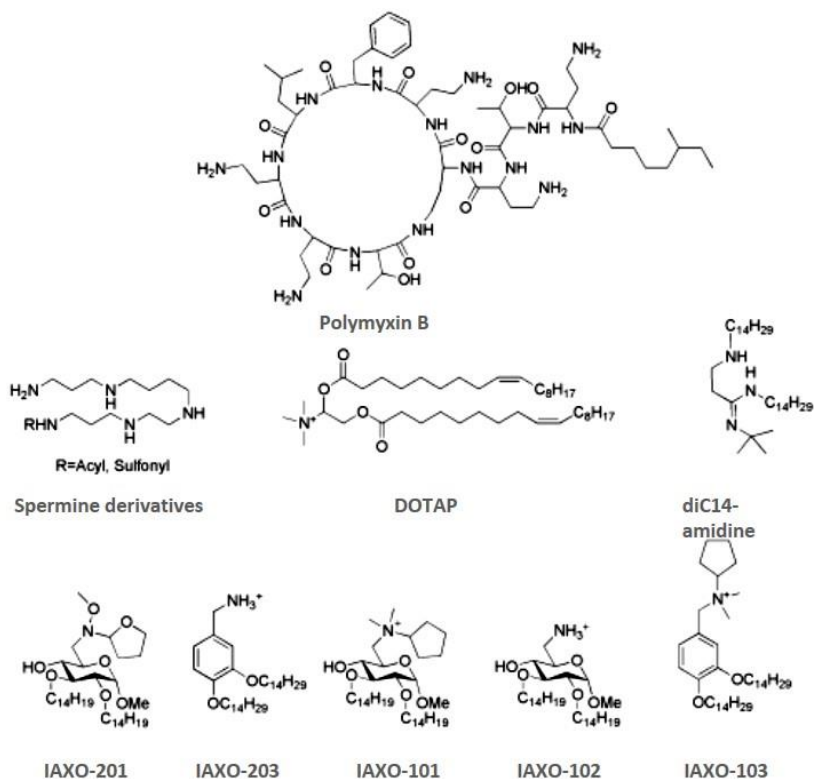
Figure 1.18. Some TLR4-modulating cationic amphiphiles.[58]

Cationic amphiphiles also act at a second level, interacting directly with LBP or CD14. As an example, diC14-amidine (Figure 1.18), a cationic lipid with an amidine polar head and two lipophilic chains, is a TLR4 agonist and induces an inflammatory reaction similar to that caused by LPS.[68]

The immunostimulatory activity of cationic lipids is generally weak and it is not sufficient to be used as vaccines adjuvants. As a consequence, most adjuvant formulations of cationic liposomes also contain bacterial components as immunostimulators. However, recent positive results, obtained by combining some cationic lipids (e.g. DOTAP and diC14-

53

amidine) and antigens, suggest that formulations of one-compound adjuvants for vaccines will be possible in the next future.[69]

A small library of glycolipids and benzylammonium lipids was synthesized (IAXO compounds, figure 1.18).[70] Compounds IAXO-101 and IAXO-102[71] resulted chemically stable, non-toxic, potent TLR4 antagonists. In these compounds a methyl α-D-glucopyranoside is alkylated in C-2 and C-3 positions with C14 alkyl chains, and substituted in C-6 position with a quaternary ammonium salt (IAXO-101) or an amine (IAXO-102), which is protonated at physiological pH. IAXO-103 and IAXO-203 are the benzylammonium analogues of IAXO-101 and IAXO-102. Among these compounds, IAXO-102 and 103 turned out to be the most promising TLR4 inhibitors both *in vitro* and *in vivo*, with IC_{50} values of 5.5 and 1.7 μM respectively, and high activity in *in vivo* models of sepsis and septic shock.[70] Moreover, IAXO-101 was evaluated for its analgesic effect on neuropathic pain, one of CNS pathologies in which TLR4 signal seems to play a pivotal role.[72] Finally, IAXO-102 was found active in reducing motor neuron death, counteracting the LPS neurotoxicity, tested on an experimental model of central nervous system (CNS) inflammation.

1.5.1.3 Aggregation properties

The TLR4 agonists and antagonists described above are amphiphilic molecules with a polar (charged) head linked to a variable number of lipophilic chains. The amphiphilic character results in the formation of micelles in aqueous environment above their Critical Micellar Concentration (CMC), that is normally very low (nanomolar range).

Consequently, the concentration range relevant for biological responses and for biochemical characterization *in vitro* is generally characterized by the predominance of aggregated forms. Therefore, the mutation of the aggregation state and of the 3D form of endotoxin or synthetic molecule aggregates may directly influence the kinetics and potency of TLR4 activation and signalling, as described for natural ligands, lipid As, in previous paragraphs.[73]

Another important consequence of the amphiphilic character of these molecules is their low water solubility, which sometimes complicates their handling *in vitro* and *in vivo*, and it is associated with poor distribution (pharmacokinetic) properties.

1.5.2 Natural TLR4 modulators

Most natural bioactive and pharmacologically active compounds derive from plants and they generally are plant secondary metabolites.
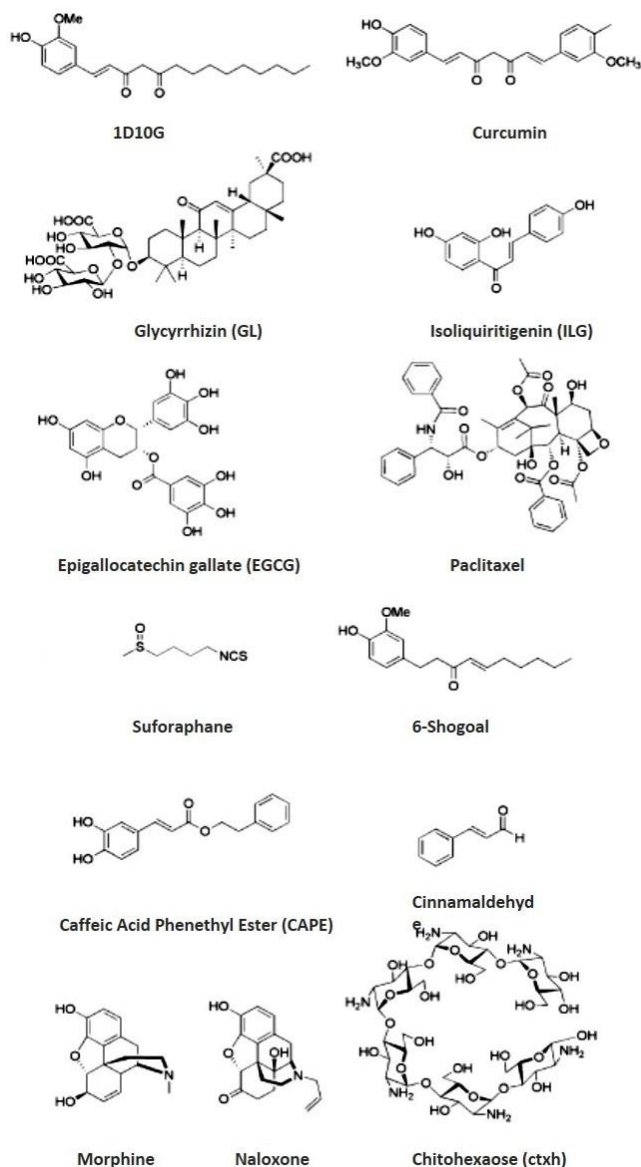

Figure 1.19. Some recently studied TLR4-modulating compounds from natural sources.[55]

Plant-based extracts provide a large number of natural immune modulators, many of which have been used in traditional medicine for centuries. Recent research efforts are directed to identify plant extracts as potential modulators of TLRs and to isolate the bioactive molecules contained in the extracts.[74] Many herbs used in traditional Chinese medicine (TCM) and Ayurvedic medicine seem to contain molecules that interfere with TLR4 activation and signalling. These include green tea, Glycyrrhiza uralensis, Magnolia officinalis, ginger (Zingiber officinalis), Salvia miltiorrhiza (red sage), and curcumin.[55]

With some exceptions, most natural TLR4-active compounds are polyphenolic and aromatic compounds, sharing interesting similarities in their chemical structures and in their mechanism of action. The chemical structures of natural compounds, whose TLR4 activity has been recently investigated, are reported in Figure 1.19.

The main mechanism of action proposed for some of these molecules is based on the formation of covalent bonds, which causes the disruption of TLR4.MD-2 heterodimer. In fact, compounds like isoliquiritigenin,[75] 6-shogaol,[76] caffeic acid phenetyl ester (CAPE),[77] and cinnamaldehyde [78] are able to form covalent adducts with solvent-exposed MD-2 and/or TLR4 cysteines. Cinnamaldehyde, 1-dehydro-10-gingerdione (1D10G), 6-shogaol, isoliquiritigenin, curcumin, and caffeic acid ester contain α,β-unsaturated carbonyl moieties that can easily react as an electrophile carbon with the nucleophilic thiol of a cysteine, thus forming Michael adducts with protein targets.[55]

Interestingly, curcumin and 1D10G do not seem to form a covalent bond with MD-2,[79] even if they are characterised by the same α,β-unsaturated carbonyl functionality.[80] They seem to inhibit the formation of TLR4 activated complex by interacting non-covalently with MD-2 and competing with endotoxin for MD-2 binding.

The polyphenolic fraction present in green tea extracts possesses anti-inflammatory and chemopreventive effects. The active compounds contained in this fraction are catechin, (−)-epicatechin (EC), (−)-epigallocatechin (EGC), (−)-epicatechin 3-gallate (ECG), and (−)-epigallocatechin 3-gallate (EGCG). Among these, EGCG is known to possess the most potent antioxidative and chemopreventive properties, and it has been demonstrated not to prevent LPS-induced dimerization of TLR4, but to inhibit the TLR4 signal downstream, blocking both MyD88- and TRIF-dependent signal pathways, by targeting IKKβ and TBK1 kinases, respectively. [63]

The variety of natural compounds active as TLR4 modulators is surprising and not so easy to be rationalised. As described, these molecules can modulate the TLR4 signalling pathway at different levels and many of the processes involved have not been completely elucidated yet.

1.6 Biological activity of olive oil phenolics

The phenolic constituents of extra virgin olive oil (EVOO) have long been associated with the numerous health benefits conferred with Mediterranean diet.[81] Olive oil phenolics have been shown to possess very interesting biological activities as anti-oxidant, anti-inflammatory and anti-thrombotic agents.[82]

Phenolic compounds are found in all the parts of the olive plant, but their nature and concentration varies greatly. Minor phenolic constituents from olive oils have been isolated and classified in six groups (Figure 1.20): phenolic acids (e.g. cinnamic acid and derivatives), phenethyl alcohols (e.g. tyrosol and hydroxytyrosol), hydroxyisochromans, flavonoids (e.g. luteolin, apigenin, taxoflavin), lignans (pinoresinol, elenoic acid), secoiridoids (e.g. oleuropein, oleuropein aglycone, ligstroside, oleocanthal).[81] These compounds have been extracted and purified from natural sources, but considerable synthetic efforts were also made to obtain some of these interesting molecules, based on either total or partial synthesis strategies.

Both the whole phenolic extracts and the single constituents have been tested for biological activity as anti-inflammatory agents, producing some interesting results. The effect of olive oil phenolic extracts on NF-κB activity on human gastric adenocarcinoma cells was evaluated. Olive oil extracts inhibited the NF-κB-driven transcription in a concentration-dependent manner, with IC_{50} values for the extracts in the range of μg/mL. [83]
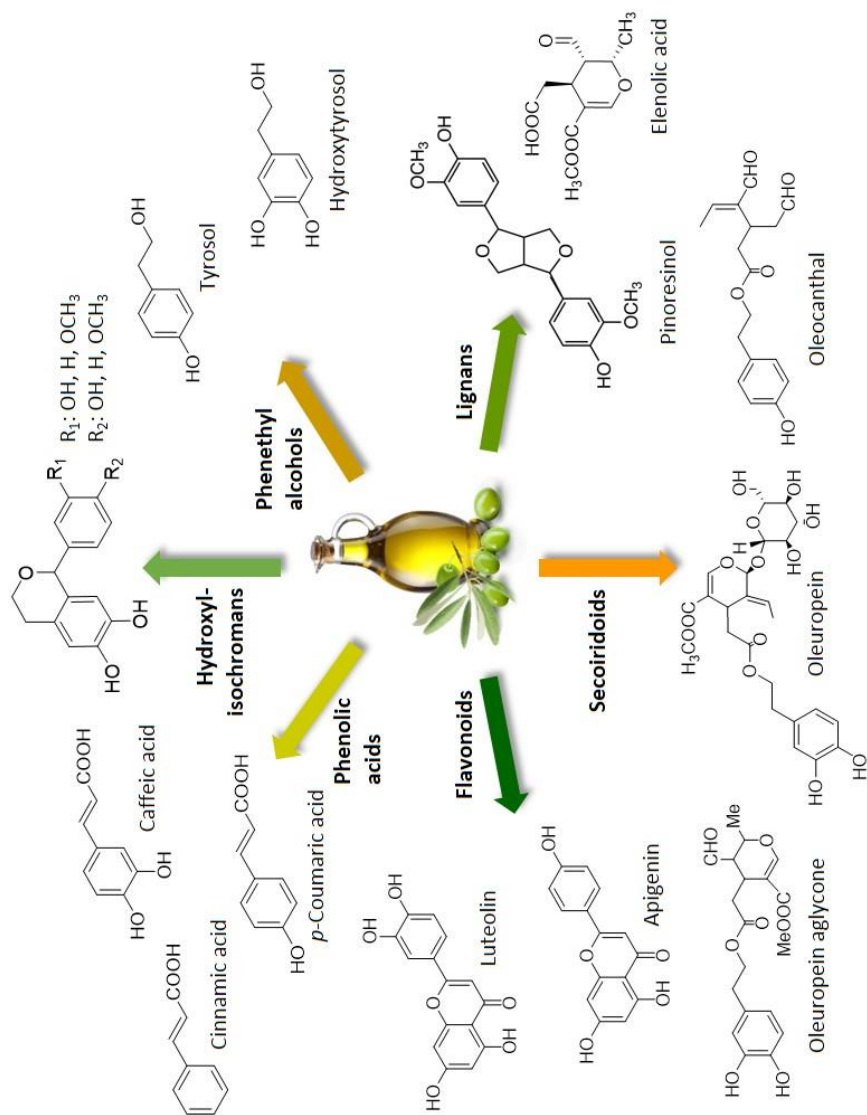
Figure 1.20. Some phenolic constituents from extra virgin olive oil belonging to the most important groups of phenols: phenolic acids, phenethyl alcohols, hydroxyl-isochromans, flavonoids, lignans, secoiridoids. Self work.

The most important phenolic compounds active as anti-inflammatory agents were found to be: oleuropein[84], hydroxytyrosol[85] and oleocanthal[86, 87].

In particular, oleuropein, the main phenolic compound in virgin olive oil, and several of its derivatives, such as oleuropein aglycone, hydroxytyrosol and their respective acetylated lipophilic forms, were tested *in vitro* and *in vivo*, and their intriguing anti-COX-1 and anti-COX-2 properties were comparable to those of some well-known anti-inflammatory drugs, such as ibuprofen and celecoxib.[88]

Oleocanthal is a component contained especially in freshly pressed extra-virgin olive oil. This molecule has a peculiar sensory property: its pungency elicits a strong stinging sensation in the back of the throat. This sensation is similar to that caused by solutions of the non-steroidal anti-inflammatory drug (NSAID) ibuprofen. The perceptual similarity between oleocanthal and ibuprofen spurred the hypothesis that the two compounds shared pharmacological activity. It was demonstrated that, regardless of structural dissimilarities, natural oleocanthal inhibits inflammation in the same way as ibuprofen, and it is even more potent on an equimolar basis.[86]

Subsequent studies have shown that oleocanthal and some derivatives exhibit various modes of action in reducing inflammatory-related diseases, including neurodegenerative diseases, specific cancer and degenerative joint diseases, since they proved to be able to down-regulate iNOS protein expression in LPS-challenged chondrocytes, resulting in a reduction of nitrite production. [87]

Moreover, in very recent studies, some flavonoids and lignans contained in olive oil, such as apigenin, luteolin and pinoresinol have been associated with anti-inflammatory activity.[89, 90] In particular, the ability of several flavonoids to modulate the production of pro-inflammatory molecules from LPS-stimulated macrophages was compared and their mechanism of action was investigated. Pre-treatment of RAW 264.7 cells with luteolin and luteolin-7-glucoside inhibited both the LPS-stimulated TNF-α and IL-6 release. Luteolin was the most potent in inhibiting cytokine production, with IC_{50} values of less than 1 µM for TNF-α release.[89]

In recent years, the interest towards natural compounds and in particular olive oil phenolic compounds has increased considerably. Even if there is, as shown previously, some evidence regarding the anti-inflammatory activity of some olive oil phenolics, this activity has not been directly correlated to the activity of TLR4 receptor system yet. Our research group tried to fill this gap, investigating the activity of olive oil phenolic extracts and of some isolated phenolic constituents on TLR4 receptor system.

Interestingly, it was found that the whole phenolic extract from each different tested extra virgin olive oil inhibits TLR4 signalling pathway, thus presenting a considerable dose-dependent antagonist activity. Moreover, some constituents of olive oil phenolic fraction were identified as very good TLR4 antagonists. In particular, luteolin and apigenin proved to be strongly active in inhibiting inflammatory responses related to the activation of the TLR4 pathway, whereas oleuropein showed a lower activity (paragraph 2.2.3.1).

The amphiphilic character of all "classical" lipid A analogues is often associated with low solubility in aqueous media, while the natural TLR4-active compounds are characterised by a better water solubility and bioavailability. In addition, synthetic modifications of natural compounds can be carried out both to increase target specificity and resistance to enzyme hydrolysis.

Aim of the work

The purpose of this PhD project is the design, the synthesis and the chemical and biological characterization of new small molecules, active as ligands of LPS-binding proteins. The LPS-binding proteins involved in this project belong to two classes: the bacterial proteins of the Lpt transport machinery and the mammalian TLR4 receptor complex, including the co-receptors LBP, CD14, MD-2.

The interest towards these biological targets is due to two aspects. The first area of interest is the development of new molecules which can bind LPS binding proteins and interfere in the correct transport of LPS to the bacterial outer membrane or which can modulate the LPS-TLR4 signalling: this can lead to the development of new drug hits. Secondly, a further interesting aspect is the elucidation of both the biological processes involved in the LPS biogenesis and its recognition by the innate immunity receptors. In fact, a deep study concerning the interaction of the natural ligand and/or synthetic small molecules with LPS binding proteins is very useful to understand the molecular basis of these biological processes.

The research project of the thesis can be divided in two parts, the first focused on the LPS interaction with Lpt transport proteins, the second based on the study of LPS interaction with TLR4 receptor system.

The Lpt Transport Machinery and the LptC protein

The functionality of Gram-negative outer membrane is essential to bacterial viability and requires the correct placement of LPS in the outer leaflet. Therefore, the LPS biogenesis represents an ideal target for the

development of novel antibiotics against Gram-negative bacteria. While the structures of Lpt proteins have been elucidated, little is known about the mechanism of LPS transport and little data is currently available on Lpt-LPS binding. The present project is part of a wider work, which has the objects of elucidating the binding of the LPS to the proteins LptA and LptC, evaluating the precise mechanism of LPS transport to the outer membrane and determining some thermodynamic and kinetic parameters of the binding. A second target of this project concerns the production of new synthetic molecules and their screening to evaluate their ability to interfere with the binding of the natural ligand, thus representing potential scaffolds to develop antibiotics against Gram-negative bacteria. In particular, this thesis project is focused on the protein LptC.

The development of a new tool to study *in vitro* the binding of the natural ligand, the LPS, to LptC was required. Radiolabeled LPS is generally used for binding studies, but fluorescence labeling can be used as an alternative, safer method. The main problems related to the use of fluorescent LPS are the low sensitivity of measurements with commercial fluorescent LPS, due to the low level of fluorescence incorporation, and the risk to alter LPS activity and binding properties through the introduction of the bulky fluorescent moiety. Consequently, the production of a fluorescent LPS, with higher incorporation ratio of fluorophore, which retains the biological activity of the natural ligand, was needed to obtain a satisfying fluorescent probe. To study the interaction between LPS and LptC, different techniques have been used, in particular Nuclear Magnetic Resonance (NMR). With reference to the second target

of this project, some synthetic molecules were designed and synthesized, in order to obtain potential LptC ligands and, in perspective, potential Gram-negative antibiotics. A fluorescent moiety was also needed to be present in these compounds, in order to use them as fluorescent probes for interaction studies with the protein LptC.

The innate immunity receptors: the TLR4 receptor system

In recent years, our research group was mainly focused on the study of innate immunity receptors TLR4, MD-2 and CD14 through the use of synthetic molecules able to interfere with their activity. Synthetic small molecules able to modulate TLR4 activity are a powerful mean not only to study the receptor system, but also to obtain vaccine adjuvants (agonists) or anti-inflammatory agents (antagonists). Although many lipid A mimetics were obtained in recent years, the development of safer and more active compounds is still needed.

A criterion for the entire synthetic project was the structure simplification. Since full lipid A mimetics are molecules with very complicated chemical structures and their syntheses involve a lot of chemical reactions, we applied the concept of simplification both to the chemical structures and the synthetic procedures to obtain small-molecule ligands of LPS-binding proteins.

Specific binding of amino glycolipids and aromatic ammonium salts to CD14 was clearly demonstrated by our research group.[91-93] These compounds are active in inhibiting LPS-stimulated TLR4-dependent cytokine production in cells and *in vivo*. Among these, IAXO-102 resulted a chemically stable, non-toxic, potent TLR4 antagonist. Moreover, this

molecule presents a reactive amino group at position C-6 of the sugar, which can be easily functionalized. The synthesis of molecules derived from IAXO-102 is a target of this thesis work. In particular, IAXO-102 derivatives were obtained with the following aims in mind: employ them as fluorescent probes for binding studies, produce molecules with enhanced water solubility, and modulate the TLR4 antagonist activity.

Lipid X, a biosynthetic precursor of lipid A, whose structure corresponds to the reducing GlcNAc monosaccharide of *E. coli* lipid A, is well known for blocking LPS-induced septic shock. Due to its anti-endotoxic activity, lipid X has been considered a simplified monosaccharide scaffold for the development of TLR4 agonists and antagonists. TLR4 antagonists with a chemical structure inspired to lipid X were synthesized in our labs: they are mono- and diphosphate glycolipids. The aim of this work is the evaluation, via NMR binding experiments, of their ability to bind the innate immunity co-receptor MD-2.

The glycolipidic TLR4 antagonists obtained so far are amphiphilic molecules, often presenting low solubility in aqueous media and poor bioavailability. These characteristics can represent a problem when molecules are employed in aqueous biological environments, for instance when tested on cells, or, even worse, *in vivo*. This issue is solved when natural TLR4-active compounds are used, since they usually show good water solubility. The synthetic modification of natural compounds, however, is often required in order to increase target specificity and to improve resistance to enzyme hydrolysis. Consequently, the synthesis of new small molecules with chemical structures similar to natural TLR4 modulators was pursued, in order to produce a new generation of TLR4-

active compounds, characterised by improved pharmacokinetic properties, enhanced water solubility and reduced toxicity. In particular, very interesting anti-inflammatory properties are reported for phenolic constituents from extra virgin olive oil and our group demonstrated in a very recent screening that some phenolic extracts from extra virgin olive oils and some specific phenolic constituents from olive oil presented a very promising activity as TLR4 antagonists. Therefore, the synthesis of some analogues of these molecules is an important target to obtain a new class of potential TLR4 modulators, that can combine the advantages of natural products and the improvements derived from chemical modifications.

In addition to the production of TLR4 antagonists described so far, another target of this work is the conjugation of small-molecules TLR4 agonists to carrier proteins, in order to obtain a new class of potential vaccine adjuvants. Agonists are important in vaccine formulation, as mild TLR4 stimulation is a way to enhance the intensity and duration of antibody production and immunity response to antigens.

Chapter 2

Results and discussion

2.1 LptC ligands

LptC plays a fundamental role in LPS transport to the external surface of the bacterial outer membrane, because it is the first protein of the Lpt transport machinery that interact with the newly translocated LPS molecule in the periplasm. Here, the interaction of LptC with both the natural ligand (LPS) and synthetic molecules has been investigated by using several techniques. The production of a fluorescent LOS, the synthesis of a new fluorescent ligand and NMR binding studies will be presented in the next sections.

2.1.1 Fluorescent lipooligosaccharide (fLOS)

Binding studies between the bacterial transport protein LptC and the natural ligand, the LPS, were performed. A suitable tool was required to perform these experiments: a labeled LPS. Radiolabeled LPS is generally used for binding studies. However, for this work, a safer labeling method was preferred, replacing radioactivity with fluorescence labeling. The main issues related to the use of fluorescent LPS are related to: 1) the low sensitivity of measurements with commercial FITC-LPS due to the low level of fluorescence incorporation and 2) the risk to alter LPS activity and binding properties by introducing the fluorescent moiety. These issues were overcome by producing a fluorescently labeled LPS by fluorescein conjugation to a pure LPS, directly extracted from *E. coli* cells. The LPS used in this work is a rough type LPS from *E. coli* MG1655 (lipooligosaccharide, LOS) extracted from cells, using the Phenol-

Chloroform-light Petroleum (PCP) procedure,[94] which is a selective extraction procedure for R-type LPS (LOS). During the extraction procedure cells are not lysed, allowing for a selective isolation of LOS, recovered as a solid precipitate, easily isolated from the extraction liquid phase. Pure LOS was then labeled with fluorescein isothiocyanate (FITC), using a modified procedure from Troelstra et al.[95] Fluorescent lipooligosaccharide (**fLOS**) was obtained.[10]

The purity and the chemical identity of **fLOS** were assessed thanks to NMR and SDS-PAGE electrophoresis analyses. Discontinuous gels were used for this analysis, with 12% separating gel and 5% staking gel, stained according to the Silver Stain procedure, which is specific for LPS and LOS.
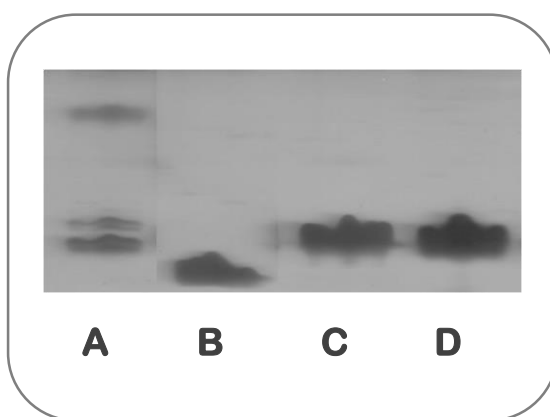
Figure 2.1. Discontinuous SDS-PAGE electrophoresis (separating gel 12%), coloured according to Silver Stain procedure. **A)** Smooth LPS from *E. coli* O55:B5 (6 µg), **B)** Deep rough LOS from *E. coli* (6 µg), **C)** LOS from *E. coli* MG1655 (6 µg), **D) fLOS** (6 µg).

The labelling ratio was calculated using the colorimetric thiobarbiturate assay[96] for Kdo (3-deoxy-D-manno-oct-2-ulosonic acid) quantification, which is a LOS marker, and spectrophotometric measures at 492 nm for

FITC quantification. The labelling ratio for **fLOS** was calculated to be 1:1 (LOS:FITC), significantly higher than the 50:1 (LPS:FITC) found for the commercial FITC-LPS (*E. coli* O111:B4) from Sigma Aldrich. High levels of fluorescein incorporation are essential to reach a reliable signal level in binding experiments.

Thus, the first issue deriving from using fluorescent LPS was clearly overcome. The second one was also overcome, because the biological activity was totally retained by **fLOS**, as shown by the Hek-Blue™ cells activation assay. It is clear from figure 2.2 that the dose-dependent TLR4 activation of **fLOS** is very similar to commercial *E. coli* LPS (Sigma-Aldrich) and native *E. coli* LOS (strain MG1655).

All the biological assays presented in this work have been performed by Dr. Stefania Sestito.
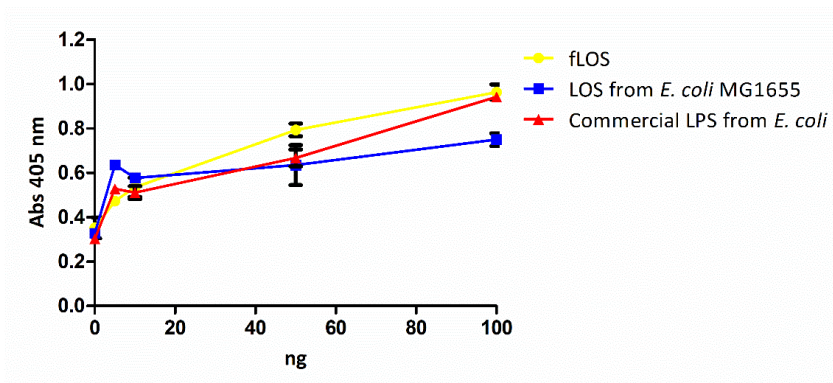
Figure 2.2. Activity assay on HEK-Blue™ cells. Activation of Hek-Blue™ cells, transfected with human CD14 and MD-2.TLR4, treated with 0-100 ng of commercial LPS from *E. coli,* native LOS from *E. coli* MG1655 and **fLOS**. TLR4 activation is monitored as sAP production.

Previous attempts to obtain pure fluorescently labeled LPSs with high level of fluorophore incorporation were performed starting from commercially available LPSs (Sigma-Aldrich). LOS from *Salmonella enterica,* serotype minnesota Re 595, and LPS from *E. coli* O55:B5 were used. Fluorescent LPSs were obtained according to the labeling procedure described above, but the products did not show a good grade of purity and homogeneity and the labeling ratios were calculated to be 12:1 and 15:1 (LOS:FITC), significantly lower than ratio calculated for **fLOS**. Consequently, **fLOS** was preferred for performing all the binding experiments, respect to these two products.

The use of fluorescent LOS (**fLOS**) with high levels of fluorescein incorporation allowed us to calculate, for the first time, the thermodynamic parameters of LOS-LptC interaction *in vitro*. A truncated version of LptC was used, lacking the first 23 amino acids of the transmembrane helix and fused to N-terminal His_6 tag (sH-LptC).

Experiments based on resin capture of the sH-LptC-**fLOS** complex gave reliable association/dissociation and saturation/competition curves. In saturation and competition experiments (Figure 2.3), **fLOS** and unlabeled LOS precursor showed a similar affinity towards LptC, with apparent calculated dissociation constants K_d of 71.4 and 52.4 μM, respectively.[10]
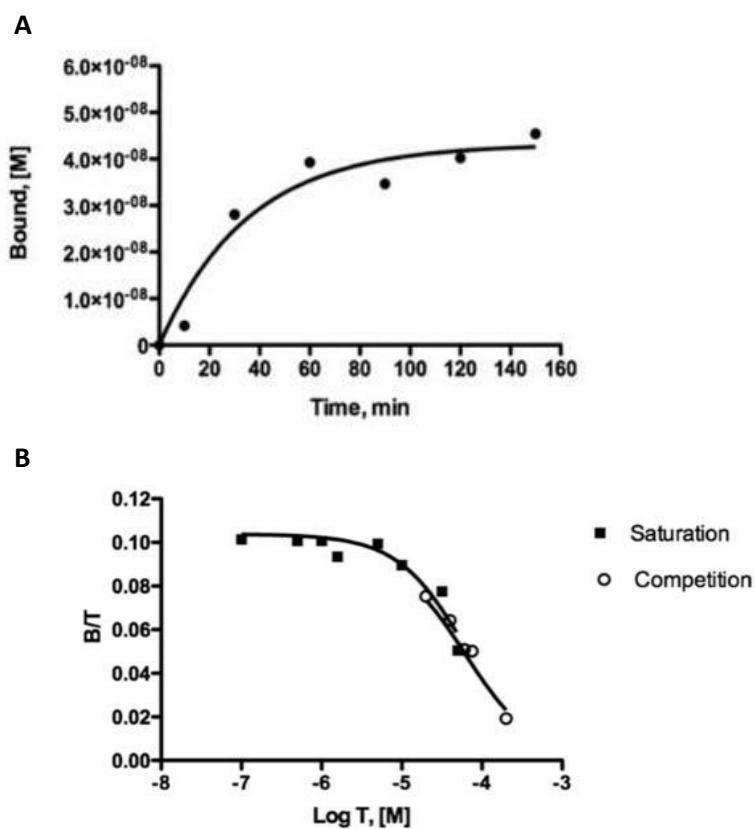
Figure 2.3. **A)** Association time-courses of **fLOS** binding to sH-LptC immobilized on Ni-NTA resin. 500 µM **fLOS** was incubated with sH-LptC RT. **B)** Saturation (0,1–50 µM **fLOS**) and competition (10 µM **fLOS** competing with increasing concentrations of unlabeled **LOS**) curves of **fLOS** binding to resin absorbed sH-LptC under pseudo-equilibrium conditions (RT, 90 min).

The very similar affinity values found for **fLOS** and LOS suggest that **fLOS** interacts with LptC similarly to unlabeled LOS.[10] Consequently, the introduction of the fluorescent moiety did not significantly alter the LOS binding properties and the biological activity, and demonstrates that **fLOS**

can be used as a tracer in quantitative analysis. Moreover, it was observed that binding of LOS to LptC is mostly irreversible, as dissociation time-course experiments with unlabeled LOS failed to displace the bound ligand. Data was confirmed by experiments based on LptC intrinsic fluorescence quenching by **fLOS** in solution. Interestingly, both methods show that **fLOS** binding to LptC is mostly irreversible, reflecting that LPS can be released from LptC only when energy is supplied by ATP or in the presence of higher affinity LptA protein, which is downstream in the Lpt bridge.

2.1.2 Synthetic, fluorescently labelled LptC ligands

Recently, we developed small molecules that interact with the LPS-binding protein CD14 with high affinity and specificity (compounds IAXO-101 and IAXO-102, Figure 2.4), thus inhibiting TLR4 activation and signaling in cells and in mice.
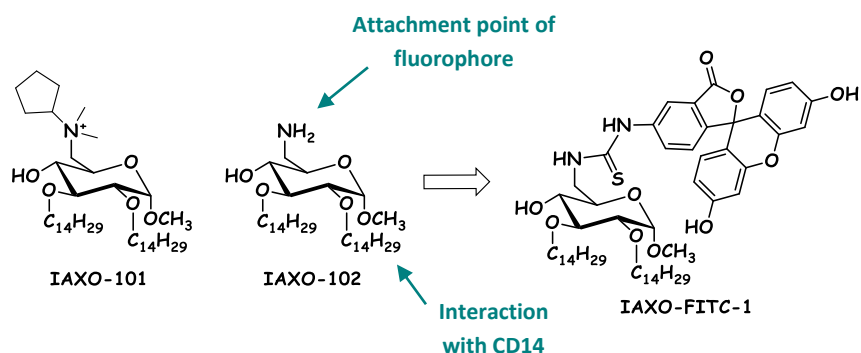
Figure 2.4. TLR4 modulators IAXO-101 and IAXO-101 and rational design of the fluorescent potential LptC ligand **IAXO-FITC-1.**

Similarly to CD14, it was demonstrated that also LptA and LptC bind LPS within the interior of the hydrophobic cavity formed by their β-sheets. Since CD14 and LptC share the same natural ligand, the possibility that compounds interfering with CD14 activity (e.g. IAXO-102) can be used as scaffolds to generate compounds able to bind/interfere with LptC was explored. Thus, new potential LptC ligands, with chemical structure based on the CD14 ligand IAXO-102 were designed (Figure 2.4).

Obviously, the introduction of a fluorescent moiety on the molecule was required, in order to perform binding studies. NMR data showed that the hydrophobic linear ether chains of IAXO-102 directly interact with CD14 binding site, thus suggesting that the conjugation of the fluorophore through the C-6 primary amine should preserve the interaction with CD14 and consequently with LptC.[92]

In **IAXO-FITC-1**, IAXO-102 is chemically linked to fluorescein, through a thiourea 3-atoms linker. The synthesis of **IAXO-FITC-1** is described in the paragraph regarding the IAXO-102-derived TLR4 antagonists (par 2.2.1.1 Scheme 2.4).

IAXO-102 and **IAXO-FITC-1** have been identified as good candidates to compete with LOS for binding to LptC.[10] Thus, both the glycolipid IAXO-102 and the fluorescent analogue **IAXO-FITC-1** were used for binding studies with LptC, based on fluorescence measurements (Figure 2.5).
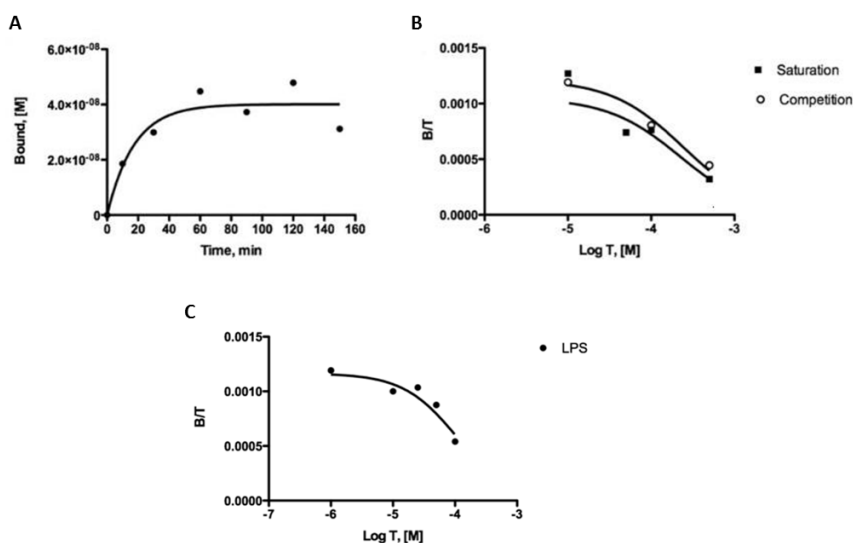
Figure 2.5. A) Association time-courses of **IAXO-FITC-1** binding to sH-LptC immobilized on Ni-NTA resin. 50 µM **IAXO-FITC-1** was incubated with sH-LptC RT for up to 150 min. **B)** Saturation (10–500 µM **IAXO-FITC-1**) and competition (50 µM **IAXO-FITC-1** competing with increasing concentrations of **IAXO-102)** curves of **IAXO-FITC-1** binding to resin absorbed sH-LptC under pseudo-equilibrium conditions (RT, 90 min). **C)** Binding curves for 50 µM **IAXO-FITC-1** competing with increasing concentrations of LPS. Binding is expressed as the concentration ratio of bound to total ligand (B/T) against the logarithm of total unlabeled ligand concentration (log T).

The fluorescent **IAXO-FITC-1** displayed faster association kinetics with LptC, but with a four-fold lower affinity for the protein (apparent K_d of 221 µM), compared to LPS, as expected for the synthetic ligand. As in the case of LPS, the presence of the fluorophore did not profoundly affect the LptC binding affinity, IAXO-102 having an apparent $K_i = 129$ µM.

Interestingly, **IAXO-FITC-1** and LPS appear to bind at the same site to the LptC protein, as demonstrated by competition experiments. As noted for LPS binding, also **IAXO-FITC-1** binding resulted mostly irreversible, suggesting a common way of interaction with the protein LptC.

Consequently, **IAXO-FITC-1** represents not only an interesting fluorescent tool to perform interaction studies on LptC, but also a scaffold for the development of a new class of antibiotics against Gram-negative bacteria.

2.1.3 NMR binding studies

NMR binding studies on the protein LptC were performed in collaboration with Dr. Cristina Airoldi (University of Milano- Bicocca).

The goal of the whole research project regarding the protein LptC is the characterization of the interaction between LptC and the natural ligand, the LPS. As described in the previous paragraph, different techniques were used to reach this goal. Here, some preliminary results obtained using Nuclear Magnetic Resonance (NMR) techniques are reported.

The commercial fluorescent probe 1-Anilinonaphthalene-8-Sulfonic Acid (ANS) was used as competing ligand to study the LptC-LPS interaction. ANS is a fluorescent dye that binds with high affinity to hydrophobic surfaces of proteins. The emission maximum of ANS undergoes a blue shift and fluorescence intensity increases significantly upon binding to low polarity regions of a protein surface.

These properties make ANS well suited to determine the affinity of hydrophobic ligands to their corresponding binding proteins, such as the binding of free fatty acids to fatty acid binding proteins.

The use of ANS for NMR binding studies was needed to deal with two issues:

1) the interaction between LPS and LptC was supposed to be too strong to be studied using direct NMR experiments, requiring competition studies based on the use of a mediator;

2) some experiments, already performed on the proteins LptA and LptC, which were based on the use of ANS as probe for fluorescence interaction studies, required to be validated, since they were indirect measurements.

First, the interaction between LptC and ANS was evaluated through mono-dimensional STD (Saturation Transfer Difference) NMR (Figure 2.6) and bi-dimensional tr-NOESY NMR experiments (Figure 2.7), performed on the protein and ligand mixture (LptC/ANS 1:40) dissolved in phosphate buffer, pH 7.4, 25°C. These experiments were run with different acquisition parameters, indicating a quite good interaction between the protein LptC and the fluorescent probe ANS. All the required control experiments were performed, resulting negative and confirming the data.

The ^{1}H NMR spectrum of the mixture of ANS and LptC, acquired in the same conditions as STD and tr-NOESY, is reported both in figures 2.6 and 2.7, as reference. Consequently, it was demonstrated, for the first time, that ANS interacts with the protein LptC.
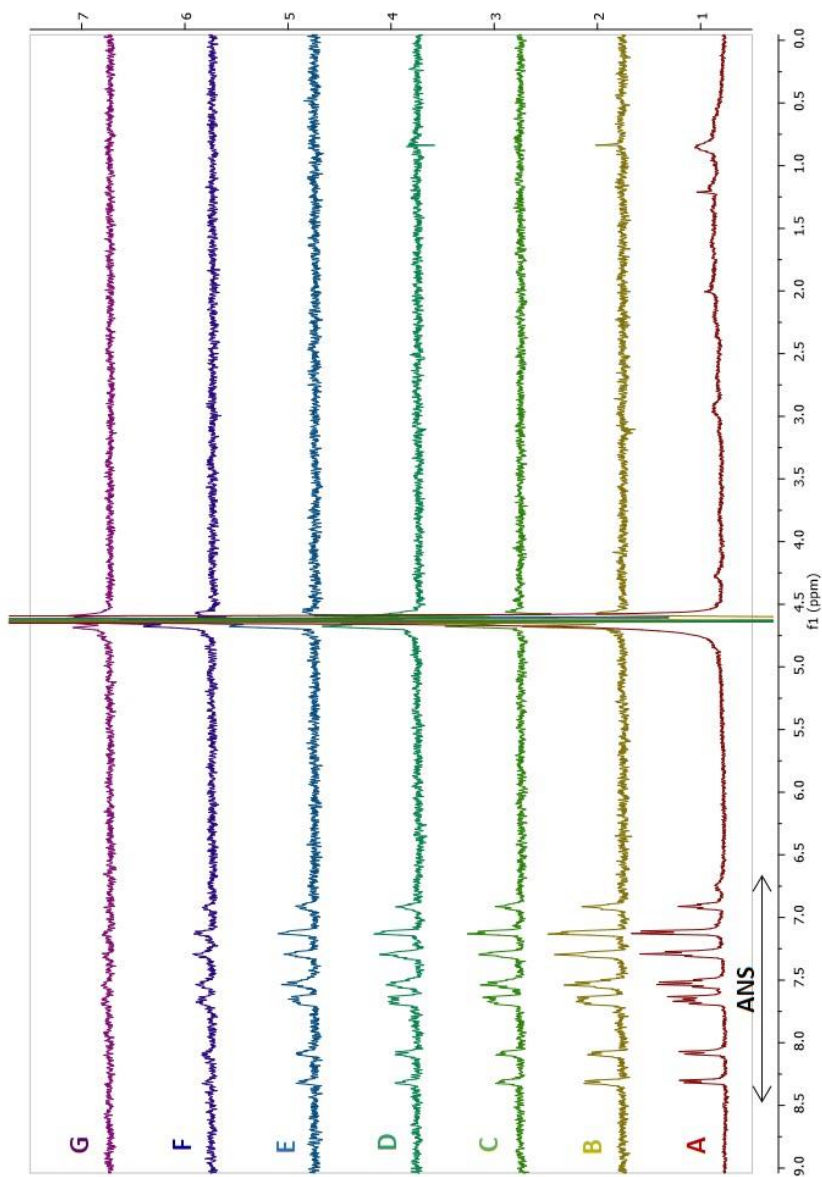
Figure 2.6. A) ^{1}H NMR spectrum of a solution of ANS (1 mM) and LptC (25 µM) in deuterated phosphate buffer pH=7.4 (10 mM), acquisition temperature 37°C, number of scans 64; **B-G)** STD NMR spectra of a solution of ANS (1 mM) and LptC (25 µM) in deuterated phosphate buffer pH=7.4 (10 mM), acquisition temperature 37°C, number of scans 768, saturation frequency -1 ppm, acquired with different saturation times: **B)** 3 s; **C)** 2 s; **D)** 1.5 s; **E)** 1 s; **F)** 0.65 s; **G)** 0.35 s.
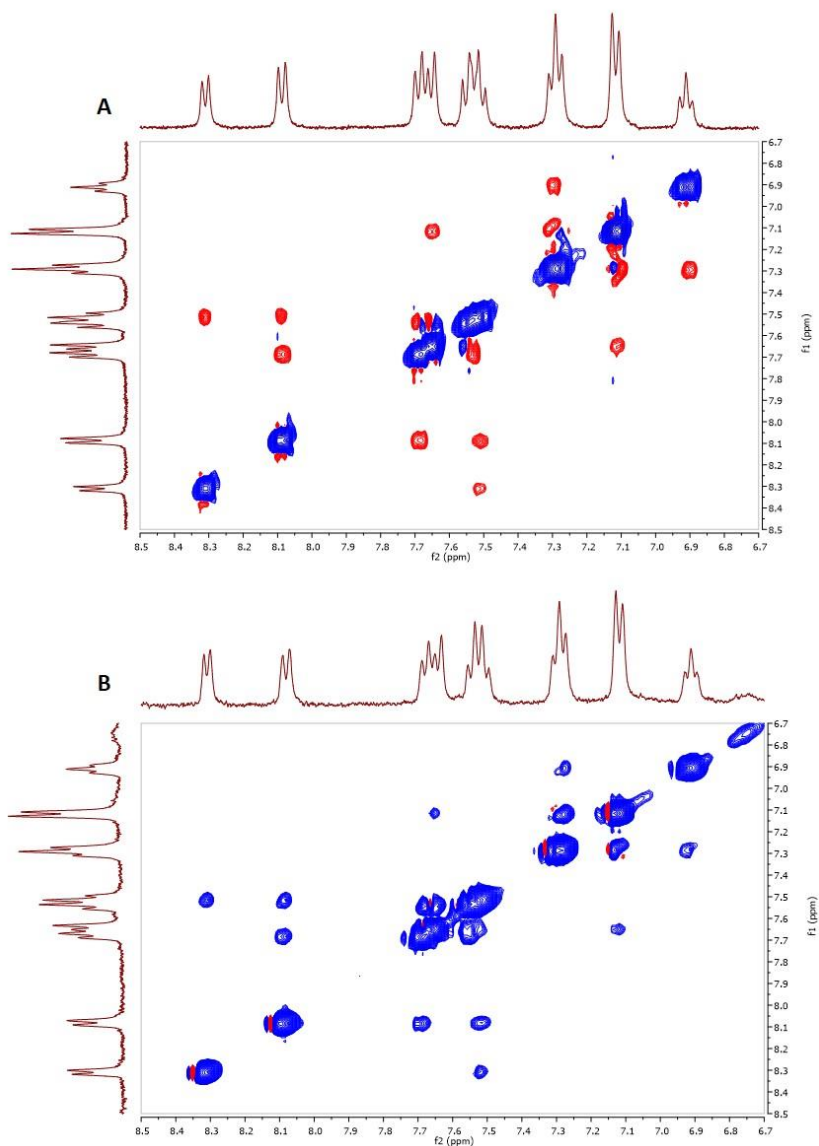
Figure 2.7. **A)** Tr-NOESY NMR spectrum of a soltution of ANS (2 mM) in deuterated phosphate buffer pH=7.4 (10 mM), acquisition temperature 25°C, number of scans 64, mixing time 200 ms, relaxation delay 1 s.; **B)**Tr-NOESY NMR spectrum of a soltution of ANS (1 mM) and LptC (25 µM) in deuterated phosphate buffer pH=7.4 (10 mM), acquisition temperature 25°C, number of scans 80, mixing time 200 ms, relaxation delay 1 s.

Then, it was necessary to investigate if the fluorescent probe (ANS) and the natural ligand (LPS) compete for the same LptC binding site. The LPS used for NMR experiments was a LOS from *E. coli* MG1655 isolated from cells and purified in our labs (Par. 2.1.1). Competition STD experiments were performed, adding increasing amounts of LPS (LptC/ANS/LPS 1:40:0.2 to LptC/ANS/LPS 1:40:10) to a mixture of LptC and ANS, as in a titration experiment.

A progressive lowering in STD signal intensities was expected for molecules sharing the same binding site. The expected decrease, however, was not observed. On the contrary, the signals became more widespread, as of the amount of added LPS increased. Moreover, a line broadening was observed in the ^{1}H NMR spectrum, too, when high amounts of LPS were added (LPS 250 μM, figure 2.8 I). Tr-NOESY experiments confirmed this unexpected behavior (Figure 2.9). The outcomes of these experiments indicated that, when LPS is added to the solution of ANS/LptC, the interaction of ANS with the other species in solution (LptC and/or LPS) do not decrease. In fact, the effects of a good interaction were still observed in ^{1}H, STD and tr-NOESY spectra, for competition experiments.

A logical explanation of this outcome could be that ANS interacted not only with the protein Lptc, but also with the other molecule in solution: the LPS. This was further investigated by STD and tr-NOESY experiments (LPS/ANS 1:20). It appeared clearly that LPS and ANS interact with each other with high affinity (Figure 2.10).
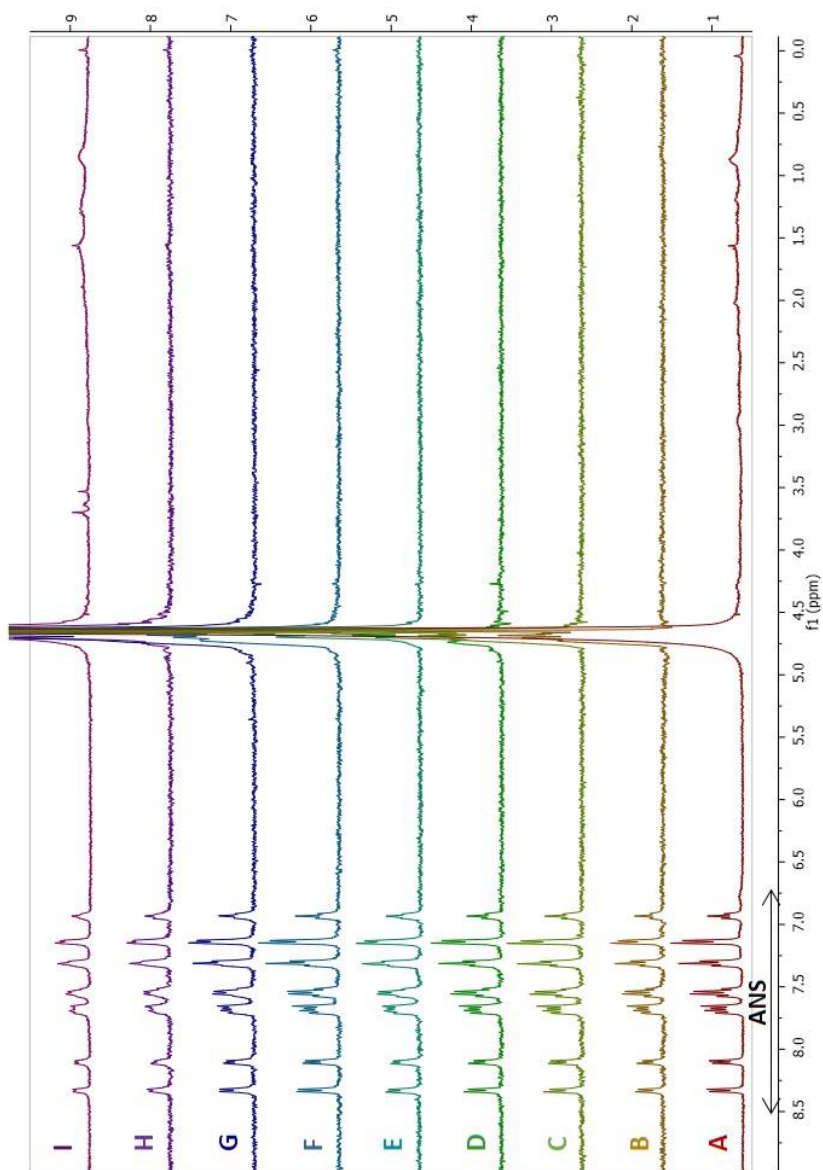
Figure 2.8. All the samples were prepared in deuterated phosphate buffer pH=7.4 (10 mM) and the acquisition temperature was 37°C. **A)** ^{1}H NMR spectrum of ANS (1 mM) and LptC (25 μM), number of scans 64; **B-H)** STD NMR spectra of ANS (1 mM) and LptC (25 μM), number of scans 768, saturation frequency -1 ppm, saturation time 2 s, to which different amounts of LPS were added: **B)** 0 mM LPS (final concentration); **C)** 5 μM LPS; **D)**

15 µM LPS; **E)** 25 µM LPS; **F)** 50 µM LPS; **G)** 100 µM LPS; **H)** 250 µM LPS; **I)** ^{1}H NMR spectrum of ANS (1 mM), LptC (25 µM) and LPS (250 µM) in number of scans 64.
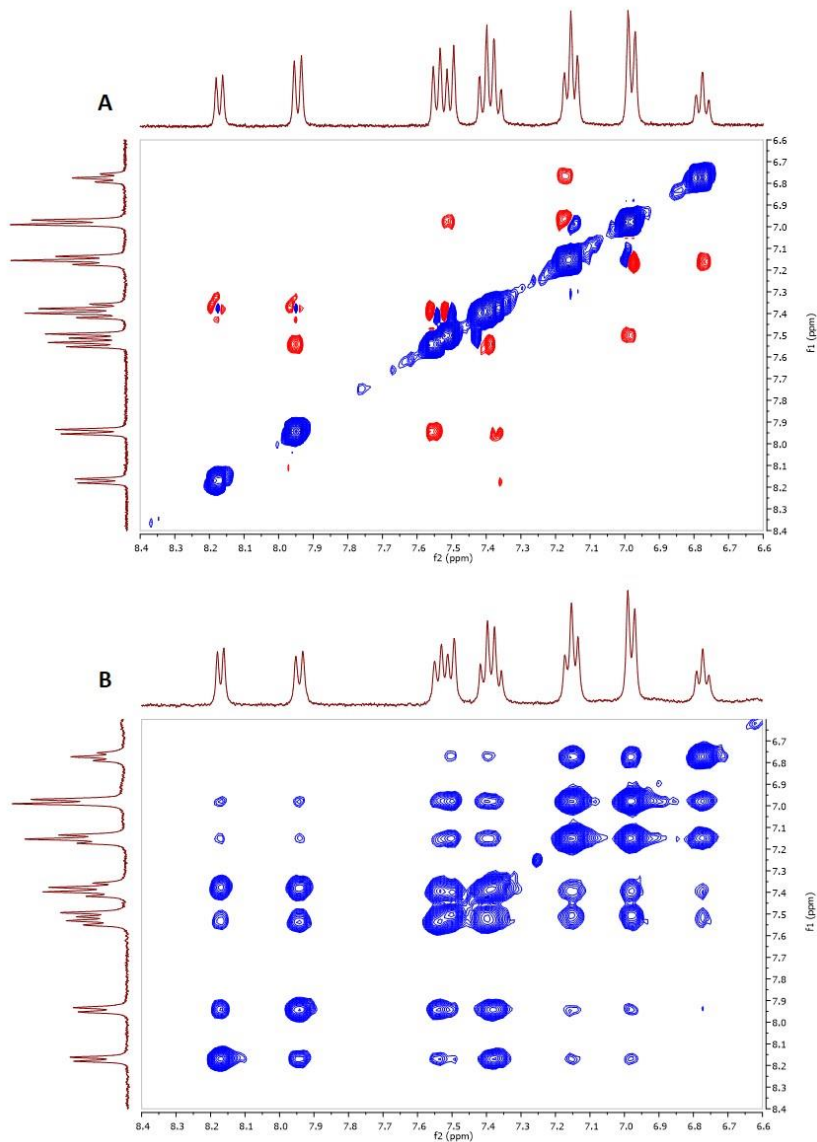
Figure 2.9. A) Tr-NOESY NMR spectrum of a solution of ANS (2 mM) in deuterated phosphate buffer pH=7.4 (10 mM), acquisition temperature 37°C, number of scans 64, mixing time 200 ms, relaxation delay 1 s; **B)** Tr-NOESY NMR spectrum of a solution of ANS

(1 mM), LptC (25 µM) and LPS (250 µM) in deuterated phosphate buffer pH=7.4 (10 mM), acquisition temperature 37°C, number of scans 64, mixing time 200 ms, relaxation delay 1 s.
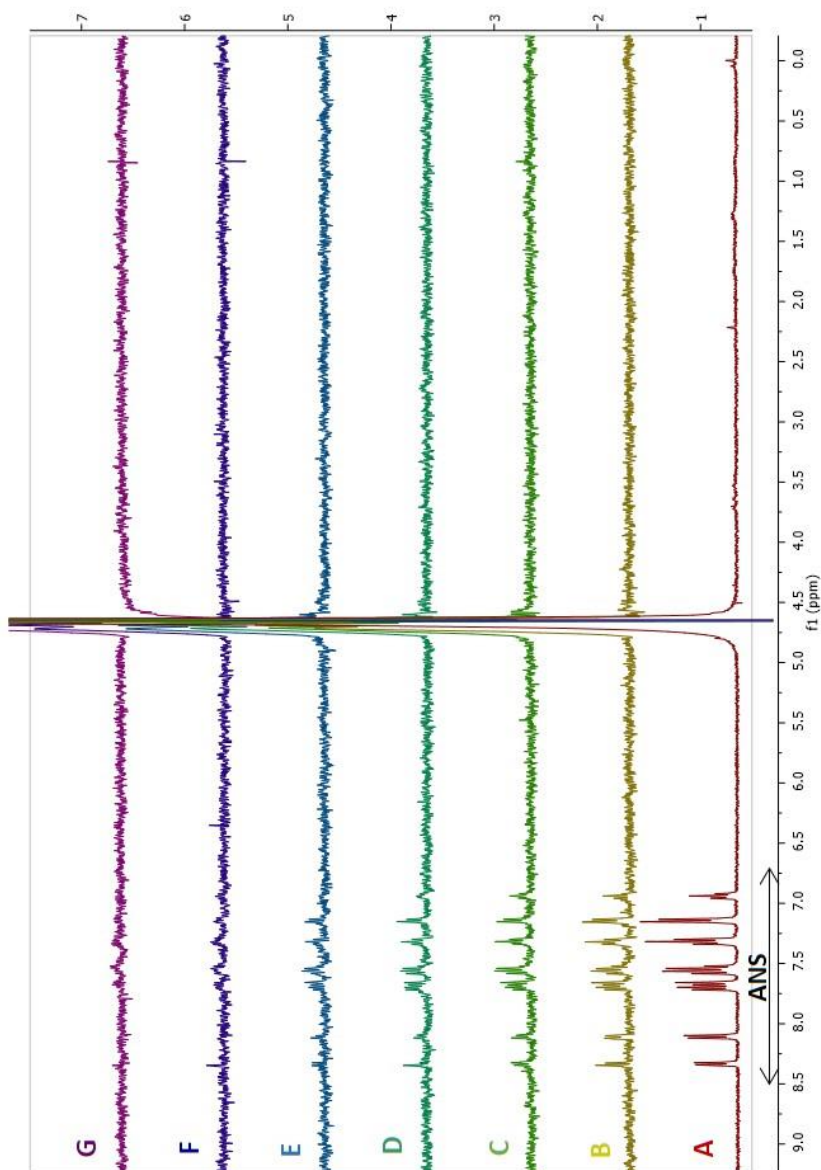
Figure 2.10. A) ^{1}H NMR spectrum of a solution of ANS (1 mM) and LPS (50 µM) in deuterated phosphate buffer pH=7.4 (10 mM), acquisition temperature 37°C, number of

scans 64; **B-G)** STD NMR spectra of a solution of ANS (1 mM) and LptC (25 µM) in deuterated phosphate buffer pH=7.4 (10 mM), acquisition temperature 37°C, number of scans 768, saturation frequency -1 ppm, acquired with different saturation times: **B)** 3 s; **C)** 2 s; **D)** 1.5 s; **E)** 1 s; **F)** 0.65 s; **G)** 0.35 s.

The hypothesis that can explain the LPS/ANS interaction is based on the formation of mixed micelles with the hydrophobic molecules of ANS intercalating the hydrophobic chains of LPS molecules. This is supported by the fact that is well known that ANS can strongly interact with the hydrophobic surfaces of proteins, being commonly used as fluorescent probe for binding studies.

The experimental finding that ANS and LPS mutually interact hampered the use of ANS as probe to study quantitatively the interaction between LptC and LPS, as initially planned. Unfortunately, even if it was demonstrated that ANS interacts with LptC, no direct evidence that the natural ligand and the fluorescent probe share the same binding site on the protein LptC can be obtained by using this method.

2.2 TLR4 modulators

The large variety of TLR4 modulators synthesized or isolated from natural sources so far has been widely described in the introduction. Here, the rational design – generally supported by computational data –, the synthesis and the chemical-biological characterization of TLR4 modulators with different chemical structures and also different effect on LPS-TLR4 signalling will be presented.

This section is divided in four sub-sections:

1) new TLR4 antagonists with chemical structure derived from the cationic amphiphile IAXO-102;

2) anionic TLR4 antagonists with chemical structures inspired to the lipid X, a precursor of lipid A;

3) natural TLR4 antagonists contained in the phenolic extracts from extra virgin olive oil and new synthetic derivatives;

4) TLR4 agonists obtained for conjugation of small-molecule TLR4 modulators to carrier proteins.

2.2.1 IAXO-102 derivatives

IAXO-102 (Figure 2.11) is the most representative compound of the first generation of cationic TLR4 antagonists synthesized in our labs. The glycolipid IAXO-102 resulted a strong TLR4 antagonist, both *in vivo* [91, 97] and *in vitro* [93, 98] (IC_{50}= 1.7 and 5.5 μM, respectively); also, it is not toxic and chemically stable.
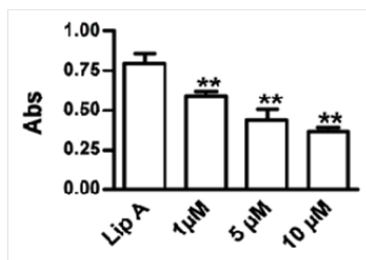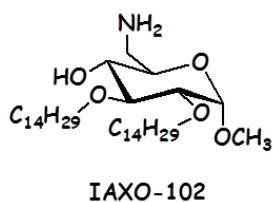
Figure 2.11. Chemical structure of the glycolipid IAXO-102 and dose-dependent inhibition of LPS-stimulated TLR4 activation by IAXO-102.

The free amino group at C-6 position of IAXO-102 allowed further modifications on this molecule to obtain new potential TLR4 modulators. Three directions were followed: fluorescent probes, dimeric IAXO-102 and a zwitterionic molecule (Scheme 2.1).
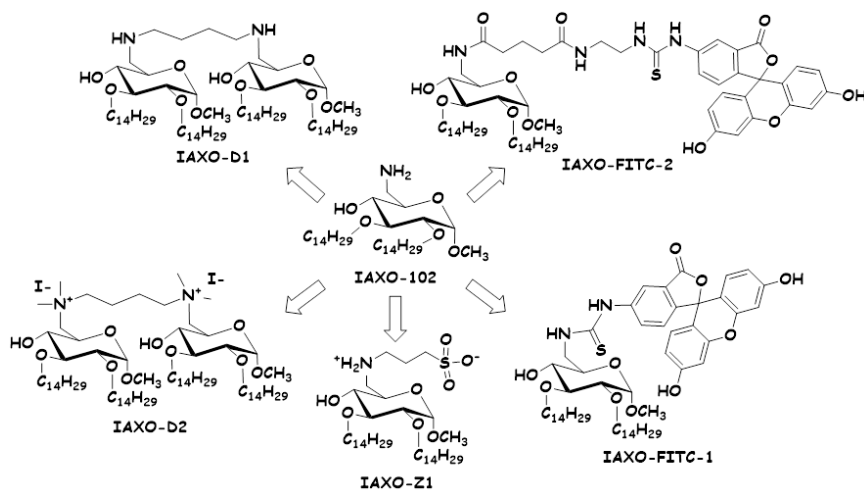
Scheme 2.1. Schematic representation of IAXO-102 derivatives projected and synthesized during this thesis work.

All the synthesis described in the next paragraphs will start from a common intermediate: the direct precursor of IAXO-102, named PMB-IAXO-102. As represented in scheme 2.2, PMB-IAXO-102 was obtained from methyl-α-D-glucopiranoside, as described previously.[70]
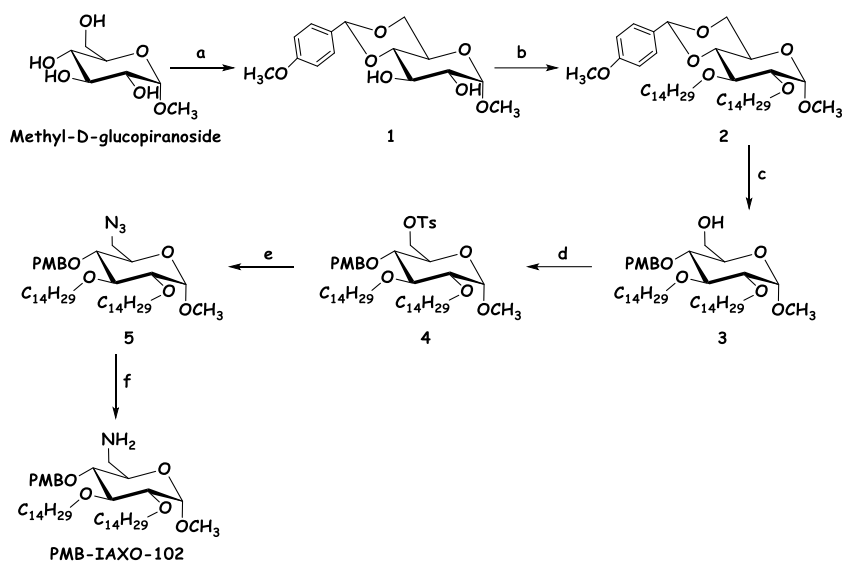
Scheme 2.2. Synthesis of PMB-IAXO-102. Reactions and conditions: **a)** Anisaldehyde dimethylacetal, CSA, DMF, 1h, 94%; **b)** $C_{14}H_{29}Br$, NaH, DMF, 3h, 74%; **c)** LiAlH$_4$, AlCl$_3$, CH$_2$Cl$_2$/Et$_2$O, 1h, 86%; **d)** TsCl, DMAP, pyridine, 24 °C, 12h, 98%; **e)** NaN$_3$, tetrabutylamonium iodide (TBAI), DMF, 75 °C, 4h, 79%; **f)** PPh$_3$, H$_2$O, THF, 70 °C, 2h, 93%.

2.2.1.1 Fluorescent probes

2.2.1.1.1 Rational design of IAXO-102-derived fluorescent ligands

All the computational studies presented in this work were performed by the research group of Dr. Sonsoles Martín Santamaría (CIB, CSIC, Madrid).

Small-molecule fluorescent probes for endotoxin co-receptor CD14 and for the receptor complex MD-2.TLR4 were developed. From a structural point of view, CD14 is characterized by a bent solenoid typical of leucine-rich repeat proteins with a large hydrophobic pocket found on the NH_2-terminal side. In the TLR4.MD-2 system, MD-2 protein is the responsible for LPS binding and is also characterized by a wide lipophilic pocket, which hosts the fatty acid (FA) chains from LPS.

The rational design of the molecules was based on the conjugation of a fluorescein dye with the high-affinity CD14 ligand IAXO-102. NMR binding data showed that the hydrophobic FA chains of IAXO-102 directly interact with the CD14 binding pocket,[92] thus suggesting that the conjugation of a fluorophore through the C-6 primary amine of IAXO-102 would not interfere with the CD14 binding.

This resulted into the design of **IAXO-FITC-1** and **IAXO-FITC- 2** (Scheme 2.3), where IAXO-102 is chemically linked to fluorescein through a thiourea 3-atoms linker (**IAXO-FITC-1**) or a glutaryl-diaminoethyl 9-atoms linker (**IAXO-FITC-2**).

Similarly, the ability of **IAXO-FITC-1** and **IAXO-FITC- 2** to act as TLR4 modulators was estimated by a computational docking study, carried out both on CD14 and TLR4.MD-2.
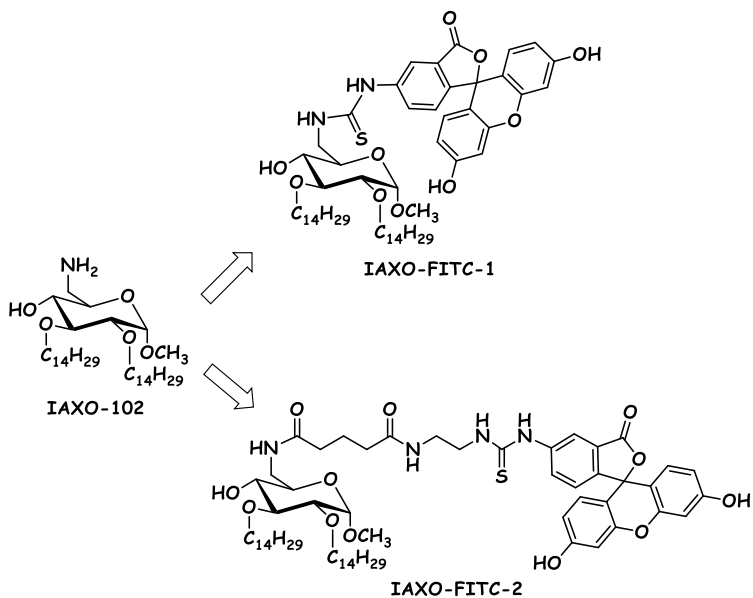
Scheme 2.3. Chemical structure of compounds **IAXO-FITC-1** and **IAXO-FITC-2**, derived from **IAXO-102.**

The calculations showed that *h*CD14 (*human* CD14) and *h*MD-2 (*human* MD-2) pockets share a similar topology in terms of solvent accessible surface area and volume (Figure 2.12). However, CD14 possesses fewer polar residues in the rim and it is capable of recognizing a few other microbial and cellular compounds, in addition to LPS.[99] Despite being very similar in lipophilicity, solvent accessible surface area and volume, the pockets of CD14 and MD-2 differ in the polarity of the rim, allowing MD-2 to be more selective than CD14 in the recognition of LPS.
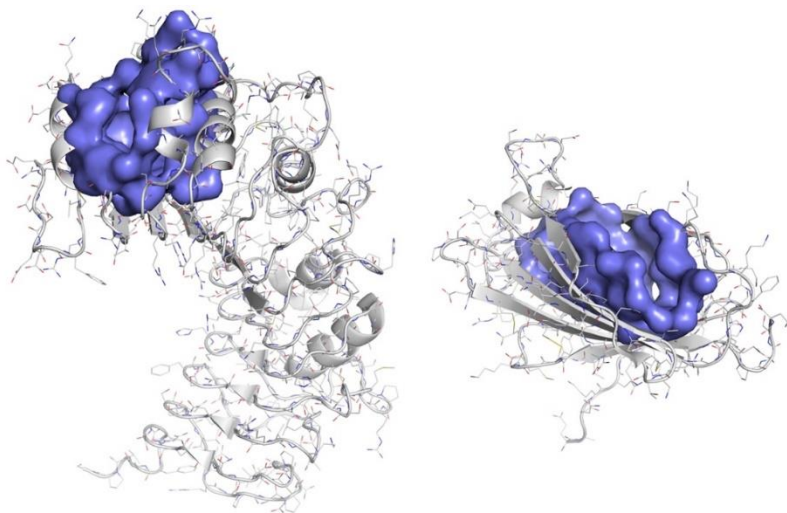
Figure 2.12. Binding pockets identified by CASTp[100] in *h*CD14 (left, PDB-ID 4GLP) and *h*MD-2 (right, PDB-ID 2E59).

Consequently, in order to estimate their CD14 binding properties, designed compounds **IAXO-FITC-1** and **IAXO-FITC-2** were submitted to docking studies by using the X-ray crystal structure of CD14 and focusing on the NH$_2$-terminal pocket, which presumably binds acylated ligands including LPS.

Since the 3D structures of CD14-bound ligands are not available, and given that the crystallographic structure for CD14 adopts a closed conformation of the pocket, thus preventing an efficient exploration by docking, a normal-mode analysis (NMA) of the protein was undertaken to represent motions and conformational changes. Then, docking calculations were performed on three different conformations of CD14, obtained by normal mode analysis, thus approaching a flexible protein docking protocol.

Calculations predicted binding poses for both compounds **IAXO-FITC-1** and **IAXO-FITC-2**, with a general tendency to bury their fatty acid chains inside the hydrophobic pocket, with the pyranose ring remaining towards the external portion. These results are in line with the binding modes proposed for other TLR4 modulators interacting with CD14.
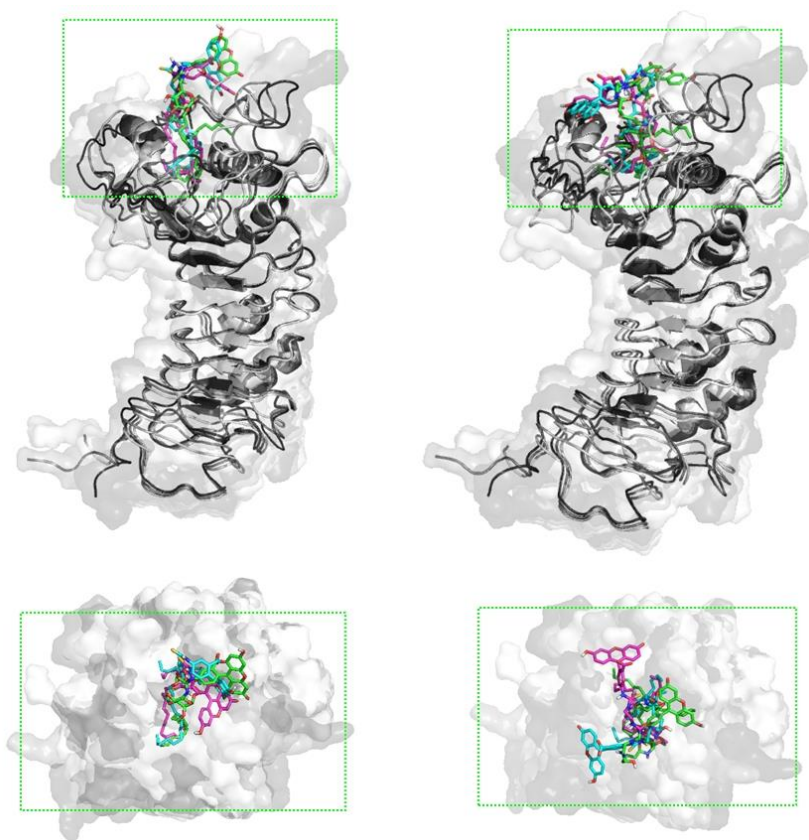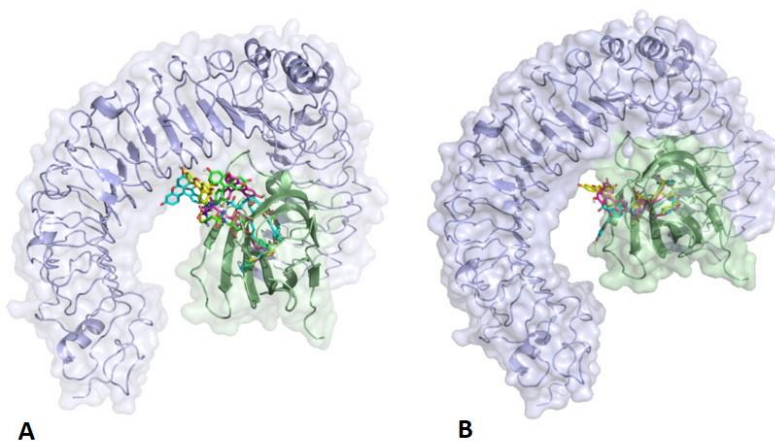

Figure 2.13. Docked poses for compound **IAXO-FITC-1** (left, lateral and top views) and compound **IAXO-FITC-2** (right, lateral and top views) binding to CD14 (PDB-ID: 4GLP). Fluorescein remains at the CD14 rim and the IAXO-102 scaffold binds into the CD14 pocket. Fatty acid chains are buried inside the hydrophobic pocket. Three different conformations of CD14 from NMA are superimposed.

The calculations predict that the thiourea linkers and the fluorescein moiety establish polar interactions with the hydrophilic rim, without adopting any preferred binding pose. This heterogeneity can be observed in the docked poses shown in figure 2.13. Especially in the case of compound **IAXO-FITC-2**, these results should not be incompatible with the fluorescein tag dangling from the CD14 into the solvent. Similar docking results were obtained for *m*CD14 (data not shown).

To evaluate putative MD-2 binding properties of compounds **IAXO-FITC-1** and **IAXO-FITC-2**, docking studies in the TLR4.MD-2 system were also performed. Since the X-ray structure of the TLR4.MD-2 complex is not available in the antagonist conformation, a hybrid model from PDB-IDs 3FXI and 2E59 was built.

Similarly to CD14, the calculations predicted binding poses for both compounds with FA chains buried inside the MD-2 hydrophobic pocket, in line with the antagonist binding pose found for lipid IVa in the crystallographic structure (PDB ID 2E59), with the thiourea linker and the fluorescein moiety outside MD-2, adopting different orientations (Figure 2.14).

In the case of compound **IAXO-FITC-2**, the longer linker allows the fluorescein moiety to reach the TLR4 region delimited by Asn361, Lys362, Gly363, and Arg264. In a dynamic environment, it is likely that the fluorescein tag fluctuates into the solvent.

Figure 2.14. Docked poses for compound **IAXO-FITC-1 (A)** and compound **IAXO-FITC-2 (B)** binding to TLR4.MD-2 (hybrid model from PDB-ID 2E59) showing three preferred binding poses.

2.2.1.1.2 Synthesis of IAXO-102-derived fluorescent ligands

Two fluorescent glycolipidic probes, derivatives of IAXO-102, have been synthesized. For the synthesis of **IAXO-FITC-1**, IAXO-102 was obtained from the protected PMB-IAXO-102 precursor.[70]

The reaction of IAXO-102 and fluorescein isothiocyanate (FITC) in dichloromethane at room temperature for 4h (Scheme 2.4), afforded the fluorescent probe **IAXO-FITC-1** (92% yield), in which fluorescein is linked to the C-6 of glucose through a thiourea bond.
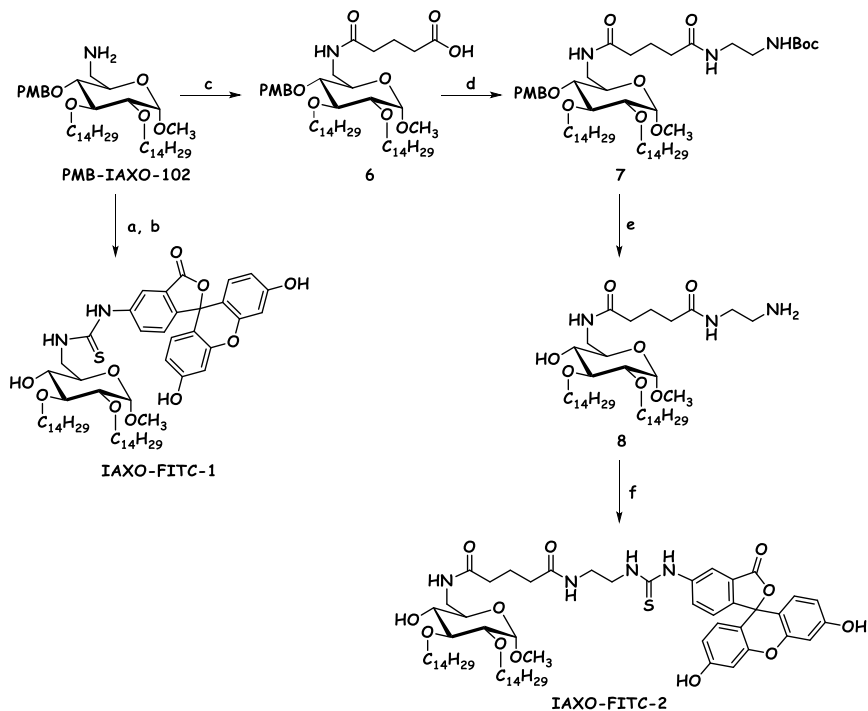
Scheme 2.4. Synthesis of compounds **IAXO-FITC-1** and **IAXO-FITC-2**. Reaction and conditions: **a)** TFA, CH$_2$Cl$_2$, RT, 1h, 98%; **b)** Fluorescein isothiocyanate (FITC), CH$_2$Cl$_2$, RT, 3.5h, 92%. **C)** Glutaric anhydride, dry pyridine, RT, 2h, yield: 87%; **d)** N-Boc-ethylenediamine, DIC, HOBt, DIPEA, dry DMF, 40°C, 40h, 67%; **e)** TFA, CH$_2$Cl$_2$, RT, 1.5h, 93%; **f)** Fluorescein isothiocyanate (FITC), CH$_2$Cl$_2$, RT, 2.5h, 50%.

Alternatively, PMB-IAXO-102 was reacted with glutaric anhydride affording compound **6**, with a free carboxylic acid function. Subsequently, the carboxylic acid derivative **6** was condensed with the mono-protected di-amine Boc-ethylendiamine in the presence of DIC, HOBt and DIPEA, obtaining compound **7**. After simultaneous Boc and PMB deprotection in acid conditions with TFA, compound **8** was obtained, bearing the free amino function at the end of the linker.

The reaction of compound **8** with FITC in dichloromethane at room temperature afforded molecule **IAXO-FITC-2**, in which the fluorescent moiety is linked to glucose through a glutaryl-diaminoethyl 9-atoms linker.

2.2.1.1.3 TLR4 activity and cellular toxicity of the IAXO-102-derived fluorescent ligands

The ability of molecules **IAXO-FITC-1** and **IAXO-FITC-2** to interfere with LPS-triggered TLR4 activation in HEK-Blue™ cells model was investigated. HEK-Blue™ cells are HEK-293 cells stably transfected with human TLR4, MD-2, and CD14 genes. Hek-Blue™ cells stably express a secreted Alkaline Phosphatase (sAP) produced upon activation of NF-kB. LPS binding activates TLR4 and NF-kB, leading to sAP secretion, detected by an alkaline phosphatase substrate in cell culture media (colorimetric assay).

In this assay, cells were pre-treated with increasing concentrations of **IAXO-FITC-1** and **IAXO-FITC-2** (from 0 to 25 µM) and then stimulated with *E. coli* LPS (10 nM). Compounds **IAXO-FITC-1** and **IAXO-FITC-2** significantly inhibited sAP production dependent from TLR4 signaling (Figure 2.15 A), with a potency similar to that of the precursor compound IAXO-102.[21] In fact, the calculated IC_{50} values for compounds **IAXO-FITC-1** and **IAXO-FITC-2** were 20.4 µM and 9.5 µM, respectively.

Compounds **IAXO-FITC-1** and **IAXO-FITC-2** showed no toxicity at the cell viability MTT test, upon the highest concentration tested for TLR4 activity (Figure 2.15 B).
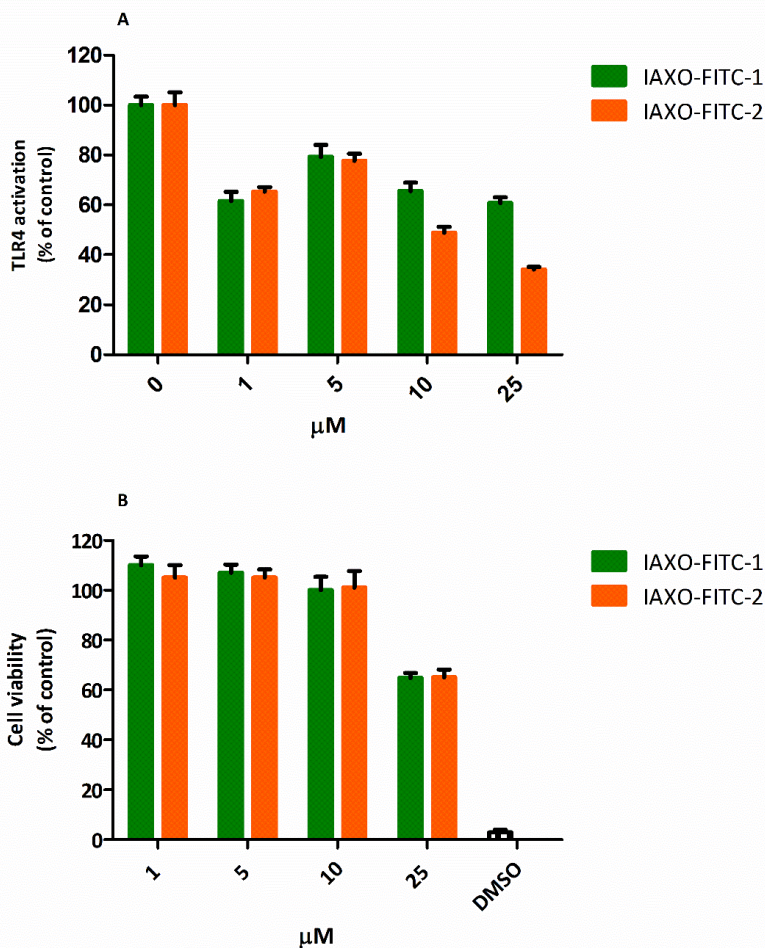
Figure 2.15. A) Dose-dependent inhibition of LPS-stimulated TLR4 activation by compounds **IAXO-FITC-1** and **IAXO-FITC-2**. HEK-293 cells, transfected with human CD14 and MD-2.TLR4, were treated with increasing concentrations of compounds (0-25 µM) and then stimulated with LPS (10 ng). TLR4 activation is monitored as sAP production. The results are normalized to activation by LPS alone and expressed as the mean of percentage ± SD (standard deviation) of 3 independent experiments **B)** Viability assay (MTT) on **IAXO-FITC-1** and **IAXO-FITC-2** (0-25 µM) in HEK-Blue cells. The results are normalized on the positive control (cells treated with PBS) and expressed as the mean of percentage ± SD of 3 independent experiments. DMSO is used as negative control.

2.2.1.2 Dimeric molecules

2.2.1.2.1 Rational design of IAXO-102-derived dimeric molecules

MD-2/IAXO-102 interaction model suggested that space is available in the MD-2 binding cavity can accommodate up to four acyl chains.

A dimeric molecule with two glucose units linked in C-6 positions, but with negatively charged sulphate groups on C-4, which showed good TLR4 antagonist activity (DDS, Figure 2.16), was recently developed by our group.[65] The TLR4 antagonist activity and the binding properties of DDS suggest that 4 acyl chains could be optimal for MD-2 binding.

Working on this issue, dimeric compounds **IAXO-D1** and **IAXO-D1** were designed, formed by two IAXO-102 units connected through a linear alkyl C4 linker attached to C-6 amine function (Figure 2.16). The alkyl linker allowed to keep almost unaltered the structure of the monomers, with the amine group still positively charged. Compound **IAXO-D1** bears two secondary amines that can be easily protonated, while in compound **IAXO-D1** two quaternary amines are present, as ammonium salt.
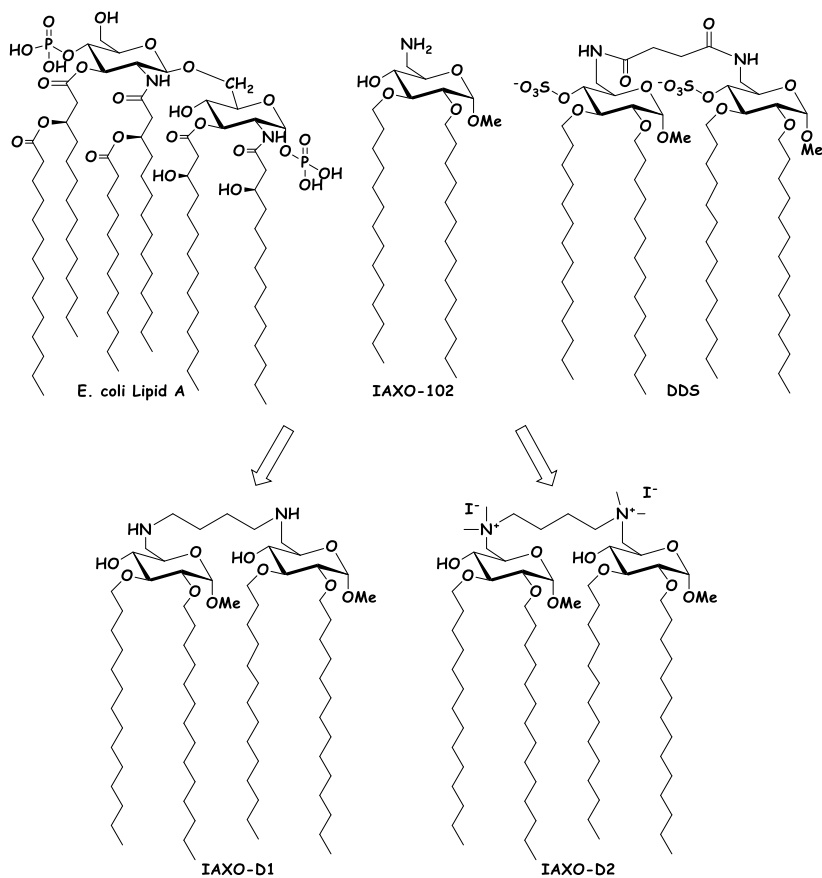
Figure 2.16. Rational design of dimeric derivatives of IAXO-102: chemical structures of *E. coli* lipid A, IAXO-102, DDS, **IAXO-D1** and **IAXO-D2**.

From docking calculations, it emerged that molecules **IAXO-D1** and **IAXO-D1** could interact more strongly than the monomer with both the co-receptors CD14 and MD-2 (data not shown).

2.2.1.2.2 Synthesis of IAXO-102-derived dimeric molecules

Compounds **IAXO-D1** and **IAXO-D2** were obtained from the common precursor PMB-IAXO-102 (Scheme 2.5).[70]
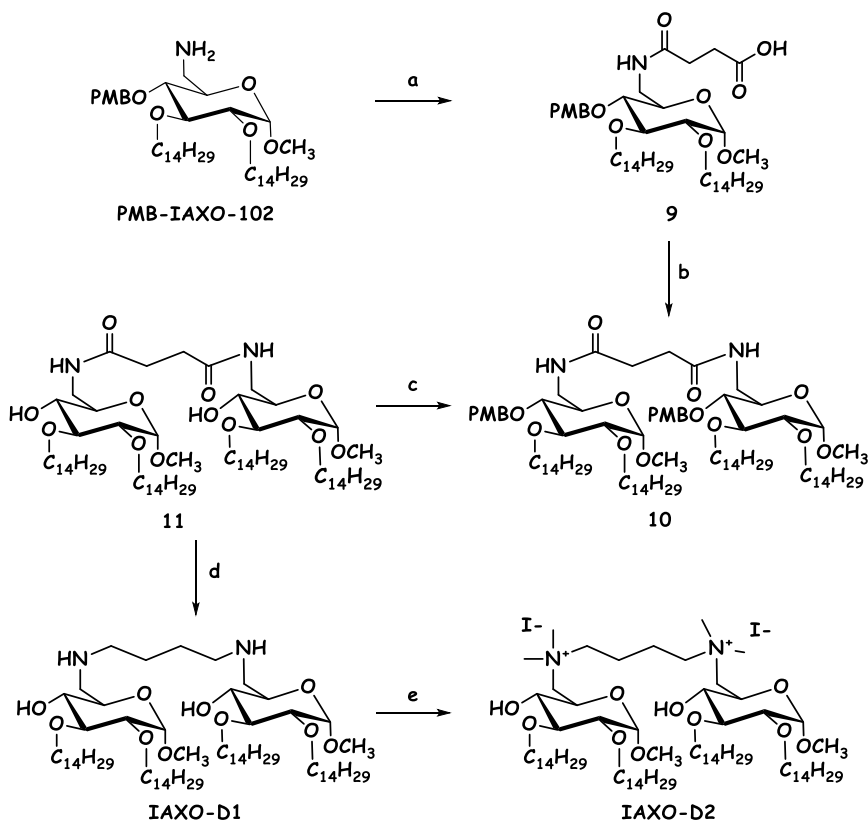
Scheme 2.5. Synthesis of cationic glycolipids **IAXO-D1** and **IAXO-D2**. Reactions and conditions: **a)** Succinic anhydride, dry pyridine, RT, 3h, 98%; **b)** PMB-IAXO-102, EDC, dry DMF, 60°C, 22h, 49%; **c)** TFA, CH_2Cl_2, RT, 1h, 95%; **d)** $LiAlH_4$, dry THF, dry CH_2Cl_2, RT, 4h, 78%; **e)** CH_3I, Na_2CO_3, dry DMF, 40°C, 24h, 89%.

Compound **11** was obtained from methyl-α-D-glucopyranoside according to published procedures.[65] Compound **11** was reacted with the reductive agent $LiAlH_4$ to efficiently reduce the amide groups to secondary amines,

obtaining compound **IAXO-D1** with a 78% yield. Compound **IAXO-D1** was reacted with CH_3I and Na_2CO_3 in DMF, affording compound **IAXO-D2** (yield 89%), with positively charged quaternary amines as a salt with iodine as counterion.

The synthetic strategies to obtain another dimeric derivative, compound **20,** are described in scheme 2.6.
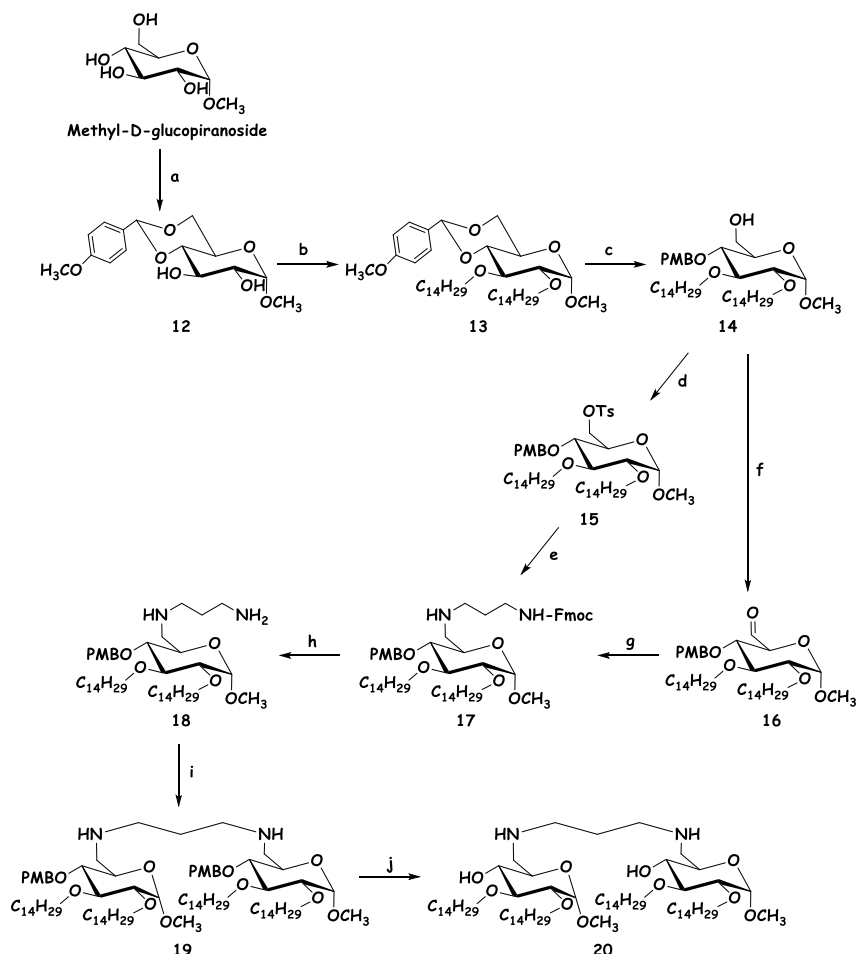
Scheme 2.6. Synthesis of compound **20**. Reactions and conditions: **a)** ADMA, CSA, DMF, 40°C, 1.5h, 94%; **b)** $C_{14}H_{29}Br$, NaH, DMF, 60°C, 3h, 76%; **c)** $LiAlH_4$, $AlCl_3$, ET_2O/CH_2Cl_2 (1:1), RT, 1h, 86%; **d)** TsCl, DMAP, Py, RT, 22h, 80%; **e)** $NH_2CH_2CH_2CH_2NHFmoc$, Et_3N, TBAI, DMF,

65°C, 24h; **f)** Dess Martin, CH_2Cl_2, RT, 2h, 99%; **g)** $NH_2CH_2CH_2CH_2NHFmoc$, $Na(Ac)_3BH$, AcOH, $CH_2Cl_2/MeOH$ (2:1), RT, 22h, 63%; **h)** Piperidine 20%, DMF, RT, 2h; **i)** Compound **16**, $Na(Ac)_3BH$, AcOH, $CH_2Cl_2/MeOH$ (2:1), RT, 72h, 58%; **j)** H_2, Pd/C, $CH_2Cl_2/MeOH$ (1:1), RT, 20h.

Docking calculations indicated that connecting two IAXO-102 molecules with a C3 or C4 linear alkyl linker, favorable binding energies with MD-2 are obtained. Besides **IAXO-D1** and **IAXO-D2** with a C4 linker, the synthesis of the dimer with a C3 linker was planned (Scheme 2.6).

Product **17** was successfully obtained through reaction steps **f** and **g**, but this synthetic strategy failed at the last step to give the desired product **20,** affording instead an unidentified product, with different chemical structure. This synthetic route was abandoned because of these difficulties and because the biological activity of **IAXO-D1** and **IAXO-D2** (Par. 2.2.1.2.3) was not good enough to justify further work on this type of compounds.

2.2.1.2.3 TLR4 activity, cellular toxicity and CMC calculations of IAXO-102 derived dimeric molecules

The activities of compounds **IAXO-D1** and **IAXO-D2** in modulating the LPS-stimulated TLR4 activation and signaling were tested in HEK-Blue™ cells.[93] Cells were treated with increasing concentrations of compounds **IAXO-D1** or **IAXO-D2** (from 10 to 200 µM) and then stimulated with LPS from *E. coli* O55:B5. Both compounds showed a concentration-dependent TLR4 antagonistic activity (Figure 2.17 A). The calculated IC_{50} for compounds **IAXO-D1** and **IAXO-D2** are 240 and 173 µM, respectively. These

compounds are less potent than the corresponding monomer IAXO-102 that inhibited TLR4 activation in HEK-blue cells with an IC_{50} of 5.5 µM. The toxicity of both compounds is very low in the concentration range used for biological characterization, as assessed by MTT test (Figure 2.17 B). At the highest concentration (200 µM), compounds **IAXO-D1** and **IAXO-D2** show a death rate of 20% and 30%, respectively.
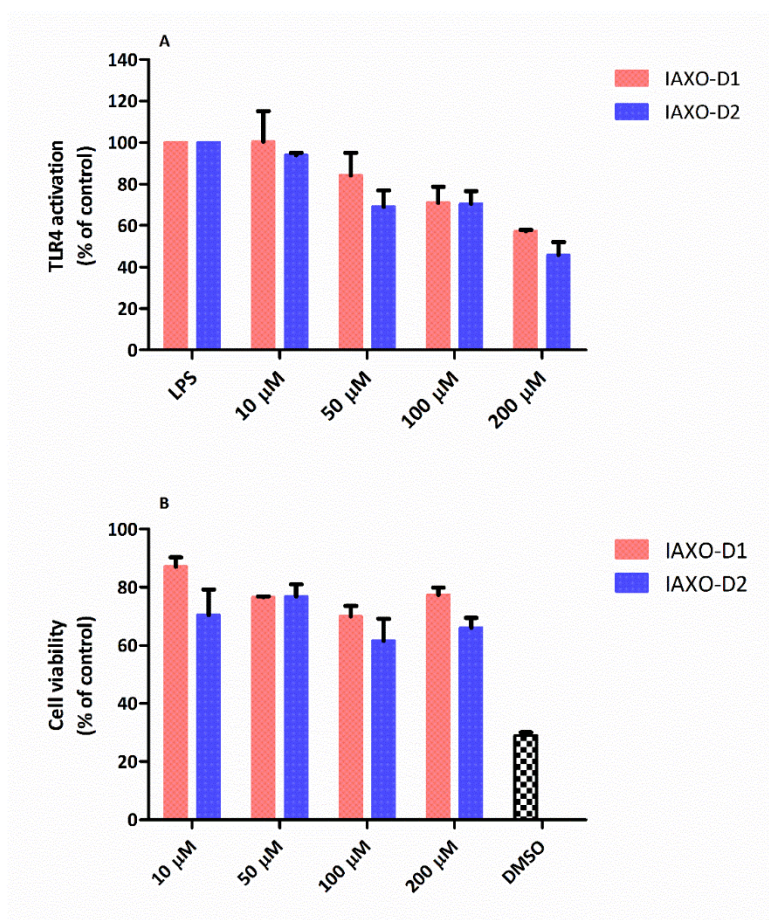
Figure 2.17. A) Concentration-dependent inhibition of LPS-stimulated TLR4 activation in HEK-blue™ cells. HEK-293 cells transfected with human CD14 and MD-2.TLR4, were

treated with increasing concentrations of compounds **IAXO-D1** or **IAXO-D2** (0-200 µM) and then stimulated with LPS (10 ng). TLR4 activation is monitored as sAP production. The results are normalized to activation by LPS alone and expressed as the mean of percentage ± SD of 3 independent experiments **B)** Viability assay (MTT) on **IAXO-D1** or **IAXO-D2** (0-200 µM) in HEK-Blue cells. DMSO is used as negative control. The results are normalized on the positive control (cells treated with PBS) and expressed as the mean of percentage ± SD of 3 independent experiments.

The aggregation properties of the cationic glycolipids **IAXO-D1** and **IAXO-D2** were investigated. The critical micelle concentrations (CMCs) for compounds **IAXO-D1** and **IAXO-D2** were determined via pyrene fluorescence measurements.[101] CMC values for compounds **IAXO-D1** and **IAXO-D2** are 18.1 µM and 29.7 µM, respectively. The low value of CMC could account for the weaker TLR4 activity of these compounds if compared to correspondent monosaccharide IAXO-102.[91] In the concentration range used for biological characterization (10 to 200 µM), compounds **IAXO-D1** and **IAXO-D2** form aggregates, so that TLR4 activity is due to very few residual free molecules that interact with CD14 and TLR4.MD-2 receptors.

2.2.1.3 Zwitterionic molecule

2.2.1.3.1 Rational design and synthesis of the zwitterionic derivative

Glycolipidic molecules like IAXO-102 always present a low solubility in water, causing several problems, especially related to the biological assays. Consequently, a zwitterionic molecule **IAXO-Z1** was designed in order to increase the solubility in aqueous media, preserving the positively charged amine group at C-6 position of the sugar.
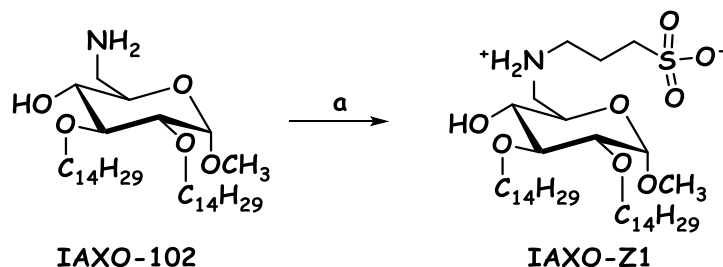
Scheme 2.7. Synthesis of **IAXO-Z1**. Reactions and conditions: **a)** 1.3-propanesultone, dry CH₃CN, 60°C, 24h, 90%.

A very simple synthesis was used to modify IAXO-102 obtaining a zwitterionc molecule with high yield (90%). The use of a sultone, a ciclic sulfonate ester, allowed to obtain compound **IAXO-Z1** in only one reaction step, starting form IAXO-102.

2.2.1.3.2 Biological activity and water solubility of the zwitterionic derivative

The water solubility of **IAXO-Z1** was enhanced with respect to the precursor IAXO-102. The biological activity of this molecule in modulating the LPS-stimulated TLR4 activation and signalling was evaluated on HEK-Blue™ cells, together with the toxicity of the compound.

IAXO-Z1 is not toxic in the concentration range used for biological characterizations (MTT test, figure 2.18 B); however, unfortunately, **IAXO-Z1** did not show any activity as TLR4 modulator (Figure 2.18 A).
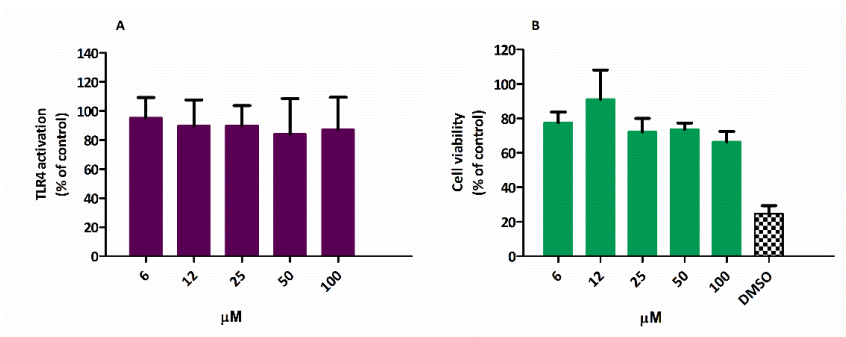
Figure 2.18. A) Dose-dependent inhibition of LPS-stimulated TLR4 activation in HEK-blue[TM] cells. HEK-293 cells transfected with human CD14 and MD-2.TLR4, were treated with increasing concentrations of compound **IAXO-Z1** (0-100 µM) and then stimulated with LPS (10 ng). TLR4 activation is monitored as sAP production. The results are normalized to activation by LPS alone and expressed as the mean of percentage ± SD of 3 independent experiments **B)** Viability assay (MTT) on **IAXO-Z1** (0-100 µM) in HEK-Blue cells. DMSO is used as negative control. The results are normalized on the positive control (cells treated with PBS) and expressed as the mean of percentage ± SD of 3 independent experiments.
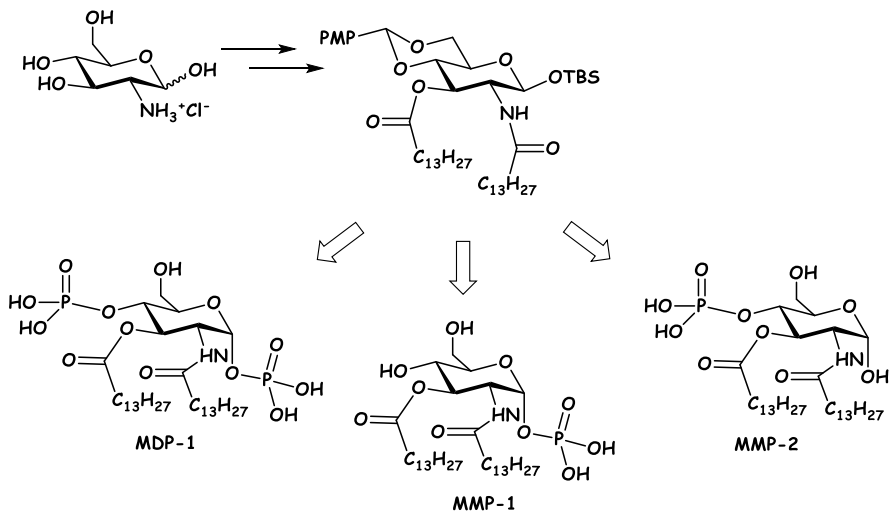
2.2.2 Anionic antagonists

The precursor of lipid A, named lipid X, is considered a simplified monosaccharide scaffold for the development of TLR4 agonists and antagonists, because of its anti-endotoxic activity, as described in the introduction.

MMP-1: $R_1=PO_3^-$, $R_2=H$
MMP-2: $R_1= H$, $R_2= PO_3^-$
MDP-1: $R_1=PO_3^-$, $R_2= PO_3^-$

E. coli lipid A   lipid X
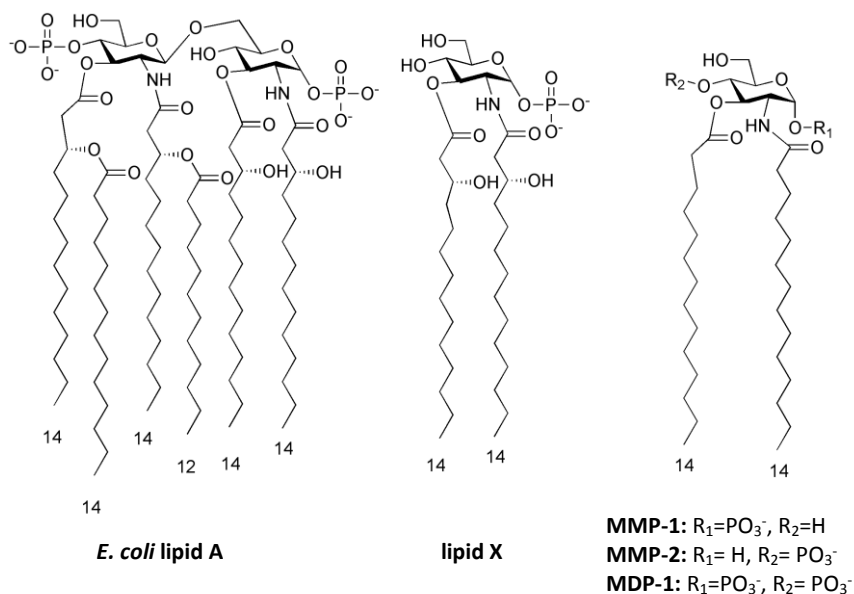
Figure 2.19. *E. coli* lipid A and its biosynthetic precursor lipid X, mono- (**MMP-1** and **MMP-2**) and di-phosphorylated (**MDP-1**) lipid X mimetics.

Three monosaccharides inspired to lipid X structure are presented: compound **MMP-1** has a phosphate ester in the anomeric (C-1) position, while **MMP-2** corresponds to a lipid X mimetic with phosphate on C-4 and **MDP-1** is phosphorylated on both C-1 and C-4 positions. Compounds **MMP-1**, **MMP-2** and **MDP-1** were synthesized in our labs using a

divergent strategy, starting from the common intermediate, obtained from the commercial D-glucosamine hydrochloride (Scheme 2.8).[66]

Scheme 2.8. Compounds **MDP-1**, **MMP-1** and **MMP-2** obtained from a common intermediate, starting from D-glucosamine hydrochloride.

2.2.2.1 TLR4 activity and cellular toxicity of anionic TLR4 antagonists

The ability of molecules **MDP-1**, **MMP-1** and **MMP-2** to interfere with LPS-triggered TLR4 activation was investigated in HEK-blue™ cells. The cells were pre-treated with increasing concentrations of synthetic monosaccharides (from 0 to 50 µM) and then stimulated with *E. coli* LPS. In this concentration range, compounds **MMP-1** and **MMP-2** were inactive or very weakly active in inhibiting LPS-stimulated TLR4 signaling, while **MDP-1** was a potent inhibitor (Figure 2.20 A).
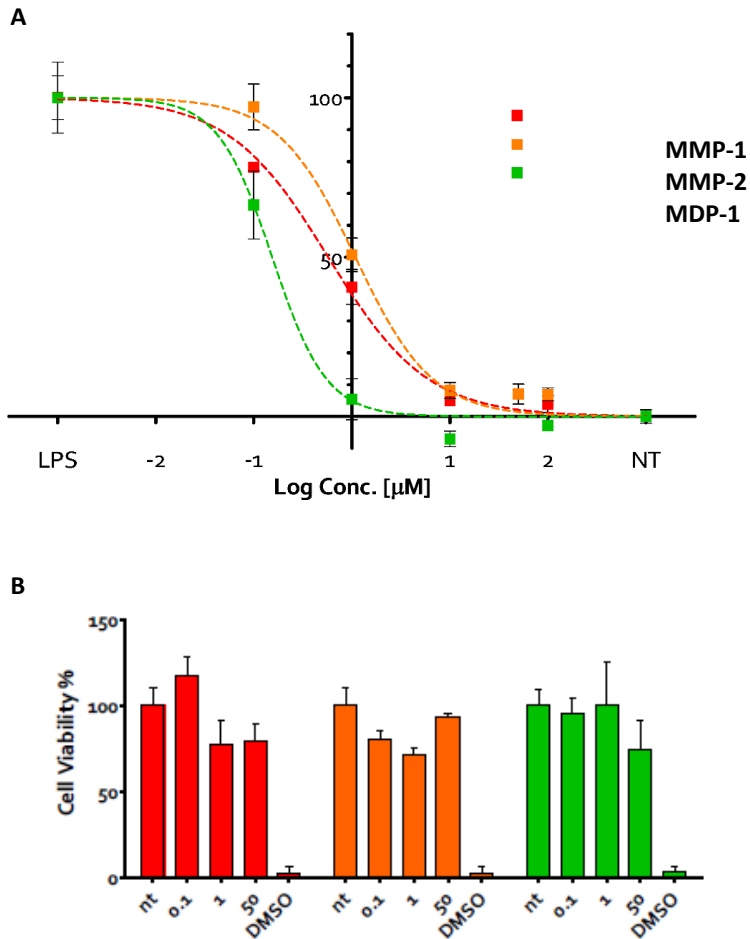
Figure 2.20. A) Dose-dependent inhibition of LPS-stimulated TLR4 activation in HEK-blue^{TM} cells. HEK-293 cells transfected with human CD14 and MD-2.TLR4, were treated with increasing concentrations of compounds **MDP-1**, **MMP-1** and **MMP-2** (0-50 μM) and then stimulated with LPS (10 ng). TLR4 activation is monitored as sAP production. The graphics are result of 3 independent experiments **B)** Viability assay (MTT) on **MDP-1**, **MMP-1** and **MMP-2** (0-50 μM) in HEK-Blue cells. DMSO is used as the negative control. The results are normalized on the positive control (cells treated with PBS) and expressed as the mean of percentage ± SD of 3 independent experiments.

Compound **MDP-1** turned out to be a potent antagonist at low LPS concentration (10 ng/mL), with a calculated IC_{50} of 0.46 µM.

The toxicity of all compounds was assessed by MTT test (Figure 2.20 B) and all compounds showed no or very limited toxicity up to the highest concentration tested (50 µM).

2.2.2.2 NMR binding experiments: interaction between the synthetic molecule MDP-1 and MD-2

NMR binding studies on the protein MD-2 were performed during a research period abroad, in the labs of Prof. Jesús Jiménez Barbero (Centro de Investigaciones Biológicas (CIB), CSIC, Madrid), within a European C.O.S.T. project.

The binding of monosaccharide **MDP-1** to MD-2 receptor was investigated by means of NMR techniques in solution. Because of the tendency of compound **MDP-1** to form stable aggregates at the concentration required for NMR measurements (150-300 µM), it turned out to be impossible to detect ligand-protein interaction by Saturation Transfer Difference (STD) experiments.

However, it was possible to record good quality ^{1}H NMR spectra of **MDP-1**, of MD-2 and of a **MDP-1**/MD-2 mixture (ratio 5:1, at a 150 µM ligand concentration, Figure 2.21).
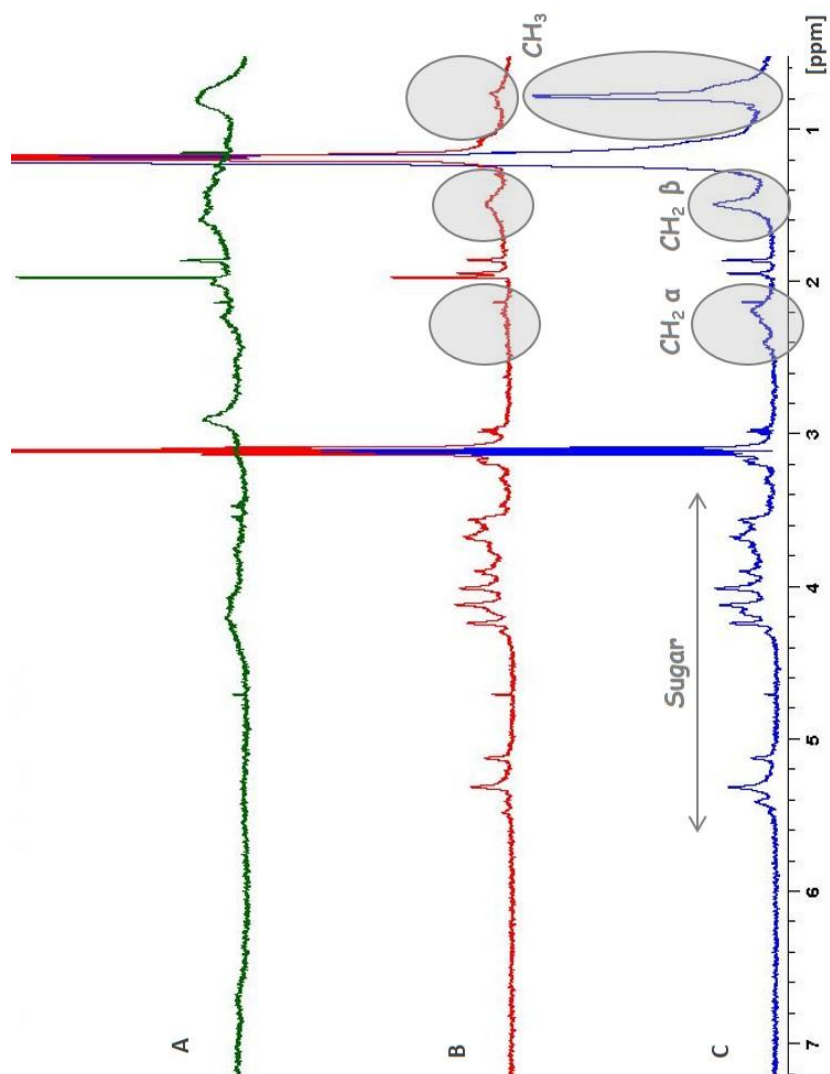
Figure 2.**21.** A) ^{1}H NMR of 30 µM MD-2 protein in deuterated acetate buffer at pH=5, 298K, 120 scans; **B)** ^{1}H NMR of 30 µM MD-2 protein and 150 µM of compound **MDP-1** in deuterated acetate buffer at pH=5, 298K, 120 scans; **C)** ^{1}H NMR of 150 µM **MDP-1** in deuterated acetate buffer at pH=5, 298K, 120 scans.

Fittingly, selective attenuation of the signals corresponding to the fatty acid C_{14} chain protons of **MDP-1** was observed upon addition of MD-2 to the monosaccharide sample solution (Figure 2.21). Although broadenings of all the resonance signals were detected, the decrease in signal intensities was significantly higher for those hydrogens belonging to the FA aliphatic chains, in particular for the signals of the Ω methyl groups and for those of the contiguous CH_2 moieties, followed by the remaining of the chain hydrogens. In contrast, the intensity of the signals corresponding to the hydrogens on the sugar ring resulted almost unaltered.

The experimentally observed reduction in intensity, due to specific line broadening of these signals, arises from the change in transverse relaxation time of these signals. This dramatic change is likely to arise from the existence of interaction between **MDP-1** and MD-2, precisely at the aliphatic side chain region. In fact, the FA chains-MD-2 interactions outlined here are reminiscent of those previously observed for positively charged amphiphiles.[8]

The data suggest the occurrence of a major interaction of both FA chains of the sugar ligand with the hydrophobic binding cavity of MD-2, also confirmed by the docking calculations (see next paragraph). The exchange process between the free and bound states provides the basis for the increased relaxation rate and the corresponding observed increase of linewidth.

Additional features of the interaction were also investigated by using DOSY (Diffusion Order SpecrtoscopY) NMR (Figure 2.22).
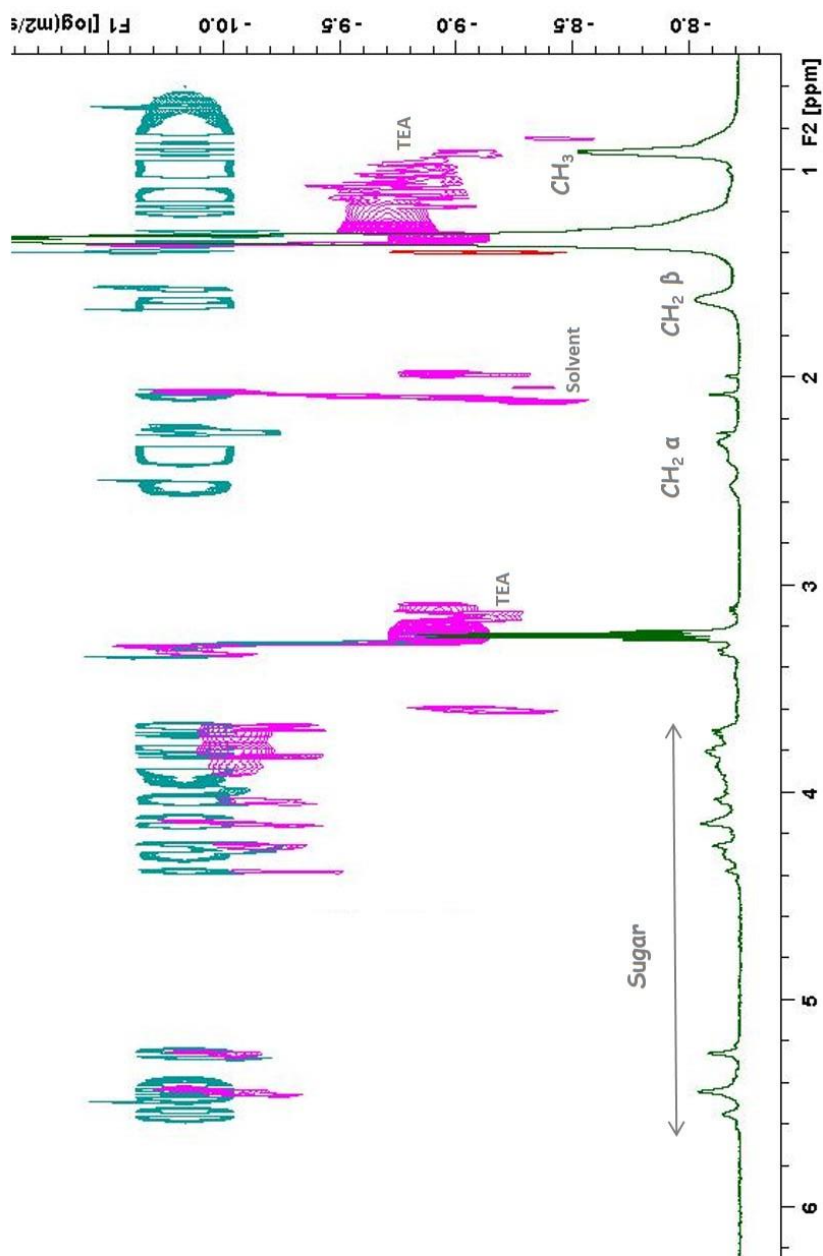
Figure 2.22. Blue: DOSY spectrum of compound **MDP-1** (300 µM) in deuterated acetate buffer at pH=5. **Magenta**: DOSY spectrum of **MDP-1**/MD-2 mixture at 5:1 molar ratio (330 µM compound **MDP-1** and 60 µM MD-2) in deuterated acetate buffer at pH = 5. **Green**: [1]H spectrum of compound **MDP-1** (300 µM) in deuterated acetate buffer at pH = 5.

First, the aggregation properties of **MDP-1** were evaluated by means of DOSY experiments. The DOSY on the free ligand showed a strikingly small diffusion coefficient, corresponding to a high molecular weight species in solution. This can be associated with the fact that molecule **MDP-1** forms relatively large aggregates in water solution.

Then, the DOSY spectrum of the **MDP-1**/MD-2 mixture (at 5:1 molar ratio) was also recorded. As stated above, the signals of the ligand aliphatic chains were no more visible in the NMR spectrum, strongly suggesting the interaction of this part of the glycolipid with MD-2. In addition, the observation of a higher diffusion coefficient for the ligand molecule indicated that the existing aggregate for isolated **MDP-1** is indeed disrupted.

## 2.2.2.3 Molecular modeling studies and docking of monosaccharide MDP-1 with CD14 and MD-2

First, the use of AutoDock and Vina programs was validated by docking the natural antagonist lipid IVa, employing the X-ray crystallographic structure of *h*MD-2 protein in complex with lipid IVa as starting geometry (PDB 2E59).[27] Both AutoDock and Vina programs satisfactorily reproduced the crystallographic binding mode, showing the four FA acyl chains inside the lipophilic pocket, and the phosphorylated glucosamine moieties located at the entrance of the cavity (data not shown).

Then, the same docking protocol was applied to compound **MDP-1**, predicting reasonable binding poses in both proteins, *h*CD14 and *h*MD-2, pointing at this compound as a suitable binder.

Analysis of the AutoDock and AutoDock Vina docked binding poses in MD-2 showed the ability of compound **MDP-1** to bind in two different fashions, with close predicted binding energies. Most of the best-docked solutions corresponded to binding poses with the two FA chains deeply confined inside the MD-2 pocket, similarly to lipid IVa. One of the FA chains establishes hydrophobic contacts and CH-π interactions with Leu74, Phe76, Phe104, and Ile117, in a similar way to the equivalent FA chain present in lipid IVa (Figure 2.23 A). The second FA chain is directed into the region delimited by Ile52, Leu54, Phe121, Ile124, Tyr131, and Ile153, a sub-pocket also occupied by a FA chain in the complex with lipid IVa. In few cases, results from docking showed a second binding mode with one FA chain going out towards Val82, and placed over Ile124 (Figure 2.23 B). Interestingly, this Ile124 moves "up" in the agonist conformation, and its position is occupied by Phe126, thus acting as an agonist/antagonist switch.

Polar interactions were also identified in the docked binding poses. One phosphate group participates in hydrogen bonds, for instance with Ser118, and is always placed near Lys58 and/or Lys122, similarly to one of the lipid IVa phosphates. The second phosphate is found in proximity of positively charged side chains, such as that from Arg96, or in other docked solutions, exposed to the outside. In addition, either amide CO group or ester CO group from compound **MDP-1** was found to establish a hydrogen

bond with the Ser120 CO group in some of the docking results. These predicted binding poses are in agreement with the NMR experiments and provide a 3D model for the interaction of the FA chains with MD-2 protein, as well as putative polar interactions involving the phosphate groups.
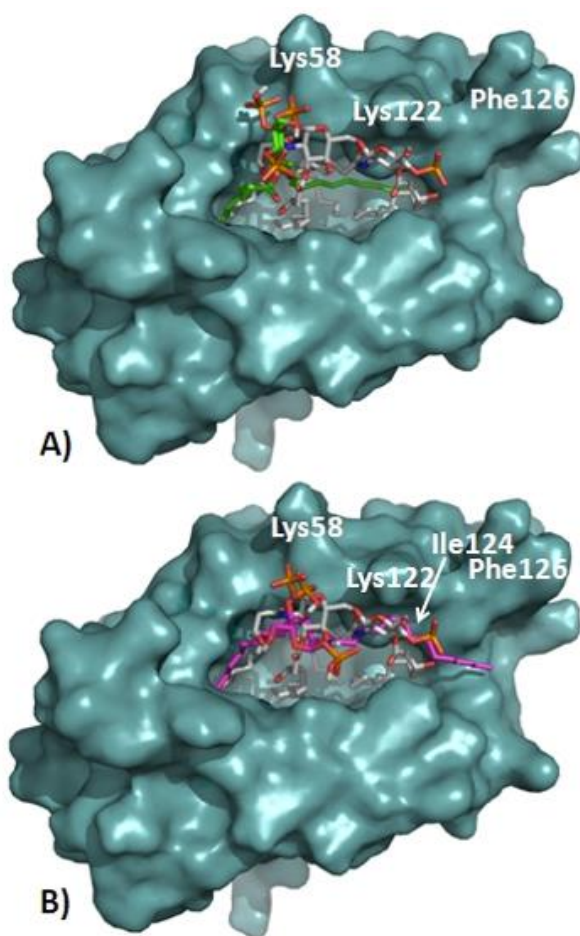
Figure 2.23. AutoDock binding poses of compound **MDP-1** characterized for having two (green) or one (magenta) FA chain oriented inside the lipophilic MD-2 pocket. Lipid IVa is shown as reference in CPK colours.

In the case of CD14, this protein also owns a highly lipophilic wide pocket as MD-2 protein, but with fewer charged residues in the opening portion. Compound **MDP-1** showed binding poses, presenting both FA chains inside the pocket, and the polar phosphate groups and sugar placed at the entrance of the cavity (data not shown).

## 2.2.3 Natural olive oil phenols and synthetic derivatives

The increasing interest of the scientific community in finding molecules of natural origin that modulate TLR4 activation and signalling, together with some disadvantages in the use of the amphiphilic glycolipids synthesized so far – poor water solubility, high tendency to form large aggregates, synthetic difficulties related to carbohydrate chemistry – prompted us to screen olive oil extracts for natural substances active as TLR4 modulators. We also planned total syntheses of new molecules with chemical structures inspired to the bioactive natural compounds.

2.2.3.1 Natural compounds from extra virgin olive oil: new TLR4 modulators

Evidence on the strong anti-inflammatory activity of some phenolic compounds from extra virgin olive oil (EVOO) increased in recent years. This important property, however, has not yet been directly correlated to the activity of these molecules on TLR4 receptor system.

In the first part of the work regarding natural compounds and derivatives, phenolic extracts from different extra virgin olive oils and some isolated phenolic constituents were tested for their activities on human TLR4.

A preliminary screening of the *in vitro* TLR4 antagonist activity of total phenolic contents extracted from Taggiasco, Tuscan and Sagra EVOO (Figure 2.24) was performed. The total phenolic fraction was extracted according to published procedures[83] and quantified through the gallic acid equivalence method (Folin Ciocalteau method).
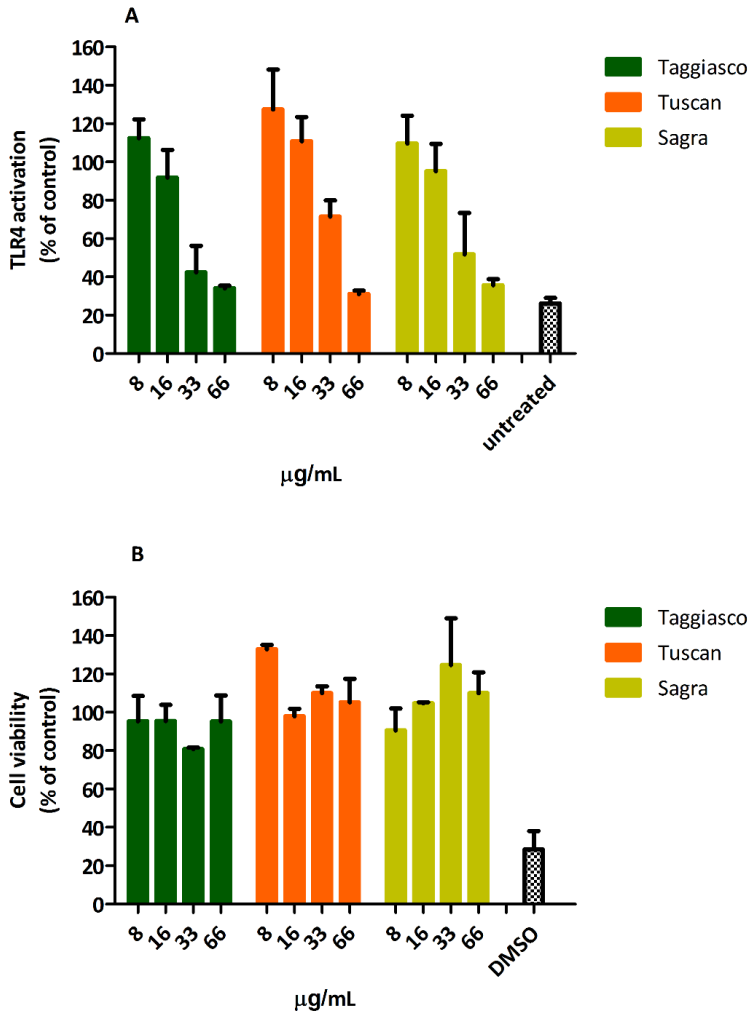
Figure 2.24. A) Dose-dependent inhibition of LPS-stimulated TLR4 activation by total phenolic extracts from different EVOOs (namely Taggiasco, Tuscan, Sagra) on HEK-293 cells transfected with human CD14 and MD-2.TLR4. Cells were treated with increasing concentrations of phenolic extracts (8-66 µg/ml) and then stimulated with LPS (10 ng). TLR4 activation is monitored as sAP production. The results are normalized to activation by LPS alone and expressed as the mean of percentage ± SD of 3 independent experiments **B)** Viability assay (MTT) on total phenolic extracts from different EVOOs in HEK-Blue cells. DMSO is used as negative control. The results are normalized on the positive control.

The phenol fractions were then tested on HEK-293 cells transfected with human TLR4, MD-2 and CD14 receptors, and all the samples proved to be able to reduce the LPS-induced TLR4 activation in a dose-dependent way, inducing a total inhibition when used at higher concentrations (Figure 2.24 A).

These activities are not associated with cellular toxicity, which was found to be very low in the concentration range used for biological tests, as assessed by MTT assay (Figure 2.24 B).

As stated, all the three samples possess very good TLR4 activity, showing some differences in the inhibition potency that could be interesting to study in deep. These results are very promising, because they suggest a correlation between the anti-inflammatory effects of the phenols from olive oil and their activity as TLR4 modulators.

Consequently, a second screening was performed on the main single constituents from the phenolic fraction of EVOO. In particular, several compounds belonging to the principal classes of phenolics contained in extra virgin olive oil were tested: phenolic acids, phenehtyl alcohols, lignans, flavonoids and secoiridoids. The majority of these molecules are commercially available (Figure 2.25).
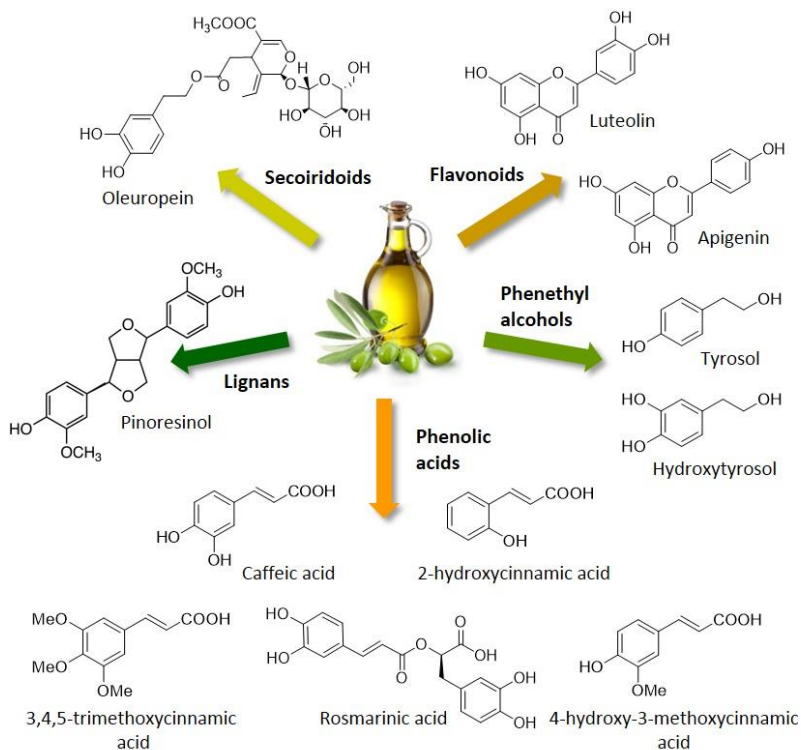
Figure 2.25. Chemical structures of principal olive oil phenolics tested for TLR4 activity: 2-hydroxycinnamic acid, 4-hydroxy-3-methoxycinnamic acid, caffeic acid, rosmarinic acid, trimethoxycinnamic acid, luteolin, apigenin, hydroxytyrosol, tyrosol, oleuropein, pinoresinol.

The compounds containing carboxylic acids, generally derivatives of cinnamic acid (2-hydroxycinnamic acid, 4-hydroxy-3-methoxycinnamic acid, caffeic acid, rosmarinic acid, trimethoxycinnamic acid), were not active in inhibiting the TLR4 pathway activation, as well as the lignan pinoresinol (Figure 2.26). Disappointingly, also tyrosol and hydroxytyrosol were inactive in inhibiting LPS-stimulated TLR4 signal, despite strong anti-inflammatory activities are reported in literature for both these phenols.
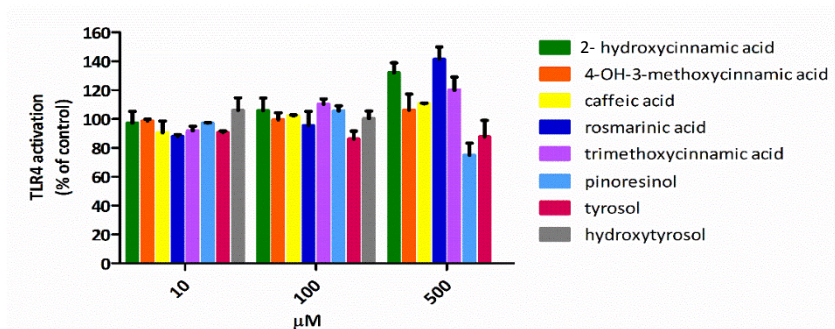
Figure 2.26. TLR4 activity of some phenolic constituents of EVOO on HEK-293 cells transfected with human CD14 and MD-2.TLR4. Cells were treated with increasing concentrations of phenolic compounds (10-500 µM) and then stimulated with LPS (10 ng). TLR4 activation is monitored as sAP production. The results are normalized to activation by LPS alone and expressed as the mean of percentage ± SD of 3 independent experiments**.**

Among the phenolic compounds screened for biological activity on TLR4 receptor system, oleuropein showed a moderate dose-dependent TLR4 antagonism (Figure 2.27), not associated with cell toxicity, as assessed by cell viability test (MTT test, not shown).
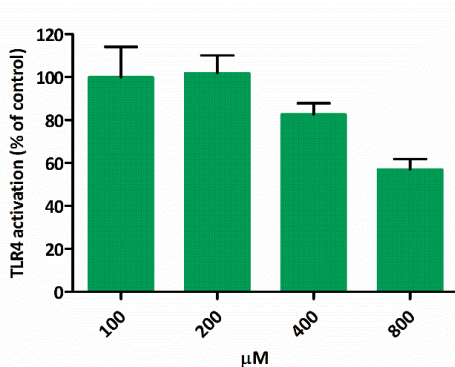
Figure 2.27. Dose-dependent inhibition of LPS-stimulated TLR4 activation by oleuropein on HEK-293 cells transfected with human CD14 and MD-2·TLR4. Cells were treated with increasing concentrations of oleuropein (100-800 µM) and then stimulated with LPS (10 ng). TLR4 activation is monitored as sAP production.

Surprisingly, the best inhibitors of LPS-induced TLR4 activation were the flavonoids apigenin and luteolin (Figure 2.28) with IC_{50} values of 15.7 and 14.3 µM, respectively. These molecules also proved not to be toxic for HEK-293 cells, as confirmed by MTT test (data not shown).
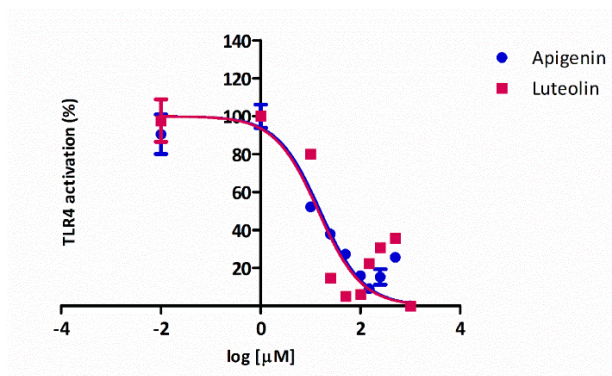
Figure 2.28. TLR4 activity of apigenin and luteolin in HEK Blue cells. Cells were treated with increasing concentrations of flavonoids (0-100 µM) and then stimulated with LPS (10 ng). TLR4 activation is monitored as sAP production. Normalized data are representative of three independent experiments. The IC_{50} values have been calculated by non-linear regression analysis using GraphPad Prism.

These results are very interesting because they pointed out for the first time that the anti-inflammatory activity of phenolic extracts from EVOO can be correlated to their activity as modulators of the TLR4 receptor system.

The single constituents of the phenolic fraction from EVOO do not elicit a so strong antagonist activity when administrated alone. Consequently, a synergic effect of the single phenolic constituents was speculated to explain the strong activity of the whole extracts as TLR4 antagonists. Alternatively, the high activity of still-unknown constituents could be

responsible for the total TLR4 activity of phenol fraction, thus suggesting a future study on the biological characterization of minor components present in EVOO phenolic fraction.

2.2.3.2 Synthesis of Oleocanthal

The molecule of oleocanthal shows very interesting biological properties. Particularly, oleocanthal has been identified to be a very strong anti-inflammatory agent.[86, 87] Consequently, there is a great interest in testing this compound as inhibitor of the TLR4 signal pathway, together with the other constituents of the phenolic fraction from olive oil described in the previous paragraph.

Oleocanthal, however, is not a commercial product. Thus, the synthesis of oleocanthal was undertaken. The synthesis of oleocanthal is quite challenging and time-consuming. The target of this thesis work was the synthesis of key intermediate **24**.

Two synthetic strategies were followed. The first route was based on that reported in literature by Smith, A. B. at al. (step **a** to **m**).[102] The second synthetic strategy was developed (step **n** to p) in our labs, with the aim of increasing the yields of the first steps and reducing the synthetic complexity of the first route.[103, 104]
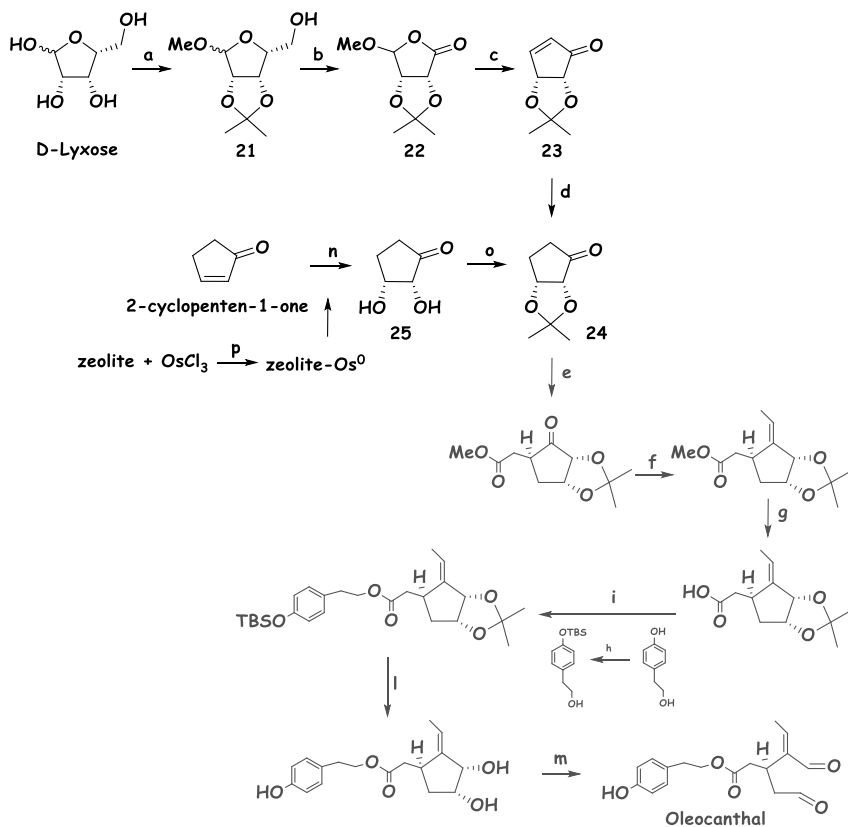
Scheme 2.9. Synthesis of oleocanthal. Reactions and conditions: **a)** DMP, HClO₄, acetone, MeOH, RT, 2h, 99%; **b)** PCC 2.5 eq, benzene, reflux in Dean Stark Trap, 110°C, o.n.; PCC 2.5 eq, benzene, reflux, o.n., 28% ; **c)** (MeO)₂POCH₂Li (in situ from dimethyl methylphosphonate and *n*-BuLi 1.6 M in hexane), THF, -78°C to 23°C, 4h, 62%; **d)** H₂, Pd/C, MeOH/CH₂Cl₂ 2:1, 4h, 98%; **e)** LiHMDS, THF, -78°C; methylbromoacetate, HMPA, Me₂Zn, -45°C; **f)** LiHMDS, EtPPh₃Br, THF; CeCl₃, THF,-78°C to 23°C; **g)** LiOH, MeOH, THF; **h)** TBSCl, imidazole, DMF; I₂, MeOH; **i)** DCC, DMAP, CH₂Cl₂, 0 to 23°C; **l)** TBAF, THF; 1N HCl, CH₃CN; **m)** NaIO₄, THF/H₂O 1:1; **n)** H₂O₂ 30%, zeolite-Os⁰, cat, acetone/ H₂O 9:1, RT, 36 h, 11%; **o)** DMP, TsOH, CH₂Cl₂, 0°C, 3h, 20%; **p)** zeolite-Y, OsCl₃·3H₂O, H₂O, 72h; NaBH₄, H₂O, 4h. Reaction steps in grey (**e** to **m**) have not been performed, yet, but they are reported in literature.

The starting material of the first route was the commercial pentose D-Lyxose. The sugar was converted into the corresponding acetal **21** using

DMP and HClO$_4$, with 99% yield. Exhaustive oxidation of **21** employing pyridinium chlorochromate (PCC) provided lactone **22**. The transformation involved both the oxidation of the primary alcohol and the cleavage of a C-C bond. To reach this goal, very harsh reaction conditions were ensured: a high amount of the strong oxidative agent PCC was used, with benzene as solvent at high temperatures - reflux in a Dean Stark trap - for a long reaction time. In order to reduce solvent toxicity, an alternative to benzene was toluene, but the change in solvent caused a decrease in yield from 28% to 21%. When the reactions were scaled up to gram scale, however, the yields decreased dramatically to 12-15%. In the subsequent step, treatment of the lactone with the lithium anion derived from dimethyl methylphosphonate and *n*-BuLi produced enone **23** (62% yield). Finally, the enone, upon hydrogenolysis with H$_2$ on Pd/C, furnished lactone **24**, with 98% yield. The issues derived from the reaction step **b**, specifically the harsh reaction conditions, the low yield and the reactant and solvent difficult handling due to the high toxicity, prompted us to find an alternative strategy to synthesize intermediate **24**.

The starting reagent of the second synthetic route was the 2-cyclopenten-1-one. The hydroxylation reaction with H$_2$O$_2$, catalysed by Zeolite-Os^0, provided the *cis*-diol **25**. The solid phase catalyst was obtained from Zeolite-Y and OsCl$_3$, as described by Zahmakiran et al.[103] The diol was protected as acetal **24** for reaction with DMP and TsOH at 0°C, with a modified procedure from Majumdar et al., 2009.[104] When this reaction was performed at room temperature and a bigger amount of TsOH was used, the presence of a predominant side product (**26a** or **26b**) was

observed, which was identified thanks to NMR and MS measurements, as shown in scheme 2.10.
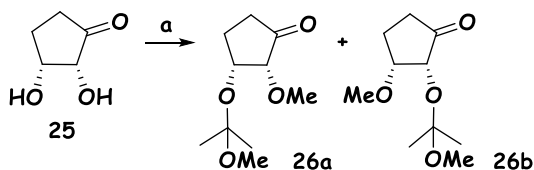
Scheme 2.10. Reactions and conditions: **a)** DMP, TsOH, RT, 2h.

The amount of side products was drastically reduced with reaction conditions described in scheme 2.9 (step **o**). The yield of the reaction, however, was 20%. In conclusion, the second synthetic strategy did not allow to increase the reaction yields, but had the advantages of milder reaction conditions and a reduced number of reaction steps.

2.2.3.3 Mimicking natural compounds: synthetic analogues of oleocanthal

2.2.3.3.1 Rational design of new oleocanthal analogues

Some new synthetic analogues of oleocanthal were designed and synthesized. Previous works on the synthesis and biological characterization of oleocanthal derivatives with anti-inflammatory activity outlined some important structural characteristics of these molecules.[87] First of all, the phenolic portion seems to be fundamental in retaining the anti-inflammatory activity, while bearing one or two phenolic OH in different positions. However, we demonstrated that

131

molecules like tyrosol and hydroxytyrosol – presenting only the phenolic portion – were not capable of inhibiting the activation of the TLR4 pathway. Consequently, in these new mimetics of oleocanthal the di-aldehyde portion was maintained. Major structural variations involved the direction of the ester bond and the length of the linker between the phenolic portion and the di-aldehyde function, together with the variation of the distance between the two aldehyde groups.

The designed analogues are presented in scheme 2.11. During this PhD project the synthesis of the first two compounds, among the six described, was performed. The synthesis of the other four analogues is still in progress.
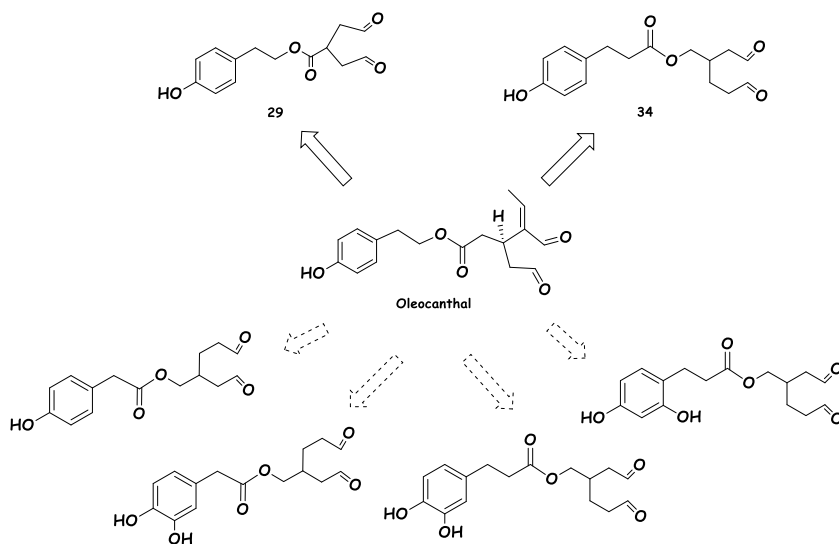

Scheme 2.11. New synthetic analogues of oleocanthal. Compound **29** and **34** were synthesized during this thesis work. The synthesis of the other derivatives is in progress.

2.2.3.3.2 Synthesis of new oleocanthal analogues

The synthesis of compound **29** was performed starting from tyrosol and 3-cyclopentenecarboxylic acid. The desired condensed product **27a** was obtained for reaction of the starting materials in presence of DCC (Dicyclohexylcarbodiimide) as condensing agent and DMAP (4-dimethylaminopyridine) as catalyst. The yield of the first reaction step was not very high (55%) because of the formation of a side product, isolated after purification and characterized as **27b**. Compound **27a** was hydroxylated with OsO$_4$ and NMO (*N*-Methylmorpholine-*N*-Oxide) in a solution of acetone/PBS buffer pH 7.4 (9:1), yielding 74% of diol **28**, after purification. When this reaction was performed in another solvent solution (tBuOH/H$_2$O 1:1), degradation of the product was observed, due to the hydrolysis of the ester bond, with a yield of 18%. It was deduced that the control of the mixture pH, obtained using PBS buffer, was fundamental.
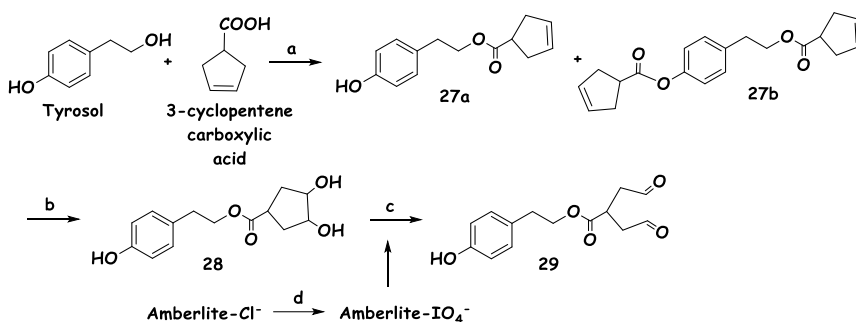

Scheme 2.12. Synthesis of compound **29**. Reactions and conditions: **a)** DCC, DMAP, CH$_2$Cl$_2$, 20h, 55%; **b)** OsO$_4$, NMO, acetone/PBS buffer pH 7.4 (9:1), 3 h, 74%; **c)** Amberlite-IO$_4^-$, CH$_3$CN/H$_2$0 10:1, 2h; **d)** Amberlite IRA-900 Cl$^-$, NaIO$_4$, H$_2$O, o.n.

Dihydroxy derivative **28** was oxidized with periodate to obtain the dialdehyde **29**. When periodate in solution (dioxane/H_2O 8:2) was used, it was very difficult to recover the product from the aqueous medium. Thus, periodate absorbed on amberlite resin was prepared for ion exchange from Amberlite IRA-900 Cl^{-} and sodium periodate and it was used to perform reaction step **c**.[105] Unfortunately, even if solid phase periodate was used, the isolation of the pure final product **29** was impossible because it probably underwent fast rearrangements, affording a mixture of products. The molecular mechanism of these rearrangements is under study.

A previous synthetic approach to obtain directly compound **29** from compound **27a** was based on ozonolysis, followed by treatment with PPh_3. O_3 was provided thanks to an ozoniser (φ=9 L/min, P=1.2 Bar, -78°C). The impossibility to recover the product after purification of the reaction mixture was first imputed to the reaction itself. After the evidence emerged from the synthetic strategy described in scheme 2.12, however, it was conjectured that the impossibility of product isolation was due to the intrinsic instability of compound **29** itself.

Some derivatives were proposed due to intramolecular rearrangements, in order to explain the product instability (Scheme 2.13). It is well known that in aqueous environments (also due to atmosphere humidity) aldehydes are in equilibrium with their hydrate forms, with different relative stabilities in relation to the molecular structures.
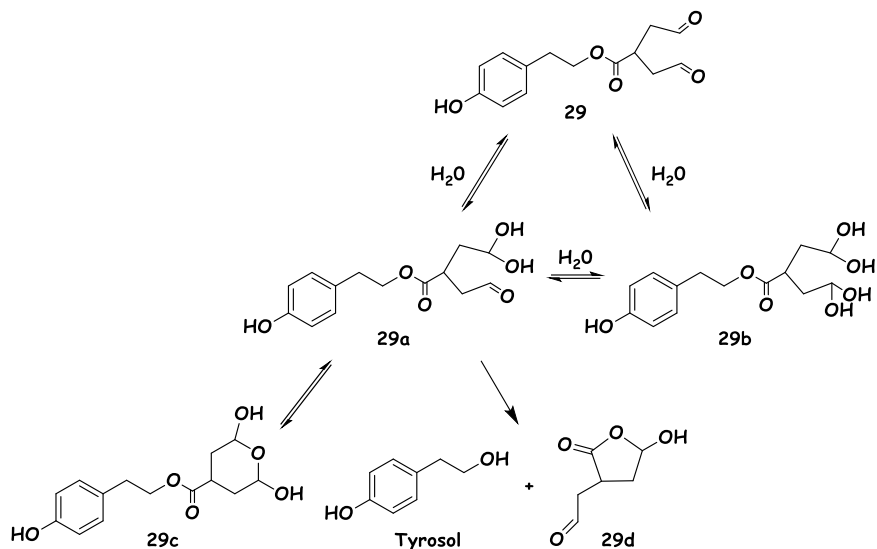
Scheme 2.13. Rearrangement hypotheses for molecule **29**.

Compound **29** presents two aldehyde functions, being able to form both a mono-hydrated derivative **29a** and a di-hydrated one **29b**. The mono-hydrated derivative can undergo further rearrangement due to nucleophilic attack of the hydroxyl group to the carbonyl group. It is reported in literature the formation of stable hydrated forms with a six-atom ring, when two aldehyde function are spaced by three atoms, as in the case of molecule **29c**.[106] Finally, the possibility of the nucleophilic attack of the hydroxyl oxygen on the ester carbonyl would lead to the hydrolysis of ester with formation of tyrosol and lactone **29d**, stabilised for the presence of a 5-atom ring.

Compound **34** was obtained starting from 3-(4-hydroxyphenyl)propionic acid (Scheme 2.14). A first attempt was made to directly react 3-(4-hydroxyphenyl)propionic acid and 3-cyclohexene-1-methanol to obtain molecule **32** in a single step, but a mixture of products was obtained instead. Consequently, the phenolic OH of 3-(4-hydroxyphenyl)propionic acid was first protected as *tert*-butyldimethylsilyl ester **30** for reaction with TBSCl (*tert*-Butyldimethylsilyl chloride) and imidazole (yield 99%).[107] The subsequent reaction with 3-cyclohexene-1-methanol, in the presence of DCC and DMAP, afforded ester **31**.
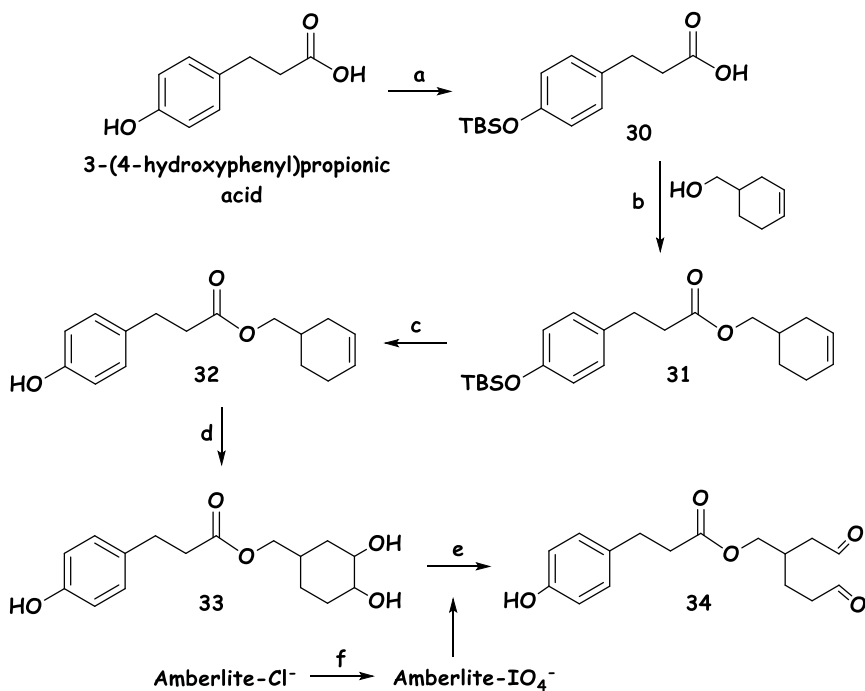
Scheme 2.14. Synthesis of compound **34**. Reactions and conditions: **a)** TBSCl, imidazole, DMF, 24h, 99%; **b)** DCC, DMAP, CH_2Cl_2, 24h, 88%; **c)** TBAF, AcOH, CH_2Cl_2, 1h, quant; **d)** OsO_4, NMO, acetone/PBS 9:1, 3h, 67%; **e)** Amberlite-IO_4^-, CH_3CN/H_2O 10:1, 2,5h, quant; **f)** Amberlite IRA-900 Cl$^-$, $NaIO_4$, H_2O, overnight.

After quantitative deprotection with TBAF (tetra-*n*-butylammonium fluoride) of the phenolic hydroxyl, compound **32** was oxidized with OsO_4 and NMO, in buffered solution (acetone/PBS buffer at pH=7.4 9:1), affording diol **33** with 67% yield. The final product **34** was obtained from diol **33** through treatment with periodate absorbed on solid phase Amberlite, as described for compound **29**.

Compound **34** was successfully isolated, with a reaction yield of 98%. Compound **34** showed a good water solubility and, in contrast with its homologue **29**, it proved to be chemically stable, even after several months, allowing to perform biological tests to evaluate its activity as TLR4 modulator.

As in the case of compound **29**, compound **34** is in equilibrium with the hydrated forms of aldehydes, but the rearrangements that causes the instability of compound **29** (scheme 2.13) do not occur, probably because compound **34** would pass through the formation of a disfavoured seven-atom ring.

2.2.3.3.3 TLR4 activity and cellular toxicity of synthetic oleocanthal analogues

The chemical instability of molecule **29** hampered its biological characterization.

The ability of molecule **34** to interfere with LPS-triggered TLR4 activation in HEK-Blue™ cells model was investigated (Figure 2.29 A). In this assay,

cells were pre-treated with increasing concentrations of compound **34** (from 0 to 100 μM) and then stimulated with *E. coli* LPS (10 nM).
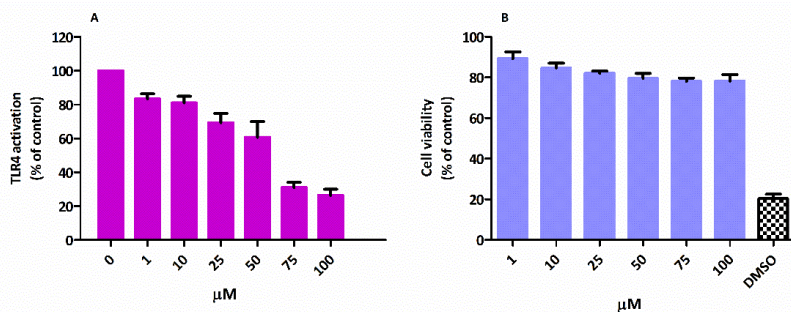
Figure 2.29. A) Dose-dependent inhibition of LPS-stimulated TLR4 activation by compound **34**. HEK-293 cells transfected with human CD14 and MD-2.TLR4, were treated with increasing concentrations of compounds (0-100 μM) and then stimulated with LPS. TLR4 activation is monitored as sAP production. The results are normalized to activation by LPS alone and expressed as the mean of percentage ± SD of 3 independent experiments. **B)** Viability assay (MTT) on compound **34** (0-100 μM) in HEK-Blue cells. DMSO is used as negative control. The results are normalized on the positive control (cells treated with PBS) and expressed as the mean of percentage ± SD of 3 independent experiments.

Compound **34** significantly inhibited TLR4-depending sAP production (Figure 2.29 A), showing a good dose-dependent TLR4 antagonism. Moreover, compound **34** was tested for its toxicity on cells (MTT test, figure 2.29 B) and it showed no toxicity at the concentrations used for HEK-Blue™ assay. Consequently, compound **34** presented very promising characteristics: it is a chemically stable, water-soluble, not toxic, good TLR4 antagonist.

2.2.4 TLR4 modulators conjugated to carrier proteins

As discussed in the introduction, non-toxic TLR4 agonists are interesting hits for the development of vaccine adjuvants. A mild TLR4 stimulation is a way to potentiate the intensity and duration of antibody production and immunity response to antigens. The project to synthesize new TLR4 agonists and to covalently conjugate immunostimulatory molecules to proteins was developed in collaboration with Lofarma (Milano), a pharmaceutical company specialised in the treatment of allergy diseases, and interested in the production of new vaccine adjuvants. In particular, these adjuvants should be used in sublingual anti-allergic vaccines. In this thesis, the conjugation of a synthetic IAXO compound and a carrier protein, the ovalbumin, was obtained. Then, Lofarma characterized the immunogenic profile of the derivative.

The glycolipidic small molecule IAXO-102, described previously (Par. 2.2.1), was selected to be conjugated to the protein ovalbumin (OVA). Data not shown in this thesis indicates that IAXO-102 works as TLR4 agonist in a specific concentration range on some cellular models.

Two conjugation strategies were performed: the first one was based on the reaction between IAXO-102 and OVA, in the presence of a bifunctional linker (ethylene glycol disuccinate bis(sulfo-N-succinimidyl) ester sodium salt). In this case, the amino group of IAXO-102 and the amino functions of surface lysines of OVA are linked through a linker with two amide bonds. The second strategy was based on the chemical functionalization of IAXO-102 with a glutarate linker, which allows the direct conjugation

of the free carboxylic acid on the small molecule to the amino groups of protein lysines, with the use of condensation agents.
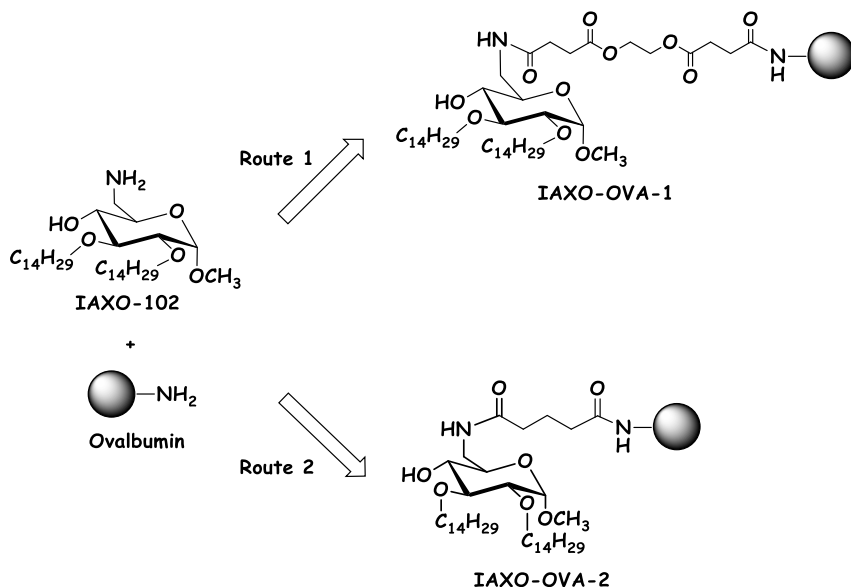

Scheme 2.15. The glycolipid IAXO-102 is conjugated to the protein ovalbumin through two different synthetic strategies, namely route 1 and route 2. The synthetic details to obtain products **IAXO-OVA-1** and **IAXO-OVA-2** are described below.

2.2.4.1 Conjugation of IAXO-102 to OVA through a bifunctional linker

An activated dicarboxilic crosslinking agent was used in order to space the small molecule from the protein, preserving the biological activity of the glycolipid. The choice to use the lysine of the protein to be linked covalently to the small molecule is due to biological requirements: the modulation of the allergoid activity of the proteic allergens that will be

used in the development of the future adjuvant is based on the derivatization of the lysine residues.
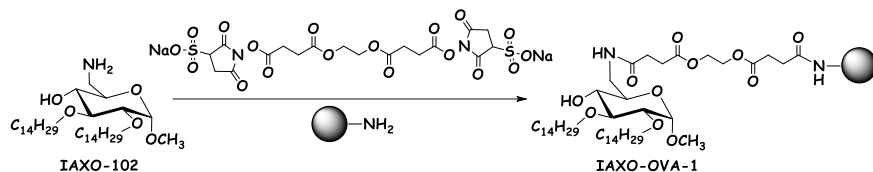
Scheme 2.16. Synthesis of **IAXO-OVA-1.** Reactions and conditions: PBS, DMSO (max 10%), 37°C, 4h.

Four experiments of conjugation were performed, varying the molar ratio between OVA, IAXO-102 and the crosslinking agent (Table 2.1)

Ovalbumin (eq)	Crosslinker (eq)	IAXO-102 (eq)
1	20	40
1	20	20
1	10	10
1	5	5

Table 2.1: Molar ratio of reagents.

The purified products were analysed on SDS-PAGE electrophoresis gel, with 12% separating gel, revealed with Blue Comassie, which is a specific coloration for proteins. Form this analysis, the present of different products emerged: a small amount of free OVA, a specie of little higher molecular weight than OVA, reasonably **IAXO-OVA-1**, and a specie of high molecular weight (90 KDa compared to the markers), reasonably indicating the formation of OVA oligomers. The amount of conjugated

OVA was higher for lower ratios among protein, crosslinking agent and IAXO-102 (1:5:5). A further purification trial was carried out, but did not give the hoped results. The evident disadvantage of this conjugation strategy lies in the formation of oligomers of OVA linked through the bifunctional linker, which does not allow obtaining the pure conjugate **IAXO-OVA-1**.

2.2.4.2 Direct conjugation of carboxylated-IAXO-102 to OVA

The second strategy was based on the synthesis of a molecule (compound **35**), which presented a linker bearing a free carboxylic function to be directly conjugated to the lysine of the protein.
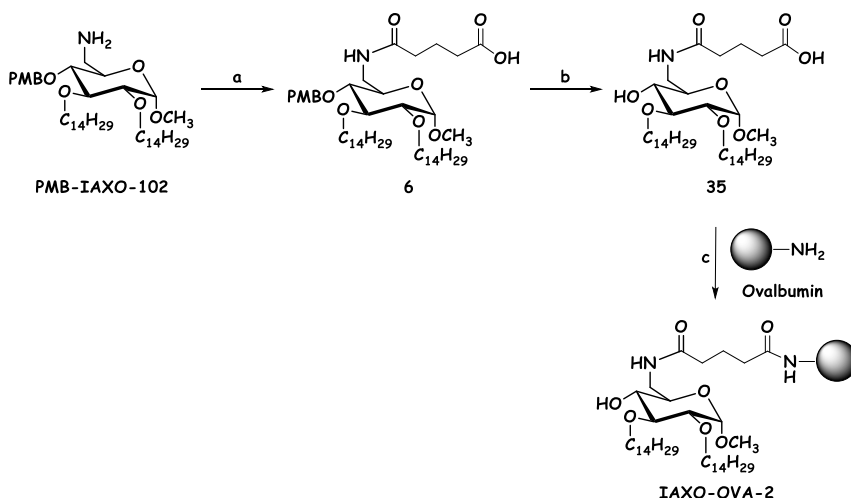
Scheme 2.17. Synthesis of **IAXO-OVA-2**. Reaction and conditions: **a)** Glutaric anhydride, dry pyridine, RT, 2h, yield: 87%; **b)** TFA, CH$_2$Cl$_2$, RT, 1.5h, 98%; **c)** Buffer: see table 2.2, 35°C, 24h.

In particular, a precursor of IAXO-102, named PMB-IAXO-102,[70] was reacted with glutaric anhydride, obtaining compound **6** as described in paragraph 2.2.1.1. Here, compound **6** was deprotected in TFA, to obtain molecule **35**. This molecule was directly reacted with OVA, using EDC as crosslinking agent.

An issue to overcome was to perfectly solubilize in an aqueous buffer the synthetic molecule **35**. Seven experiments of conjugation were performed on small amounts of reagents (1 mg OVA), varying the molar ratio between OVA, molecule **35** and EDC, and modifying the buffer composition (Table 2.2), in order to choose the best reaction conditions.

OVA (eq)	Compound 35 (eq)	EDC (eq)	Buffer
1	5	5	MES Buffer* pH=4.7
1	10	10	MES Buffer* pH=4.7
1	5	5	MES Buffer* pH=4.7, DMSO 25%
1	10	10	MES Buffer* pH=4.7, DMSO 25%
1	5	5	MES Buffer* pH=4.7, DMSO 50%
1	10	10	MES Buffer* pH=4.7, DMSO 50%
1	5	5	MES Buffer* pH=4.7, DMSO 30%

* MES Buffer: acido 2-(N-morfolino)etansolfonico 100 mM, NaCl 150 mM

Table 2.2. Reaction conditions of step **c**.

The best conditions were chosen: MES Buffer at pH=4.7, DMSO ≥ 30%; OVA:IAXO-glutarate:EDC 1:5:5 and these conditions were used for the scale up of the reaction (10 mg OVA).

The purified products were analysed on SDS-PAGE electrophoretic gel, using polyacrylamide separating gels at 15% and 12%, revealed with Blue Comassie and Silver Stain procedures.
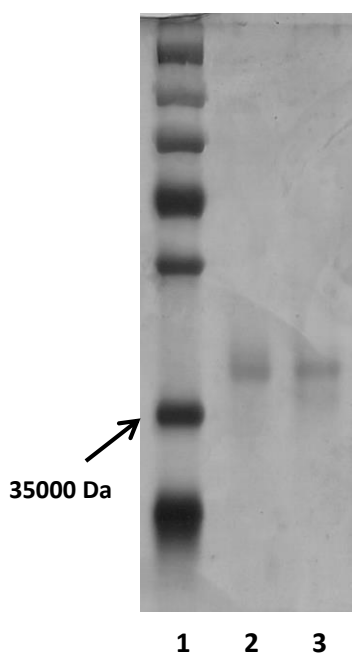
Figure 2.30. Discontinuous SDS-PAGE electrophoresis (separating gel 12%), coloured with Silver Stain procedure: **1)** molecular weight markers; **2)** Ovalbumin, 3 μg; **3)** derivative **IAXO-OVA-2**, 3 μg.

The electrophoretic analysis pointed out the presence of a specie with a molecular weight higher than OVA, comparable to that expected for the

conjugate **IAXO-OVA-2**. This conjugation strategy allowed to obtain a final product quite homogeneous, avoiding the formation of side products.

The pure final product **IAXO-OVA-2** was tested for its immunogenic activity in the labs of the pharmaceutical company Lofarma. They tested the protein ovalbumin, the protein ovalbumin associated with the small molecule IAXO-102 (co-administration) and the derivative **IAXO-OVA-2**, on murine models. The values monitored to evaluate the adjuvant activity of the compounds are the amount of IgE (Immunoglobulin E), specific antibodies responsible for allergies, and IgG2a, a subclass of Immunoglobulin G, the major responsible of secondary immune response. The ratio between IgE and IgG2a is an essential parameter to evaluate the adjuvant activity. The lowest is the ratio, the better is the adjuvant activity of the compound. The analysis of the IgE/IgG2a values revealed that the treatment of rats with **IAXO-OVA-2** is the only administration that determines the decrease of IgE/IgG2a, which is essentially due to a production reduction of specific IgE. Thus, it was found that **IAXO-OVA-2** induces a specific antibody response significantly higher than the ovalbumin alone or than the co-administration of IAXO-102 and ovalbumin, representing a promising candidate to develop new vaccine adjuvants to be employed in allergy vaccines.

Conclusions

The aim of this PhD project was the study of LPS binding proteins belonging to two classes: the bacterial proteins of the Lpt transport machinery and the mammalian TLR4 receptor complex, namely TLR4 and the co-receptors LBP, CD14, MD-2. This goal was achieved thanks to the design, synthesis, chemical and biological characterization of new small-molecule ligands of LPS binding proteins.

Characterization of LptC interaction with natural and synthetic ligands: the development of new potential antibiotics

The study of the bacterial transport protein LptC required the development of new chemical tools. First, a fluorescent-labelled natural ligand (**fLOS**) was obtained, with incorporation ratio of fluorophore 50 times higher than the commercial product. The newly developed fluorescent LOS also retained the biological activity of the natural ligand. All these characteristics made **fLOS** an innovative, safe and sensitive tool to be employed as fluorescent probe in interaction studies with LptC. The high levels of fluorescein incorporation of **fLOS** allowed us to calculate, for the first time, the thermodynamic parameters of LOS-LptC interaction *in vitro*, with an apparent dissociation constant K_d of 71.4 for **fLOS** and 52.4 µM for unlabeled LOS.

Subsequently, a synthetic glycolipid containing a fluorophore was designed and synthesized in order to make it a potential LptC ligand. The fluorescent glycolipid **IAXO-FITC-1** was used for binding studies with LptC, based on fluorescence measurements. As for the natural ligand, also

IAXO-FITC-1 K_d was calculated, resulting in a value of 221 μM. **IAXO-FITC-1** interacts with LptC, but with lower affinity than the natural ligand. Through competition experiments, it was also demonstrated that **IAXO-FITC-1** and LPS bind at the same site to the LptC protein, thus suggesting a common mechanism of action on LptC. The evidence obtained indicates that **IAXO-FITC-1** can be a useful tool for fluorescence interaction studies on LptC and, even more important, it represents a prototype for the development of new antibiotics targeting the LPS transport in Gram-negative bacteria.

Finally, a preliminary interaction study on LptC was performed, using NMR techniques. The fluorescent probe 1-Anilinonaphthalene-8-Sulfonic Acid (ANS) was used as a mediator to study LptC-LPS interaction. The interaction between LptC and ANS was evaluated through STD and tr-NOESY NMR experiments. These experiments pointed out, for the first time, a strong interaction between the protein LptC and the fluorescent probe ANS. Then, competitive STD experiments were performed, in order to verify if ANS and the natural ligand, the LPS, shared the same binding site on LptC. However, an unexpected outcome was observed: apparently, LPS was not able to displace ANS from LptC. This can be explained by the hypothesis that the LPS and ANS can interact with each other, forming mixed micelles, as demonstrated by other NMR experiments. Unfortunately, these results suggest that it is not possible to study the interaction between LptC and LPS by NMR, using ANS as probe.

In conclusion, the dissection of single steps of LPS binding and release through the Lpt transport chain provides important information on the

molecular mechanisms underlying LPS transport. Moreover, the ability to block LPS transport to the cell surface by small molecules seems an appealing new strategy to gain access to a new generation of antibiotics targeting multi-resistant Gram-negative bacteria. The rational optimization of the molecular structures of these hit compounds, with the aim of improving bioavailability, cell penetration and LptC affinity, could afford the first generation of Gram-negative bacteria-specific antibiotics targeting the LPS transport mechanism.

Characterization of the interaction of TLR4 receptor system with natural and synthetic ligands: new lead compounds targeting TLR4

Although in recent years many TLR4 modulators were synthesized or isolated from natural sources, the need for safer and more active compounds has not decreased. The large panel of TLR4 modulators (agonists or antagonists) developed, with very different chemical structures among each other, is representative of a complex recognition process of LPS from the TLR4 receptor system (including co-receptors LBP, CD14 and MD2). This variety of chemical structures of LPS binding-protein ligands is reflected in the molecules designed and synthesized during this thesis project.

Firstly, new TLR4 antagonists with chemical structures derived from the cationic amphiphile IAXO-102 were designed, with the support of computational data, and then synthesized and studied for their biological activity as TLR4 modulators. IAXO-102 is the most representative member of a first generation of glycolipids active as strong TLR4 antagonists. In

particular, two fluorescent derivatives of IAXO-102, named **IAXO-FITC-1** and **IAXO-FITC-2**, were produced in order to employ them as fluorescent probes for interaction studies. Computational studies suggested the synthesis of the dimeric molecules **IAXO-D1** and **IAXO-D2**, composed of two units of IAXO-102, linked through a 4-atom linker at the C-6 amine position of the sugar. With the aim of improving the water solubility of these amphiphiles – always an important issue when glycolipids are used in biological environments – we projected a zwitterionic derivative of IAXO-102, **IAXO-Z1**, preserving the charged amino group at C-6 position through the introduction of a sultone moiety. All the five new molecules were tested for their biological activity as antagonists of the TLR4 receptor system: **IAXO-FITC-1** and **IAXO-FITC-2** demonstrated to be good dose-dependent antagonists, retaining the activity of the precursor IAXO-102. **IAXO-D1** and **IAXO-D2** also showed antagonist activity, but with lower potency with respect to the precursor IAXO-102, reasonably because of the very low CMC values. **IAXO-Z1** did not show any TLR4 activity. To summarize, among the different glycolipids obtained using IAXO-102 as scaffold, the two fluorescent molecules are the most promising ones, representing not only very good TLR4 modulators, but also useful fluorescent tools for interaction studies on the receptors.

Secondly, a panel of three anionic TLR4 antagonists with chemical structures inspired to the lipid X, a precursor of lipid A, was prepared. One of these anionic glycolipids, **MDP-1**, bearing two phosphate groups, was the most promising one, presenting a potent antagonist activity. This molecule was studied for its interaction with the purified co-receptor MD-2 through NMR binding experiments, indicating a good interaction of the

acyl chains portion of the glycolipid with the protein binding site. These results were in line with computational calculations.

The amphiphilic character of the synthetic glycolipids described so far is often a disadvantage when used in biological environments, because it is associated with low solubility in aqueous media and poor bioavailability. Consequently, at a later stage of this PhD project, the interest moved towards TLR4 modulators from natural sources, which are generally characterized by good water solubility, low toxicity and good bioavailability. In particular, natural TLR4 antagonists, contained in the phenolic extracts from extra virgin olive oil, and new synthetic derivatives inspired to natural compounds were developed. A preliminary screening of phenolic extracts from extra virgin olive oil and of the most abundant compounds contained in the extracts indicates that phenolic extracts and some phenolic compounds, such as apigenin, luteolin and oleuropein, present a very good activity as TLR4 antagonists. Interestingly, this result related for the first time the well-known anti-inflammatory activity of phenolic extracts from olive oils to their activities on the TLR4 receptor system. Oleocanthal, a non-commercial phenolic constituent from olive oil, was very promising because of its well-known anti-inflammatory properties, suggesting that it would be interesting to test its activity on TLR4. Thus, the challenging synthesis of this molecule was undertaken and a key intermediate was obtained with an optimised procedure. The synthetic modification of natural compounds is generally required to increase target specificity and resistance to enzyme hydrolysis, in order to produce a new generation of biologically active compounds with improved pharmacokinetic properties and reduced toxicity. Therefore,

the synthesis of some analogues of phenolic constituents of olive oil was an important target to obtain a new class of potential TLR4 modulators. Two molecules were obtained, namely compound **29** and **34**. As compound **29** underwent fast rearrangement, its isolation resulted impossible and it could not be tested on cells. Compound **34**, on the other hand, was very stable, water soluble, non-toxic and presented a very good activity as a dose-dependent TLR4 antagonist. Consequently, not only a new class of natural compounds active as TLR4 modulators was identified, but also a new and potent TLR4 antagonist, with chemical structure inspired to natural phenols from olive oil, was projected and obtained.

Finally, to complete the panel of TLR4 modulators synthesized during this work, a TLR4 antagonist was also projected. The potential vaccine adjuvant was obtained from the conjugation of a small-molecule TLR4 agonist with a carrier protein. The glycolipid IAXO-102, which was known to switch to agonist activity when used in a specific concentration range, was conjugated through a linker to the protein ovalbumin. The pharmaceutical company Lofarma tested the originally developed conjugate for its immunogenic profile, pointing out that **IAXO-OVA-2** is a good prototype for a new class of vaccine adjuvants, which can be used to formulate new sublingual vaccines against allergies.

In conclusion, the study of the molecular mechanisms at the basis of LPS recognition from the essential bacterial transport protein LptC and from the mammalian innate immunity receptor system is fundamental both for the full elucidation of these important biological processes and for the identification of new and more efficient therapeutics against Gram-

negative bacteria and all the TLR4 related pathologies. During this work, synthetic small molecules, with different and original chemical structures, were produced to reach this goal. New small molecules were designed and synthesized to interfere somehow with the LptC-LPS and/or TLR4-LPS recognition processes. The ability of the new synthetic small-molecules to interact with the LPS binding proteins was investigated by several biochemical and analytical techniques, revealing interesting aspects of the binding mechanisms. These results perpetuate the scientific interest towards the field of LPS-binding proteins and emphasize how important it is to constantly work to reach an in-depth understanding of the molecular mechanisms associated with LPS biosynthesis and recognition.

Chapter 3

Materials and methods

3.1 LOS extraction and purification

For rough LPS (LOS, Ra-LPS) extraction, *E. coli* strain MG1655 was grown at 37°C in LD for 16 h. This culture was diluted 1:100 in fresh medium and grown until mid-logarithmic phase (OD_{600}, 0.6). Cells were then harvested by centrifugation (5000 g, 20 min), washed in 50 mM NaH_2PO_4 [pH 8.0] and stored at - 20°C before extraction.[10] LOS was selectively extracted from dry cells using PCP procedure (Phenol-Chloroform-light Petroleum).[94] Briefly, a solution of aqueous 90% Phenol-Chloroform-light Petroleum (2:5:8 v/v/v), to which solid phenol was added until limpidness, was prepared. Dry cells (9,73 g) were suspended in PCP solutions (2.5%, w/v), stirred for 30 minutes and extracted three times. Then, the light solvents were removed under vacuum and LOS was precipitated from the remaining phenol solution by adding water. The solid was centrifuged, collected, suspended in water and dialysed (cut-off 1000 Da) against distilled water for 3 days. Finally, it was lyophilized, and 85 mg of pure LOS were recovered (yield: 0.9 % w_{LOS}/w_{cells}). The sample obtained from this procedure was screened for the occurrence of contaminants by ^{1}H NMR spectroscopy and discontinuous SDS-PAGE (Sodium Dodecyl Sulphate Polyacrylamide Electrophoresis).[108] The gel was prepared with 15% separating gel (lower gel) and 5% stacking gel (upper gel). The gel was stained according to the Silver Stain procedure for Lipopolysaccharide,[109] which has a sensitivity limit of 1 µg for S-type LPS and 10 µg for of R-type LPS.

Gels were realized as reported: 15% separating gel (lower gel), 5 % stacking gel (upper gel).

	Separating gel (15%)	Stacking gel (5%)
Acrylamide	2500 µl	335 µl
Tris*-HCl 1.5M pH 8.8	1250 µl	- - - - - -
Tris-HCl 0.5M pH 6.8	- - - - - -	500 µl
H₂O MilliQ	1250 µl	1150 µl
APS**	25 µl	15 µl
TEMED***	2.5 µl	2.5 µl
Bromophenol Blue (4% w/v)	- - - - - -	15 µl

*Tris: 2-hydroxymethyl-2-methyl-1,3-propaendiol

**APS: ammonium persulfate

***TEMED: N, N, N', N'-tetramethylene-ethylenediamine

Table 3.1. Reagents for SDS-PAGE gel preparation.

Samples were prepared from aqueous solutions (1 mg/ml) of LPS and were conveniently denatured. Denaturation was performed by adding a volume of sample buffer corresponding to 25% of the sample volume and it was carried out at 100°C for 5 minutes. Commercial samples of LPS from *E. coli* were used as standards. The sample buffer composition was: 2-mercaptoethanol (0.5 mL), as reducing agent; glycerol (2.5 mL), to increase the density of the solution; 3% bromophenol blue (33 µL), as indicator; Tris 1 M pH 6.8 (0.6 mL); SDS 20% (2 mL), as denaturing agent; Milli-Q water until 10 mL.

The electrophoretic analyses were performed on Mini Protean III Bio-Rad system, run at 150 V (constant voltage). The gels were run into the

electrophoresis buffer: TRIS (3 g), glycine (14.4 g), SDS (1 g) in one litre Milli-Q water.

Silver Stain Procedure[109]: The gel was left 1 hour in the fixative solution (40% methanol, 5% acetic acid). Then, it was kept for 20 minutes in the oxidative solution of $NaIO_4$ (100 mg in 100 mL of fixative solution) and washed three times with Milli-Q water (10 min), to remove the excess of oxidant. It was treated with aqueous silver nitrate (0.1 %) for 30 minutes and subsequently it was quickly washed with Milli-Q water (3 seconds). Then, the colouration was developed treating the gel with an aqueous solution of Na_2CO_3 (3%) and formaldehyde (0.02%). The stain development was stopped with a solution of acetic acid (1%). Finally, the gel was washed with Milli-Q water and dried.

3.1.1 LOS conjugation to FITC

LOS from *E. coli* MG1655, obtained according to the described procedure, was labelled with fluorescein using the following procedure. FITC (fluorescein isothiocyanate) was conjugated to LOS, using an optimized protocol of a published procedure.[95] LOS (20 mg) was treated with a solution of triethylamine 0.5% (10 mL) and sonicated on ice for 15 min, then adding a solution of EDTA 100 mM (1 mL). A solution of HCl 1 M was added until a pH value of 5 was reached. A solution of 100 mg FITC in 0.25 M borate buffer (pH=10.5) was added (4 mL) and the mixture was sonicated for 5 min. After addition of 1.6% sodium deoxycholate (5 mL), the solution was stirred at 37°C for 30 h. The reaction mixture was centrifuged at 10000g to eliminate aggregates and the supernatant was

dialyzed (cut-off 1000 Da) against NaCl 137 mM. The sample was concentrated and purified with a PD-10 desalting column (Sephadex G-25) eluted with water. Fractions containing **fLOS** were collected and lyophilized (16 mg). To evaluate the labeling efficiency, a ratio between LOS and FITC concentrations in the sample was calculated. The concentration of FITC was determined spectrophotometrically at 492 nm (extinction coefficient for FITC 85000 M^{-1} cm^{-1}). The concentration of LOS was determined using the thiobarbiturate assay[96], which allows to evaluate the level of KDO (2-keto-3-deoxyoctulosonic acid), a marker sugar for LPS. In these measurements, a sample of commercial LPS-FITC from Sigma Aldrich was used as a reference. A labeling ratio of LOS:FITC 1:1 was calculated for the sample, while the reference showed a labeling ratio of about 50:1 (LPS:FITC).

3.2 Chemistry, general procedures

All the reagents were commercially available and used without further purification unless indicated otherwise. All solvents were anhydrous grade unless indicated otherwise. When dry conditions were required, the reactions were carried out in oven-dried glassware under a slight pressure of argon. Reaction were magnetically stirred and monitored by Thin-Layer Chromatography (TLC) on silica gel. TLC was performed on Silica Gel 60 F254 plates (Merck) with UV detection. Flash column chromatography was performed on silica gel 230–400 mesh (Merck). The petroleum ether used as eluent in chromatography has boiling range of 40–60°C. ^{1}H and ^{13}C NMR spectra were recorded on a Varian 400 MHz MERCURY instrument at 300 K. Chemical shifts are reported in ppm downfield from TMS as internal standard. Mass spectra were recorded on ESI-MS triple quadrupole (model API2000 QTrap™, Applied Biosystems).

Molecules synthesized for the first time during this PhD project are characterized using ^{1}H NMR, 2D-COSY NMR and APT NMR or 2D-HSQC NMR spectroscopy for ^{1}H and ^{13}C chemical shifts and MS spectrometry for m/z values. Molecules synthesized during this thesis work, but previously characterized in other works are characterized only by ^{1}H NMR, 2D-COSY NMR spectroscopy and MS spectrometry. NMR spectra are reported in the section Supporting Information.

Compound IAXO-FITC-1. IAXO-102 was obtained from PMB-IAXO-102 according to published procedures.[70] IAXO-102 (60 mg, 0.10 mmol) and fluorescein isothiocyanate (40 mg, 0.10 mmol) were dissolved in CH_2Cl_2 (6 mL) and reacted at room temperature for 3.5 h, then TLC showed

complete consumption of starting materials. The solution was concentrated *in vacuo* and the crude purified by flash chromatography (AcOEt/EtP 8:2) affording **IAXO-FITC-1** (90 mg, 92%) as orange powder. R_f= 0.74 (AcOEt);

^{1}H NMR (400 MHz, CD$_3$OD, 25°C, TMS) δ (ppm) = 8.07 (s, 1H; H-1'), 7.65 (d, ^3J(H,H)= 7.4 Hz, 1H; H-2'), 7.05 (d, ^3J(H,H)= 8.2 Hz, 1H; H-3'), 6.59–6.52 (m, 4H; H-4', H-4'', H-6', H-6''), 6.43 (dd, J_{ortho}(H,H)= 8.7 Hz, J_{meta}(H,H)= 2.3 Hz, 2H; H-5', H-5''), 4.78 (s, 1H, H-1), 3.87 (m, 1H; NH), 3.79 (m, 1H; NH), 3.65-3.46 (m, 5H; H-4, 2CH$_2$-α chains), 3.33 (m, 2H; H-3, H-6a), 3.20 (m, 6H; OCH$_3$, H-2, H-5, H-6b), 1.47 (m, 4H; 2CH$_2$-β chains), 1.17 (m, 44H, 22CH$_2$ chains), 0.78 (t, ^3J= 6.7 Hz); ^{13}C NMR (100 MHz, CD$_3$OD, 25°C, TMS) δ (ppm)=169.97, 152.89, 128.95, 102.11, 97.74, 80.14, 73.27, 70.83, 54.26, 31.67, 30.07, 29.77, 29.42, 29.38, 29.22, 29.08, 25.88, 25.82, 22.33, 13.04; m/z calcd. for C$_{56}$H$_{82}$N$_2$O$_{10}$S 974.6, found 975.7 [M+H]$^+$.
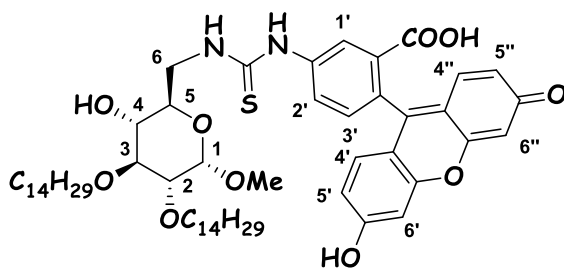
Compound 6. PMB-IAXO-102 (300 mg, 0.43 mmol) and glutaric anhydride (97 mg, 0.86 mmol) were dissolved in dry pyridine (12.4 mL) under argon atmosphere, and reacted at room temperature for 2 h. The solution was concentrated *in vacuo* and the crude was dissolved in CH$_2$Cl$_2$ and washed with HCl 1 M solution, then the organic phase was dried with anhydrous

sodium sulphate and evaporated *in vacuo*. The crude product was purified by flash chromatography (AcOEt/EtP 9:1) affording **6** as a white powder (303 mg, 87%). R_f= 0.57 (AcOEt/MeOH 9:1);

^{1}H NMR (400 MHz, CDCl$_3$, 25°C, TMS) δ(ppm)= 7.32 (d, ^3J(H,H)= 8.6 Hz, 2H; Ar), 6.88 (d, ^3J(H,H)= 8.7 Hz, 2H; Ar), 5.73 (s, 1H; NH), 4.77 (d, ^3J(H,H)= 10.2 Hz, 1H; H-7a), 4.72 (d, ^3J(H,H)= 3.4 Hz, 1H; H-1), 4.53 (d, ^3J(H,H)= 10.1 Hz, 1H; H-7b), 3.91 – 3.51 (m, 10H; H-3, H-4, H-5, OCH$_3$, 2CH$_2$-⍺ chains), 3.43 – 3.14 (m, 6H; H-2, H-6a, H-6b, OCH$_3$ PMB), 2.40 (t, ^3J(H,H)= 7.0 Hz, 2H; 2H-8), 2.20 (m, 2H; 2H-10), 1.97 (m, 2H; 2H-9), 1.61 (m, 4H; 2CH$_2$-β chains), 1.29 (m, 44H; 22CH$_2$ chains), 0.87 (t, ^3J(H,H)= 6.7 Hz, 6H; 2CH$_3$ chains); ^{13}C NMR (100 MHz, CD$_3$OD, 25°C, TMS) δ(ppm)= 177.73, 172.25, 159.42, 130.13,113.93, 97.73, 81.55, 80.64, 78.21, 74.68, 73.78, 71.80, 68.81, 55.20, 39.76, 35.27, 32.97, 31.91, 30.59, 30.02, 29.69, 29.37, 26.26, 26.04, 22.69, 20.63, 19.76, 14.14; m/z calcd. for C$_{48}$H$_{85}$NO$_9$: 819.6, found 820.7 m/z [M+H]$^+$.
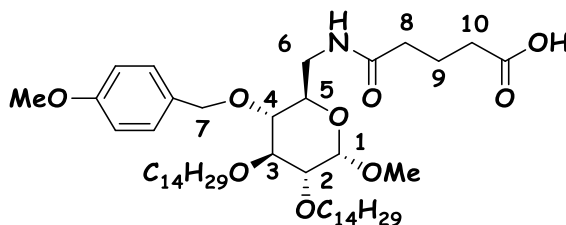
Compound 7. *N*-Boc-ethylenediamine (56.5 µL, 0.36 mmol), HOBt (60.2 mg, 0.45 mmol), DIC (68.9 µL, 0.45 mmol) and DIPEA (152.5 µL, 0.90 mmol) were added to a solution of compound **6** (244 mg, 0.30 mmol) in dry DMF (3.5 mL), under argon atmosphere at 0°C. The mixture was

heated at 40°C and stirred for 40h. The solution was concentrated *in vacuo;* then, the crude was dissolved in CH_2Cl_2 and washed with HCl 1 M solution, $NaHCO_3$ sat. solution and brine. The organic phase was dried with anhydrous sodium sulphate and evaporated *in vacuo*. The crude product was purified by flash chromatography (AcOEt/MeOH 7:3) to obtain **7** as a white powder (193 mg, 67%). R_f= 0.55 (AcOEt/MeOH 95:5);

^{1}H NMR (400 MHz, $CDCl_3$, 25°C, TMS): δ (ppm)= 7.33 (d, ^3J(H,H)= 8.6 Hz, 2H; Ar), 6.88 (d, ^3J(H,H)= 8.6 Hz, 2H; Ar), 6.36 (s, 1H; NH), 5.84 (s, 1H; NH), 5.00 (s, 1H; NH), 4.78 (d, ^3J(H,H)= 10.3 Hz, 1H; H-7a), 4.72 (d, ^3J(H,H)= 3.3 Hz, 1H; H-1), 4.54 (d, ^3J(H,H)= 10.2 Hz, 1H; H-7b), 3.90–3.52 (m, 10H; H-3, H-4, H-5, OCH_3, $2CH_2$-α chains), 3.44 – 3.13 (m, 10H; H-2, H-6a, H-6b, OCH_3 PMB, 2H-11, 2H-12), 2.21 (m, 4H; 2H-8, 2H-10), 1.94 (m, 2H; 2H-9), 1.62 (m, 4H; $2CH_2$-β chains), 1.43 (m, 9H; $3CH_3$ Boc), 1.25 (m, 44H; $22CH_2$ chains), 0.87 (t, ^3J(H,H)= 6.7 Hz, 6H; $2CH_3$ chains); ^{13}C NMR (100 MHz, $CDCl_3$/CD_3OD 3:1, 25°C, TMS) δ (ppm)= 173.07, 172.42, 159.28, 130.24, 130.08, 113.19, 97.84, 81.50, 80.68, 79.61, 78.21, 74.64, 73.77, 71.78, 68.91, 55.31, 40.57, 39.61, 35.33, 31.89, 30.63, 30.05, 29.70, 29.50, 29.37, 28.33, 26.28, 26.03, 22.69, 21.86, 14.12; m/z calcd. for $C_{55}H_{99}N_3O_{10}$ 961.6, found 962.8 m/z $[M+H]^+$.
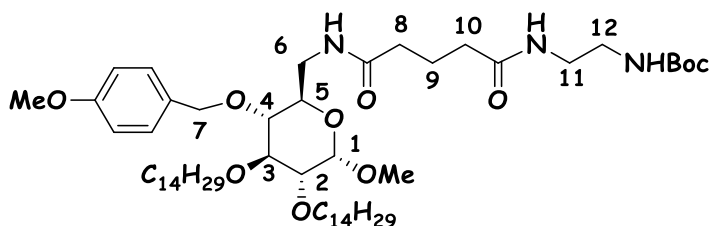
Compound 8. Compound **7** (193 mg, 0.20 mmol) was dissolved in CH_2Cl_2 (2 mL); then, the solution was cooled at 0°C and TFA (1 mL) was added. After 1.5 h the solution was concentrated *in vacuo* and the residue was treated with $NaHCO_3$ sat. solution, until basic pH was reached. The solid was filtered and washed with water, then triturated with EtP. Compound **8** was recovered after filtration as a white powder (75 mg, 73%). R_f= 0.1 (AcOEt/MeOH 9:1);

^{1}H NMR (400 MHz, CD_3OD, 25°C, TMS) δ(ppm) = 4.73 (s, 1H; H-1), 3.75 (t, ^3J(H,H)= 6.7 Hz, 2H; CH_2-α chains), 3.64 – 3.27 (m, 12H; H-3, CH_2-α chains, H-4, H-5, H-6a, H-6b, H-11a, OCH_3, H-12a), 3.26 – 3.13 (m, 2H; H-2, H-11b), 2.83 (t, ^3J(H,H)= 5.7 Hz, 1H; H-12b), 2.23 (m, 4H; 2H-8, 2H-10), 1.90 (m, 2H; 2H-9), 1.57 (m, 4H; $2CH_2$-β chains), 1.24 (m, 44H; $22CH_2$ chains), 0.86 (t, ^3J(H,H)= 6.6 Hz, 6H; $2CH_3$ chains); ^{13}C NMR (100 MHz, $CDCl_3$/CD_3OD 3:1, 25°C, TMS) δ(ppm)= 178.62, 101.77, 84.68, 84.19, 75.52, 75.15, 74.08, 58.65, 44.32, 43.93, 38.91, 35.74, 34.11, 33.84, 33.52, 33.19, 29.89, 26.48, 25.69, 17.67; m/z calcd. for $C_{42}H_{83}N_3O_7$ 741.6, found 742.8 m/z $[M+H]^+$.
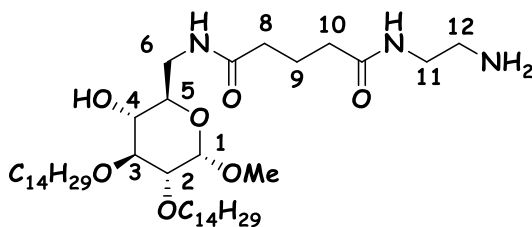
Compound IAXO-FITC-2. Compound **8** (63 mg, 0.085 mmol) and fluorescein isothiocyanate (FITC) (33 mg, 0.085 mmol) were dissolved in CH_2Cl_2/DMF 3:1 solution (2 mL) and reacted at room temperature for 2.5

h. The reaction mixture was concentrated *in vacuo* and the crude was purified by flash chromatography (AcOEt/MeOH 9:1), affording **IAXO-FITC-2** as orange powder (48 mg, 50%). R_f= 0.60 (AcOEt/MeOH 9:1);

^{1}H NMR (400 MHz, CD$_3$OD, 25°C, TMS) δ(ppm)= 8.10 (s, 1H; H-1'), 7.74 (d, ^3J(H,H)= 8.3 Hz, 1H; H-2'), 7.17 (d, ^3J(H,H)= 8.3 Hz, 1H; H-3'), 6.68 (m, 4H; H-4' H-4'', H-6', H-6''), 6.54 (dd, J_{ortho}(H,H)= 8.7 Hz, J_{meta}(H,H)= 2.2 Hz, 2H; H-5', H-5''), 4.74 (d, ^3J(H,H)= 3.4 Hz, 1H; H-1), 3.73 (m, 4H; 2CH$_2$-α-chains), 3.64 −3.32 (m, 11H; H-3, H-4, H-5, H-6a, H-6b, OCH3, CH$_2$-12, H-11a), 3.24 −3.12 (m, 2H; H-2, H-11b), 2.25 (t, ^3J(H,H)= 7.2 Hz, 4H; 2H-8, 2H-10), 1.91 (t, ^3J(H,H)= 7.4 Hz, 2H; 2H-9), 1.54 (m, 4H; 2 CH$_2$-β- chains), 1.28 (m, 44H; 22 CH$_2$ chains), 0.89 (t, ^3J(H,H)= 6.7 Hz, 6H; 2CH$_3$ chains); ^{13}C NMR (100 MHz, CD$_3$OD, 25°C, TMS) δ(ppm)= 174.60, 174.45, 169.67, 128.98, 109.76, 97.55, 80.91, 80.07, 73.21, 71.45, 70.79, 70.13, 54.06, 39.86, 38.30, 34.76, 31.68, 30.01, 29.77, 29.46, 29.12, 25.83, 22.37, 21.85, 13.07; m/z calcd. for C$_{63}$H$_{94}$N$_4$O$_{12}$S 1130.7, found 1131.8 m/z [M+H]$^+$.
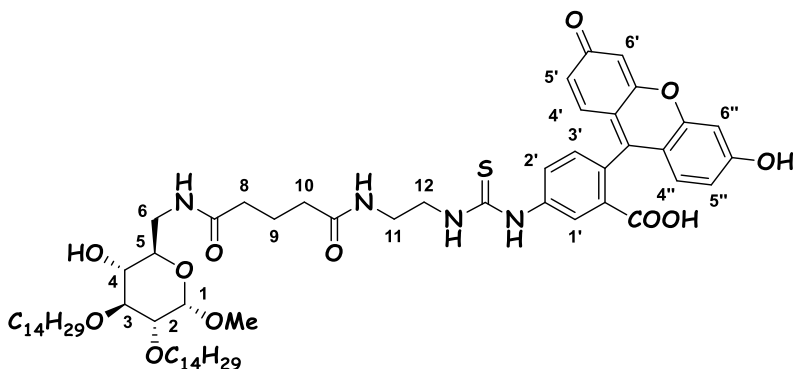
Compound IAXO-D1. Compound **11** was obtained from PMB-IAXO-102 according to published procedures.[65] LiAlH$_4$ (43 mg, 1.12 mmol) was

suspended in dry THF (5 mL), under argon atmosphere, and a solution of **11** (177 mg, 0.14 mmol) in dry CH_2Cl_2 (3 mL) was added. The mixture was stirred at 50° C for 4 h, when the TLC (CH_2Cl_2/MeOH 9:1, 1% NH_3) showed complete consumption of starting materials. The reaction was cooled to 0° C and quenched with AcOEt and MeOH. The solution was evaporated *in vacuo* and the crude was dissolved in CH_2Cl_2 and stirred with a saturated aqueous solution of Rochelle salt (potassium sodium tartrate, $KNaC_4H_4O_6$) for 2 h. The water phase was extracted with CH_2Cl_2; then, the organic phase was dried with anhydrous sodium sulphate and evaporated *in vacuo*. The crude was purified by flash chromatography (CH_2Cl_2/MeOH 95:5, 0,1% TEA) affording **IAXO-D1** (134 mg, 78%) as white powder. R_f= 0.43 (CH_2Cl_2/MeOH 9:1, 1% NH_3);

^{1}H NMR (400 MHz, CDCl$_3$, 25°C, TMS) δ (ppm) = 4.77 (d, ^3J(H,H)= 3.0 Hz, 2H; H-1, H-1'), 3.82 (dd, ^3J(H,H)= 16.0, 7.3 Hz, 2H; H-5, H-5'), 3.71 (m, 4H; 2CH$_2$-α chains), 3.64-3.36 (m, 14H; 2CH$_2$-α chains, H-3, H-3', 2OCH$_3$, H4, H-4'), 3.27 (dd, ^3J(H,H)= 9.4, 3.5 Hz, 2H; H-2, H-2'), 2.92 (m, 4H; CH$_2$-6, CH$_2$-6'), 2.73 (m, 4H; CH$_2$-7, CH$_2$-7'), 1.67 (m, 4H; CH$_2$-8, CH$_2$-8'), 1.57 (m, 8H; 4CH$_2$-β chains), 1.30 (m, 88H, 44CH$_2$ chains), 0.87 (t, ^3J= 6.7 Hz, 12H; 4CH$_3$);
^{13}C NMR (100 MHz, CD$_3$OD, 25°C, TMS) δ (ppm)= 98.12, 80.64, 79.82, 73.28, 71.79, 70.63, 67.45, 54.90, 48.74, 47.17, 29.79, 29.25, 23.14, 13.07; m/z calcd. for $C_{74}H_{148}N_2O_{10}$: 1225.1 found 1225.8 [M+H]$^+$.
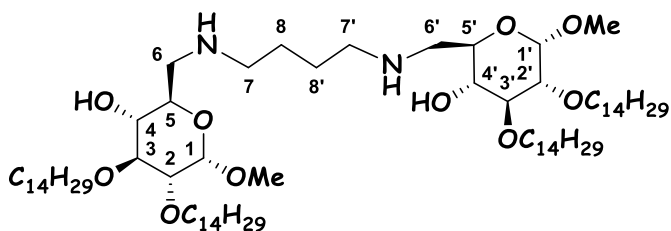
Compound IAXO-D2. Compound **IAXO-D1** (30 mg, 0.024 mmol) was dissolved in dry DMF (1 mL) under argon atmosphere, then Na_2CO_3 (23 mg, 0.15 mmol) and CH_3I (6.7 µl, 0.11 mmol) were added and the mixture was stirred at 40° C for 24 h. The solution was concentrated *in vacuo* and the crude was triturated in Et_2O, affording **IAXO-D2** as a white powder (27 mg, 73%). R_f= 0.02 (AcOEt/MeOH 8:2);

^{1}H NMR (400 MHz, $CDCl_3$, 25°C, TMS) δ(ppm)= 4.77 (d, ^3J(H,H)= 3.0 Hz, 2H; H-1, H-1'), 4.16-3.67 (m,12H; H-5, H-5', 2CH_2-α chains, H-6, H-6', CH_2-7, CH_2-7'), 3.65-3.54 (m, 6H; 2CH_2-α chains, H-3, H-3'), 3.53-3.43 (m, 8H; H-6, H-6', 2OCH_3), 3.39-3.25 (m, 14H; H-4, H-4', 4NCH_3), 3.20 (m, 2H; H-2, H-2'), 2.17 (m, 4H; CH_2-8, CH_2-8'), 1.56 (m, 8H; 4CH_2-β chains), 1.21 (m, 88H, 44CH_2 chains), 0.87 (t, ^3J= 6.7 Hz, 12H; 4CH_3); ^{13}C NMR (100 MHz, $CDCl_3$, 25°C, TMS) δ (ppm)=99.28, 79.85, 79.55, 73.75, 71.89, 71.50, 66.86, 65.84, 65.26, 57.47, 53.12, 52.03, 30.17, 29.44, 19.69, 13.98; m/z calcd. for $C_{78}H_{159}N_2O_{10}$: 1283.2, found 641.8 m/z $[M/2]^+$.
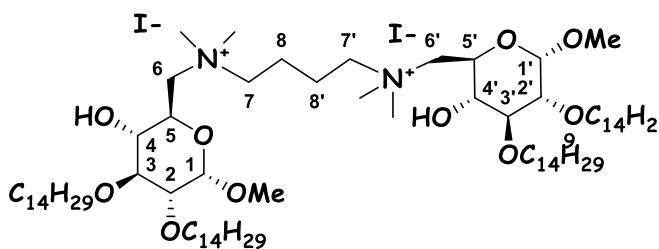
Compound IAXO-Z1. Compound IAXO-102 (97 mg, 0.17 mmol) was dissolved in dry CH_3CN (2 mL), under argon atmosphere and the solution

was heated to 65°C. A solution of 1,3-propanesultone (15 µL, 0.17 mmol) in dry CH$_3$CN (0.5 mL) was added dropwise and the reaction mixture was stirred at 65°C for 24 h. The reaction mixture was concentrated *in vacuo* and the crude was purified by flash chromatography (AcOEt/MeOH 8:2), affording **IAXO-Z1** as white powder (108 mg, 90%). R_f= 0.75 (AcOEt/MeOH 6:4);

^{1}H NMR (400 MHz, CD$_3$OD-CDCl$_3$ 3:1, 25°C, TMS) δ(ppm)= 4.84 (under water signal; H-1), 3.75 (m, 3H; H-3, H-5, CH-α-chains), 3.68 –3.51 (m, 3H; CH$_2$-α-chains), 3.46 (s, 3H; OCH$_3$), 3.44-3.34 (m, 2H; H-4, H-6), 3.28-3.16 (m, 3H; H-2, CH$_2$-7), 3.09 (m, 1H; H-6'), 2.94 (t, ^3J(H,H)= 6.5 Hz, 2H; CH$_2$-9), 2.15 (m, 2H; CH$_2$-8), 1.61 (m, 4H; 2CH$_2$-β-chains), 1.31 (m, 44H; 22 CH$_2$-chains), 0.89 (m, 6H; 2CH$_3$-chains); ^{13}C NMR (100 MHz, CD$_3$OD-CDCl$_3$ 6:1, 25°C, TMS) δ(ppm)= 98.34, 80.89, 80.41, 73.48, 71.52, 55.41, 50.29, 49.00, 30.24, 26.75, 13.89; m/z calcd. for C$_{38}$H$_{77}$NO$_8$S 707.5, found 708.7 m/z [M+H]$^+$, 706.7 m/z [M-H]$^-$.
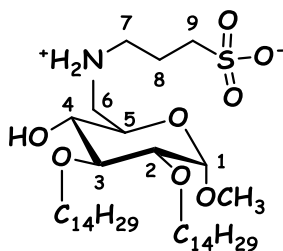
Compound 21. D- (-)-Lyxose (5 g, 33.30 mmol) was suspended in acetone (40 mL) and DMP (10 mL, 83.26 mmol) was added. HClO4 60% (2.33 mL, 34.97 mmol) was added drop wise at 0°C. The reaction mixture was stirred at 0°C for 30 min and RT for 2 h. Then, MeOH (7 mL) was added and the

reaction mixture was stirred RT for 3 more hours. The reaction was cooled to 0° C and quenched with a solution of Na_2CO_3 (3.2 g in 10 mL of H_2O). The solid precipitate was filtered and the solution was concentrated *in vacuo*; the crude was dissolved in Et_2O and washed with brine. The organic phase was dried with anhydrous sodium sulphate and evaporated *in vacuo*, affording **21** as a light yellow oil (6.745 g, 99%). It was used for subsequent reactions without further purifications. R_f= 0.53 (EtP/AcOEt 4:6);

^{1}H NMR (400 MHz, CDCl₃, 25°C, TMS) δ (ppm) = 4.94 (s, 1H; H-1), 4.78 (dd, [3]*J*(H,H)= 5.9, 3.8 Hz, 1H; H-2), 4.58 (d, [3]*J*(H,H)= 5.9, 1H; H-3), 4.04 (m, 1H; H-4), 3.95 (m, 2H; CH_2-5), 3.33 (s, 3H; OCH_3), 2.17 (s, 1H; OH), 1.47 (s, 3H; CH_3), 1.30 (s, 3H; CH_3); m/z calcd. for $C_9H_{16}O_5$ 204.10, found 205.2 m/z [M+H]⁺.
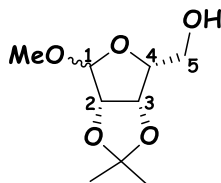
Compound 22. Compound **21** (160 mg, 0.78 mmol) was dissolved in dry benzene (15 mL), under argon atmosphere. The reaction flask was equipped with a Dean-Stark apparatus filled with the solvent. The system was brought to reflux (80°C) and PCC (420 mg, 1.95 mmol) was added in five portions over 2.5 h. The reaction mixture was stirred at reflux overnight. After cooling to RT, celite powder was added and stirred for 30 min. Then, the mixture was filtered. The solution was recovered and the Dean-Stark apparatus was assembled again, filled with fresh solvent and

brought to reflux, again. PCC was added (420 mg, 1.95 mmol) in five portions over 2.5 h. It was stirred at reflux overnight. After cooling to RT, celite powder was added and stirred for 30 min; then, the mixture was filtered. Solvents were evaporated *in vacuo* and the crude was purified on flash chromatography (EtP/AcOEt 7:1) affording **22** (70 mg, 28%). R_f= 0.78 (EtP/AcOEt 4.5:5.5);

^{1}H NMR (400 MHz, CDCl$_3$, 25°C, TMS) δ (ppm) = 5.33 (s, 1H; H-1), 4.80 (d, ^3J(H,H)= 5.4, 1H; H-2), 4.55 (d, ^3J(H,H)= 5.4, 1H; H-3), 3.52 (s, 3H; OCH$_3$), 1.45 (s, 3H; CH$_3$), 1.37 (s, 3H; CH$_3$); m/z calcd. for C$_8$H$_{12}$O$_5$ 188.07, found 189.2 m/z [M+H]$^+$.
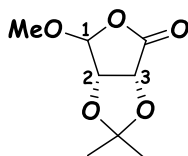
Compound 23. Dimethyl methylphosphonate (57 µL, 0.53 mmol) was dissolved in dry THF (4 mL) and cooled to -78°C. Then, *n*-BuLi 1.6 M in hexane (330 µL, 0.53 mmol) was slowly added dropwise and stirred for 30 min. A solution of **22** (100 mg, 0.53 mmol) in dry THF (1 mL) was added and it was stirred at -78°C for 2.5 h and at RT for 30 min. The reaction was cooled to 0° C and quenched with AcOEt. The mixture was washed with H$_2$O and the organic phase was dried with anhydrous sodium sulphate and evaporated *in vacuo*, affording **23** (50 mg, 62%). R_f= 0.60 (EtP/AcOEt 6:4);

^{1}H NMR (400 MHz, CDCl$_3$, 25°C, TMS) δ (ppm) =7.60 (dd, ^3J(H,H)= 5.9, 2.2, 1H; H-2), 6.21 (d, ^3J(H,H)= 5.9, 1H; H-1), 5.26 (dd, ^3J(H,H)= 5.4, 1.7, 1H; H-

3), 4.46 (d, ^3J(H,H)= 5.5, 1H; H-4), 1.41 (s, 6H; CH$_3$); m/z calcd. for m/z calcd. for C$_8$H$_{10}$O$_3$ 154.06, found 155.1 m/z [M+H]$^+$.
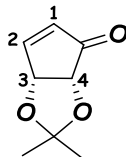

Compound 24. Compound **23** (65 mg, 0.42 mmol) was dissolved in dry CH$_2$Cl$_2$/MeOH 1:2 (6 mL), under argon atmosphere, and a catalytic amount of Pd/C was added. H$_{2(g)}$ was supplied and the reaction mixture was stirred RT for 4 h. The solid catalyst was eliminated after filtration on a celite cake and the solvents were evaporated under *vacuo*, affording **24** (64 mg, 98%) as white powder. R_f= 0.79 (EtP/AcOEt 6:4).

Alternatively, compound **25** (500 mg, 4.30 mmol) was dissolved in dry CH$_2$Cl$_2$ (10 mL), under argon atmosphere and the reaction was cooled to 0°C. DMP (5 mL, 43.05 mmol) and TsOH (4 mg, 0.022 mmol) were added and the reaction mixture was stirred for 3 h. The reaction was treated with NaHCO$_3$ sat. solution to neutralise the acid residue. The mixture was washed with brine and the water phase was washed with AcOEt. The organic phases were pooled, dried with anhydrous sodium sulphate and evaporated *in vacuo*. The crude was purified by flash chromatography (EtP/AcOEt 9:1), affording **24** (126 mg, 20%) as white powder. R_f= 0.62 (EtP/AcOEt 1:1);

^{1}H NMR (400 MHz, CDCl$_3$, 25°C, TMS) δ (ppm) = 4.83 (m, 1H; H-3), 4.18 (m, 1H; H-4), 2.58 (m, 1H; CH-2), 2.27 (m, 2H; CH$_2$-1), 2.04 (m, 1H; CH-2'), 1.41

(s, 3H; CH$_3$), 1.34 (s, 3H; CH$_3$) ; m/z calcd. for C$_8$H$_{10}$O$_3$ 156.08, found 157.1 m/z [M+H]$^+$.
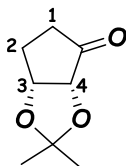
Zeolite-Os^0 catalyst. OsCl$_3$·xH$_2$0 (77 mg) was dissolved in H$_2$0 (100 mL). Zeolite Y was added (1 g) and the suspension was stirred for 72 h. When the supernatant switched from a dark colour to colourless, the catalyst was filtered, washed with water three times and dried under *vacuo*. Then the powder was slowly added (over 2 h) to a stirring aqueous solution of NaBH$_4$ (150 mM, 250 mL) and it was stirred for two more hours. After filtration and washing with water, the solid catalyst was dried under *vacuo* overnight. **Zeolite-Os^0** was recovered as a grey powder (1 g).

Compound 25. 3-Cyclopenten-1-one (0.5 mL, 5.97 mmol) was dissolved in a mixture of acetone/water (9:1, 30 mL) and 30% H$_2$O$_2$ (925 µL, 29.85 mmol, in 5 portions) and Zeolite-Os^0 catalyst (300 mg) were added. The reaction was stirred RT for 36 h. After centrifugation (6000 rpm, 10 min x 2), the supernatant was treated with NaHSO$_3$ under stirring for 10 min. After filtration on a celite cake, the solvents were evaporated and the crude was purified on flash chromatography (EtP/AcOEt 5:5), affording **25** (74 mg, 11%). R_f= 0.11 (EtP/AcOEt 4:6));

^{1}H NMR (400 MHz, CDCl$_3$, 25°C, TMS) δ (ppm) = 4.39 (m, 1H; H-3), 4.13 (m, 1H; H-4), 2.34 (m, 2H; CH$_2$-1), 2.14 (m, 2H; CH$_2$-2); ^{13}C NMR (100 MHz, CDCl$_3$, 25°C, TMS) δ (ppm)= 216.76, 78.70, 69.96, 30.75, 24.36; m/z calcd. for C$_5$H$_8$O$_3$ 116.05, found 139.1 m/z [M+Na]$^+$.
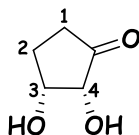

Compound 27a. 3-cyclopentene-1-carboxylic acid (300 µL, 2.47 mmol) was dissolved in dry CH$_2$Cl$_2$ (5 mL) and DCC was added (612 mg, 2.96 mmol), under argon atmosphere, and it was stirred RT for 30 min. A suspension of tyrosol (375 mg, 2.71 mmol) and DMAP (cat) in CH$_2$Cl$_2$ (5 mL) was added in five portions during 2 h. The reaction was stirred RT overnight. After filtration, the solvents were evaporated *in vacuo* and the crude was purified on flash chromatography (EtP/AcOEt 9:1), affording **27a** (110 mg, 55%) and **27b**, as side product. R_f= 0.84 (EtP/AcOEt 1:1);

^{1}H NMR (400 MHz, CDCl$_3$, 25°C, TMS) δ (ppm) = 7.23 (d, ^3J(H,H)= 8.4 Hz, 2H; H-A3, H-A5), 7.02 (d, ^3J(H,H)= 8.4 Hz, 2H; H-A2, H-A6), 5.71 (m, 2H; CH-6, CH-7), 3.84 (t, ^3J(H,H)= 6.5 Hz, 2H; CH$_2$-2), 3.37 (m, 1H; CH-4), 2.85 (m, 2H, CH$_2$-1), 2.79 (m, 4H, CH$_2$-5, CH$_2$-8); ^{13}C NMR (100 MHz, CDCl$_3$, 25°C, TMS) δ (ppm)= 175.33, 149.95, 136.31, 130.42, 129.38, 121.99, 64.00, 42.06, 39.00, 36.82; m/z calcd. For C$_{14}$H$_{16}$O$_3$: 232.1 found 255.2 m/z [*M*+Na]$^+$, 233.2 m/z [*M*+H]$^+$.
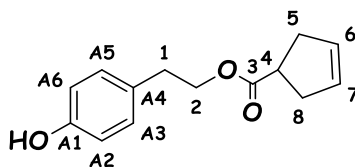
Compound 28. Compound **27a** (200 mg, 0.86 mmol) was dissolved in a mixture of acetone/PBS buffer (pH=7.4) 9:1 (5 mL) and NMO (202 mg, 1.72 mmol) and OsO_4 25% in *t*-BuOH (440 µL, 0.044 mmol) were added. The reaction was stirred RT for 3 h. The reaction mixture was treated with a solution of $NaHSO_3$ (140 mg in 1.4 mL of water) and stirred for 1h. The solution was concentred *in vacuo*, diluted with CH_2Cl_2 and washed with brine. The organic phase was dried with anhydrous sodium sulphate and evaporated *in vacuo*. The crude was purified by flash chromatography (EtP/AcOEt 2:8), affording **28** (170 mg, 74%) as white powder. R_f= 0.15 (EtP/AcOEt 4:6);

^{1}H NMR (400 MHz, CD$_3$OD, 25°C, TMS) δ (ppm) = 7.24 (d, ^3J(H,H)= 8.1 Hz, 2H; H-A3, H-A5), 6.97 (d, ^3J(H,H)= 8.3 Hz, 2H; H-A2, H-A6), 4.11 (m, 2H; CH-6, CH-7), 3.74 (t, ^3J(H,H)= 6.9 Hz, 2H; CH$_2$-2), 3.32 (m, 1H; CH-4), 2.81 (t, ^3J(H,H)= 6.9 Hz, 2H, CH$_2$-1), 2.10 (m, 4H, CH$_2$-5, CH$_2$-8); ^{13}C NMR (100 MHz, CD$_3$OD, 25°C, TMS) δ (ppm)= 175.40, 149.55, 136.69, 129.57, 121.00, 73.14, 63.70, 38.97, 38.16, 33.85; m/z calcd. for $C_{14}H_{18}O_5$: 266.1 found 267.2 m/z [*M*+H]$^+$, 284.2 m/z [*M*+H$_2$O]$^+$, 289.2 m/z [*M*+Na]$^+$.
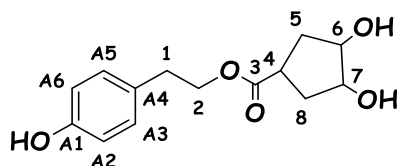
Amberlite-IO$_4^-$. Amberlite IRA-900 Cl$^-$ was suspended in water (20 mL) and NaIO$_4$ (2 g) was added. The mixture was vigorously stirred RT for 6 h. The solvent was decanted and a fresh solution of NaIO$_4$ (2 g) in water (20 mL) was added and stirred overnight. The resin was filtered and washed with water (4 x 20 mL), THF (2 x 10 mL) and Et$_2$O (2 x 10 mL) and dried under *vacuo* over night. **Amberlite-IO$_4^-$** was recovered (1.707 g).

Compound 29. Compound **28** (47 mg, 0.18 mmol) was dissolved in CH$_3$CN/H$_2$O 14:1 (1.5 mL) and **Amberlite-IO$_4^-$** resin (220 mg, 0.35 mmol IO$_4^-$) was added. The reaction was stirred RT for 2 h. The reaction mixture was filtered and the solvents evaporated *in vacuo*. A mixture of **29** and rearrangement and degradation products was recovered (36 mg). R_f= 0.11; 0.28 (CH$_2$Cl$_2$/MeOH 95:5).
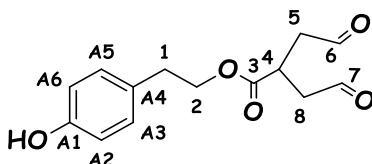
Compound 30. 3-(4-hydroxyphenyl)propionic acid (50 mg, 0.30 mmol) was dissolved in dry DMF (1 mL), under argon atmosphere. TBSCl (91 mg, 0.60 mmol) and imidazole (82 mg, 1.20 mmol) were added and the reaction was stirred RT for 24 h. The solvent was evaporated *in vacuo* and the crude was dissolved in Et$_2$O and washed with brine. The organic phase was dried with anhydrous sodium sulphate and evaporated *in vacuo*. The crude was dissolved in THF (1.5 mL) and MeOH (4 mL) and a solution of

K_2CO_3 (0.7 M, 1.3 mL) were added dropwise and stirred for 20 min. Solvents were evaporated and the crude was dissolved with Et_2O and brine and a solution of HCl was added dropwise until pH=6 was reached. Then, the organic phase was extracted, dried with anhydrous sodium sulphate and evaporated *in vacuo*. Compound **30** (506 mg, 92%) was obtained without further purifications. R_f= 0.46 (EtP/AcOEt 1:1);

^{1}H NMR (400 MHz, $CDCl_3$, 25°C, TMS) δ (ppm) = 7.04 (d, ^3J(H,H)= 8.5 Hz, 2H; H-A3, H-A5), 6.74 (d, ^3J(H,H)= 8.5 Hz, 2H; H-A2, H-A6), 2.88 (t, ^3J(H,H)= 7.8 Hz, 2H; CH_2-1), 2.64 (t, ^3J(H,H)= 7.8 Hz, 2H; CH_2-2), 0.97 (s, 9H, CH_3 t-Bu), 0.18 (s, 6H, CH_3 Si); ^{13}C NMR (100 MHz, $CDCl_3$, 25°C, TMS) δ (ppm)= 179.09, 154.5, 132.78, 129.15, 120.07, 35.83, 29.82, 25.68, 4.45; m/z calcd. For $C_{15}H_{24}O_3Si$: 280.15, found 281.2 m/z [M+H]$^+$.
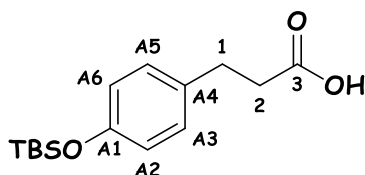
Compound 31. Compound **30** (120 mg, 0.43 mmol) was dissolved in dry CH_2Cl_2 (4 mL) and DCC was added (104 mg, 0.51 mmol), under argon atmosphere, and it was stirred RT for 30 min. Then, 1-cycloesen-4-olo (45 μL, 0.39 mmol) and DMAP (cat) were added. The reaction was stirred RT for 20 h. After filtration, the solvents were evaporated *in vacuo* and the crude was purified on flash chromatography (EtP/AcOEt 98:2), affording **31** (125 mg, 78%). R_f= 0.88 (EtP/AcOEt 6:4);

^{1}H NMR (400 MHz, $CDCl_3$, 25°C, TMS) δ (ppm) = 7.04 (d, ^3J(H,H)= 8.5 Hz, 2H; H-A3, H-A5), 6.74 (d, ^3J(H,H)= 8.5 Hz, 2H; H-A2, H-A6), 5.65 (q, ^3J(H,H)=

12.5 Hz, 2H; CH-7, CH-8), 3.96 (d, ^3J(H,H)= 6.6 Hz 2H; CH$_2$-4), 2.88 (t, ^3J(H,H)= 7.8 Hz, 2H; CH$_2$-1), 2.60 (t, ^3J(H,H)= 7.8 Hz, 2H; CH$_2$-2), 2.04 (m, 2H; CH$_2$-9), 1.91 (m, 1H; CH-5), 1.74 (m, 2H; CH$_2$-6), 1.26 (m, 2H, CH$_2$-10), 0.97 (s, 9H, CH$_3$ t-Bu), 0.17 (s, 6H, CH$_3$ Si); ^{13}C NMR (100 MHz, CDCl$_3$, 25°C, TMS) δ (ppm)= 173.16, 154, 133.15, 129.11, 127.01, 125.48, 119.98, 68.72, 36.17, 32.97, 30.26, 28.11, 25.67, 25.34, 24.28, 18.17, 4.45; m/z calcd. For C$_{22}$H$_{34}$O$_3$Si: 374.23 found 397.3 [M+Na]$^+$.
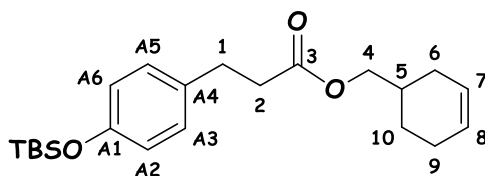
Compound 32. Compound **31** (100 mg, 0.27 mmol) was dissolved in dry CH$_2$Cl$_2$ (5 mL), under argon atmosphere, and it was cooled to 0°C. Then, a solution of TBAF (211 mg, 0.67 mmol) and AcOH (61 µL, 1.07 mmol) in CH$_2$Cl$_2$ (2 mL) was added dropwise. The reaction was stirred RT for 24 h. The reaction mixture was washed with NaHCO$_3$ sat. solution. The organic phase was dried with anhydrous sodium sulphate and evaporated *in vacuo*. The crude was purified by flash chromatography (EtP/AcOEt 8:2), affording **32** (70 mg, 100%) as white powder. R_f= 0.17 (EtP/AcOEt 9:1);

^{1}H NMR (400 MHz, CDCl$_3$, 25°C, TMS) δ (ppm) = 7.06 (d, ^3J(H,H)= 8.4 Hz, 2H; H-A3, H-A5), 6.74 (d, ^3J(H,H)= 8.5 Hz, 2H; H-A2, H-A6), 5.65 (m, 2H; CH-7, CH-8), 3.97 (d, ^3J(H,H)= 6.6 Hz 2H; CH$_2$-4), 2.88 (t, ^3J(H,H)= 7.7 Hz, 2H; CH$_2$-1), 2.61 (t, ^3J(H,H)= 7.7 Hz, 2H; CH$_2$-2), 2.04 (m, 2H; CH$_2$-9), 1.90 (m, 1H; CH-5), 1.71 (m, 2H; CH$_2$-6), 1.27 (m, 2H, CH$_2$-10); ^{13}C NMR (100 MHz, CDCl$_3$, 25°C, TMS) δ (ppm)= 173.16, 154, 133.15, 129.11, 127.01, 125.48,

119.98, 68.72, 36.17, 32.97, 30.26, 28.11, 25.67, 24.28; m/z calcd. For $C_{16}H_{20}O_3$: 260.14 found 261.4 $[M+H]^+$.
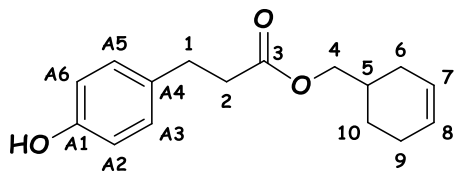
Compound 33. Compound **32** (110 mg, 0.42 mmol) was dissolved in a mixture of acetone/PBS buffer (pH=7.4) 9:1 (2.5 mL) and NMO (98 mg, 0.84 mmol) and OsO_4 25% in t-BuOH (210 μL, 0.021 mmol) were added. The reaction was stirred RT for 3 h. The reaction mixture was treated with a solution of $NaHSO_3$ (70 mg in 0.7 mL of water) and stirred for 1h. The solution was concentred *in vacuo*, diluted with CH_2Cl_2 and washed with brine. The organic phase was dried with anhydrous sodium sulphate and evaporated in vacuo. The crude was purified by flash chromatography (EtP/AcOEt 2:8), affording **33** (105 mg, 67%) as white powder. R_f= 0.13 (EtP/AcOEt 4:6);
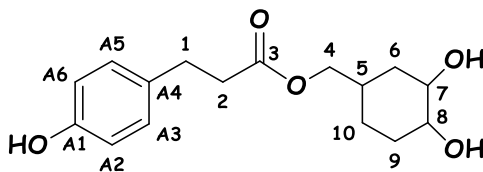
^1H NMR (400 MHz, CD_3OD, 25°C, TMS) δ (ppm) = 7.01 (d, ^3J(H,H)= 8.4 Hz, 2H; H-A3, H-A5), 6.68 (d, ^3J(H,H)= 8.4 Hz, 2H; H-A2, H-A6), 3.88 (m, 2H; CH_2-4), 3.49 (m, 2H; CH-7, CH-8), 2.82 (t, ^3J(H,H)= 7.1 Hz, 2H; CH_2-1), 2.57 (t, ^3J(H,H)= 7.4 Hz, 2H; CH_2-2), 1.96 (m, 1H; CH-5), 1.63 (m, 2H; CH_2-6), 1.40-1.24 (m, 4H, CH_2-9, CH_2-10); ^{13}C NMR (100 MHz, CD_3OD, 25°C, TMS) δ (ppm)= 173.44, 155.38, 131.13, 128.95, 114.17, 71.08, 68.35, 35.67, 30.80, 29.63, 26.68, 21.39; m/z calcd. For $C_{16}H_{22}O_5$: 294.15 found 317.3 $[M+Na]^+$.

179

Compound 34. Compound **33** (36 mg, 0.12 mmol) was dissolved in CH$_3$CN/H$_2$O 10:1 (1.1 mL) and **Amberlite-IO$_4$$^-$** resin (150 mg, 0.24 mmol IO$_4$$^-$) was added. The reaction was stirred RT for 2 h. The reaction mixture was filtered, washed with CH$_3$CN and Et$_2$O and the solvents were evaporated *in vacuo*. Compound **34** was recovered (35 mg, 100%) as white powder. R_f= 0.22 (CH$_2$Cl$_2$/MeOH 95:5);

^{1}H NMR (400 MHz, DMSO d-6, 25°C, TMS) δ (ppm) = 9.61 (d, ^3J(H,H)= 9.5 Hz, 2H; H-7, H-8), 9.14 (s, 1H, OH), 6.97 (d, ^3J(H,H)= 8.4 Hz, 2H; H-A3, H-A5), 6.63 (d, ^3J(H,H)= 8.4 Hz, 2H; H-A2, H-A6), 3.90 (dd, ^3J(H,H)= 19.2, 5.8 Hz, 2H; CH$_2$-4), 2.70 (t, ^3J(H,H)= 7.5 Hz, 2H; CH$_2$-1), 2.57-2.40 (m, 4H; CH$_2$-2, CH$_2$-6), 2.36 (m, 2H; CH$_2$-9), 2.18 (m, 1H; CH-5), 1.49 (m, 2H, CH$_2$-10; ^{13}C NMR (100 MHz, DMSO d-6, 25°C, TMS) δ (ppm)= 203.32, 202.99, (C-8, C-7), 177.65 (C-3), 156.03 (C-A1), 130.87 (C-A4), 129.48 (C-A3, C-A5), 115.50 (C-A2, C-A6), 66.20 (C-4), 45.41 (C-9), 40.77 (C-6), 35.87 (C-2), 31.81 (C-4), 29.89 (C-1), 23.35 (C-10); m/z calcd. For C$_{16}$H$_{20}$O$_5$: 292.13 found 315.20 m/z [*M*+Na]$^+$.
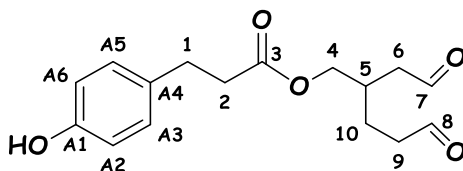
Compound 35. Compound **6** (43 mg, 0.5 mmol) was dissolved in CH_2Cl_2 (2 mL) and it was cooled to 0°C. Then, TFA (1 mL) was added dropwise. The reaction was stirred RT for 1.5 h. The mixture was washed with water and the organic phase was dried with anhydrous sodium sulphate and evaporated *in vacuo*. The crude was triturated with Et_2O, affording **35** (16 mg, 46%). R_f= 0.15 (AcOEt/MeOH 9:1);

^{1}H NMR (400 MHz, $CDCl_3$, 25°C, TMS) δ(ppm)= 6.13 (m, 1H, NH), 4.72 (m, 1H; H-1), 3.95 (m, 1H; H-6), 3.77 (m, 2H; CH_2-α chains), 3.55 (m, 4H; H-3, H-5, CH_2-α chains), 3.38 (s, 3H, OCH_3), 3.30 – 3.12 (m, 3H; H-2, H-4, H-6'), 2.43 (m, 2H; CH_2-9), 2.34 (m, 2H; CH_2-7), 1.99 (m, 2H; CH_2-8), 1.57 (m, 4H; $2CH_2$-β chains), 1.24 (m, 44H; $22CH_2$ chains), 0.87 (t, ^3J(H,H)= 6.7 Hz, 6H; $2CH_3$ chains); ^{13}C NMR (100 MHz, $CDCl_3$, 25°C, TMS) δ(ppm)= 178.17, 172.435, 101.57, 84.74, 84.05, 75.68, 75.25, 73.85, 56.66, 39.81, 36.02, 34.00, 34.11, 33.62, 33.17, 30.03, 26.68, 25.73, 17.68; m/z calcd. for $C_{40}H_{77}NO_8$: 699.56, found 700.8 m/z $[M+H]^+$.
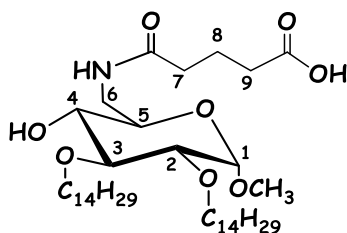
3.3 NMR spectroscopy binding studies

3.3.1 Interaction studies between LptC and LPS

NMR experiments were recorded on a Varian 400 MHz Mercury. The protein LptC was lyophilized and dissolved in 10 mM deuterated phosphate buffer, pH 7.4 just before use. ANS was dissolved in 10 mM deuterated phosphate buffer, pH 7.4 and added to the protein solution to a final concentration of 1 mM. Lyophilized LOS from *E. coli* MG1655 was dissolved in 10 mM deuterated phosphate buffer, pH 7.4, or used as powder, to be added to the protein-ANS solution. The pH of each sample was verified with a Microelectrode (Mettler Toledo) for 5 mm NMR tubes and adjusted with small amounts of NaOD or DCl. All pH values were corrected for isotope effect. The acquisition temperature was 298K. Basic sequences were employed for ^{1}H, 2D-NOESY and STD experiments. For STD, a train of Gaussian-shaped pulses of 50 ms each was employed to saturate selectively the protein envelope; the total saturation time of the protein envelope was adjusted by the number of shaped pulses and was varied between 3 s and 0.35 s.

3.3.2 Interaction studies between TLR4 antagonists and MD-2

NMR experiments were performed with a Bruker 600 MHz DRX spectrometer equipped with a cryoprobe. ^{1}H NMR spectra were recorded at 298 K, by acquisition of 120 scans. DOSY spectra were recorded at 311 K with the stebpgls19 Bruker pulse sequence by acquisition of 160 scans, with a diffusion time of 300 ms, a gradient length of 1.9 ms and a gradient

ramp from 2% to 95% in 32 linear steps. Protein samples were prepared by diluting the stock solution of MD-2 (0.11 mM in deuterated acetate buffer at pH 5) with the same buffer. Ligand samples were prepared by dissolving the solid compound **MPD-1** in deuterated acetate buffer at pH 5. For ^{1}H NMR experiments the final concentrations reached for the analyzed samples were 30 µM MD-2 and 150 µM compound **MPD-1**, whereas for DOSY experiments final concentrations of 60 µM MD-2 and 300 µM compound **MPD-1** were needed.

3.4 Biological characterization

3.4.1 HEK-blue^{TM} assay

HEK-Blue-TLR4 cells (InvivoGen) were cultured according to manufacturer's instructions. Briefly, cells were cultured in DMEM high glucose medium supplemented with 10% fetal bovine serum (FBS), 2 mM glutamine, 1x Normocin (InvivoGen), 1x HEK-Blue Selection (InvivoGen). Cells were detached by the use of a cell scraper and the cell concentration was estimated using Trypan Blue (Sigma Aldrich). The cells were diluted in DMEM high glucose medium, supplemented as described before and seeded in multiwell plate at a density of $2x10^4$ cells per well in 200 µL. After overnight incubation (37°C, 5% CO_2, 95% humidity), supernatant was removed, cell monolayers were washed with warm PBS without Ca^{2+} and Mg^{2+} and treated with compounds (from 0 to 200 µM) dissolved in DMSO-ethanol (1:1). After 30 minutes, the cells were stimulated with 10 ng/ml of LPS from *E. coli* O55:B5 (Sigma Aldrich) and incubated overnight at 37°C, 5% CO_2 and 95% humidity. As a control, the cells were treated with or without LPS (10 ng/ml) alone. Then, the supernatants were collected and 50µL of each sample was added to 100 µL PBS, pH 8, 0.84 mM para-Nitrophenylphosphate (pNPP) for a final concentration of 0.8 mM pNPP. Plates were incubated for 2-4 h in the dark at RT and then the plate reading was assessed by using a spectrophotometer at 405 nm (LT 4000, Labtech). The results were normalized with positive control (LPS alone) and expressed as the mean of percentage ± SD of 3 independent experiments.

3.4.2 MTT cell viability assay

HEK-Blue cells were seeded in 100 µL DMEM without Phenol Red at a density of 2×10^4 cells per well. After overnight incubation, 10 µL compounds (from 0 to 200 µM) were added and the plates were incubated overnight at 37 °C, 5% CO_2, 95% humidity. DMSO and PBS were included as controls. Then 10 µl of MTT solution (5 mg/mL in PBS) were added to each well. After 3 h incubation (37 °C, 5% CO_2, 95% humidity), HCl 0.1 N in isopropanol was added (100 µl/well) to dissolve formazan crystals. Formazan concentration in the wells was determined measuring the absorbance at 570 nm (LT 4000, Labtech). The results were normalized with untreated control (PBS) and expressed as the mean of percentage ± SD of 3 independent experiments.

3.4.3 Determination of CMC (Critical Micelle Concentration)

To assess the amphiphilicity, the critical micelle concentrations (CMC) of compounds have been determined using an established fluorescence technique based on pyrene. This extremely hydrophobic dye is preferentially incorporated in the interior of micelles. The onset of micelle formation can be observed in a shift of the fluorescence excitation spectra of the samples at an emission wavelength of 372 nm. In the concentration range of aqueous micellar solutions, a shift of the excitation band in the 335 nm region toward higher wavelengths confirms the incorporation of pyrene in the hydrophobic interior of micelles. The ratio of the fluorescence intensities at 339 and 335 nm was used to quantify the shift of the broad excitation band. The critical micelle concentrations were

determined from the crossover point in the low concentration range. Fluorescence spectra were recorded with an F-2500 Hitachi spectrofluorophotometer and conventional 1 cm quartz cuvettes at 37 ± 0.1 °C, using 2.5 mm excitation and emission slits.

3.5 Computational studies

3D coordinates of compounds were built with the aid of Maestro (version 9.3, Schrödinger, LLC, New York, NY, 2012). Molecular mechanics optimization (UFF force field), semi-empirical calculations (AM1), and DFT (B3LYP/6–31G*) were subsequently applied by the use of Gaussian03. Final geometry was submitted to MD simulations with implicit water and MM3* as force field, by use of Schrödinger Maestro 9.3 Impact 5.8, [Maestro, v. 9.3, Schrödinger, LLC, New York, NY, 2012. Suite 2012: Impact v. 5.8, Schrödinger, LLC, New York, NY, 2012] and the MM3* force field, dielectric constant 80.0, number of MD steps 100, and time step of 0.001 ps. 3D coordinates of *human* MD-2 protein (from PDB ID: 2E59), and CD14 protein (from PDB ID: 1WWL) were refined and minimized through the use of the Protein Preparation Wizard module of Maestro and the Amber force field. In the case of CD14, only the sequence from Ala3 to Leu130 was considered for docking purposes. Compounds were docked into both MD-2 and CD14 proteins with the aid of AutoDock 4.2., and separately with the aid of AutoDock Vina 1.1.2. Predicted binding energies ranged from –2 to –6 kcalmol–1 in the AutoDock results and from –6 to –9 kcal mol–1 in the AutoDock Vina results. For MD-2 the Autogrid grid point spacing was set at 0.375 Å, center coordinates of the grid box were – 0.379, 17.201, 16.216 (x, y, z), and number of grid points in xyz was 58, 92, 82. For CD14 the Autogrid grid point spacing was set at 0.375 Å, center coordinates of the grid box were 13.500, 51.000, 56.500 (x, y, z), leading to 66, 72, 88 (x, y, z) grid points. All the allowed torsional bonds were considered rotatable. Docking calculations with AutoDock were performed using the Genetic Algorithm (number of runs 250, number of

individuals in population 150). Docking calculations with AutoDock Vina were also performed. Coordinates and dimensions of grid boxes, starting geometries, and general methodology were the same as for AutoDock. 3D structures of the docked complexes were optimized by performing MD simulations with Impact (implicit water, and AMBER* force field).

3.6 Conjugation of TLR4 modulators to carrier proteins

Conjugation of IAXO-102 to OVA through a bifunctional linker. Four experiments of conjugation were performed, varying the molar ratio between OVA, IAXO-102 and crosslinking agent (Table 2.1).

The protein OVA and the crosslinking agent were dissolved in PBS buffer pH=7.4; then, a solution of IAXO-102 in DMSO/EtOH (10:1) was added, keeping a maximum DMSO concentration in the reaction mixture of 10%. It was stirred at 37 °C for 4 h. The reaction mixture was passed through a PD-10 desalting column, eluted with water and the product was lyophilized. After dissolution in a minimum volume of water, the protein content was determined with the Bradford reactive method. The purified products were analysed on SDS-PAGE electrophoresis gel, with 12% separating gel, revealed with Blue Comassie, which is specific for proteins, or Silver stain procedure, which is more sensitive. The product was further purified on a Sephadex G-100 exclusion resin, in order to remove the high-molecular weight species.

The samples for SDS-PAGE were prepared and the electrophoretic analyses were performed as described in paragraph 3.1.

Blue Comassie Coloration. The gel was washed with Milli-Q water three times (10 min each) and it was left for 2 hours in a fixative solution (40% methanol, 5% acetic acid). Then, it was treated with the Blue Comassie (Sigma Aldrich) solution for 16 hours. The gel was washed with the fixative solution three times, to remove the deep blue colour**.**

Gels were realised as reported: 12% separating gel (lower gel), 5 % stacking gel (upper gel).

	Separating gel (12%)	Stacking gel (5%)
Acrylamide	2000 µl	335 µl
Tris-HCl 1.5M pH 8.8	1250 µl	- - - - - -
Tris-HCl 0.5M pH 6.8	- - - - - -	500 µl
H$_2$O MilliQ	1750 µl	1150 µl
APS	25 µl	15 µl
TEMED	2.5 µl	2.5 µl
Bromophenol Blue (4% w/v)	- - - - - -	15 µl

Table 3.2. Reagents for SDS-PAGE gel preparation.

Direct conjugation of carboxylated-IAXO-102 to OVA. Compound **35** was obtained as described in the paragraph 3.2. Seven experiments of conjugation were performed on small amounts of reagents, varying the molar ratio between OVA, molecule **35** and EDC, and modifying the buffer composition (Table 2.2), in order to choose the best reaction conditions.

Compound **35** and condensing agent EDC were dissolved in the buffer and stirred at 35°C for 1h. The buffer pH was monitored during the procedure. Then, the protein OVA was added and the reaction mixture was stirred at 35°C for 24h. The reaction solution was passed through a PD-10 desalting column, eluted with water, and lyophilized. When a higher amount of

reagents was used (10 mg scale), a dialysis against water (cut off 14000 Da, 72 h) was preferred to the desalting column. After dissolution in a minimum volume of water, the protein content was determined with the Bradford reactive method. The purified products were analysed on SDS-PAGE electrophoresis gel, with 12% separating gel, revealed with Blue Comassie or Silver stain procedure, as described above. **IAXO-OVA-2** was obtained as pure and homogeneous product (2.6 mg).

Supporting information

NMR characterization of synthetic compounds

Characterization of the synthetic compounds obtained during this PhD project are reported in the Chapter Materials and Methods, together with complete lists of ^{1}H and ^{13}C chemical shifts.

In this section, ^{1}H NMR and APT NMR or 2D-HSQC NMR spectra are reported for new molecules, while ^{1}H NMR spectra are reported for known compounds.

Compound IAXO-FITC-1. ^{1}H NMR and ^{13}C-APT NMR spectra.

17.25
26.53
30.01
30.08
33.29
33.58
33.63
33.96
34.26
35.87
75.02
75.84
77.47
84.31
84.97
90.32
102.01
104.44
106.28
114.17
133.04
156.90

f1 (ppm)
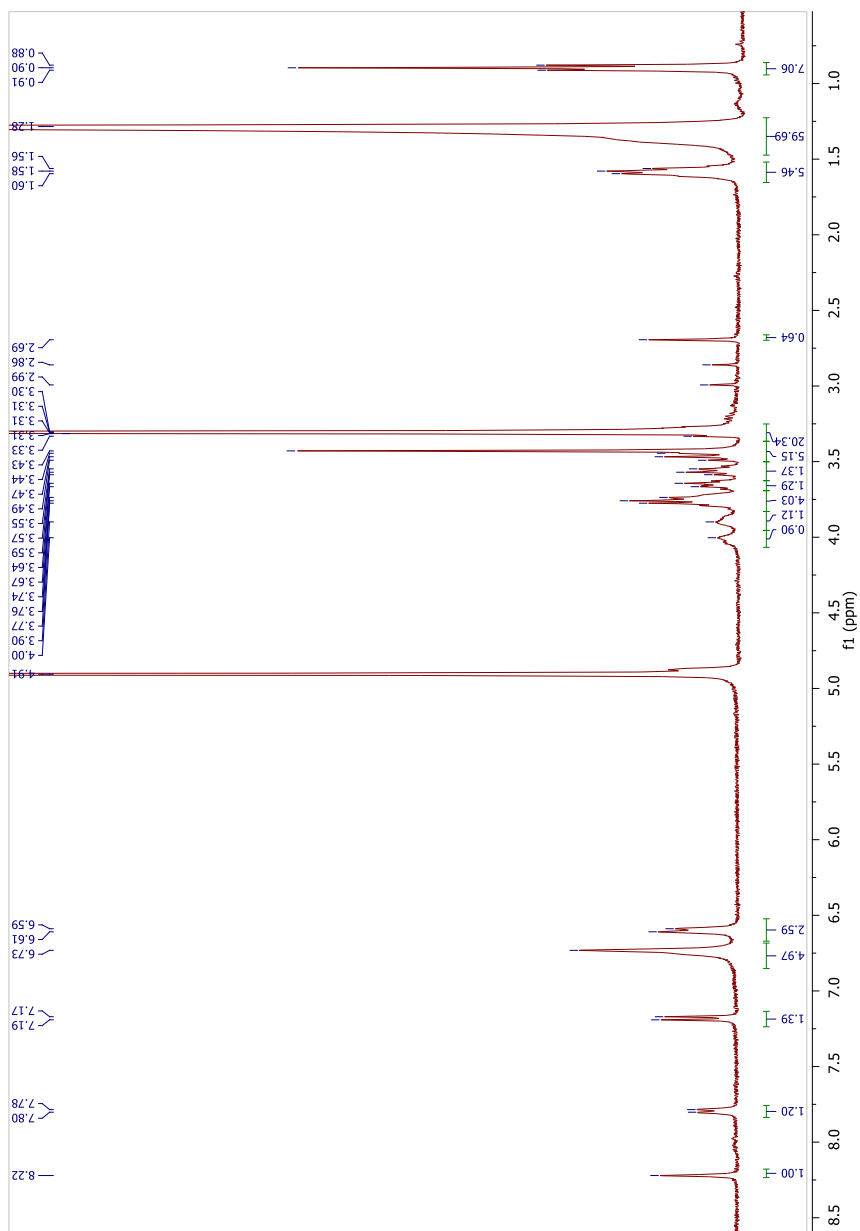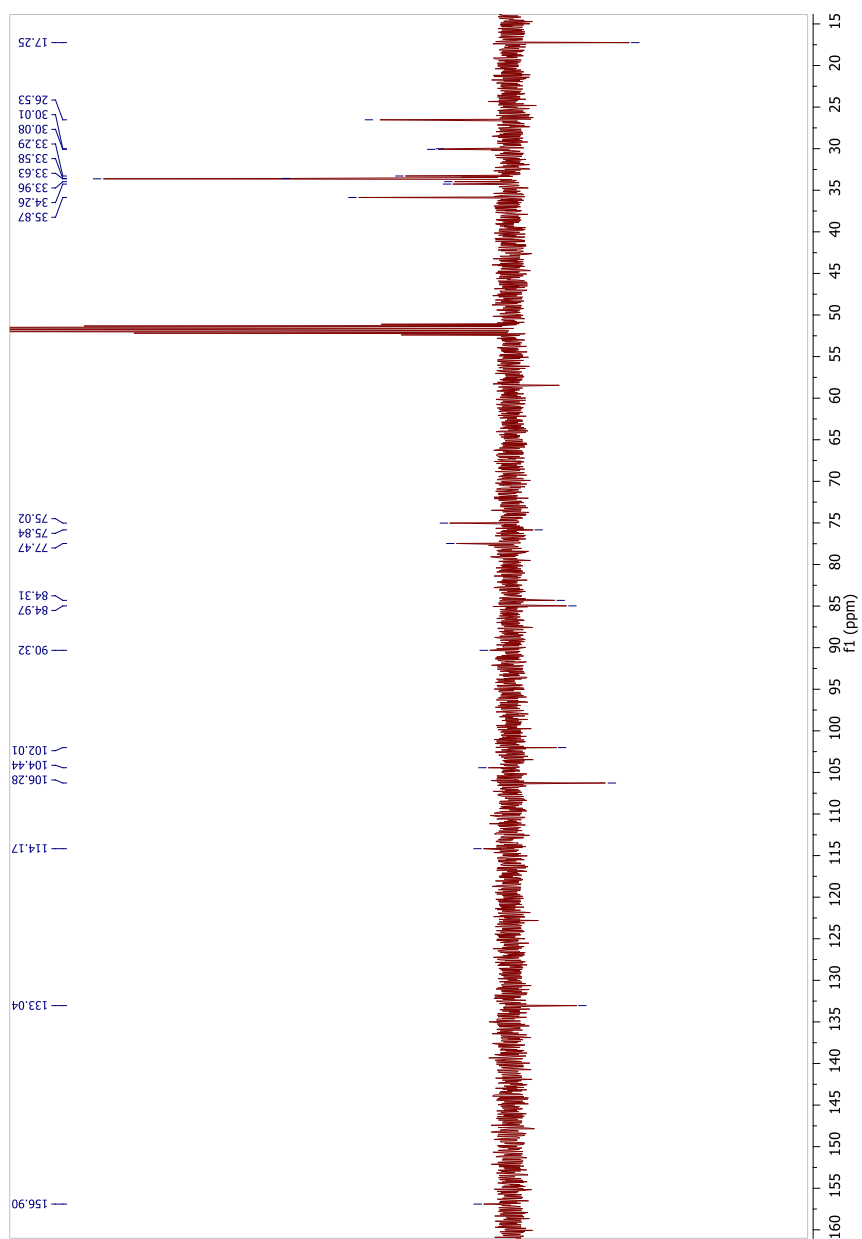
Compound 6. ^{1}H NMR and ^{13}C-APT NMR spectra.
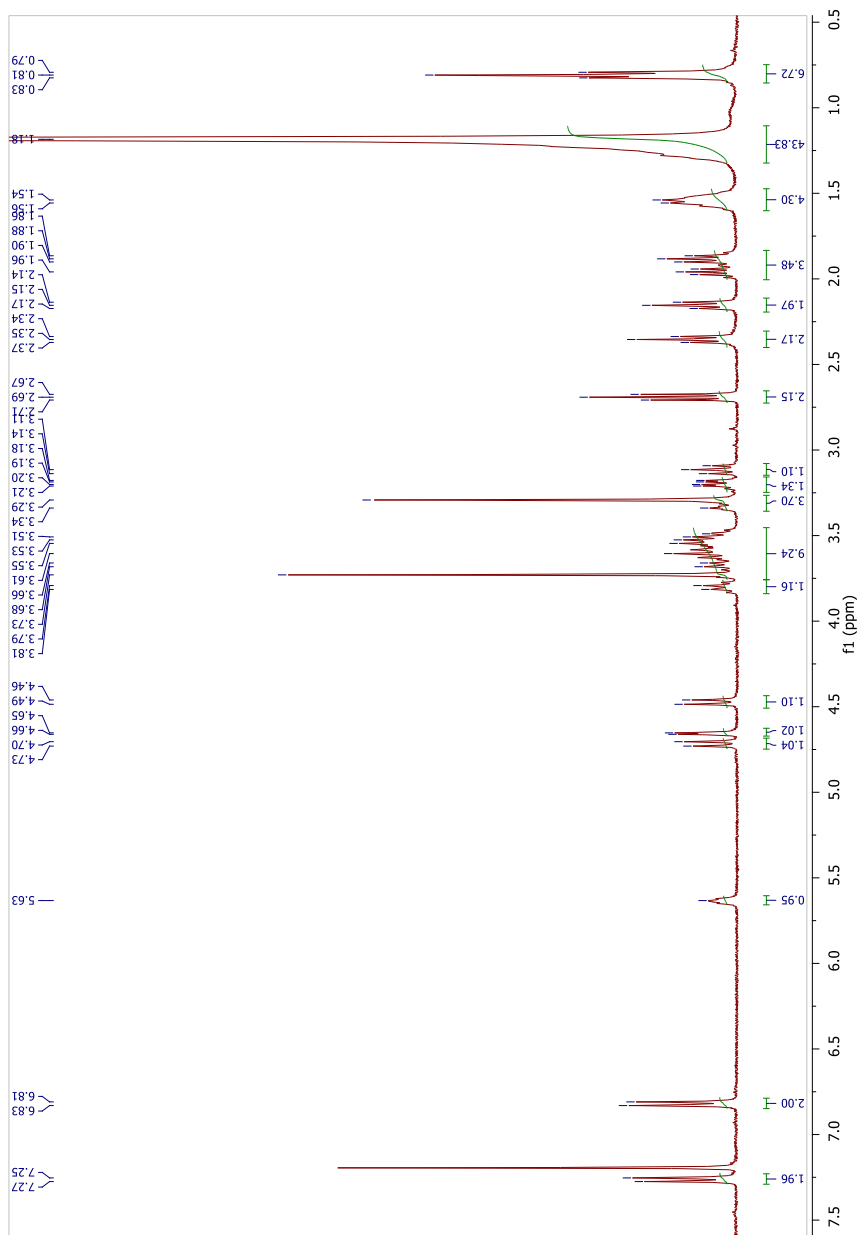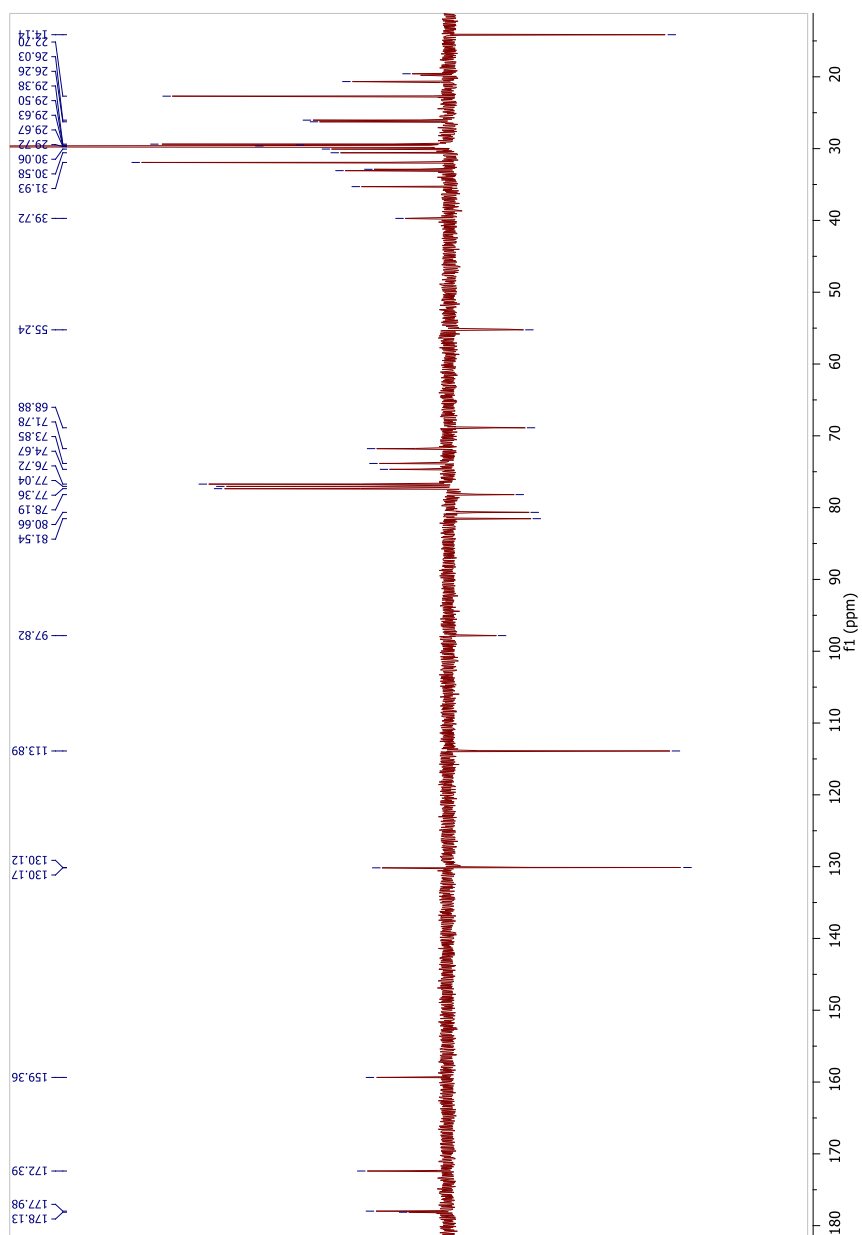
Compound 7. ^{1}H NMR and ^{13}C-APT NMR spectra.
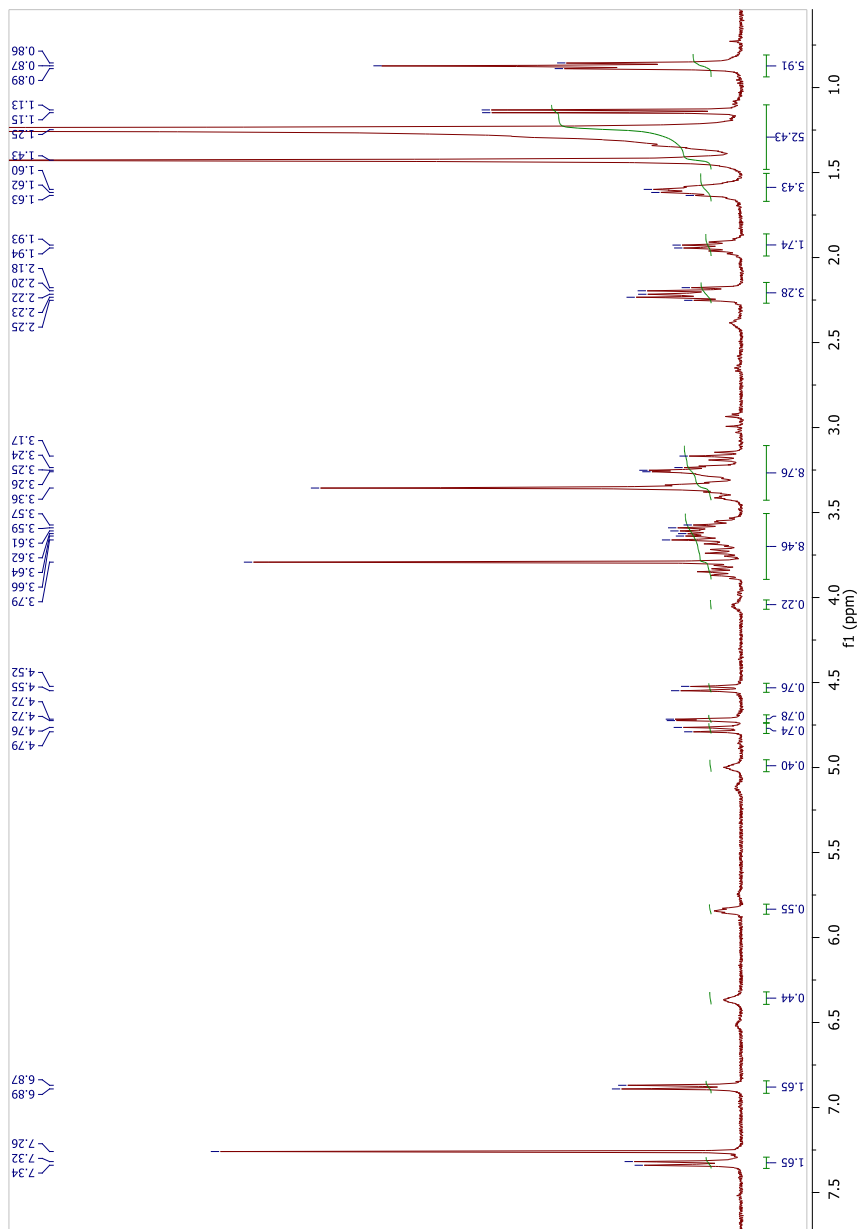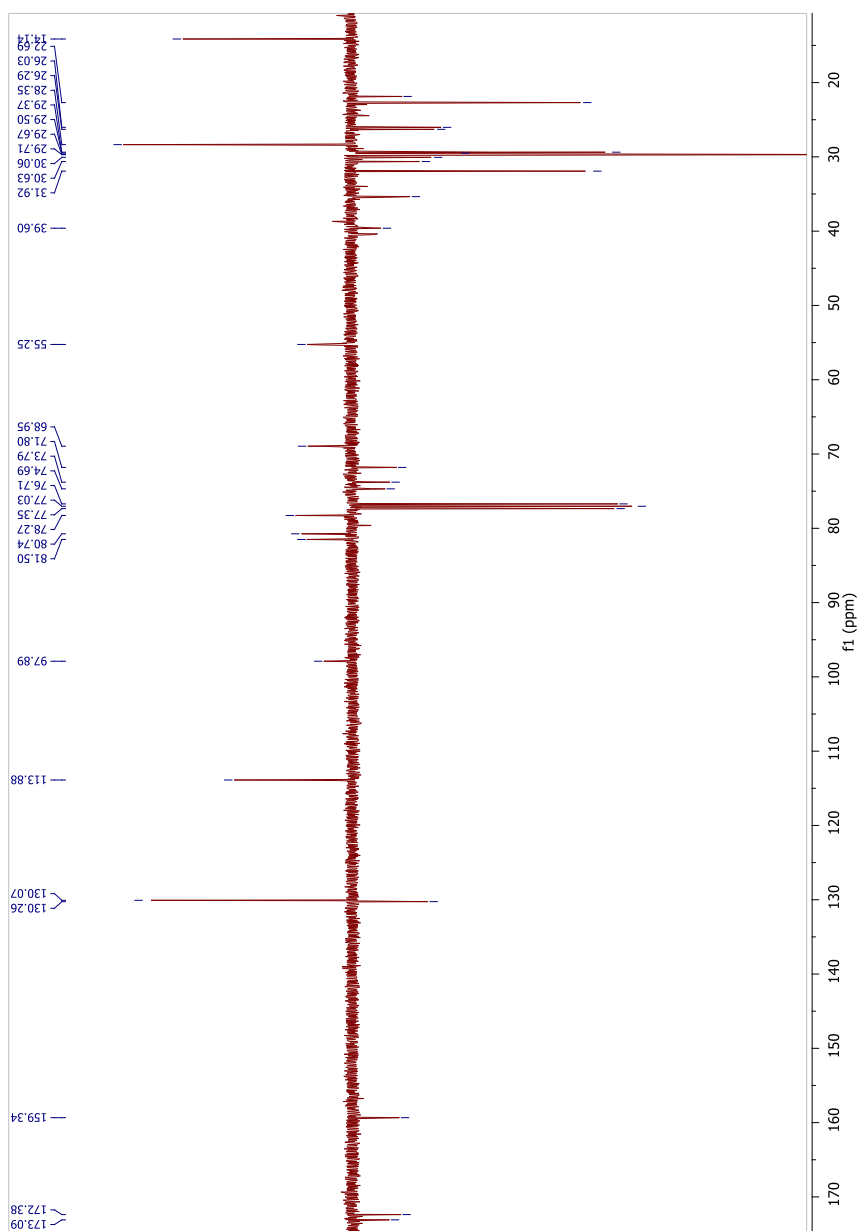
Compound 8. ^{1}H NMR and ^{13}C-APT NMR spectra.

25.70
26.48
29.87
29.92
33.19
33.34
33.52
33.88
34.14
35.76
38.94
43.94
44.34
51.74
51.96
52.17
52.38
52.60
52.81
53.02

75.51
77.76
81.02
81.34
81.66

178.65

185.64

f1 (ppm)
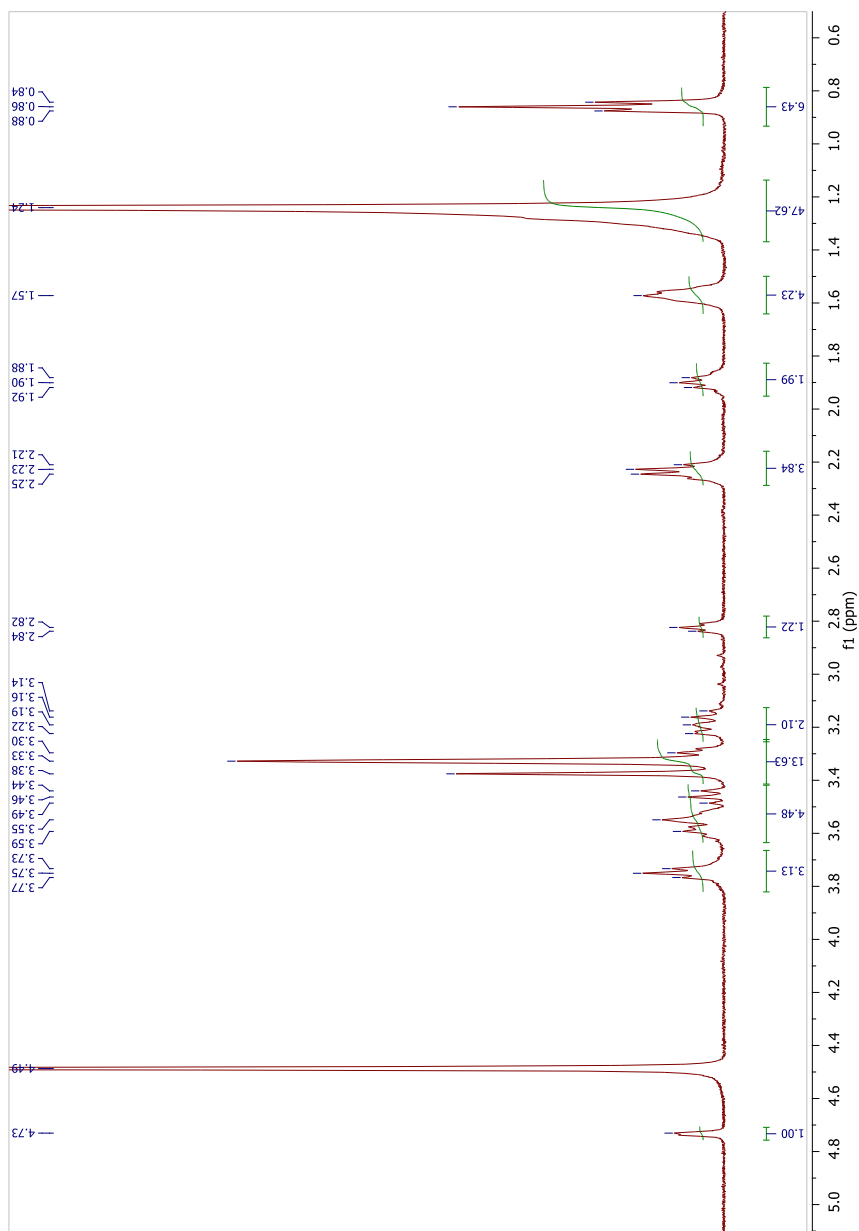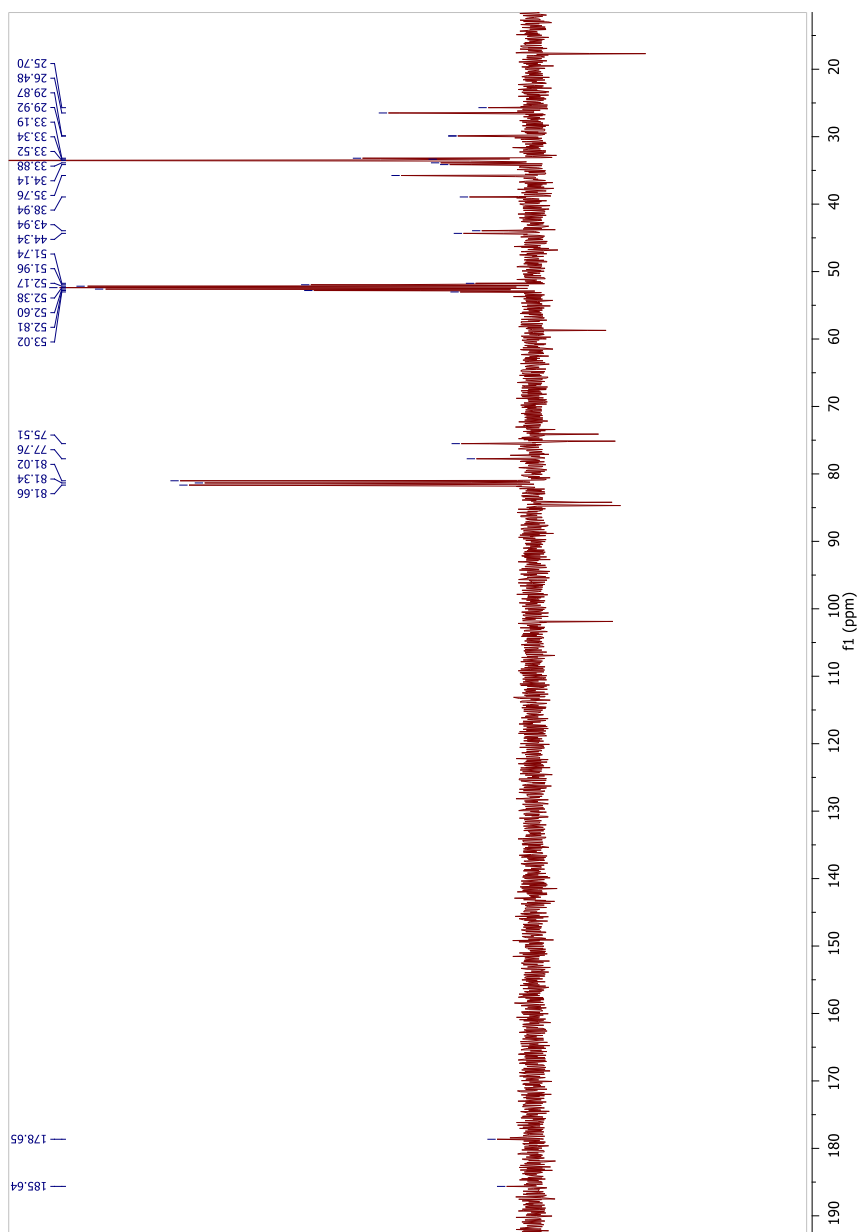
Compound IAXO-FITC-2. ^{1}H NMR and ^{13}C-APT NMR spectra.
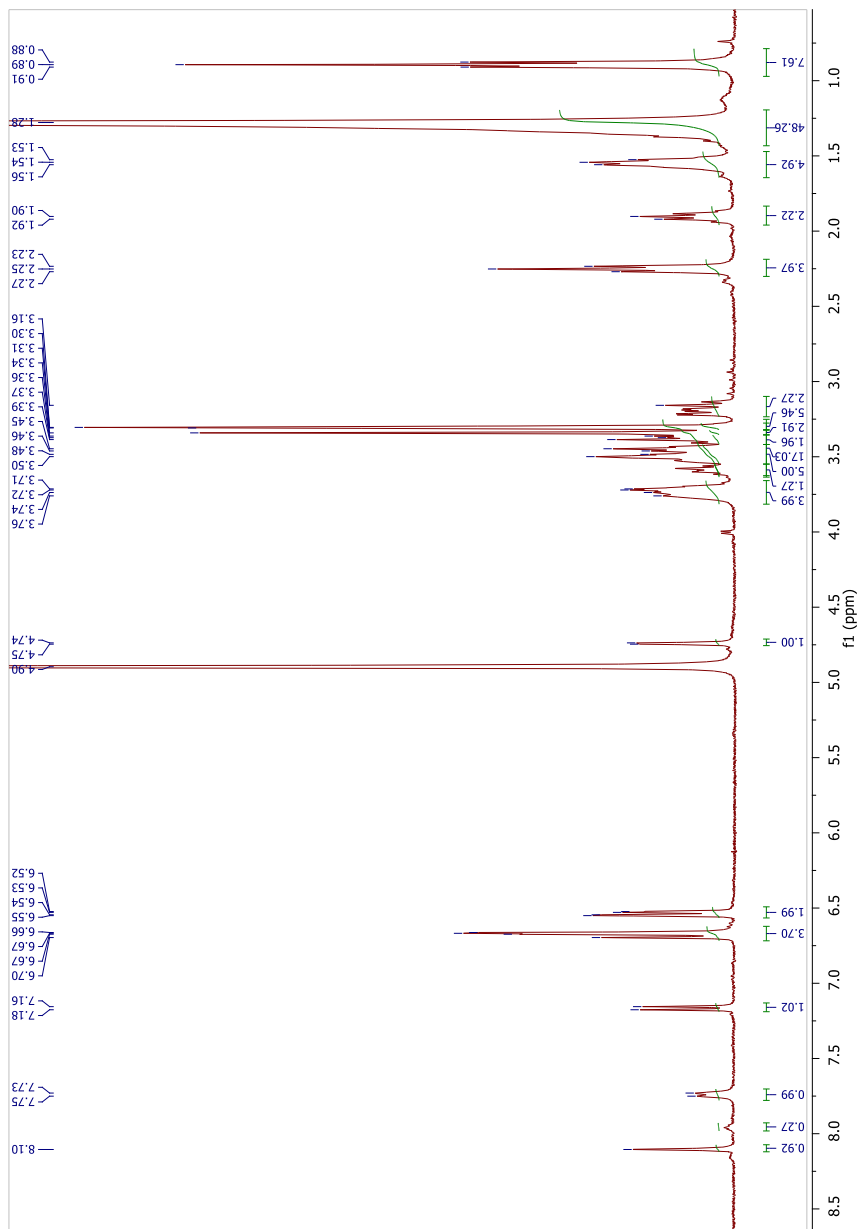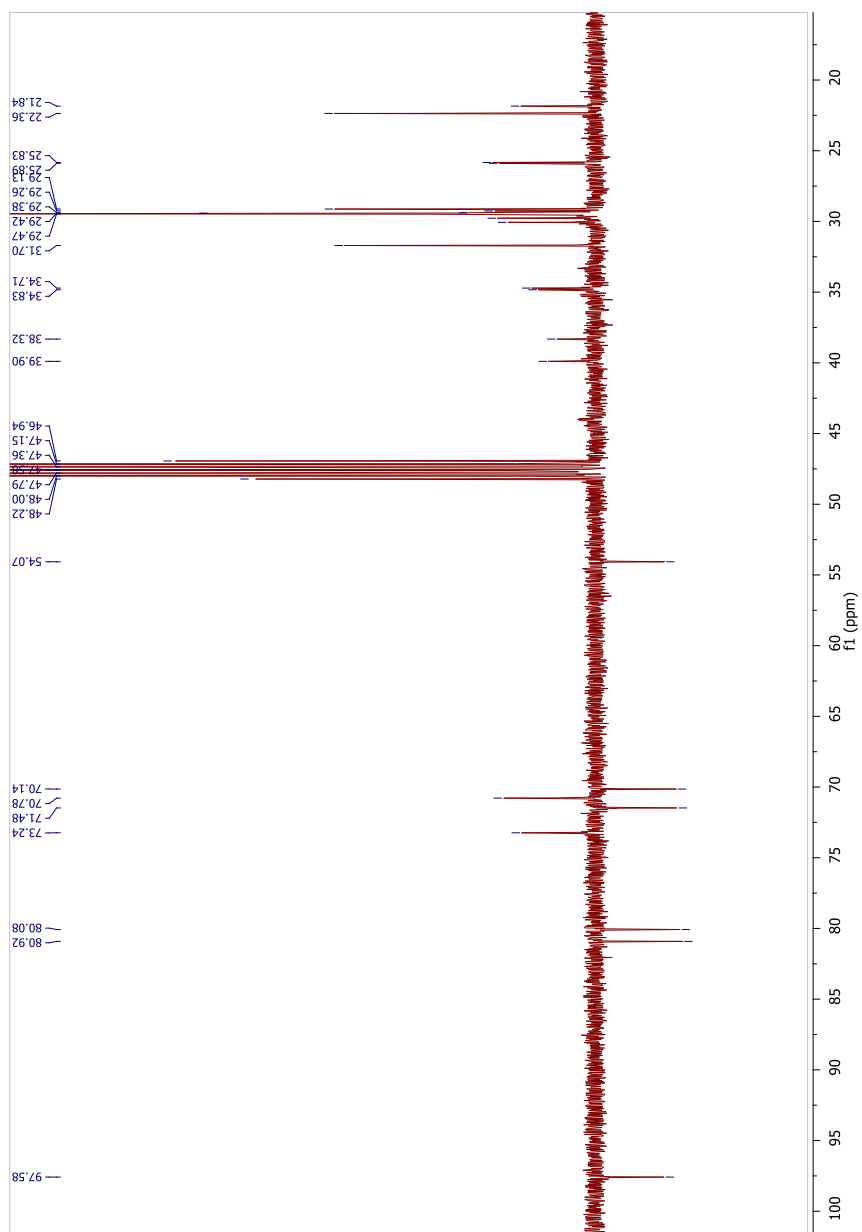
Compound IAXO-D1. ^{1}H NMR and gHSQC NMR spectra.
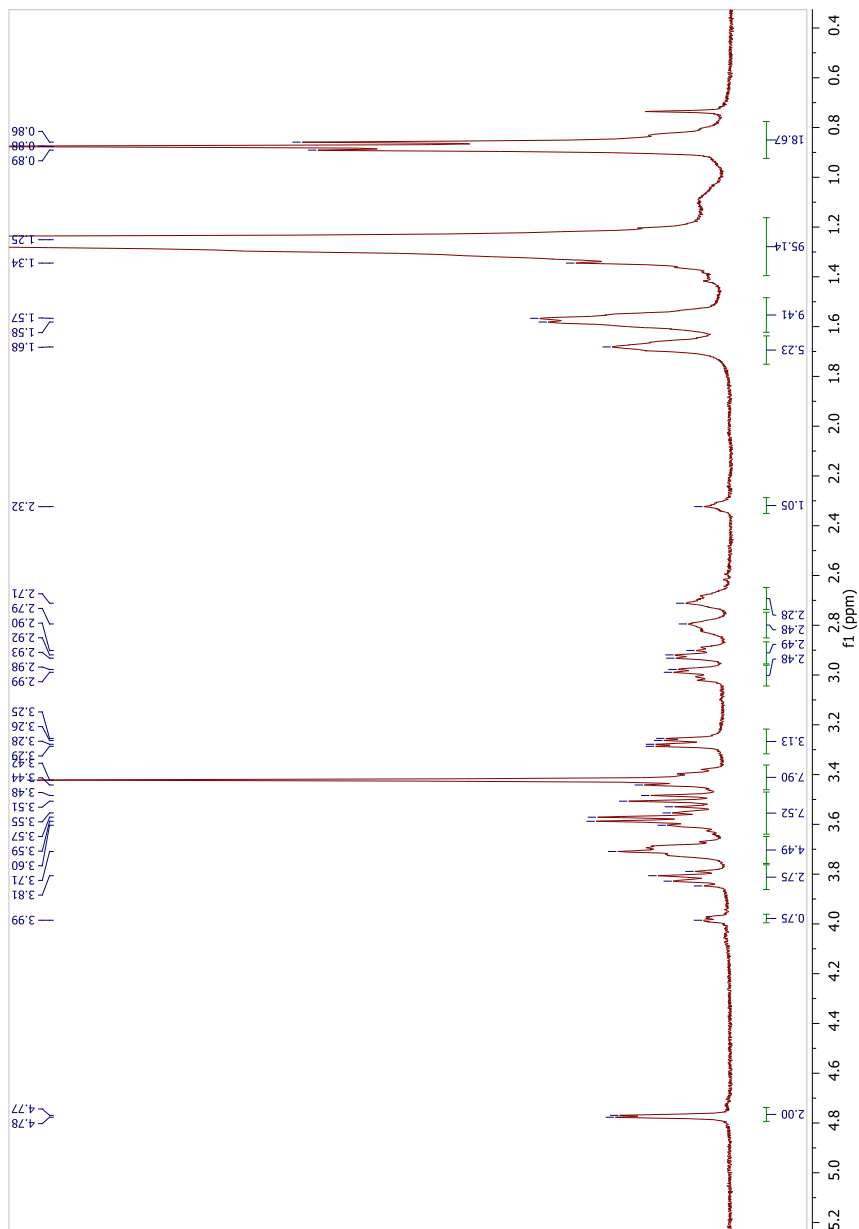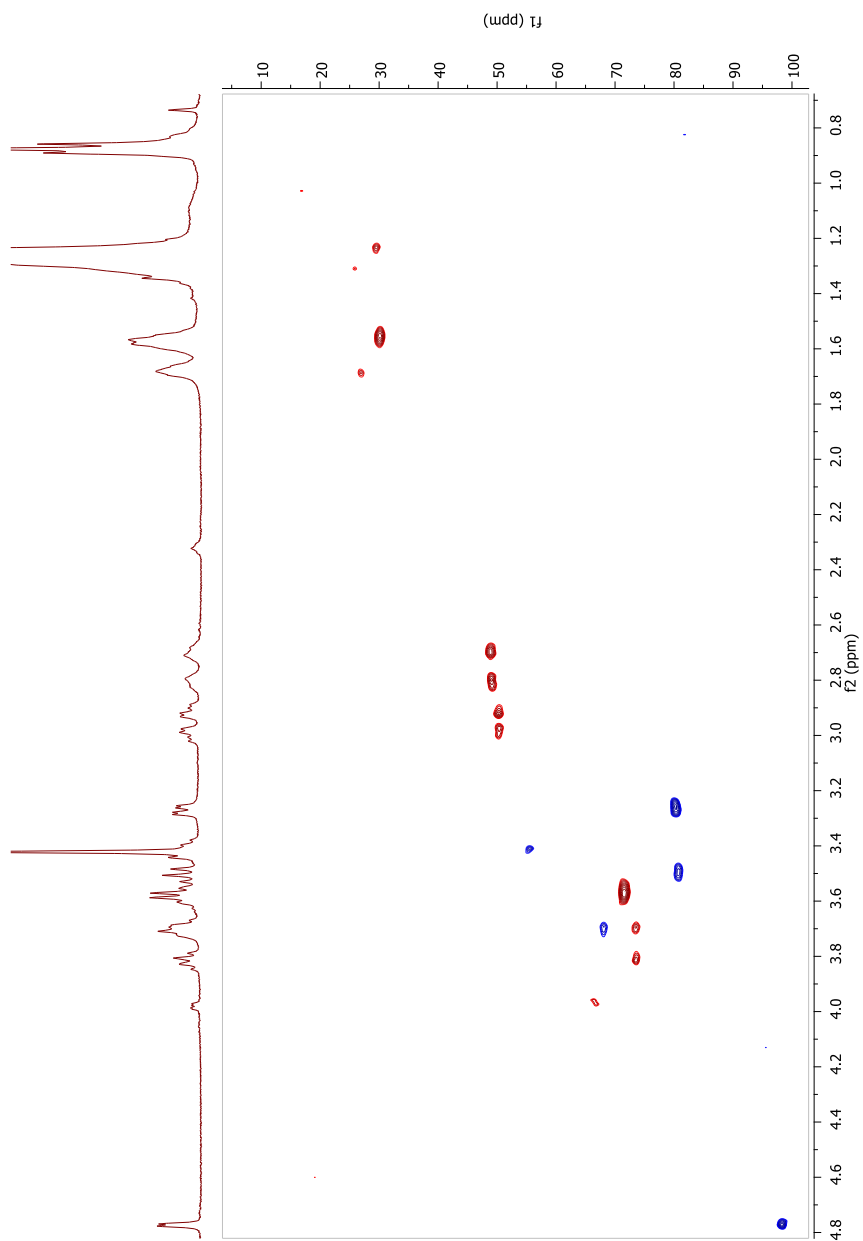
Compound IAXO-D2. ^{1}H NMR and gHSQC NMR spectra.
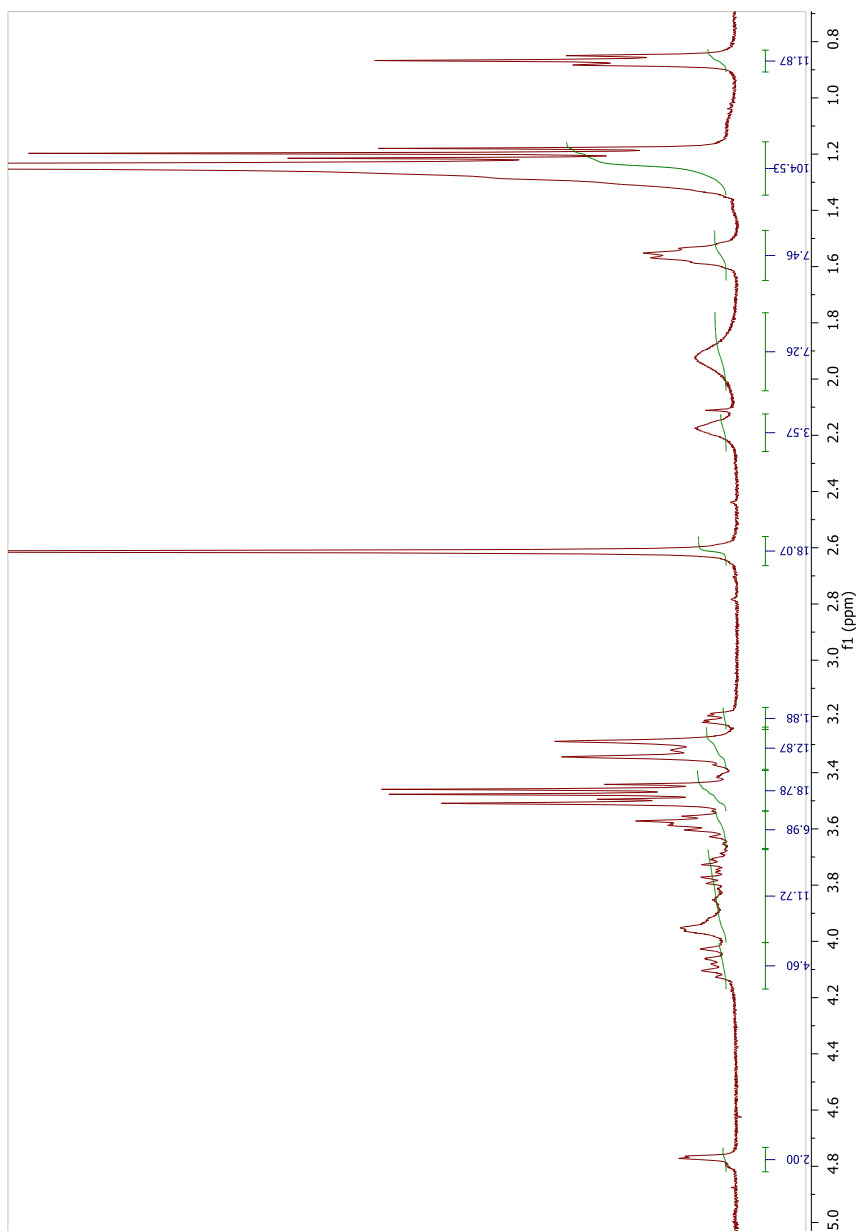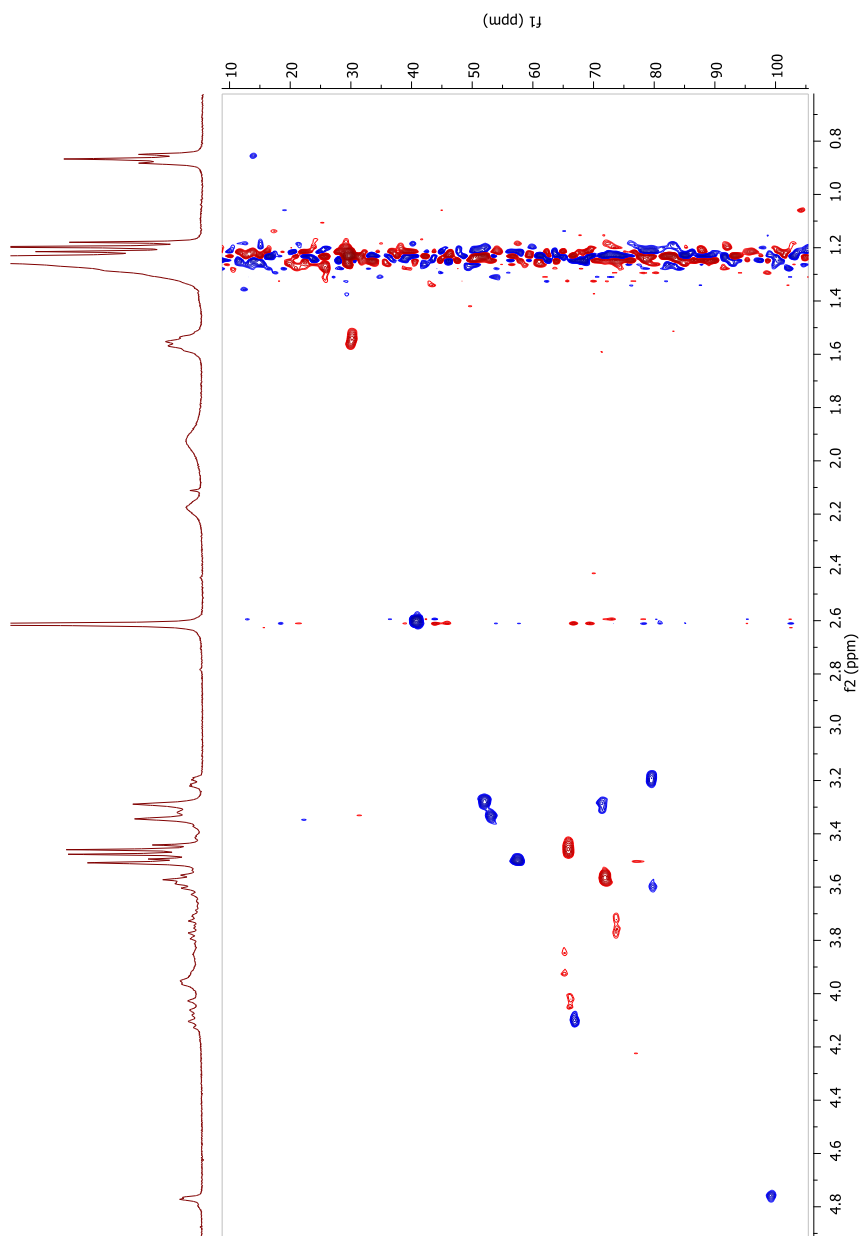
Compound IAXO-Z1. ^{1}H NMR and gHSQC NMR spectra.
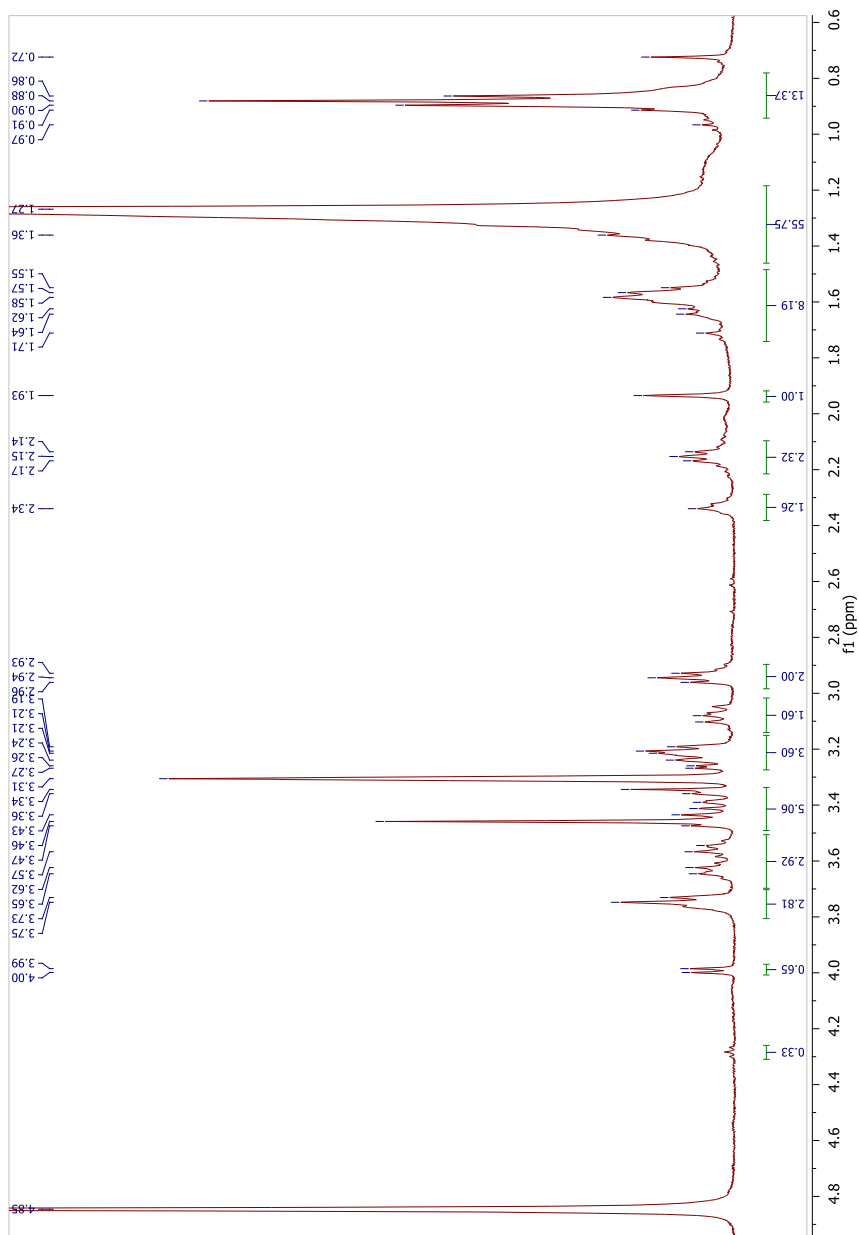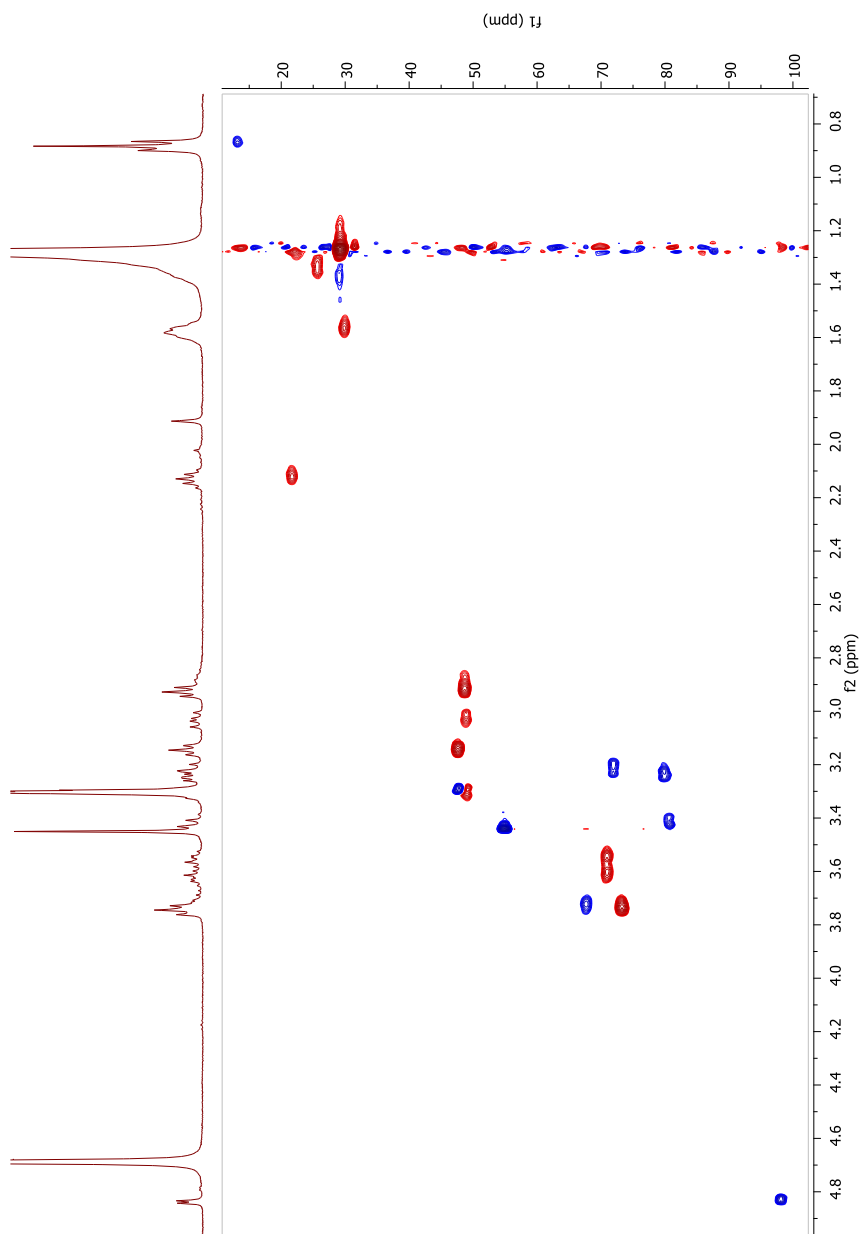
Compound 21. ^{1}H NMR spectrum.
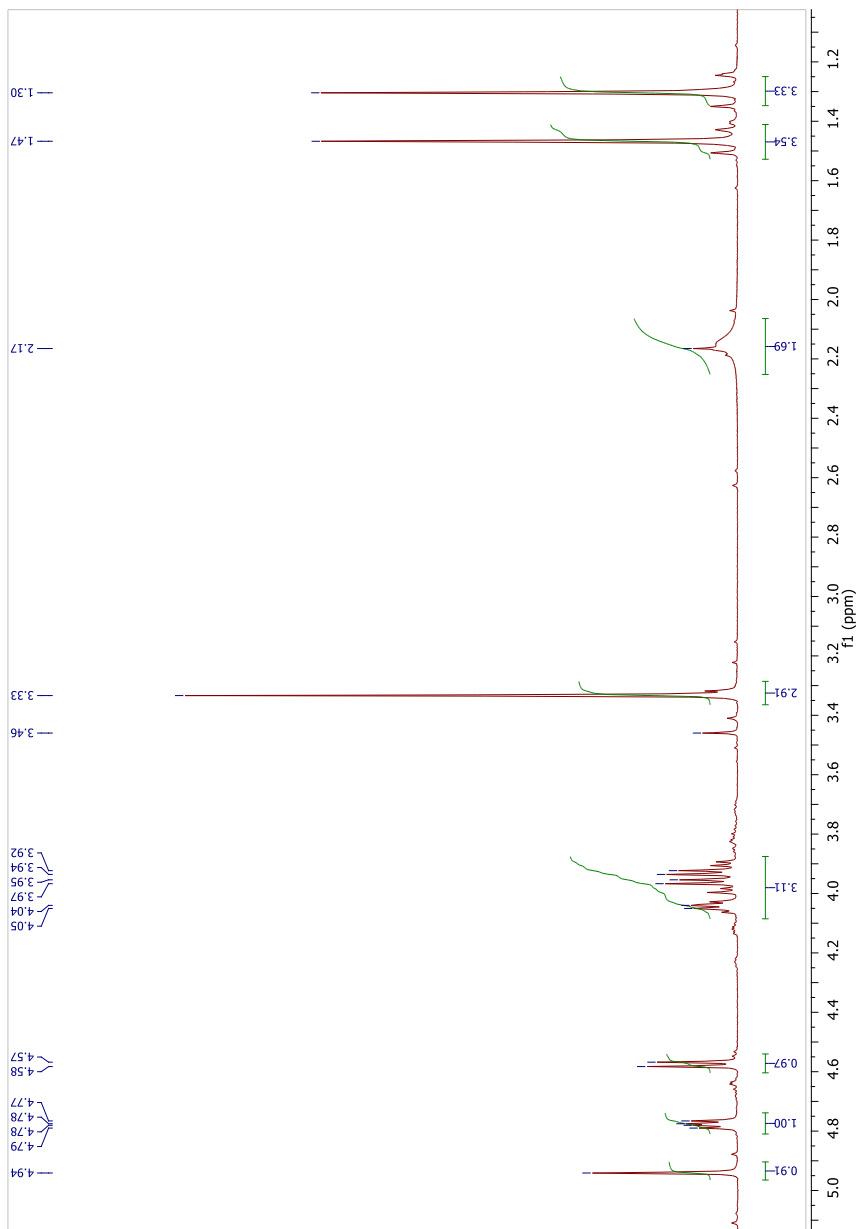
Compound 22. ^{1}H NMR spectrum.
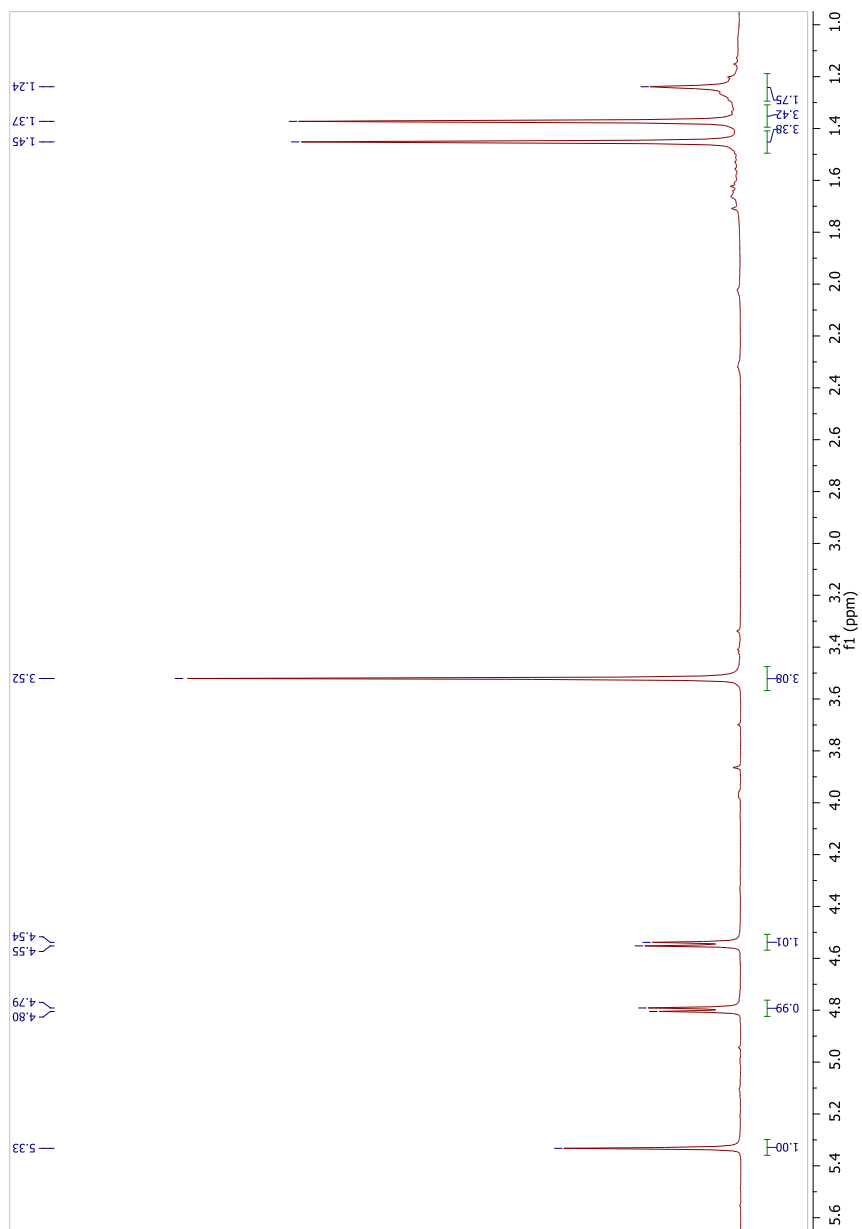
Compound 23. ^{1}H NMR spectrum.
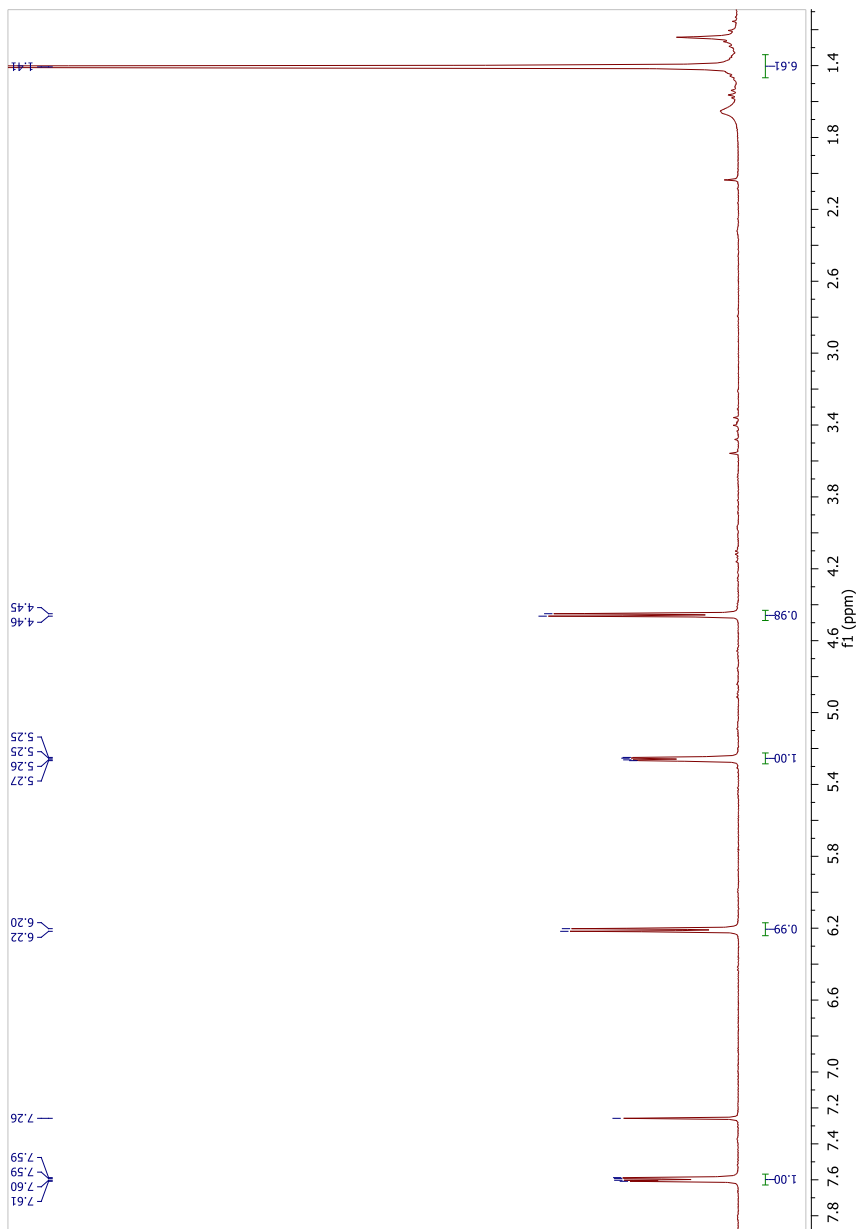
Compound 24. ^{1}H NMR spectrum.
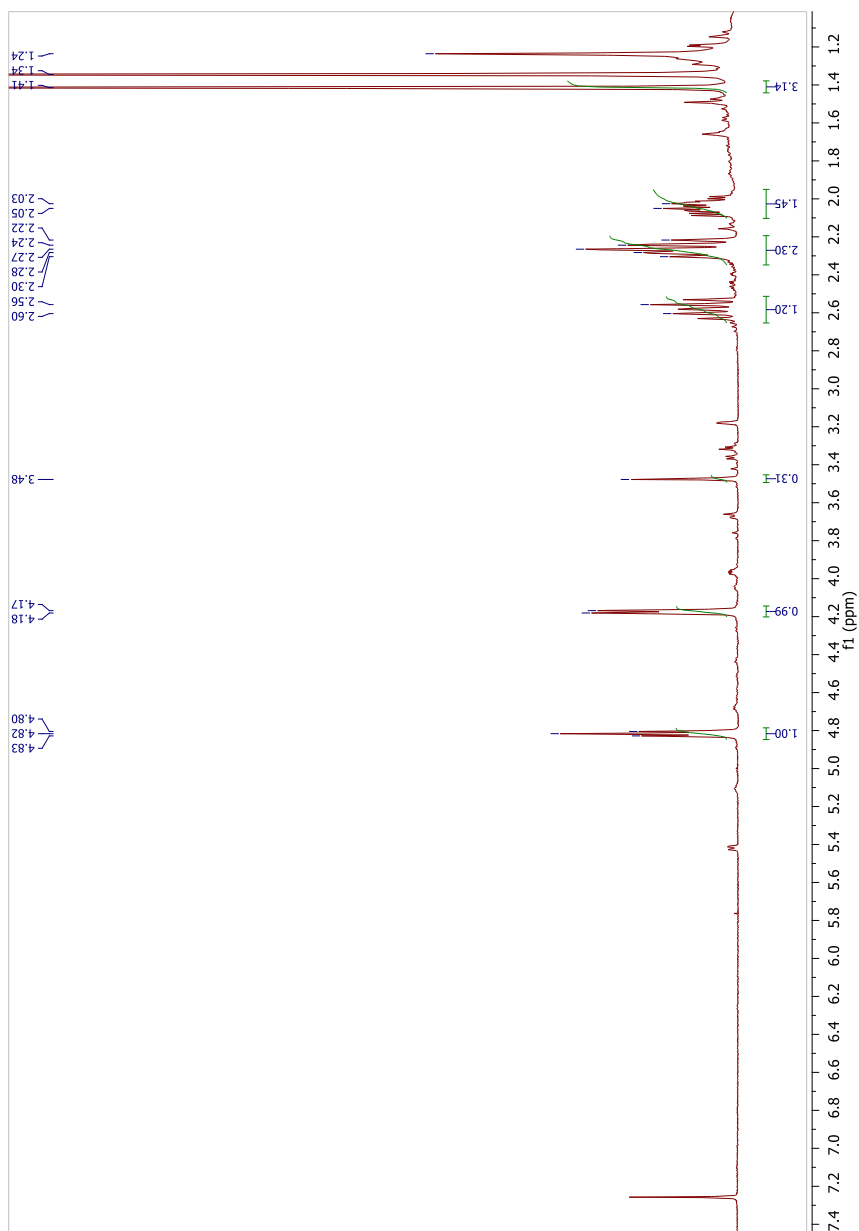
Compound 25. ^{1}H NMR and ^{13}C-APT NMR spectra.

24.36
29.03
30.75
34.03

69.86

76.74
77.06
77.38
78.70

216.76

f1 (ppm)
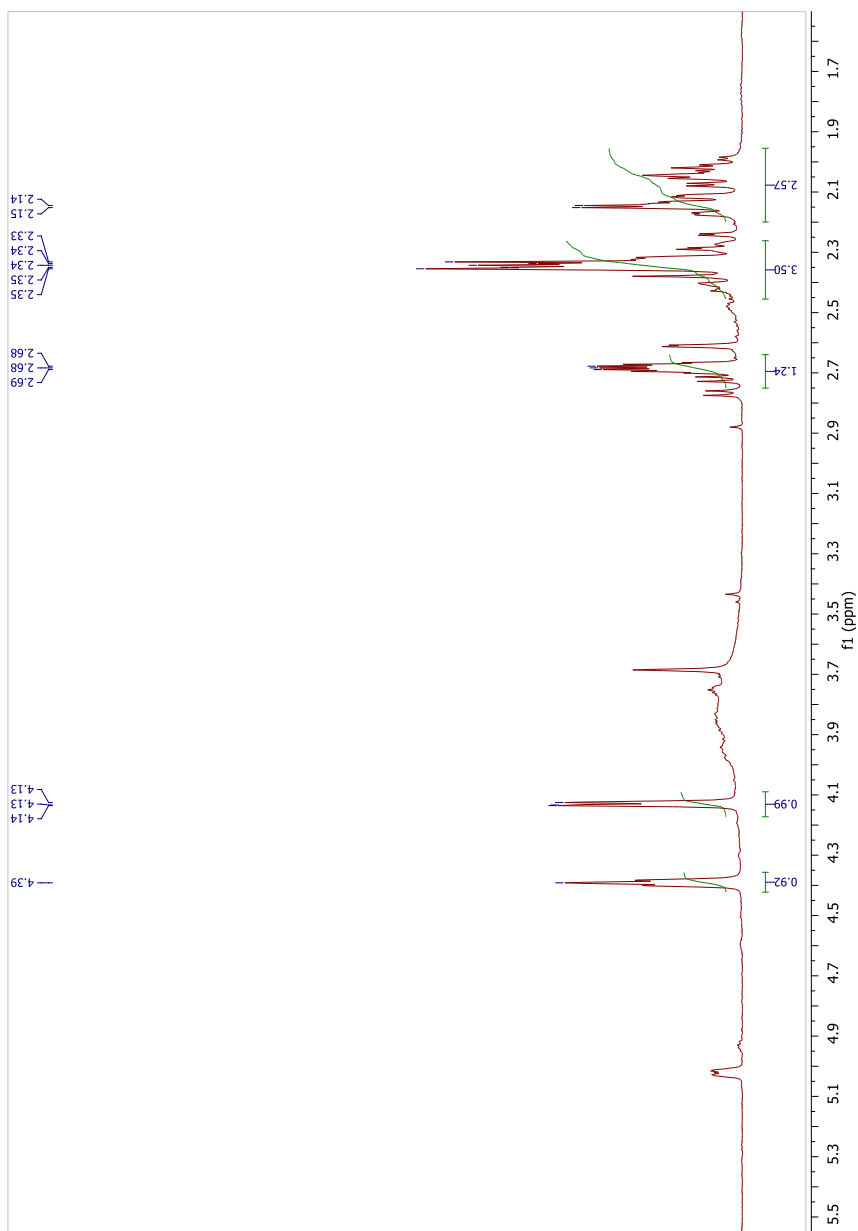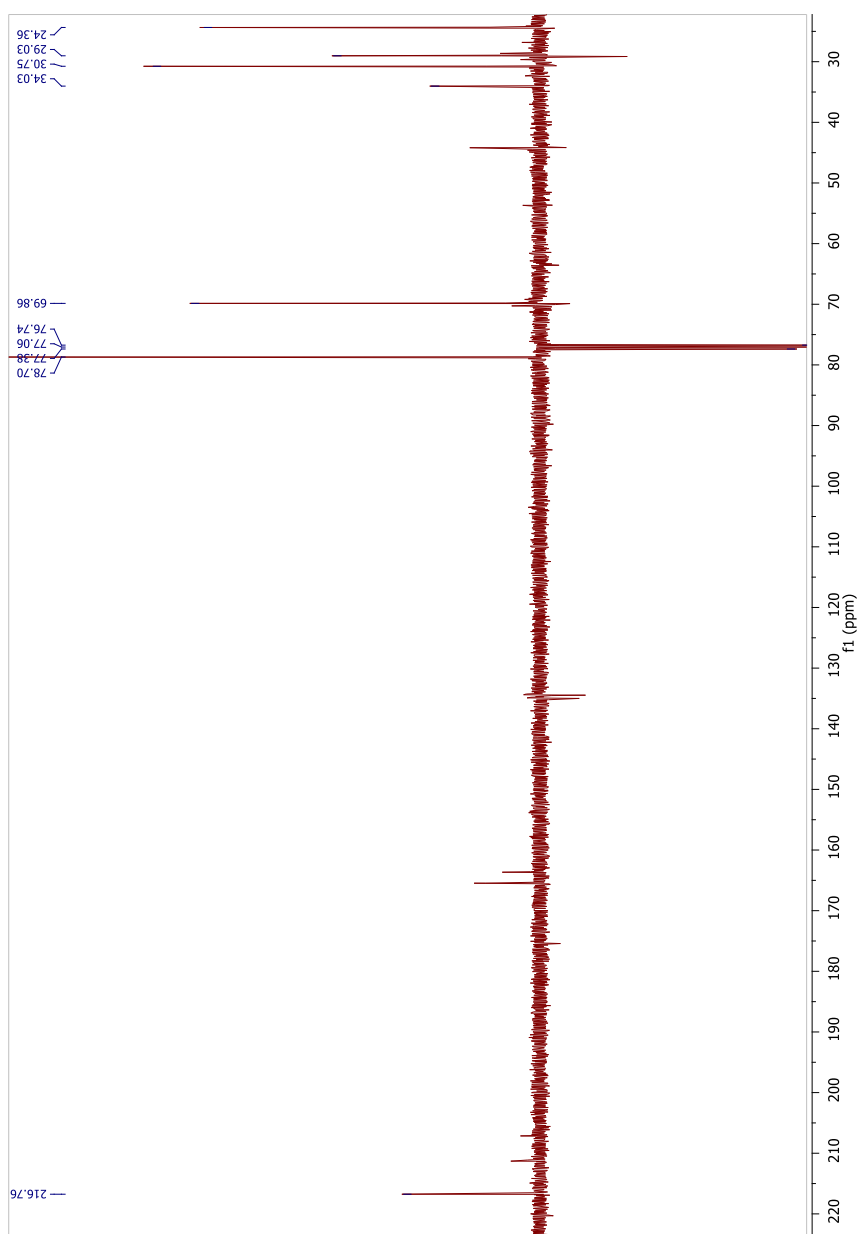
Compound 27a. ^{1}H NMR and ^{13}C-APT NMR spectra.
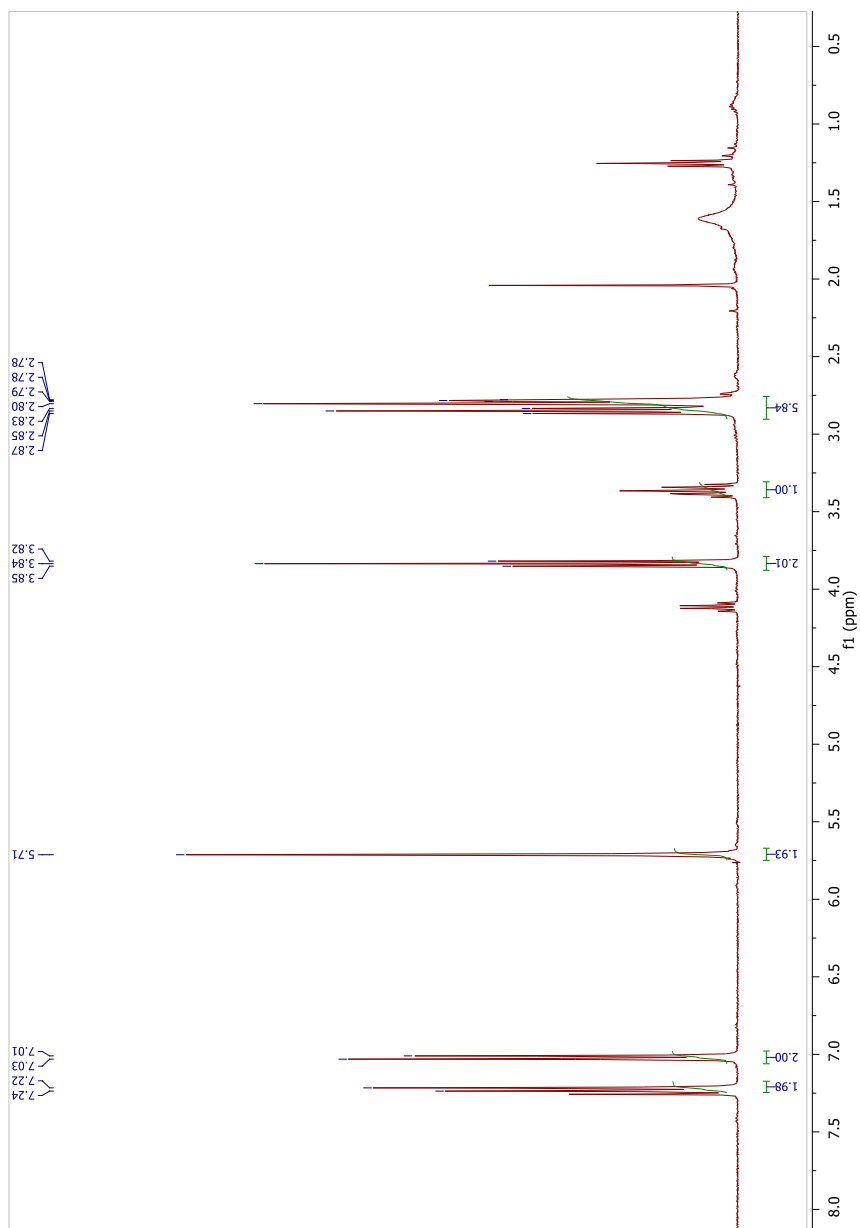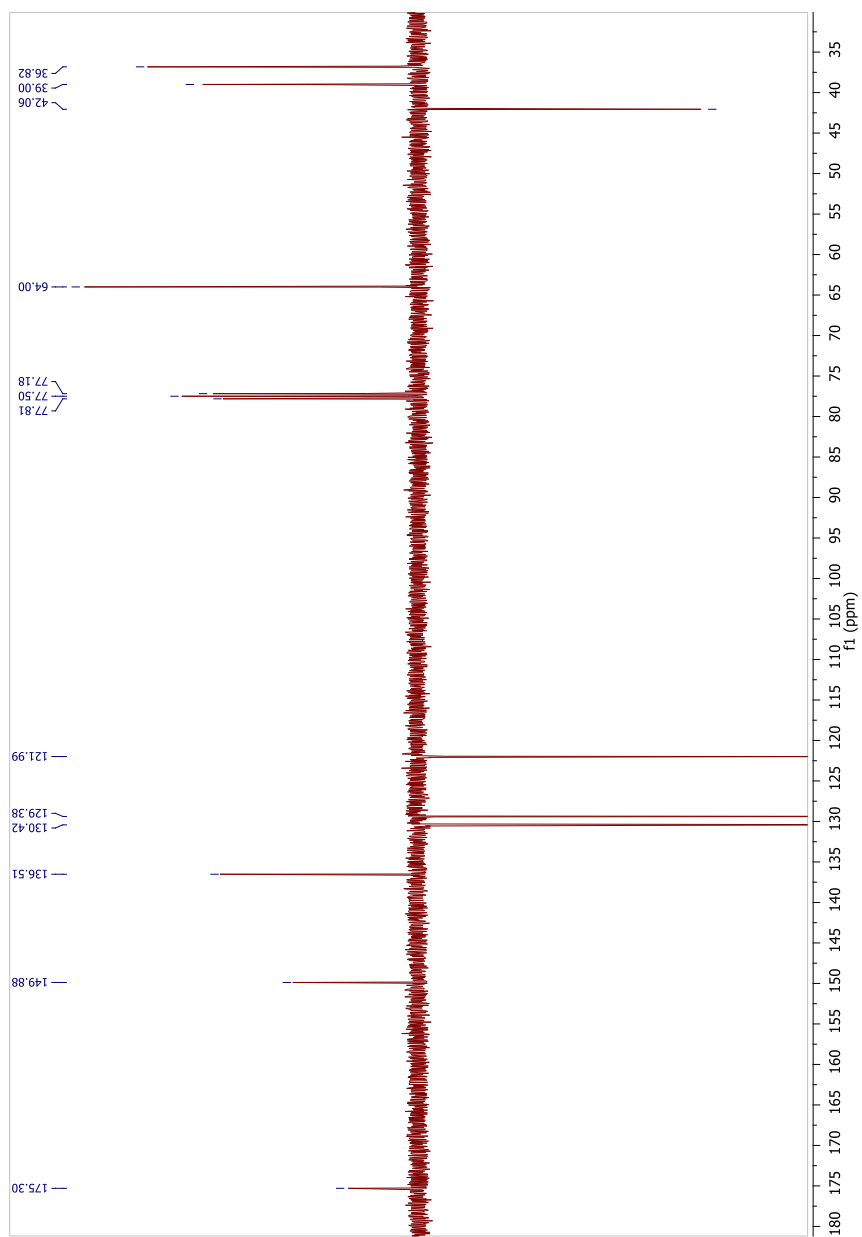
Compound 28. ^{1}H NMR and ^{13}C-APT NMR spectra.

33.85
38.16
38.97
47.08
47.30
47.51
47.94
48.15
48.36
62.70
73.14
121.00
129.57
136.69
149.25
175.40

f1 (ppm)
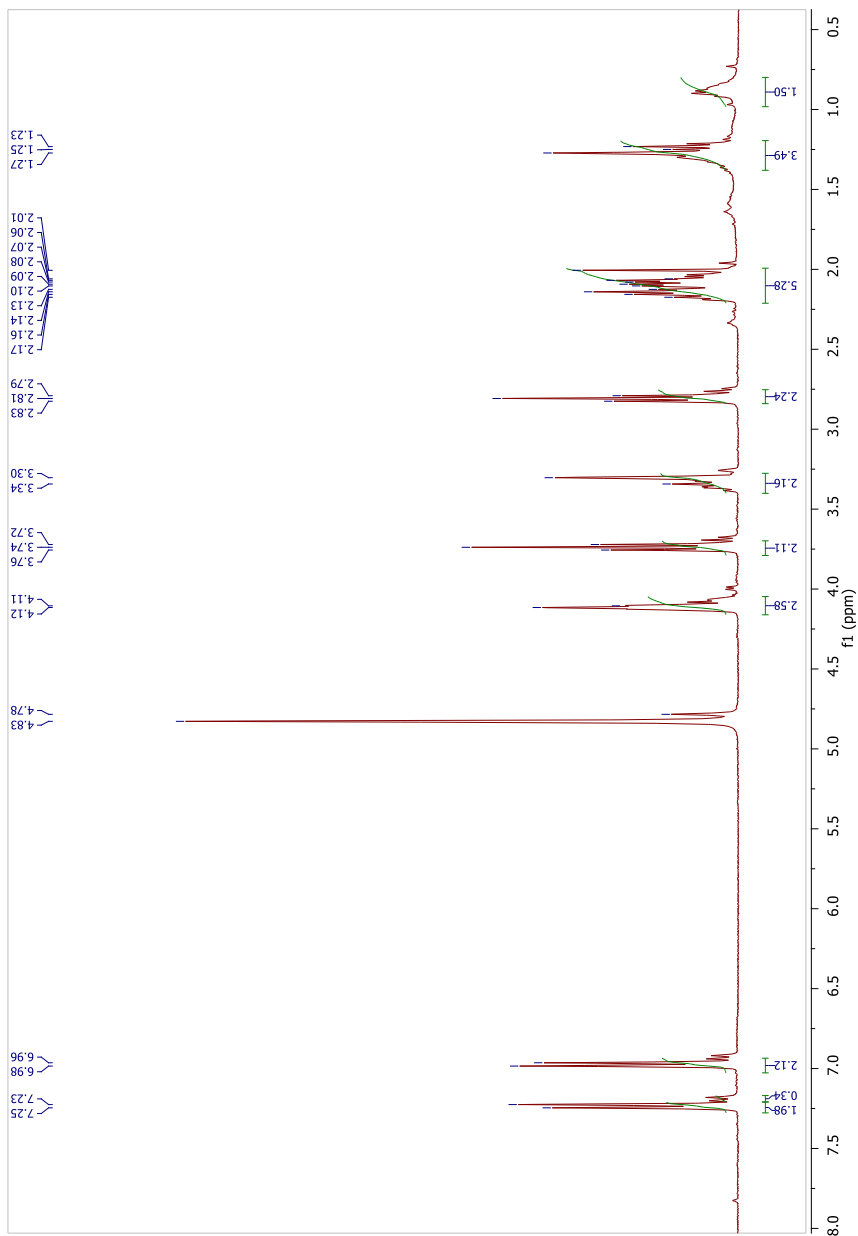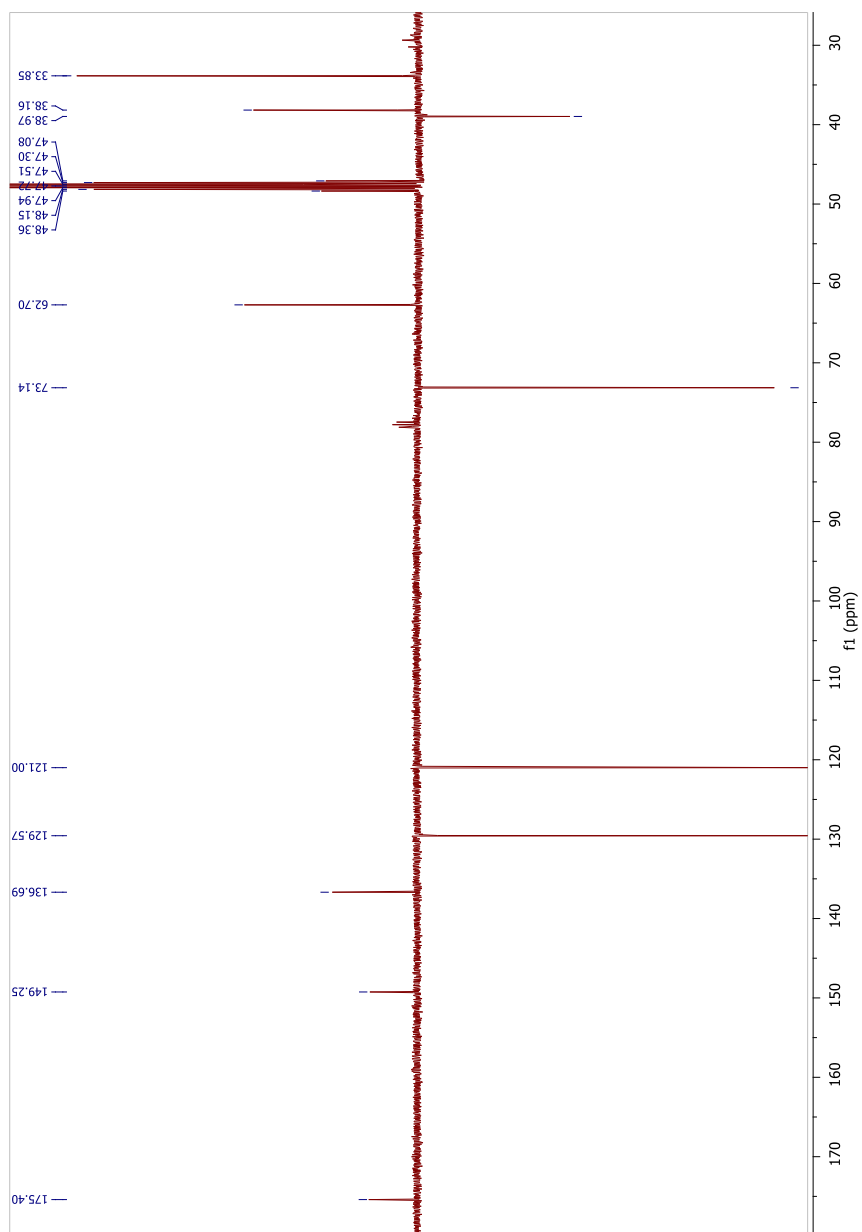
Compound 30. ^{1}H NMR and ^{13}C-APT NMR spectra.
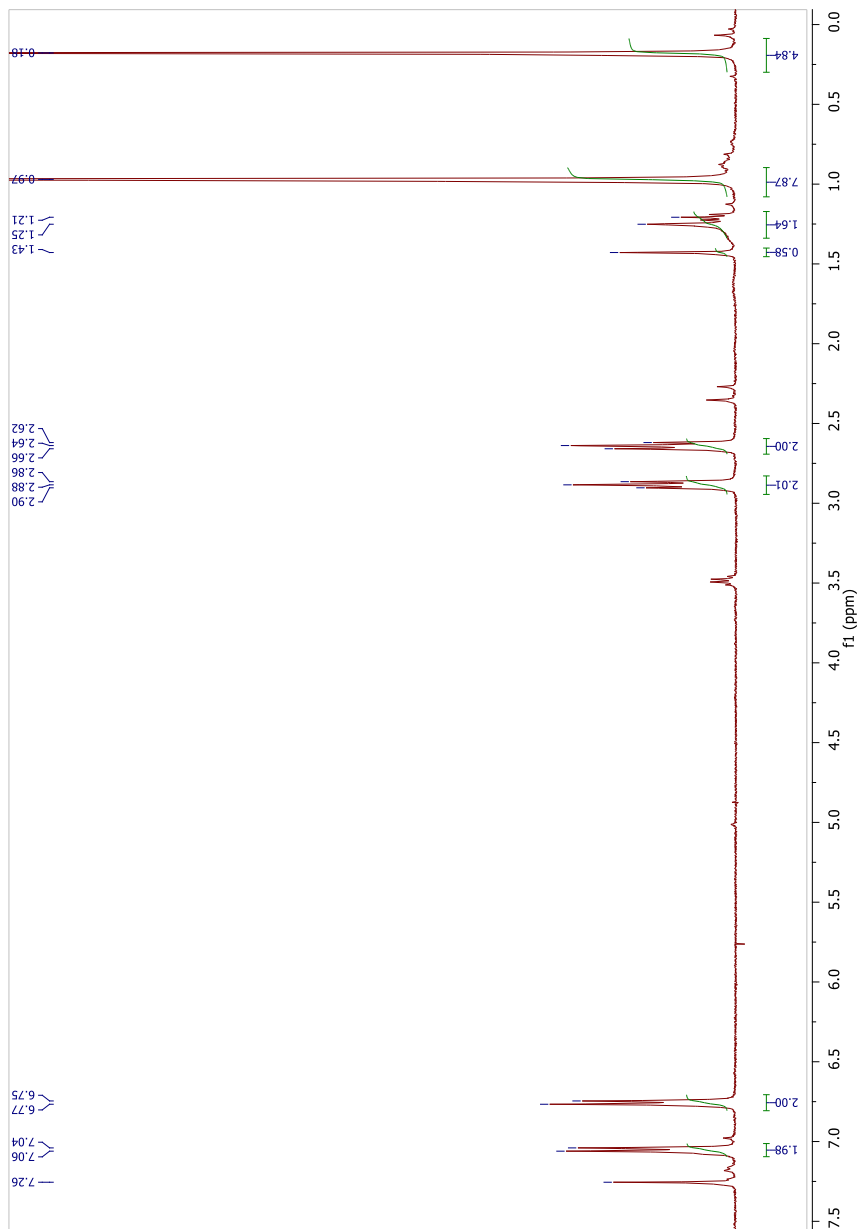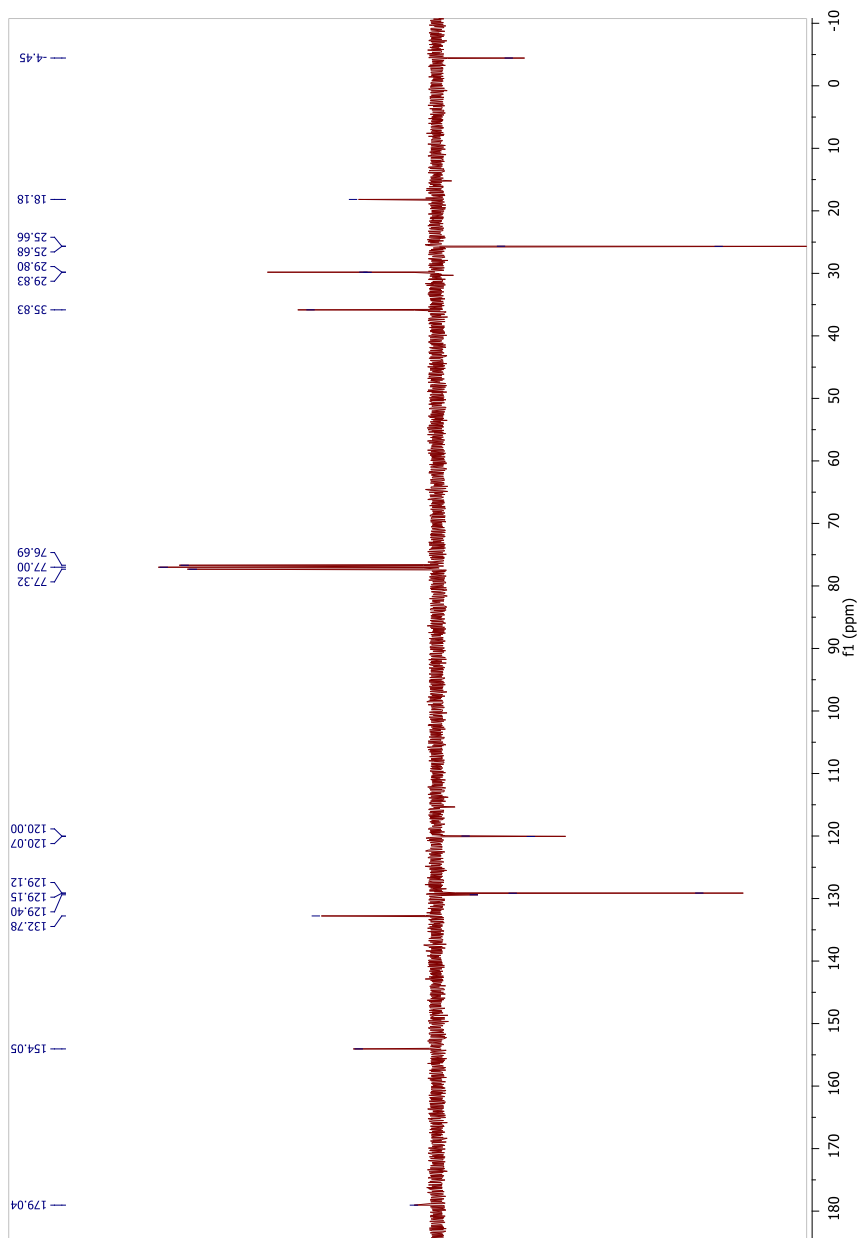
Compound 31. ^{1}H NMR and ^{13}C-APT NMR spectra.

18.17

24.38
25.24
25.67
28.11
30.26
32.97
36.17

68.70

76.69
77.00
77.32

119.98

125.48
127.01
129.12
133.15

153.96

173.14

f1 (ppm)
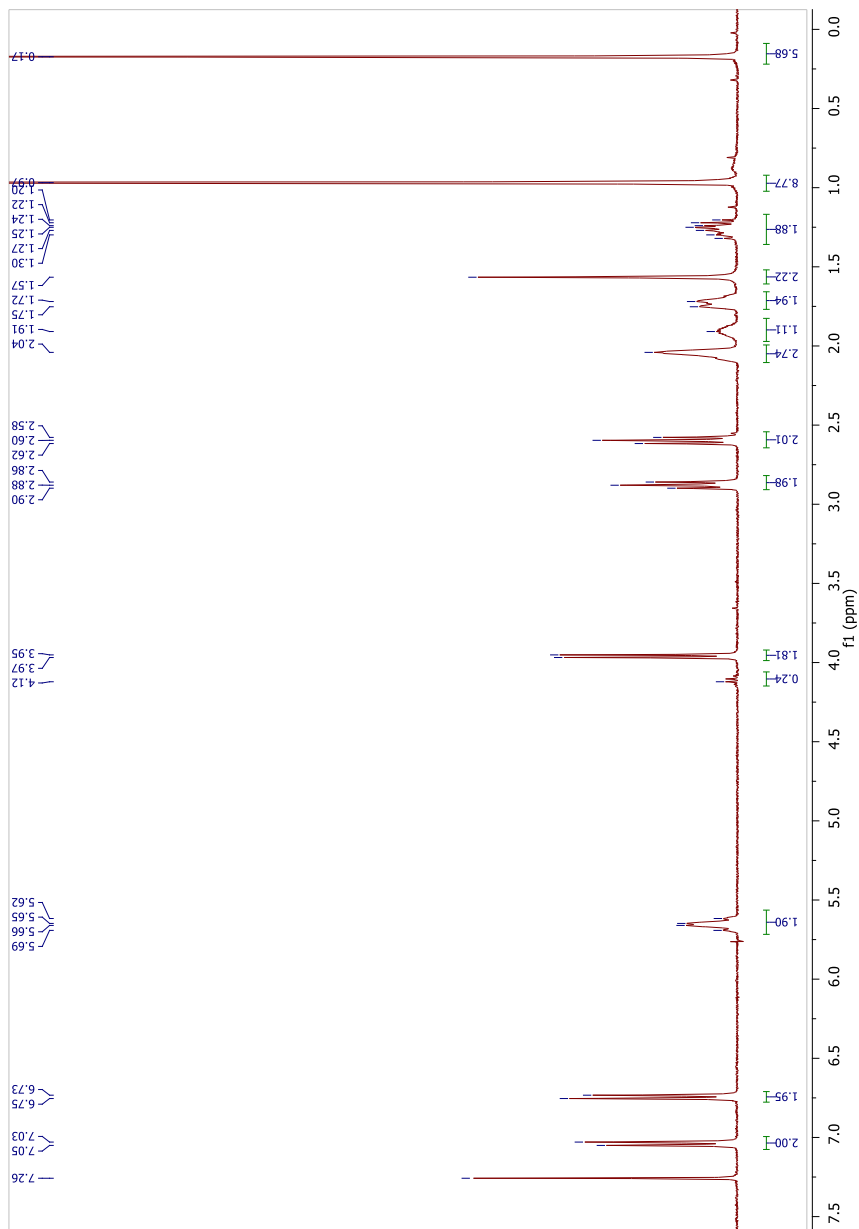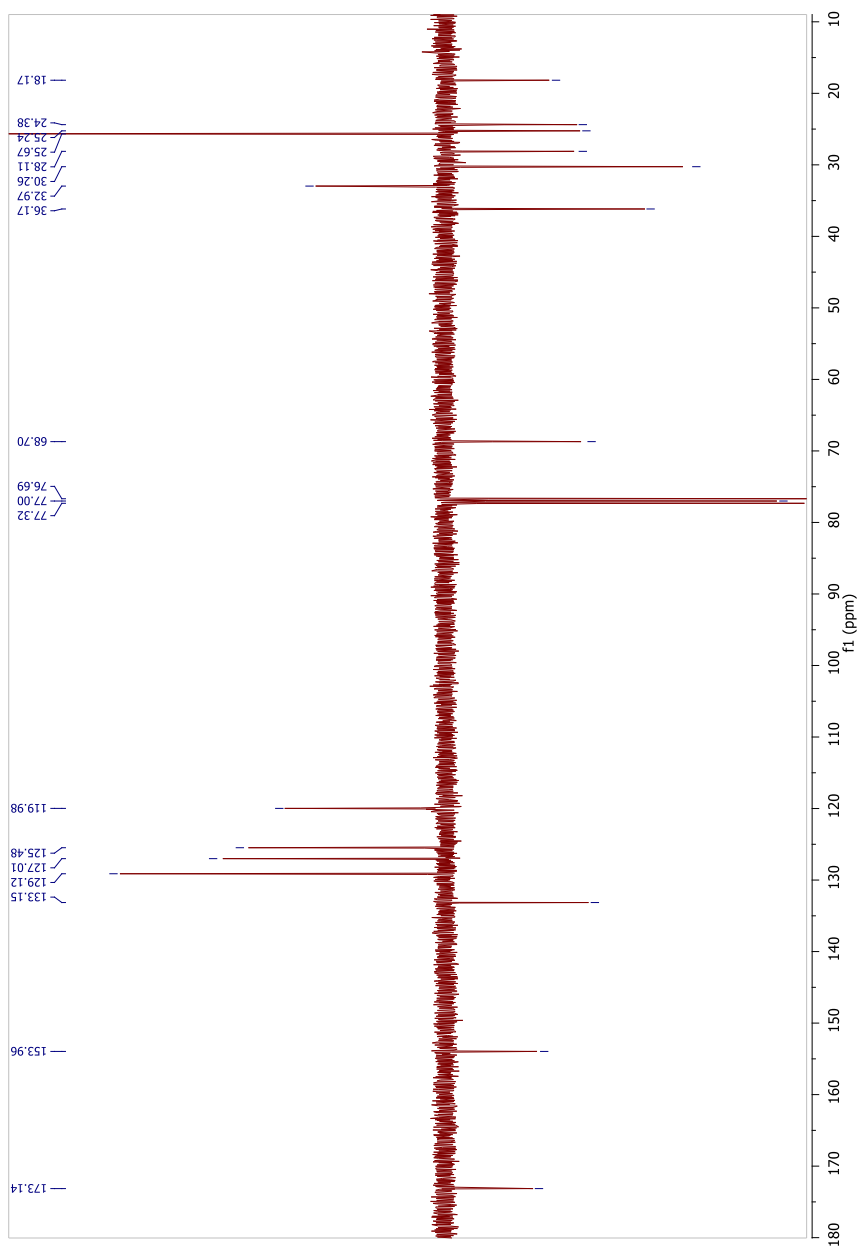
Compound 32. ^{1}H NMR and ^{13}C-APT NMR spectra.
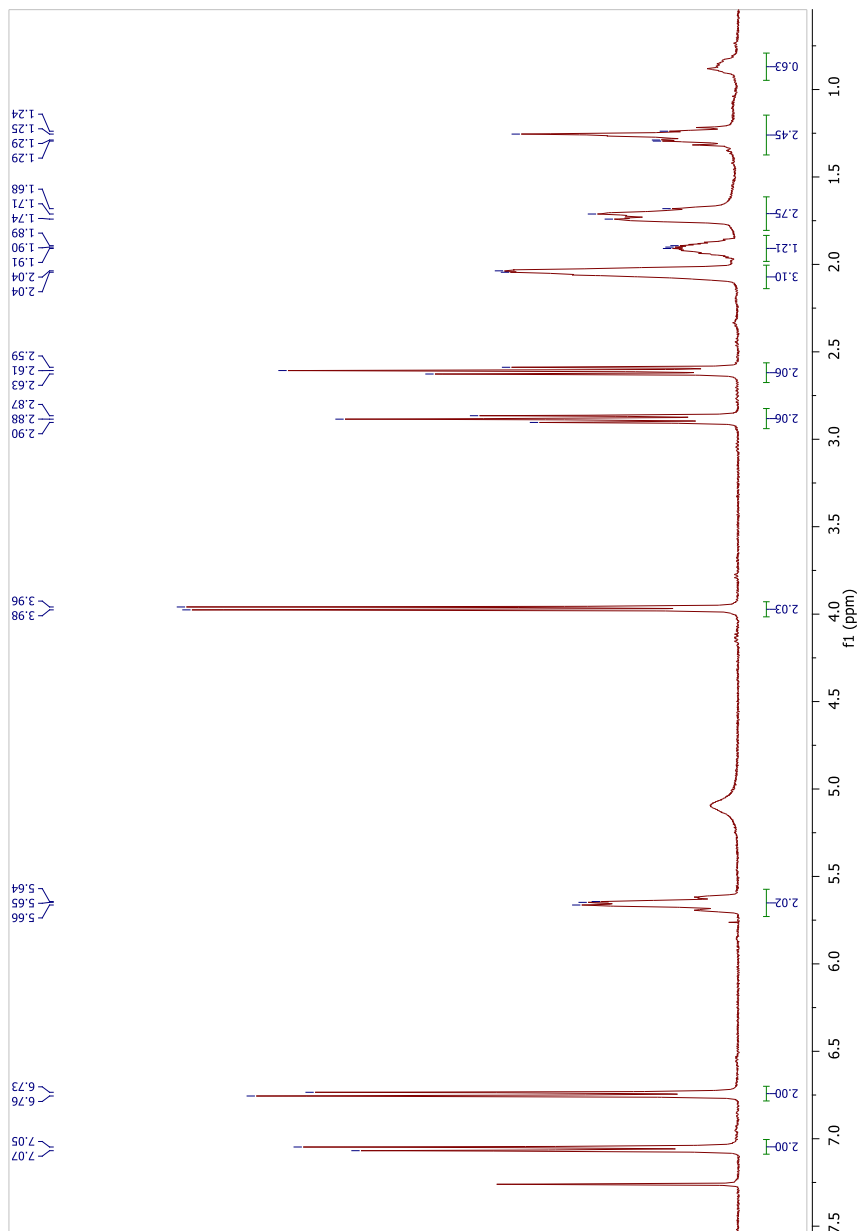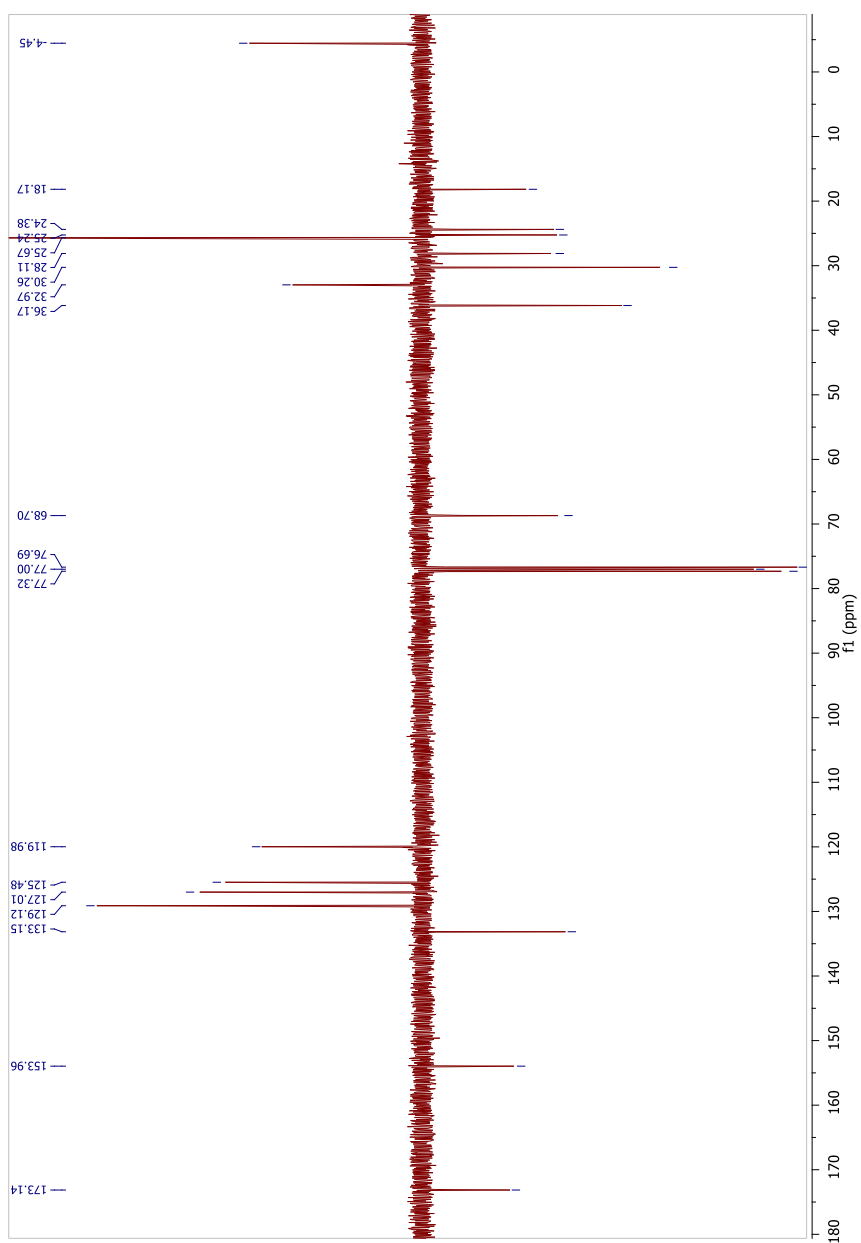
Compound 33. ^{1}H NMR and ^{13}C-APT NMR spectra.

10.00

21.74
21.76
26.95
29.68
29.86
29.96
30.84
35.56
35.83

46.93
47.14
47.36
47.57
47.78
47.99
48.21

68.39
68.47
68.58
70.91
71.28

114.74
114.76

128.83
131.18

155.39

173.43

f1 (ppm)
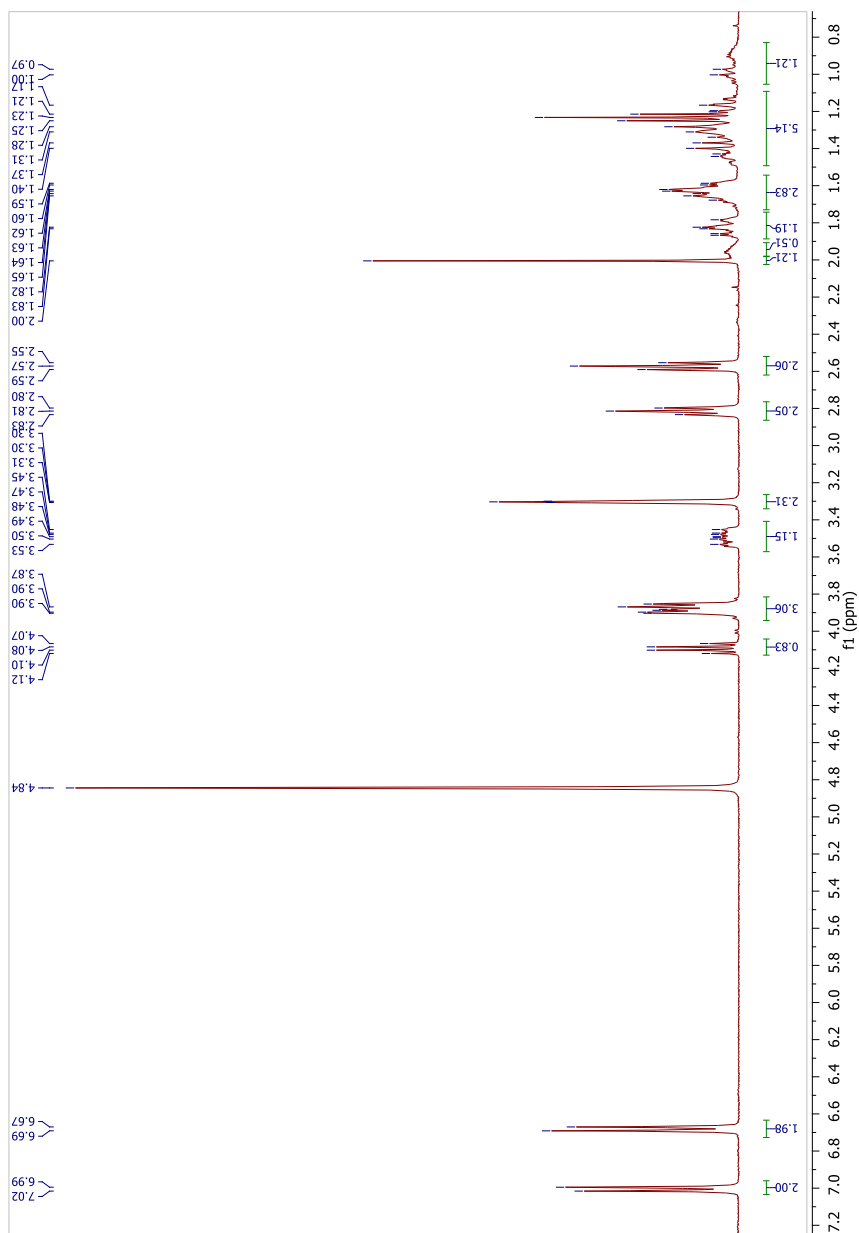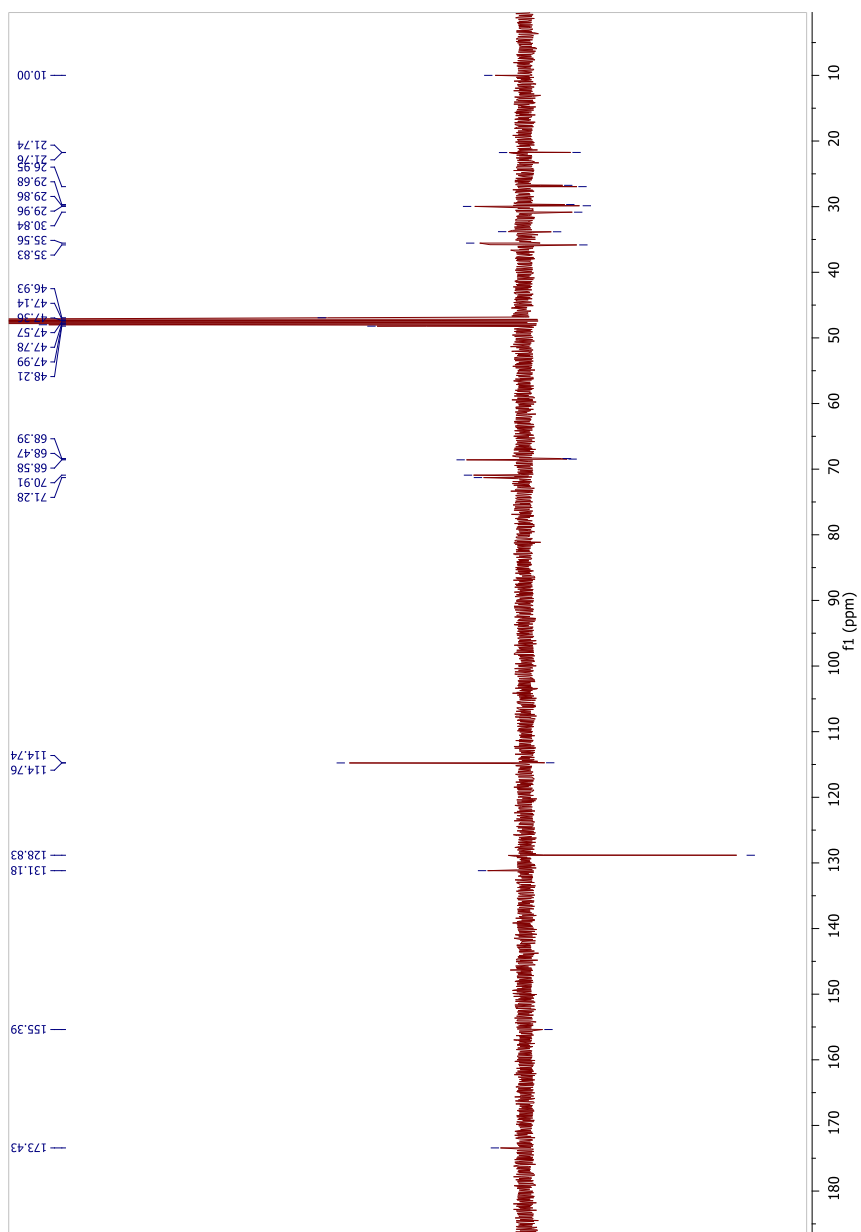
Compound 34. ^{1}H NMR and ^{13}C-APT NMR spectra.

23.35
29.89
31.81
35.87
39.53
39.74
39.95
40.16
40.37
45.41
66.20
115.50
129.48
130.87
156.03
172.65
202.97
203.35

f1 (ppm)
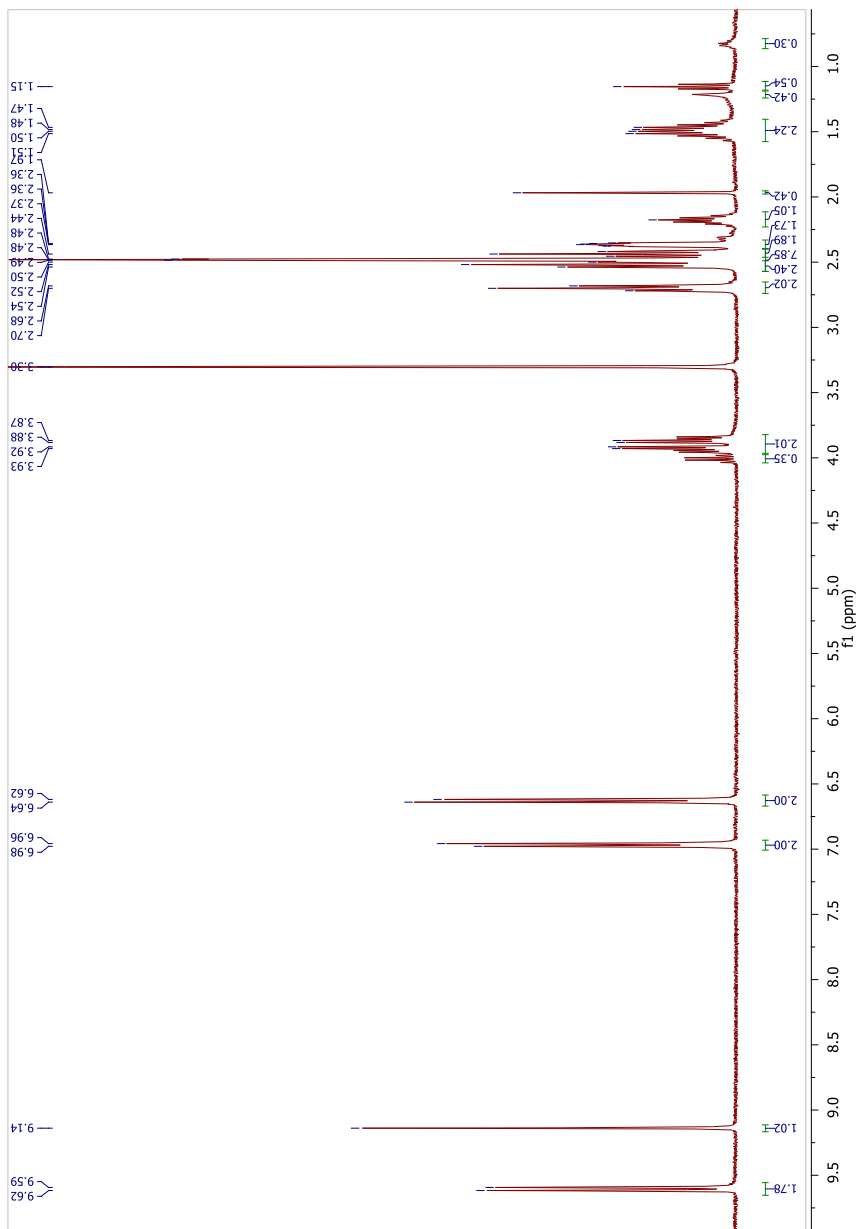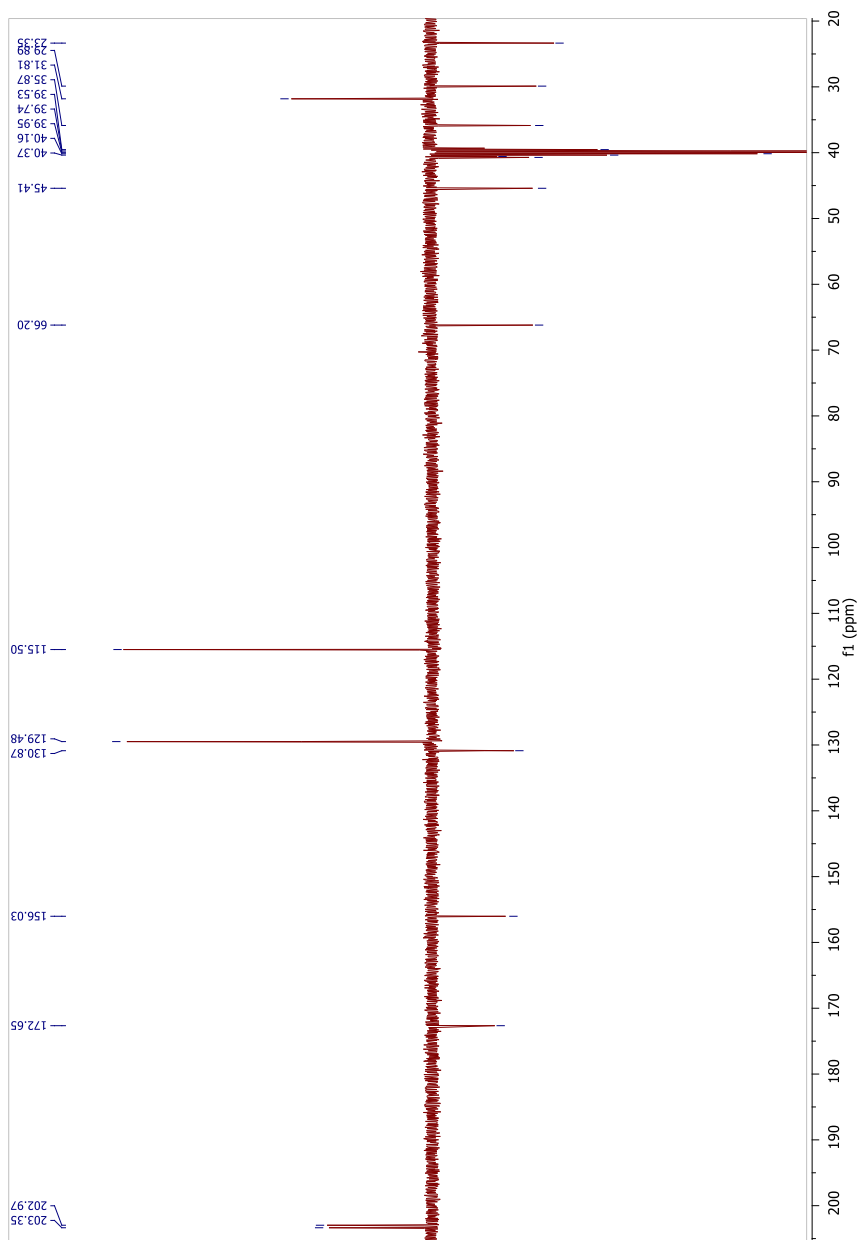
Compound 35. ^{1}H NMR spectrum.
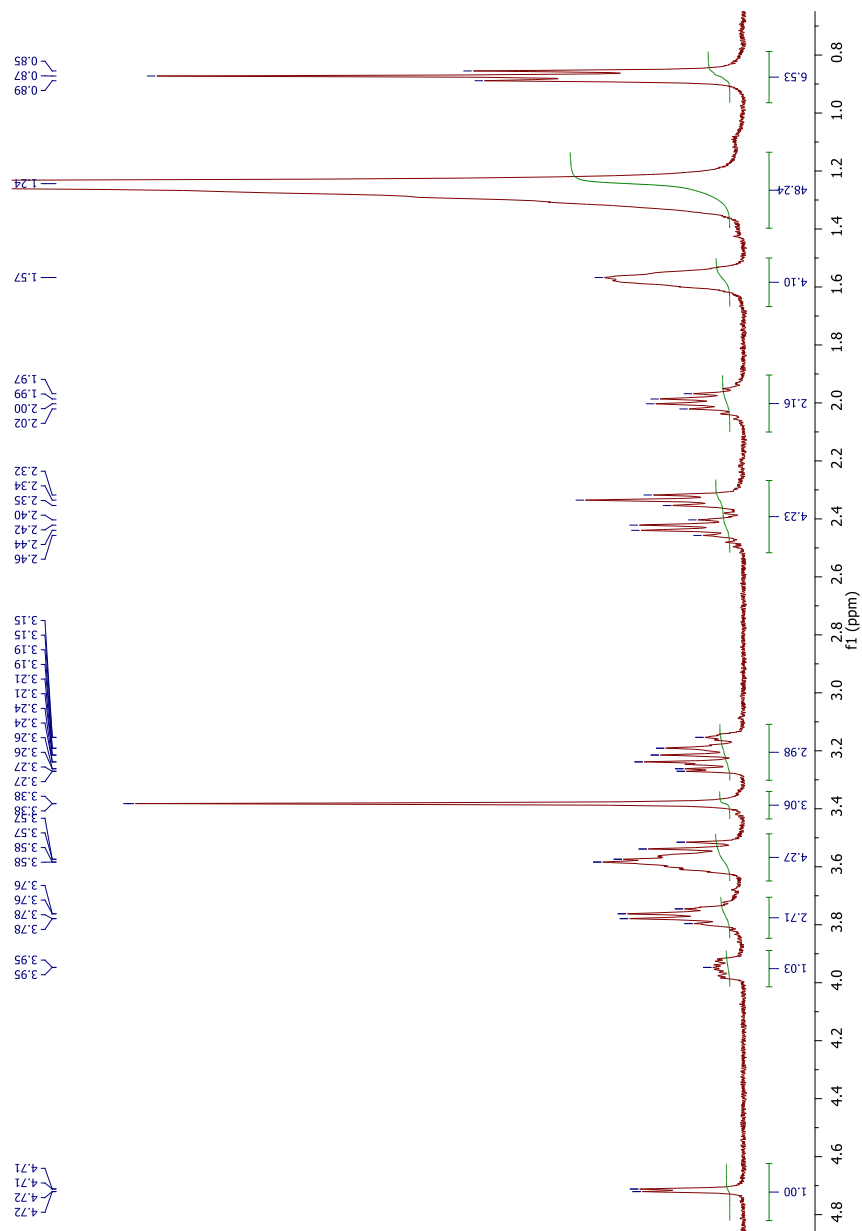
References

1. Beveridge, T. J., Use of the gram stain in microbiology. *Biotech Histochem* **2001,** *76* (3), 111-8.
2. Raetz, C. R.; Whitfield, C., Lipopolysaccharide endotoxins. *Annu Rev Biochem* **2002,** *71*, 635-700.
3. Vollmer, W.; Blanot, D.; de Pedro, M. A., Peptidoglycan structure and architecture. *FEMS Microbiol Rev* **2008,** *32* (2), 149-67.
4. Vollmer, W., Structural variation in the glycan strands of bacterial peptidoglycan. *FEMS Microbiol Rev* **2008,** *32* (2), 287-306.
5. Galanos, C.; Freudenberg, M. A.; Lüderitz, O.; Rietschel, E. T.; Westphal, O., Chemical, physicochemical and biological properties of bacterial lipopolysaccharides. *Prog Clin Biol Res* **1979,** *29*, 321-32.
6. Alexander, C.; Rietschel, E. T., Bacterial lipopolysaccharides and innate immunity. *J Endotoxin Res* **2001,** *7* (3), 167-202.
7. Rietschel, E. T.; Wollenweber, H. W.; Zähringer, U.; Lüderitz, O., Lipid A, the lipid component of bacterial lipopolysaccharides: relation of chemical structure to biological activity. *Klin Wochenschr* **1982,** *60* (14), 705-9.
8. Rudick, C. N.; Jiang, M.; Yaggie, R. E.; Pavlov, V. I.; Done, J.; Heckman, C. J.; Whitfield, C.; Schaeffer, A. J.; Klumpp, D. J., O-antigen modulates infection-induced pain states. *PLoS One* **2012,** *7* (8), e41273.
9. Huber, M.; Kalis, C.; Keck, S.; Jiang, Z.; Georgel, P.; Du, X.; Shamel, L.; Sovath, S.; Mudd, S.; Beutler, B.; Galanos, C.; Freudenberg, M. A., R-form LPS, the master key to the activation ofTLR4/MD-2-positive cells. *Eur J Immunol* **2006,** *36* (3), 701-11.
10. Sestito, S. E.; Sperandeo, P.; Santambrogio, C.; Ciaramelli, C.; Calabrese, V.; Rovati, G. E.; Zambelloni, L.; Grandori, R.; Polissi, A.; Peri, F., Functional characterization of E. coli LptC: interaction with LPS and a synthetic ligand. *Chembiochem* **2014,** *15* (5), 734-42.
11. Doerrler, W. T., Lipid trafficking to the outer membrane of Gram-negative bacteria. *Mol Microbiol* **2006,** *60* (3), 542-52.
12. Polissi, A.; Georgopoulos, C., Mutational analysis and properties of the msbA gene of Escherichia coli, coding for an essential ABC family transporter. *Mol Microbiol* **1996,** *20* (6), 1221-33.
13. Raetz, C. R., Biochemistry of endotoxins. *Annu Rev Biochem* **1990,** *59*, 129-70.

14. Buetow, L.; Smith, T. K.; Dawson, A.; Fyffe, S.; Hunter, W. N., Structure and reactivity of LpxD, the N-acyltransferase of lipid A biosynthesis. *Proc Natl Acad Sci U S A* **2007,** *104* (11), 4321-6.

15. Crowell, D. N.; Anderson, M. S.; Raetz, C. R., Molecular cloning of the genes for lipid A disaccharide synthase and UDP-N-acetylglucosamine acyltransferase in Escherichia coli. *J Bacteriol* **1986,** *168* (1), 152-9; Crowell, D. N.; Reznikoff, W. S.; Raetz, C. R., Nucleotide sequence of the Escherichia coli gene for lipid A disaccharide synthase. *J Bacteriol* **1987,** *169* (12), 5727-34.

16. Garrett, T. A.; Kadrmas, J. L.; Raetz, C. R., Identification of the gene encoding the Escherichia coli lipid A 4'-kinase. Facile phosphorylation of endotoxin analogs with recombinant LpxK. *J Biol Chem* **1997,** *272* (35), 21855-64; Garrett, T. A.; Que, N. L.; Raetz, C. R., Accumulation of a lipid A precursor lacking the 4'-phosphate following inactivation of the Escherichia coli lpxK gene. *J Biol Chem* **1998,** *273* (20), 12457-65.

17. Brozek, K. A.; Hosaka, K.; Robertson, A. D.; Raetz, C. R., Biosynthesis of lipopolysaccharide in Escherichia coli. Cytoplasmic enzymes that attach 3-deoxy-D-manno-octulosonic acid to lipid A. *J Biol Chem* **1989,** *264* (12), 6956-66.

18. Brozek, K. A.; Raetz, C. R., Biosynthesis of lipid A in Escherichia coli. Acyl carrier protein-dependent incorporation of laurate and myristate. *J Biol Chem* **1990,** *265* (26), 15410-7.

19. Onishi, H. R.; Pelak, B. A.; Gerckens, L. S.; Silver, L. L.; Kahan, F. M.; Chen, M. H.; Patchett, A. A.; Galloway, S. M.; Hyland, S. A.; Anderson, M. S.; Raetz, C. R., Antibacterial agents that inhibit lipid A biosynthesis. *Science* **1996,** *274* (5289), 980-2.

20. Alaimo, C.; Catrein, I.; Morf, L.; Marolda, C. L.; Callewaert, N.; Valvano, M. A.; Feldman, M. F.; Aebi, M., Two distinct but interchangeable mechanisms for flipping of lipid-linked oligosaccharides. *EMBO J* **2006,** *25* (5), 967-76.

21. Santambrogio, C.; Sperandeo, P.; Villa, R.; Sobott, F.; Polissi, A.; Grandori, R., LptA assembles into rod-like oligomers involving disorder-to-order transitions. *J Am Soc Mass Spectrom* **2013,** *24* (10), 1593-602; Freinkman, E.; Okuda, S.; Ruiz, N.; Kahne, D., Regulated assembly of the transenvelope protein complex required for lipopolysaccharide export. *Biochemistry* **2012,** *51* (24), 4800-6.

22. Sperandeo, P.; Cescutti, R.; Villa, R.; Di Benedetto, C.; Candia, D.; Dehò, G.; Polissi, A., Characterization of lptA and lptB, two essential genes implicated in lipopolysaccharide transport to the outer membrane of Escherichia coli. *J Bacteriol* **2007,** *189* (1), 244-53; Sperandeo, P.; Lau,

F. K.; Carpentieri, A.; De Castro, C.; Molinaro, A.; Dehò, G.; Silhavy, T. J.; Polissi, A., Functional analysis of the protein machinery required for transport of lipopolysaccharide to the outer membrane of Escherichia coli. *J Bacteriol* **2008,** *190* (13), 4460-9.

23. Chng, S. S.; Gronenberg, L. S.; Kahne, D., Proteins required for lipopolysaccharide assembly in Escherichia coli form a transenvelope complex. *Biochemistry* **2010,** *49* (22), 4565-7.

24. Robinson, J. A., Max Bergmann lecture protein epitope mimetics in the age of structural vaccinology. *J Pept Sci* **2013,** *19* (3), 127-40.

25. Narita, S.; Tokuda, H., Biochemical characterization of an ABC transporter LptBFGC complex required for the outer membrane sorting of lipopolysaccharides. *FEBS Lett* **2009,** *583* (13), 2160-4.

26. Villa, R.; Martorana, A. M.; Okuda, S.; Gourlay, L. J.; Nardini, M.; Sperandeo, P.; Dehò, G.; Bolognesi, M.; Kahne, D.; Polissi, A., The Escherichia coli Lpt transenvelope protein complex for lipopolysaccharide export is assembled via conserved structurally homologous domains. *J Bacteriol* **2013,** *195* (5), 1100-8.

27. Sperandeo, P.; Villa, R.; Martorana, A. M.; Samalikova, M.; Grandori, R.; Dehò, G.; Polissi, A., New insights into the Lpt machinery for lipopolysaccharide transport to the cell surface: LptA-LptC interaction and LptA stability as sensors of a properly assembled transenvelope complex. *J Bacteriol* **2011,** *193* (5), 1042-53.

28. Okuda, S.; Freinkman, E.; Kahne, D., Cytoplasmic ATP hydrolysis powers transport of lipopolysaccharide across the periplasm in E. coli. *Science* **2012,** *338* (6111), 1214-7.

29. Linton, K. J.; Higgins, C. F., Structure and function of ABC transporters: the ATP switch provides flexible control. *Pflugers Arch* **2007,** *453* (5), 555-67.

30. Tran, A. X.; Trent, M. S.; Whitfield, C., The LptA protein of Escherichia coli is a periplasmic lipid A-binding protein involved in the lipopolysaccharide export pathway. *J Biol Chem* **2008,** *283* (29), 20342-9.

31. Tran, A. X.; Dong, C.; Whitfield, C., Structure and functional analysis of LptC, a conserved membrane protein involved in the lipopolysaccharide export pathway in Escherichia coli. *J Biol Chem* **2010,** *285* (43), 33529-39.

32. Suits, M. D.; Sperandeo, P.; Dehò, G.; Polissi, A.; Jia, Z., Novel structure of the conserved gram-negative lipopolysaccharide transport protein A and mutagenesis analysis. *J Mol Biol* **2008,** *380* (3), 476-88.

33. Linton, K. J., Structure and function of ABC transporters. *Physiology (Bethesda)* **2007,** *22*, 122-30.
34. Akira, S.; Uematsu, S.; Takeuchi, O., Pathogen recognition and innate immunity. *Cell* **2006,** *124* (4), 783-801; Ausubel, F. M., Are innate immune signaling pathways in plants and animals conserved? *Nat Immunol* **2005,** *6* (10), 973-9.
35. Janeway, C. A.; Medzhitov, R., Innate immune recognition. *Annu Rev Immunol* **2002,** *20*, 197-216.
36. Beutler, B., Toll-like receptors: how they work and what they do. *Curr Opin Hematol* **2002,** *9* (1), 2-10.
37. Schmidt, C., Clinical setbacks for toll-like receptor 9 agonists in cancer. *Nat Biotechnol* **2007,** *25* (8), 825-6.
38. Medzhitov, R., Toll-like receptors and innate immunity. *Nat Rev Immunol* **2001,** *1* (2), 135-45.
39. Miyake, K., Innate recognition of lipopolysaccharide by Toll-like receptor 4-MD-2. *Trends Microbiol* **2004,** *12* (4), 186-92.
40. Beutler, B.; Du, X.; Poltorak, A., Identification of Toll-like receptor 4 (Tlr4) as the sole conduit for LPS signal transduction: genetic and evolutionary studies. *J Endotoxin Res* **2001,** *7* (4), 277-80.
41. Kim, H. M.; Park, B. S.; Kim, J. I.; Kim, S. E.; Lee, J.; Oh, S. C.; Enkhbayar, P.; Matsushima, N.; Lee, H.; Yoo, O. J.; Lee, J. O., Crystal structure of the TLR4-MD-2 complex with bound endotoxin antagonist Eritoran. *Cell* **2007,** *130* (5), 906-17.
42. Cighetti, R. Design, synthesis and biological characterization of new small-molecule TLR4 modulators. Università di Milano Bicocca, 2014.
43. O'Neill, L. A.; Bowie, A. G., The family of five: TIR-domain-containing adaptors in Toll-like receptor signalling. *Nat Rev Immunol* **2007,** *7* (5), 353-64.
44. Park, B. S.; Song, D. H.; Kim, H. M.; Choi, B. S.; Lee, H.; Lee, J. O., The structural basis of lipopolysaccharide recognition by the TLR4-MD-2 complex. *Nature* **2009,** *458* (7242), 1191-5.
45. Ohto, U.; Fukase, K.; Miyake, K.; Shimizu, T., Structural basis of species-specific endotoxin sensing by innate immune receptor TLR4/MD-2. *Proc Natl Acad Sci U S A* **2012,** *109* (19), 7421-6.
46. Yu, L.; Phillips, R. L.; Zhang, D.; Teghanemt, A.; Weiss, J. P.; Gioannini, T. L., NMR studies of hexaacylated endotoxin bound to wild-type and F126A mutant MD-2 and MD-2·TLR4 ectodomain complexes. *J Biol Chem* **2012,** *287* (20), 16346-55.

47. Needham, B. D.; Trent, M. S., Fortifying the barrier: the impact of lipid A remodelling on bacterial pathogenesis. *Nat Rev Microbiol* **2013,** *11* (7), 467-81.

48. Jerala, R., Structural biology of the LPS recognition. *Int J Med Microbiol* **2007,** *297* (5), 353-63.

49. Kim, J. I.; Lee, C. J.; Jin, M. S.; Lee, C. H.; Paik, S. G.; Lee, H.; Lee, J. O., Crystal structure of CD14 and its implications for lipopolysaccharide signaling. *J Biol Chem* **2005,** *280* (12), 11347-51.

50. Zanoni, I.; Granucci, F., Role of CD14 in host protection against infections and in metabolism regulation. *Front Cell Infect Microbiol* **2013,** *3*, 32.

51. Zanoni, I.; Ostuni, R.; Marek, L. R.; Barresi, S.; Barbalat, R.; Barton, G. M.; Granucci, F.; Kagan, J. C., CD14 controls the LPS-induced endocytosis of Toll-like receptor 4. *Cell* **2011,** *147* (4), 868-80.

52. Gioannini, T. L.; Teghanemt, A.; Zhang, D.; Coussens, N. P.; Dockstader, W.; Ramaswamy, S.; Weiss, J. P., Isolation of an endotoxin-MD-2 complex that produces Toll-like receptor 4-dependent cell activation at picomolar concentrations. *Proc Natl Acad Sci U S A* **2004,** *101* (12), 4186-91; Gioannini, T. L.; Teghanemt, A.; Zhang, D.; Levis, E. N.; Weiss, J. P., Monomeric endotoxin:protein complexes are essential for TLR4-dependent cell activation. *J Endotoxin Res* **2005,** *11* (2), 117-23.

53. Shimazu, R.; Akashi, S.; Ogata, H.; Nagai, Y.; Fukudome, K.; Miyake, K.; Kimoto, M., MD-2, a molecule that confers lipopolysaccharide responsiveness on Toll-like receptor 4. *J Exp Med* **1999,** *189* (11), 1777-82.

54. Hotchkiss, R. S.; Karl, I. E., The pathophysiology and treatment of sepsis. *N Engl J Med* **2003,** *348* (2), 138-50.

55. Peri, F.; Calabrese, V., Toll-like receptor 4 (TLR4) modulation by synthetic and natural compounds: an update. *J Med Chem* **2014,** *57* (9), 3612-22.

56. Kanzler, H.; Barrat, F. J.; Hessel, E. M.; Coffman, R. L., Therapeutic targeting of innate immunity with Toll-like receptor agonists and antagonists. *Nat Med* **2007,** *13* (5), 552-9.

57. Mata-Haro, V.; Cekic, C.; Martin, M.; Chilton, P. M.; Casella, C. R.; Mitchell, T. C., The vaccine adjuvant monophosphoryl lipid A as a TRIF-biased agonist of TLR4. *Science* **2007,** *316* (5831), 1628-32.

58. Calabrese, V.; Cighetti, R.; Peri, F., Molecular simplification of lipid A structure: TLR4-modulating cationic and anionic amphiphiles. *Mol Immunol* **2014**.

59. Mueller, M.; Lindner, B.; Kusumoto, S.; Fukase, K.; Schromm, A. B.; Seydel, U., Aggregates are the biologically active units of endotoxin. *J Biol Chem* **2004,** *279* (25), 26307-13; Gutsmann, T.; Schromm, A. B.; Brandenburg, K., The physicochemistry of endotoxins in relation to bioactivity. *Int J Med Microbiol* **2007,** *297* (5), 341-52.

60. Brandenburg, K.; Wiese, A., Endotoxins: relationships between structure, function, and activity. *Curr Top Med Chem* **2004,** *4* (11), 1127-46.

61. Wang, X.; Quinn, P. J., Endotoxins: lipopolysaccharides of gram-negative bacteria. *Subcell Biochem* **2010,** *53*, 3-25.

62. Manavalan, B.; Basith, S.; Choi, S., Similar Structures but Different Roles - An Updated Perspective on TLR Structures. *Front Physiol* **2011,** *2*, 41.

63. Youn, H. S.; Lee, J. Y.; Saitoh, S. I.; Miyake, K.; Kang, K. W.; Choi, Y. J.; Hwang, D. H., Suppression of MyD88- and TRIF-dependent signaling pathways of Toll-like receptor by (-)-epigallocatechin-3-gallate, a polyphenol component of green tea. *Biochem Pharmacol* **2006,** *72* (7), 850-9.

64. Chun, K. H.; Seong, S. Y., CD14 but not MD2 transmit signals from DAMP. *Int Immunopharmacol* **2010,** *10* (1), 98-106.

65. Piazza, M.; Calabrese, V.; Damore, G.; Cighetti, R.; Gioannini, T.; Weiss, J.; Peri, F., A synthetic lipid A mimetic modulates human TLR4 activity. *ChemMedChem* **2012,** *7* (2), 213-7.

66. Cighetti, R.; Ciaramelli, C.; Sestito, S. E.; Zanoni, I.; Kubik, Ł.; Ardá-Freire, A.; Calabrese, V.; Granucci, F.; Jerala, R.; Martín-Santamaría, S.; Jiménez-Barbero, J.; Peri, F., Modulation of CD14 and TLR4·MD-2 activities by a synthetic lipid A mimetic. *Chembiochem* **2014,** *15* (2), 250-8.

67. Lonez, C.; Vandenbranden, M.; Ruysschaert, J. M., Cationic lipids activate intracellular signaling pathways. *Adv Drug Deliv Rev* **2012,** *64* (15), 1749-58.

68. Wilmar, A.; Lonez, C.; Vermeersch, M.; Andrianne, M.; Pérez-Morga, D.; Ruysschaert, J. M.; Vandenbranden, M.; Leo, O.; Temmerman, S. T., The cationic lipid, diC14 amidine, extends the adjuvant properties of aluminum salts through a TLR-4- and caspase-1-independent mechanism. *Vaccine* **2012,** *30* (2), 414-24.

69. Chen, W.; Yan, W.; Huang, L., A simple but effective cancer vaccine consisting of an antigen and a cationic lipid. *Cancer Immunol Immunother* **2008,** *57* (4), 517-30; Tanaka, T.; Legat, A.; Adam, E.; Steuve, J.; Gatot, J. S.; Vandenbranden, M.; Ulianov, L.; Lonez, C.;

Ruysschaert, J. M.; Muraille, E.; Tuynder, M.; Goldman, M.; Jacquet, A., DiC14-amidine cationic liposomes stimulate myeloid dendritic cells through Toll-like receptor 4. *Eur J Immunol* **2008,** *38* (5), 1351-7.

70. Piazza, M.; Rossini, C.; Della Fiorentina, S.; Pozzi, C.; Comelli, F.; Bettoni, I.; Fusi, P.; Costa, B.; Peri, F., Glycolipids and benzylammonium lipids as novel antisepsis agents: synthesis and biological characterization. *J Med Chem* **2009,** *52* (4), 1209-13.

71. Piazza, M.; Calabrese, V.; Baruffa, C.; Gioannini, T.; Weiss, J.; Peri, F., The cationic amphiphile 3,4-bis(tetradecyloxy)benzylamine inhibits LPS signaling by competing with endotoxin for CD14 binding. *Biochem Pharmacol* **2010,** *80* (12), 2050-6.

72. Liu, T.; Gao, Y. J.; Ji, R. R., Emerging role of Toll-like receptors in the control of pain and itch. *Neurosci Bull* **2012,** *28* (2), 131-44.

73. Schromm, A. B.; Howe, J.; Ulmer, A. J.; Wiesmüller, K. H.; Seyberth, T.; Jung, G.; Rössle, M.; Koch, M. H.; Gutsmann, T.; Brandenburg, K., Physicochemical and biological analysis of synthetic bacterial lipopeptides: validity of the concept of endotoxic conformation. *J Biol Chem* **2007,** *282* (15), 11030-7.

74. Chahal, D. S.; Sivamani, R. K.; Isseroff, R. R.; Dasu, M. R., Plant-based modulation of Toll-like receptors: an emerging therapeutic model. *Phytother Res* **2013,** *27* (10), 1423-38.

75. Park, S. J.; Youn, H. S., Suppression of homodimerization of toll-like receptor 4 by isoliquiritigenin. *Phytochemistry* **2010,** *71* (14-15), 1736-40.

76. Ahn, S. I.; Lee, J. K.; Youn, H. S., Inhibition of homodimerization of toll-like receptor 4 by 6-shogaol. *Mol Cells* **2009,** *27* (2), 211-5.

77. Kim, S. Y.; Koo, J. E.; Seo, Y. J.; Tyagi, N.; Jeong, E.; Choi, J.; Lim, K. M.; Park, Z. Y.; Lee, J. Y., Suppression of Toll-like receptor 4 activation by caffeic acid phenethyl ester is mediated by interference of LPS binding to MD2. *Br J Pharmacol* **2013,** *168* (8), 1933-45.

78. Youn, H. S.; Lee, J. K.; Choi, Y. J.; Saitoh, S. I.; Miyake, K.; Hwang, D. H.; Lee, J. Y., Cinnamaldehyde suppresses toll-like receptor 4 activation mediated through the inhibition of receptor oligomerization. *Biochem Pharmacol* **2008,** *75* (2), 494-502.

79. Gradisar, H.; Keber, M. M.; Pristovsek, P.; Jerala, R., MD-2 as the target of curcumin in the inhibition of response to LPS. *J Leukoc Biol* **2007,** *82* (4), 968-74.

80. Youn, H. S.; Saitoh, S. I.; Miyake, K.; Hwang, D. H., Inhibition of homodimerization of Toll-like receptor 4 by curcumin. *Biochem Pharmacol* **2006,** *72* (1), 62-9.

81. Sperry, J. B.; Smith III, A. B., Chemical Synthesis of Diverse Phenolic Compounds Isolated From Olive Oils. In *Olive and Olive Oils in Health and Disease Prevention*, Elsevier, Ed. 2010; pp 1439-1464.

82. Cicerale, S.; Conlan, X. A.; Sinclair, A. J.; Keast, R. S., Chemistry and health of olive oil phenolics. *Crit Rev Food Sci Nutr* **2009,** *49* (3), 218-36.

83. Sangiovanni, E.; Colombo, E.; Fumagalli, M.; Abbiati, F.; Caruso, D.; Dell'Agli, M., Inhibition of NF- κB activity by minor polar components of extra-virgin olive oil at gastric level. *Phytother Res* **2012,** *26* (10), 1569-71.

84. Visioli, F.; Poli, A.; Gall, C., Antioxidant and other biological activities of phenols from olives and olive oil. *Med Res Rev* **2002,** *22* (1), 65-75.

85. Maiuri, M. C.; De Stefano, D.; Di Meglio, P.; Irace, C.; Savarese, M.; Sacchi, R.; Cinelli, M. P.; Carnuccio, R., Hydroxytyrosol, a phenolic compound from virgin olive oil, prevents macrophage activation. *Naunyn Schmiedebergs Arch Pharmacol* **2005,** *371* (6), 457-65.

86. Beauchamp, G. K.; Keast, R. S.; Morel, D.; Lin, J.; Pika, J.; Han, Q.; Lee, C. H.; Smith, A. B.; Breslin, P. A., Phytochemistry: ibuprofen-like activity in extra-virgin olive oil. *Nature* **2005,** *437* (7055), 45-6.

87. Iacono, A.; Gómez, R.; Sperry, J.; Conde, J.; Bianco, G.; Meli, R.; Gómez-Reino, J. J.; Smith, A. B.; Gualillo, O., Effect of oleocanthal and its derivatives on inflammatory response induced by lipopolysaccharide in a murine chondrocyte cell line. *Arthritis Rheum* **2010,** *62* (6), 1675-82.

88. Procopio, A.; Alcaro, S.; Nardi, M.; Oliverio, M.; Ortuso, F.; Sacchetta, P.; Pieragostino, D.; Sindona, G., Synthesis, biological evaluation, and molecular modeling of oleuropein and its semisynthetic derivatives as cyclooxygenase inhibitors. *J Agric Food Chem* **2009,** *57* (23), 11161-7.

89. Xagorari, A.; Papapetropoulos, A.; Mauromatis, A.; Economou, M.; Fotsis, T.; Roussos, C., Luteolin inhibits an endotoxin-stimulated phosphorylation cascade and proinflammatory cytokine production in macrophages. *J Pharmacol Exp Ther* **2001,** *296* (1), 181-7.

90. Xagorari, A.; Roussos, C.; Papapetropoulos, A., Inhibition of LPS-stimulated pathways in macrophages by the flavonoid luteolin. *Br J Pharmacol* **2002,** *136* (7), 1058-64.

91. Piazza, M.; Rossini, C.; Della Fiorentina, S.; Pozzi, C.; Comelli, F.; Bettoni, I.; Fusi, P.; Costa, B.; Peri, F., Glycolipids and Benzylammonium Lipids as Novel Antisepsis Agents: Synthesis and Biological Characterization. *Journal of Medicinal Chemistry* **2009,** *52* (4), 1209-1213.

92. Piazza, M.; Yu, L.; Teghanemt, A.; Gioannini, T.; Weiss, J.; Peri, F., Evidence of a Specific Interaction between New Synthetic Antisepsis Agents and CD14. *Biochemistry* **2009,** *48* (51), 12337-12344.

93. Piazza, M.; Calabrese, V.; Baruffa, C.; Gioannini, T.; Weiss, J.; Peri, F., The cationic amphiphile 3,4-bis(tetradecyloxy)benzylamine inhibits LPS signaling by competing with endotoxin for CD14 binding. *Biochemical Pharmacology* **2010,** *80* (12), 2050-2056.

94. Galanos, C.; Lüderitz, O.; Westphal, O., A new method for the extraction of R lipopolysaccharides. *Eur J Biochem* **1969,** *9* (2), 245-9.

95. Troelstra, A.; Antal-Szalmas, P.; de Graaf-Miltenburg, L. A.; Weersink, A. J.; Verhoef, J.; Van Kessel, K. P.; Van Strijp, J. A., Saturable CD14-dependent binding of fluorescein-labeled lipopolysaccharide to human monocytes. *Infect Immun* **1997,** *65* (6), 2272-7.

96. Brade, H.; Galanos, C., A method to detect 2-keto-3-deoxyoctanat and related compounds on pherograms and chromatograms. *Anal Biochem* **1983,** *132* (1), 158-9.

97. Bettoni, I.; Comelli, F.; Rossini, C.; Granucci, F.; Giagnoni, G.; Peri, F.; Costa, B., Glial TLR4 receptor as new target to treat neuropathic pain: Efficacy of a new receptor antagonist in a model of peripheral nerve injury in mice. *Glia* **2008,** *56* (12), 1312-1319.

98. Peri, F.; Granucci, F.; Costa, B.; Zanoni, I.; Marinzi, C.; Nicotra, F., Inhibition of lipid A stimulated activation of human dendritic cells and macrophages by amino and hydroxylamino monosaccharides. *Angewandte Chemie-International Edition* **2007,** *46* (18), 3308-3312.

99. Kim, J.; Lee, C.; Jin, M.; Lee, C.; Paik, S.; Lee, H.; Lee, J., Crystal structure of CD14 and its implications for lipopolysaccharide signaling. *J Biol Chem* **2005,** *280* (12), 11347-51.

100. Liang, J.; Edelsbrunner, H.; Woodward, C., Anatomy of protein pockets and cavities: measurement of binding site geometry and implications for ligand design. *Protein Sci* **1998,** *7* (9), 1884-97.

101. Hofmann, A. M.; Wurm, F.; Frey, H., Macromolecules, 2011; Vol. 44, pp 4648-4657.

102. Smith, A. B.; Sperry, J. B.; Han, Q., Syntheses of (-)-oleocanthal, a natural NSAID found in extra virgin olive oil, the (-)-deacetoxy-oleuropein aglycone, and related analogues. *J Org Chem* **2007,** *72* (18), 6891-900.

103. Zahmakiran, M.; Akbayrak, S.; Kodaira, T.; Ozkar, S., Osmium(0) nanoclusters stabilized by zeolite framework; highly active catalyst in the aerobic oxidation of alcohols under mild conditions. *Dalton Trans* **2010,** *39* (32), 7521-7.

104.   Majumdar, D.; Alexander, M. D.; Coward, J. K., Synthesis of isopeptide epoxide peptidomimetics. *J Org Chem* **2009,** *74* (2), 617-27.

105.   Harrison, C.; Hodge, P., Polymer-supported Periodate and Iodate as Oxidizing Agents. *J.C.S Perkin* **1982**, 509-511.

106.   Buckley, S., LaurenceMarc, Synthesis of mevalonic acid lactone via a meso-dialdehyde: a model for desymmetrization. *ARKIVOC* **2002,** *7*, 46-56.

107.   Solladiè, G.; Gressot-Kempf, L., Chiral Sulphoxides in Asymmetric Synthesis: Enantioselective Synthesis of Tarchonanthuslactione. *Tetrahedron Asimmetry* **1996,** *7* (8), 2371-2379.

108.   Laemmli, U. K., Cleavage of structural proteins during the assembly of the head of bacteriophage T4. *Nature* **1970,** *227* (5259), 680-5.

109.   Kittelberger, R.; Hilbink, F., Sensitive silver-staining detection of bacterial lipopolysaccharides in polyacrylamide gels. *J Biochem Biophys Methods* **1993,** *26* (1), 81-6.

Collaborations

NMR studies on the protein LptC: Dr. Cristina Airoldi[1]

LptC team: Dr. Paola Sperandeo[1], Prof. Alessandra Polissi[1], Dr.Carlo Santambrogio[1], Prof. Rita Grandori[1]

Computational studies: Dr. Lucia Perez Regidor[2], Dr. Lukasz Kubic[2], Dr. Sonsoles Martìn-Santamarìa[2]

NMR studies on the protein MD-2: Dr. Ana Ardá Freire[2], Prof. Jesús Jiménez-Barbero[2]

Expression of the protein MD-2: Prof. Roman Jerala[3]

CMC measurements: Dr. Julio Rodriguez-Lavado[4]

Vaccine adjuvants team: Dr. Matilde Forcella[1], Dr. Paola Fusi[1], LOFARMA[5]

---

[1] Università degli Studi di Milano Bicocca, Milan, Italy

[2] Centro de Investigaciones Biológicas - CSIC, Madrid, Spain

[3] National Institute of Chemistry, Ljubljana, Slovenia

[4] Universidad de Sevilla, Siviglia, Spain

[5] LOFARMA S.P.A., Milan, Italy

Publications and communications

Publications

1. R. Cighetti, <u>C. Ciaramelli</u>, S. E. Sestito, I. Zanoni, Ł. Kubik, A. Ardá-Freire, V. Calabrese, F. Granucci, R. Jerala, S. Martín-Santamaría, J. Jiménez-Barbero and F. Peri (**2013**), Modulation of CD14 and TLR4.MD-2 activities by a synthetic lipid A mimetic, *ChemBioChem*, *14*: 1-10.

2. S. E. Sestito, P. Sperandeo, C. Santambrogio, <u>C. Ciaramelli</u>, V. Calabrese, G.E. Rovati, L. Zambelloni, R. Grandori, A, Polissi and F. Peri (**2014**), Functional Characterization of *E. coli* LptC: Interaction with LPS and a Synthetic Ligand. *ChemBioChem*, *15*: 734–742.

Communications

1. <u>C. Ciaramelli</u>, V. Calabrese, F. Peri, New Molecules Active On TLR4-LPS Signalling: Synthetic Lipid A analogues and chemically modified LPS, poster contribution, XIII Convegno Scuola sulla Chimica dei Carboidrati, Certosa di Pontignano, Siena, Italy, June 2012.

2. <u>C. Ciaramelli</u>, V. Calabrese, F. Peri, New Molecules Active On TLR4-LPS Signalling: Synthetic Lipid A analogues and chemically modified LPS, poster contribution, 26th International Carbohydrate Symposium, Madrid, Spain, July 2012.

3. F. Peri, V. Calabrese, F. Granucci, I. Zanoni, J. Weiss, T. Gioannini, C. <u>Ciaramelli, R. </u>Cighetti, S. Sestito, M. Piazza, Carbohydrate-

derived synthetic molecules active on endotoxin/TLR4 signaling, oral contribution, 26th International Carbohydrate Symposium, Madrid, Spain, July 2012.

4. F. Peri, V. Calabrese, C. Ciaramelli, S. Sestito, R. Cighetti. Carbohydrate-derived synthetic molecules targeting TLR4: from antisepsis drugs to central nervous system therapeutics, oral contribution, 10th Carbohydrate Bioengineering Meeting, Prague, Czech Republic, April 2013.

5. C. Ciaramelli, V. Calabrese, S. E. Sestito, F. Peri, Towards new TLR4 active small molecules, poster contribution, XXXVIII "*Attilio Corbella*" *Summer School* on Organic Synthesis, Gargnano (BS), Italy, June 2013.

6. C. Ciaramelli, V. Calabrese, S. E. Sestito, F. Peri, Fluorescent probes: TLR4 active small molecules and chemically modified LPS, poster contribution, ICI satellite meeting, SM7 "Endotoxin, TLR4 signaling and beyond", Cinisello Balsamo, Milano, Italy, August 2013.

7. F. Peri, J.Weiss, T. Gioannini, M. Piazza, V. Calabrese, F. Granucci, I. Zanoni, D. Prosperi, A. Polissi, C. Ciaramelli, S. E. Sestito, R. Cighetti, S. Gugliotta, Toll-like receptor 4 (TLR4) modulation by synthetic molecules, oral contribution, ICI satellite meeting, SM7 "Endotoxin, TLR4 signaling and beyond", Cinisello Balsamo, Milano, Italy, August 2013.

8. S. E. Sestito, C. Ciaramelli, V. Calabrese, L. Zambelloni, P. Sperandeo, G.E. Rovati, A, Polissi and F. Peri, LptC-PLS binding: a new target for antibacterial compounds, poster contribution,ICI

satellite meeting, SM7 "Endotoxin, TLR4 signaling and beyond", Cinisello Balsamo, Milano, Italy, August 2013.

9. S. E. Sestito, <u>C. Ciaramelli</u>, V. Calabrese, P. Sperandeo, L. Zambelloni, G.E. Rovati, A, Polissi and F. Peri, LptC-PLS binding: a new target for antibacterial compounds, poster contribution, 24th Joint Glycobiology Meeting, Wittenberg, Germany, November 2013.

10. <u>C. Ciaramelli</u>, V. Calabrese, S. E. Sestito, F. Peri, Fluorescent probes: TLR4 active small molecules and chemically modified LPS, poster contribution, BtBs Day, University of Milan Bicocca, Milano, Italy, December 2013.

11. V. Calabrese, R. Cighetti, <u>C. Ciaramelli</u>, S. E. Sestito, S. Gugliotta, L. Zambelloni, D. Zaccarin, M. Claseri, F. Peri. Small molecules: from design to biological characterization, oral contribution, BtBs Day, University of Milan Bicocca, Milano, Italy, December 2013.

12. <u>C. Ciaramelli</u>, V. Calabrese, S. E. Sestito, R. Cighetti F. Peri, Synthesis and characterization of new small molecules active on LPS binding proteins, oral and poster contribution, XXXIX "*Attilio Corbella*" *Summer School* on Organic Synthesis, Gargnano (BS), Italy, June 2014.

13. <u>C. Ciaramelli</u>, V. Calabrese, S. E. Sestito, R. Cighetti, F. Peri, New small molecules active on LPS binding proteins, oral and poster contribution, XIV Convegno Scuola sulla Chimica dei Carboidrati, Certosa di Pontignano, Siena, Italy, June 2014.

Awarded as the best contribution to the Congress by Giotto Biotech.

14. F. Peri, <u>C. Ciaramelli</u>, V. Calabrese, S. E. Sestito, R. Cighetti. New perspectives in therapeutic targeting of Toll-Like Receptor 4 (TLR4) with synthetic glycolipids, oral contribution, XIV Convegno Scuola sulla Chimica dei Carboidrati, Certosa di Pontignano, Siena, Italy, June 2014.

15. S. E. Sestito, <u>C. Ciaramelli</u>, V. Calabrese, P. Sperandeo, G.E. Rovati, A, Polissi and F. Peri, LptC-PLS binding: a new target for antibacterial compounds, poster contribution, FEBS Advanced Course: Ligand-binding Theory and Practice, Novè Hrady, Czech Republic, June 2014.

16. V. Calabrese, F. Peri, <u>C. Ciaramelli</u>, S. E. Sestito, R. Cighetti, From Lipid A-like structures to simplified small molecules active on TLR4, oral contribution, XXV Congresso della Società Chimica Italiana, Arcavacata di Rende (CS), Italy, September 2014.

17. F. Peri, V. Calabrese, <u>C. Ciaramelli,</u> S. E. Sestito, R. Cighetti, Synthetic glycolipids active on TLR4 receptor: a new generation of therapeutics, oral contribution, XXV Congresso della Società Chimica Italiana, Arcavacata di Rende (CS), Italy, September 2014.

Modulation of CD14 and TLR4·MD-2 Activities by a Synthetic Lipid A Mimetic

Roberto Cighetti,[a] Carlotta Ciaramelli,[a] Stefania Enza Sestito,[a] Ivan Zanoni,[a] Łukasz Kubik,[b, c] Ana Ardá-Freire,[d] Valentina Calabrese,[a] Francesca Granucci,[a] Roman Jerala,[e] Sonsoles Martín-Santamaría,[b] Jesus Jiménez-Barbero,[d] and Francesco Peri*[a]

Monosaccharide lipid A mimetics based on a glucosamine core linked to two fatty acid chains and bearing one or two phosphate groups have been synthesized. Compounds **1** and **2**, each with one phosphate group, were practically inactive in inhibiting LPS-induced TLR4 signaling and cytokine production in HEK-blue cells and murine macrophages, but compound **3**, with two phosphate groups, was found to be active in efficiently inhibiting TLR4 signal in both cell types. The direct interaction between compound **3** and the MD-2 coreceptor was investigated by NMR spectroscopy and molecular modeling/

docking analysis. This compound also interacts directly with the CD14 receptor, stimulating its internalization by endocytosis. Experiments on macrophages show that the effect on CD14 reinforces the activity on MD-2·TLR4 because compound **3**'s activity is higher when CD14 is important for TLR4 signaling (i.e., at low LPS concentration). The dual targeting of MD-2 and CD14, accompanied by good solubility in water and lack of toxicity, suggests the use of monosaccharide **3** as a lead compound for the development of drugs directed against TLR4-related syndromes.

Introduction

Activation of Toll-like receptor 4 (TLR4) and subsequent intracellular signaling in response to minute amounts of circulating endotoxins (Gram-negative bacterial lipopolysaccharides, LPSs), results in the rapid triggering of proinflammatory processes necessary for optimal host immune responses to invading Gram-negative bacteria in mammalians.[1] TLR4 does not bind directly to LPSs, and TLR4 activation by endotoxin is a complex event, involving the participation of other LPS-binding proteins—namely LBP, CD14, and MD-2—and ending with the for-

mation of the activated (TLR4·MD-2·LPS)₂ complex.[2] In particular, CD14 was the first identified Pattern Recognition Receptor (PRR) that binds directly to LPSs,[3] and chaperones the formation of the (TLR4·MD-2·LPS)₂ complex.[4] At low endotoxin concentrations CD14 has a fundamental role in assisting the formation of the signaling complex and the consequent initiation of the MyD88-dependent pathway leading to NF-κB activation. In contrast, CD14 is not indispensable for the activation of this pathway when LPS is more concentrated.[5]

CD14 is also required for endotoxin-induced TLR4 endocytosis[6] and relocalization of the entire LPS receptor complex into the endosome, where a second signaling pathway, namely the TRIF-dependent pathway, leading to a second wave of NF-κB and IRF3 activation and inflammatory cytokine production initiates. It has recently been observed that TLR4 antagonists, such as Eritoran,[7] lipid IVa, and cationic glycolipids,[8] strongly interact with CD14 and inhibit the formation of CD14·endotoxin complex. Excessively potent and deregulated TLR4 activation and signaling causes serious systemic syndromes such as fatal septic shock, associated with a high mortality (20–30%),[9] and organ-specific syndromes. CD14-dependent TLR4 activation in the central nervous system (CNS) by endogenous factors has been recently related to a wide array of inflammatory neurological diseases such as amyotrophic lateral sclerosis (ALS),[10] neuropathic pain,[11] and Alzheimer's disease (AD).[12] Efficient and selective TLR4 antagonists with chemical structures simpler than that of lipid A are therefore required for the development of potential new drugs with a wide array of medical and pharmacological applications (from sepsis to CNS pathologies).[13]

[a] R. Cighetti, C. Ciaramelli, S. E. Sestito, Dr. I. Zanoni, Dr. V. Calabrese, F. Granucci, Prof. F. Peri
Department of Biotechnology and Biosciences
University of Milano–Bicocca
Piazza della Scienza 2, 20126 Milano (Italy)
E-mail: francesco.peri@unimib.it

[b] Ł. Kubik, Prof. S. Martín-Santamaría
Department of Chemistry and Biochemistry, Faculty of Pharmacy
Universidad CEU San Pablo
Urb. Montepríncipe, 28668 Boadilla del Monte, Madrid (Spain)

[c] Ł. Kubik
Department of Biopharmaceutics and Pharmacodynamics
Medical University of Gdańsk
Gen. Józefa Hallera 107 Street, 80-416 Gdańsk (Poland)

[d] Dr. A. Ardá-Freire, Prof. J. Jiménez-Barbero
Department of Chemical and Physical Biology
Centro de Investigaciones Biológicas, CIB-CSIC C/
Ramiro de Maeztu 9, 28040 Madrid (Spain))

[e] Prof. R. Jerala
Department of Biotechnology, National Institute of Chemistry
Hajdrihova 19, 1000 Ljubljana (Slovenia

Supporting information for this article is available on the WWW under http://dx.doi.org/10.1002/cbic.201300588.

The LPS lipid A moiety (cf. Scheme 1), which anchors LPSs to the outer membranes of Gram-negative bacteria, is responsible for the immunostimulatory activity of LPSs.[14,15] Lipid A consists of a 1,4-β-diphosphorylated diglucosamine backbone to which variable numbers of fatty acid (FA) acyl chains of different length are covalently linked.[15] The numbers and structures of the acyl chains, as well as the two phosphate groups, determine the agonistic activity of lipid A.

Lipid X (Scheme 1), a biosynthetic precursor of lipid A with a structure that corresponds to the reducing GlcNAc monosac-

compounds with different acylation patterns (including compound **1**, named GLA-26, with two linear acyl chains) acted as agonists in murine macrophages and antagonists in human monocytes.[18,20] Compound **2**, with a phosphate group at C-4, has been described (compound 880.244)[21] as a very 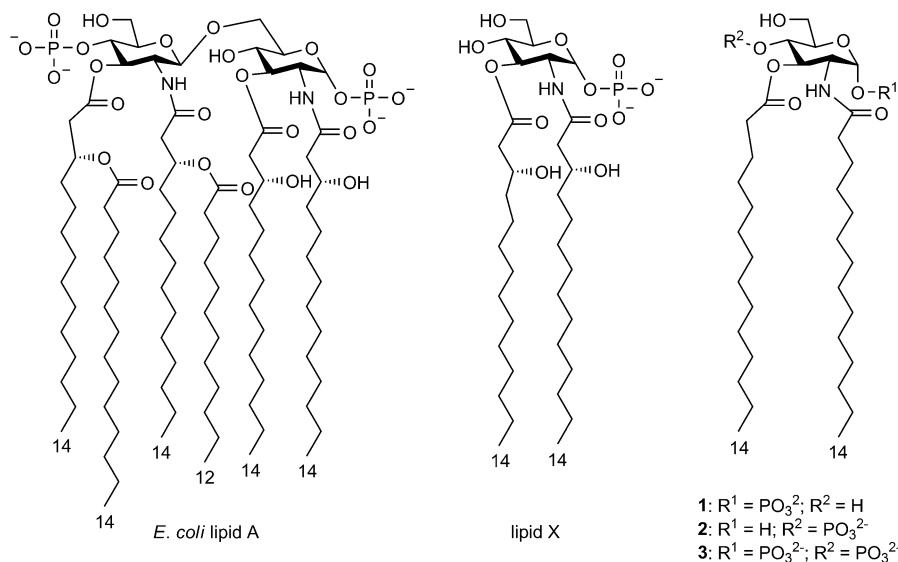weak TLR4 modulator.[21,22] Of all lipid X synthetic analogues, the diphosphoryl lipid X (Scheme 1) showed the most potent antagonist activity on both murine macrophages and human monocytes.[23] Compound **3** closely resembles diphosphoryl lipid X, but its structure is further simplified by the removal of the C-3 hydroxy groups on the FA chains.

Results and Discussion

Synthesis of lipid X mimetics 1–3

Compounds **1**–**3** were synthesized by using a divergent strategy starting from the common intermediate **4** (Scheme 2),[24] obtained from commercial D-glucosamine hydrochloride. Compound **4** was treated with PPh₃ in THF/H₂O to transform the azido group into an amine (compound **5**) and was then acylated in the C-2 and C-3 positions with myristic acid in the presence of the condensing agent 1-ethyl-3-(3-dimethylaminopropyl)carbodiimide (EDC), thus affording **6**. Monosaccharide **6** was deprotected at the anomeric (C-1) po-

Scheme 1. *E. coli* lipid A and its biosynthetic precursor lipid X, together with mono- (**1** and **2**) and diphosphorylated (**3**) lipid X mimetics.

charide of *Escherichia coli* lipid A, blocks LPS-induced septic shock and priming of TLR4-dependent human neutrophils.[16] Because of its anti-endotoxic activity[17] lipid X has been considered a simplified monosaccharide scaffold for the development of TLR4 agonists and antagonists.

Here we present the synthesis and biological characterization of monosaccharides **1**–**3** (Scheme 1): compound **1** corresponds to a lipid X mimetic with an α-anomeric phosphate, whereas **2** has a phosphate ester at the C-4 position, and **3** is phosphorylated at both C-1 and C-4 positions. Natural lipid A and lipid X have the (C-1) anomeric phosphate exclusively in the α-configuration, and the stereochemistry at the anomeric bond is very important for biological activity.[15] Accordingly, we introduced anomeric (C-1) phosphate esters into compounds **1** and **3** through stereoselective reactions that exclusively afforded the α-configuration.

Extensive structure–activity studies are available for lipid X mimetics based on a GlcNac monosaccharide with a C-4 phosphate group and acylated in the C-2 and C-3 positions with different linear and branched FA chains.[18,19] Whereas compounds with two C₁₄ FA acyl chains—at C-3 and one at C-2—have TLR4 agonist activity in human and mouse macrophages,

sition with tetrabutylammonium fluoride (TBAF) and AcOH to afford **7**, which was phosphorylated with tetrabenzyl diphosphate in the presence of lithium bis(trimethylsilyl)amide to afford the α-anomer **8** exclusively. Catalytic hydrogenolysis in the presence of Pd/C allowed simultaneous removal of the *p*-methoxybenzylidene group and the benzyl groups on the phosphate, affording compound **1**.

Alternatively, the benzylidene protecting group of compound **6** was reductively opened by treatment with NaCNBH₃ in dry THF to provide compound **9**, protected as a *p*-methoxybenzyl (PMB) ether at C-4. Compound **9** was phosphitylated with dibenzyl *N,N*-diisopropylphosphoramidite and imidazolium triflate and was then oxidized to a phosphate with *m*-chloroperbenzoic acid to obtain **10**. Compound **10** was deprotected at C-1 with TBAF and AcOH to afford **11**, and subsequent catalytic hydrogenolysis in the presence of Pd/C allowed compound **2** to be obtained.

To give access to compound **3**, compound **6** was treated with NaCNBH₃; this resulted in regioselective opening of the benzylidene ring and formation of the C-6 PMB ether. This reaction was quenched by addition of an acidic solution (HCl, 1 M in dioxane at pH 1.5 for 1 h); this promoted the removal of

Scheme 2. Reagents and conditions: a) PPh$_3$, THF/H$_2$O, 60 °C, 87%; b) myristic acid, EDC, DMAP, CH$_2$Cl$_2$, 97%; c) TBAF, AcOH, THF, −15 °C to RT, 76%; d) tetrabenzyl diphosphate, LiN(TMS)$_2$, dry THF, −78 to −20 °C, 43%; e) H$_2$, Pd/C, AcOH, dry MeOH/CH$_2$Cl$_2$, quant.; f) NaCNBH$_3$, 4 Å MS, dry THF, 84%; g) (BnO)$_2$PNiPr$_2$, imidazolium triflate, dry CH$_2$Cl$_2$, then m-CPBA, 0 °C, 42%; h) TBAF, AcOH, THF, −15 °C to RT, 57%; i) H$_2$, Pd/C, AcOH, dry MeOH/CH$_2$Cl$_2$, quant.; j) tetrabenzyl diphosphate, LiN(TMS)$_2$, dry THF, −78 to −20 °C, 71%; k) H$_2$, Pd/C, AcOH, dry MeOH/CH$_2$Cl$_2$, quant.; l) NaCNBH$_3$, 4 Å MS, dry THF, then HCl in dioxane until pH 1.5, 61%; m) (BnO)$_2$PNiPr$_2$, imidazolium tosylate, dry CH$_2$Cl$_2$, then m-CPBA, 0 °C, 38%.

Inhibition of LPS-induced, TLR4-dependent NF-κB activation in HEK-blue cells

The abilities of molecules **1**, **2**, and **3** to interfere with LPS-triggered TLR4 activation were first investigated in HEK-blue cells. HEK-blue cells are HEK293 cells stably transfected with human TLR4, MD-2, and CD14 genes. In addition, HEK-blue cells stably express a secreted alkaline phosphatase (sAP) produced upon activation of NF-κB. LPS binding activates TLR4 and NF-κB, leading to sAP secretion, which is detected in cell culture media by an alkaline phosphatase substrate.

When supplied alone, compounds **1**–**3** were unable to stimulate TLR4-dependent sAP production at a range of concentrations between 0 and 50 μM, thus confirming the lack of any agonist activity for the three monosaccharides on human TLR4. Cells were then pretreated with increasing concentrations of the synthetic monosaccharides (from 0 to 50 μM) and then stimulated with E. coli O55:B5 LPS (100 ng mL^{-1}). In this concentration range compounds **1** and **2** were weakly active in inhibiting LPS-stimulated TLR4 signaling, whereas **3** was active. The experiment was also run for compound **3** at two LPS concentrations (10 ng mL^{-1} and 1 μg mL^{-1}) by administrating LPS 30 min after the pretreatment with compound **3**. At both these LPS concentrations the percentage activation of HEK cells reached similar values, thus indi-

cating that the lower concentration (10 ng mL^{-1}) also saturated the signal corresponding to TLR4-dependent NF-κB stimulation (100% on the vertical scale, Figure 1). Compound **3** turned out to be more active as an antagonist at the low LPS concentration (10 ng mL^{-1}), with a calculated IC$_{50}$ of 0.46 μM, whereas when LPS was more concentrated the IC$_{50}$ was increased to 3.42 μM (Figure 2). As a negative control a HEK-293 cell line (InvivoGen) transfected with the same plasmids as HEK-blue but without TLR4, MD-2, and CD14 genes was used, and no effect was observed (data not shown). The toxicities of all com-

the anomeric tert-butyldimethylsilyl (TBDMS) protective group, thus providing compound **12** in one reaction step. Double phosphorylation at C-1 (stereoselective) and C-4 positions the phosphoramidite plus oxidation method and subsequent catalytic hydrogenolysis afforded monosaccharide **3**.
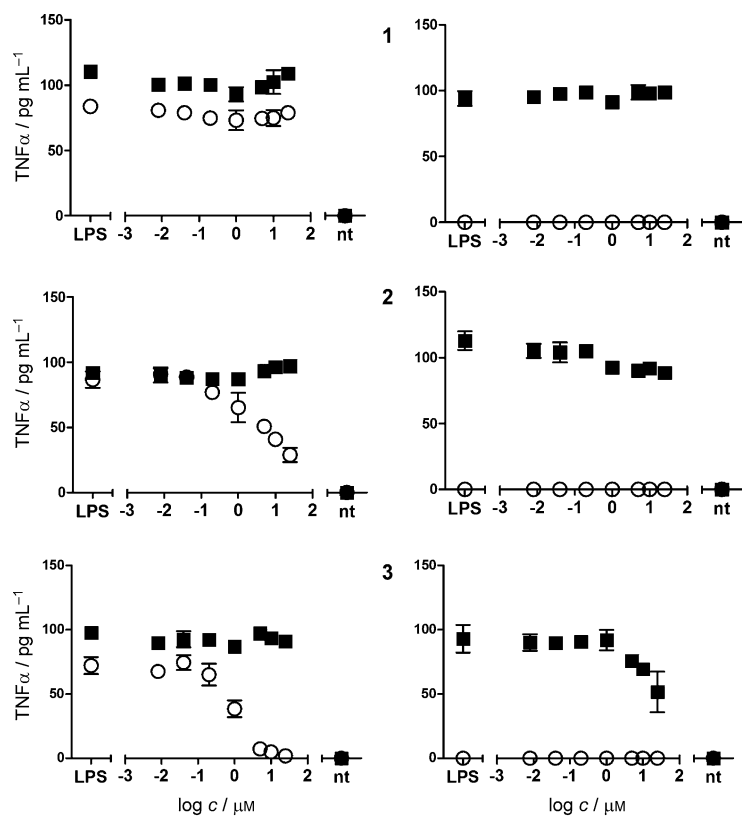
Compounds **1**, **2** and **3** were recovered as triethylammonium salts after hydrogenolysis and then treated with Amberlite IR 120 Na$^+$ exchange resin to change the counterion. The final compounds used for biological characterization contained sodium as counterion for the phosphate groups.

Figure 1. Effects of compounds **1**–**3** on LPS-induced TNF-α production by BM-derived macrophages. WT or CD14−/− BM macrophages were preincubated with synthetic compounds for 30 min and then treated either with a high LPS concentration (1 µg mL⁻¹, ■) or a low one (10 ng mL⁻¹, ○). Readout was the TNF-α production after one night's incubation.

Inhibition of LPS-induced TLR4 activation in murine macrophages

The abilities of compounds **1**–**3** to modulate the LPS-stimulated TLR4 pathway were further investigated in bone-marrow-derived murine macr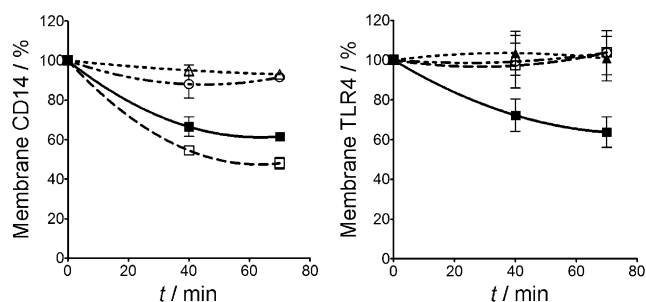ophages (BMMΦs). TNF-α production was determined from TLR4–MyD88 pathway activation. BMMΦs from wild-type and CD14−/− mice were treated with increasing concentrations (0–50 µM) of compounds **1**–**3** in DMEM+BSA (0.03%) in the presence or in the absence of LPS. Two LPS concentrations (10 and 1000 ng mL⁻¹) were tested, and LPS was administered 30 min after pretreatment with the synthetic compounds.

The LPS-induced TNF-α production after one night's incubation was assessed by ELISA test (Figure 1). As expected, the high concentration of smooth LPS also activated TLR4 signaling in the absence of CD14,[5] whereas at the low LPS concentration the signal was absent in CD14-defective cells. Compound **1** was inactive in both cell types, whereas molecule **2** showed a weak antagonist effect on wt macrophages at low LPS concentration. Compound **3** showed a dose-dependent LPS antagonistic activity in wt cells at the low LPS concentration and in CD14−/− at the high LPS concentration (Figure 1). The antagonist activity on both wt and CD14-defective cells suggests that molecule **3** competes with LPS in interaction both with CD14 and with the MD-2·TLR4 complex.

Figure 2. HEK-blue cells assay. Compound **3** inhibits LPS-triggered TLR4 activation in a dose-dependent way (monitored as sAP colorimetric reaction, normalized data, n = 3 experiments). Low concentrations of LPS (10 ng mL⁻¹; ○) gave an IC₅₀ value of 0.46 µM for compound **3**; high LPS doses (1 µg mL⁻¹; ■) shifted the IC₅₀ to 3.42 µM.

Compound 3 selectively stimulates endocytosis of CD14 (and not of the MD-2·TLR4 complex)

Because CD14 favors the activation of the TLR4–MyD88 pathway at low LPS doses, and because compounds **2** and **3** are more active as inhibitors at low LPS concentrations, we evaluated whether CD14 could be directly targeted by the synthetic compounds. We analyzed the capacities of compounds **1**–**3** to induce CD14 and MD-2·TLR4 complex internalization in BMMΦs. CD14 is in fact efficiently internalized together with the entire LPS receptor complex after LPS or lipid A binding, and this process has been demonstrated to be directed by CD14 in a TLR-independent manner.[6] BMMΦs were incubated with compounds **1**–**3** at a concentration of 10 µM, and the amounts of CD14 remaining at the cell surface over time were analyzed by flow cytometry. Compound **3**, showing the best antagonistic activity, was also capable of efficiently inducing CD14 internalization, whereas compounds **1** and **2** did not show any effect on CD14 surface expression (Figure 3). Interestingly, MD-2·TLR4 complex was not internalized after exposure to compounds **1**–**3** (Figure 3). These results suggest that compound **3**, an antagonist of the TLR4 signal pathway, can interact directly with CD14, causing its internalization.

pounds were assessed by MTT tests, and all compounds showed no or very limited toxicity up to the highest concentration tested (50 µM; see the Supporting Information).

Figure 3. Internalization of CD14 (left) and TLR4 (right) induced by compounds **1** (▲), **2** (○), and **3** (□). BMMΦs were treated with LPS (1 µg mL^{-1}; ■) or with the synthetic compounds, and the systems were incubated at 37 °C for the times indicated. Flow cytometry was then used to examine receptor endocytosis by determining the surface levels of the proteins indicated. Panels represent the mean fluorescence intensity (MFI) of specific receptor staining at each time point.

NMR binding experiments—interaction between synthetic compound 3 and MD-2

The binding of monosaccharide **3** to the MD-2 receptor in solution was then investigated by means of NMR techniques. Because of the tendency of compound **3** to form stable aggregates at the concentrations required for NMR measurements (150–300 µM), it turned out to be impossible to detect ligand–protein interaction by saturation transfer difference (STD) experiments. However, it was possible to record good-quality ^{1}H NMR spectra of **3**, of MD-2, and of a **3**/MD-2 mixture (ratio 5:1, at a 150 µM ligand concentration, Figure 4). Selective attenuation of the signals corresponding to the fatty acid C$_{14}$ chain protons of **3** was observed upon addition of MD-2 to the monosaccharide sample solution (Figure 4). Although broadening of all the resonance signals was detected, the decrease in signal intensities was significantly higher for those hydrogen atoms belonging to the FA aliphatic chains, in particular for
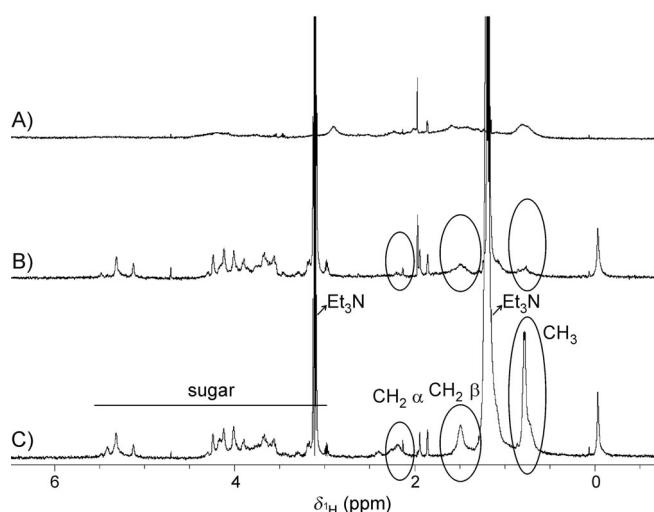
the signals of the ω-methyl groups and for those of the contiguous CH$_2$ moieties, followed by the rest of the chain hydrogen atoms. In contrast, the intensities of the signals corresponding to the hydrogen atoms on the sugar ring proved to be practically unaltered.

The experimentally observed reductions in intensity, due to specific line broadening of these signals, arise from the changes in the transverse relaxation times of these signals. This dramatic change likely arises from the existence of interaction between **3** and MD-2, precisely focused at the aliphatic side chain region. In fact, the FA chains–MD-2 interactions outlined here are reminiscent of those previously observed for positively charged amphiphiles.[8] These data suggest the existence of a major interaction of both FA chains of the sugar ligand with the hydrophobic binding cavity of MD-2, as also confirmed by docking calculations (see below). The exchange process between the free and the bound states provides the basis for the increased relaxation rate and the corresponding observed increases in line width.

Additional features of the interaction were also investigated by DOSY (diffusion ordered spectroscopy) NMR. Firstly, the aggregation properties of **3** were evaluated by use of DOSY. The DOSY of the free ligand showed a strikingly small diffusion coefficient, corresponding to a high-molecular-weight species in solution. This evidence can be correlated with the observation that compound **3** forms relatively large aggregates (Figure S2 in the Supporting Information) in water solution. The DOSY spectrum of the **3**/MD-2 mixture (at 5:1 molar ratio) was then also recorded. As stated above, the signals of the ligand aliphatic chains were no longer visible in the NMR spectrum, thus strongly suggesting the interaction of this part of the molecule with MD-2. In addition, the observation of a higher diffusion coefficient for the ligand molecule indicated that the existing aggregate for isolated **3** is indeed disrupted (see the Supporting Information).

Molecular modeling studies and docking of monosaccharide 3 with CD14 and MD-2

Docking studies were performed with the AutoDock[25] and AutoDock Vina[26] programs, by the protocol described in the Experimental Section. Firstly, the use of these computational programs was validated by docking the natural antagonist lipid IVa, with employment of the X-ray crystallographic structure of the human MD-2 protein in complexation with lipid IVa (PDB ID: 2E59) as the starting geometry.[27] Both the AutoDock and the Vina programs satisfactorily reproduced the crystallographic binding mode, showing the four FA acyl chains inside the lipophilic pocket, and the phosphorylated glucosamine moieties located at the entrance to the cavity (data not shown).

Once the docking procedures were validated, the same docking protocol was applied to compound **3**. Reasonable binding poses were predicted in both proteins (CD14 and MD-2), thus pointing to this compound being a suitable binder. The docked theoretical MD-2 binding energies for compounds **1** and **2** were significantly higher than that for compound **3**, by at least 8 kJ mol^{-1} (data not shown), thus pointing to

Figure 4. A) ^{1}H NMR of 30 µM MD-2 protein in deuterated acetate buffer at pH 5, 298 K, 120 scans. B) ^{1}H NMR of 30 µM MD-2 protein and 150 µM compound **3** in deuterated acetate buffer at pH 5, 298 K, 120 scans. C) ^{1}H NMR of 150 µM compound **3** in deuterated acetate buffer at pH 5, 298 K, 120 scans.

a more favorable binding process for **3**. Analysis of the Auto-Dock and AutoDock Vina docked binding poses in MD-2 showed the ability of compound **3** to bind in two different fashions, with close predicted binding energies. Most of the best docked solutions corresponded to binding poses with the two FA chains deeply confined inside the MD2 pocket, similarly to what had been seen with lipid IVa. One of the FA chains establishes hydrophobic contacts and CH–π interactions with Leu74, Phe76, Phe104, and Ile117, in a similar way to the equivalent FA chain present in lipid IVa (Figure 5 A). The second FA chain is directed into the region delimited by Ile52, Leu54,

Figure 5. AutoDock binding poses of compound **3** characterized with either two (green) or one (magenta) FA chains oriented inside the lipophilic MD-2 pocket. Lipid IVa is shown as reference in CPK colors.

Phe121, Ile124, Tyr131, and Ile153, a subpocket also occupied by a FA chain in the complex with lipid IVa. In few cases, results from docking showed a second binding mode, with one FA chain extending towards Val82 and placed over Ile124 (Figure 5 B). Interestingly, this Ile124 moves "up" in the agonist conformation, and its position is occupied by Phe126, thus acting as an agonist/antagonist switch.

Polar interactions were also identified in some of the docked binding poses. One phosphate group participates in hydrogen bonds—with Ser118, for instance—and is always located in the vicinity of Lys58 and/or Lys122, similarly to one of the lipid IVa phosphates. The second phosphate group is found in the vicinity of positively charged side chains, such as that from Arg96 or, in other docked solutions, exposed to the outside. In addition, in some of the docking results either the amide CO group or an ester CO group from compound **3** was found to establish a hydrogen bond with the Ser120 CO group. These predicted binding poses are in agreement with the NMR experiments and provide a 3D model for the interaction of the

FA chains with MD-2 protein, as well as for putative polar interactions involving the phosphate groups.

Docking calculations for compound **3** into CD14 were also carried out. In this case, the CD14 protein, like the MD-2 protein, also possesses a highly lipophilic wide pocket, but with fewer charged residues in the opening portion. Compound **3** showed binding poses presenting both FA chains inside the pocket, with the polar phosphate groups and sugar placed at the entrance of the cavity (Figure S3), thus supporting the experimental evidence of CD14 binding properties for this compound.

Conclusions

With the aim of obtaining TLR4 antagonists with chemical structures simpler than that of lipid A, mono- and diphosphate lipid X analogues (compounds **1**–**3**) were synthesized. Monosaccharides **1** and **2**, with one phosphate group linked to the anomeric (C-1) and the C-4 positions, respectively, showed weak antagonism in HEK-blue cells and macrophages. Monosaccharide **3**, a diphosphorylated lipid X analogue lacking the C-3 hydroxy groups on its FA acyl chains, proved to be active in inhibiting, in a dose-dependent way, the LPS-stimulated NF-κB activation in HEK-blue cells (Figure 2) and LPS-induced TNF-α production in macrophages (Figure 1). Monosaccharide **3** was much more active in inhibiting cytokine production at low LPS concentrations (10 ng mL^{-1}) than it was at higher ones (1 μg mL^{-1}, Figure 1). When the LPS concentration is low, the CD14-catalyzed extraction of LPS monomers from aggregates in solution and LPS presentation to the MD-2·TLR4 complex is essential for TLR4 activation and signaling.[5] On the other hand, it has been reported that highly concentrated LPS can bind directly to the MD-2·TLR4 complex and activate the TLR4 cascade without the need for the CD14 chaperone.

The higher activity of compound **3** under the experimental conditions under which CD14 contributes to TLR4 activation is a first indication that compound **3** probably interferes both in LPS/MD-2·TLR4 and in LPS/CD14 interactions. This behavior is reminiscent of that of a first generation of positively charged monosaccharides we developed that blocked in vitro and in vivo TLR4 activation[28] mainly by displacing endotoxin from CD14 interaction.[8]

The capacity of compound **3** to stimulate CD14 internalization (Figure 3) provides further evidence of a direct interaction between the synthetic molecule and CD14. The interaction with MD-2 has been characterized by NMR studies, allowing the identification of the FA acyl chain moieties as the part of compound **3** that directly interacts with MD-2 (Figure 4). Once again, analogously with what has been observed with synthetic cationic amphiphiles,[8] the FA acyl chains of the molecule proved to interact with MD-2 more strongly than the sugar part. Computational models for this complex have shown that the most stable docked complexes always correspond to binding poses in which the FA chains of compound **3** are deep inside the MD-2 pocket; this is consistent with the NMR observation of FA chain–protein interactions. Additionally, polar interactions of the phosphate groups with the outer polar resi-

dues can be identified in some of the binding poses. Overall, our calculations thus provide a theoretical 3D view of the interaction of this compound with MD-2. A docked model for CD14 in complexation with compound **3**, in accordance with the experimental results, has also been proposed.

Monosaccharide **3** is a promising lead for the development of drugs targeting TLR4 activation in a variety of medical settings.[9–13] This nontoxic TLR4 antagonist shows a high water solubility (completely soluble up to 1 mM concentration), in contrast with lipid A and lipid A mimetics, previously developed by us and by other groups, that suffer from poor solubility in aqueous media.[13] This is an important prerequisite for good bioavailability and favorable pharmacokinetic (distribution) properties. The critical micelle concentrations (CMCs) for compounds **1**–**3** were determined through pyrene fluorescence measurements.[29] The CMC values for compounds **1**, **2**, and **3** are 13, 28, and 9 μM, respectively. The TLR4 antagonist activity of compound **3** is observed in cells at concentration values below the CMC (IC_{50} from 0.46 to 3.2 μM). In this concentration range compound **3** is mainly in the monomeric form in solution. In contrast, at the higher concentrations required for NMR experiments (from 150 to 330 μM) compound **3** prevalently exists in the form of aggregates in solution. According to the data presented in this study, compound **3** interacts efficiently with both MD-2(·TLR4) and CD14 receptors. Multiple targeting could explain and contribute to the compound's efficacy in blocking TLR4 signaling.

Experimental Section

Chemistry

General procedures: All reagents were commercially available and used without further purification unless indicated otherwise. All solvents were anhydrous grade unless indicated otherwise. When dry conditions were required, the reactions were carried out in oven-dried glassware under a slight pressure of argon. Reactions were magnetically stirred and monitored by thin-layer chromatography (TLC) on silica gel. TLC was performed with Silica Gel 60 F254 plates (Merck) and UV detection or use of a molybdate developing solution [aqueous H_2SO_4 (5%) with $(NH_4)_6Mo_4O_7\cdot4H_2O$ (4%) and 0.2% $Ce(SO_4)_2$] followed by heating at 120 °C. Flash column chromatography was performed on silica gel 230–400 mesh (Merck). The petroleum ether used as eluent in chromatography has a boiling range of 40–60 °C. ¹H and ¹³C NMR spectra were recorded with a Varian 400 MHz Mercury instrument at 298 K. Chemical shifts are reported in ppm downfield from TMS as internal standard. Mass spectra were recorded with an ESI-MS triple quadrupole instrument (model API2000 QTrap, Applied Biosystems).

Phosphoryl 2-deoxy-3-O-tetradecanoyl-2-tetradecanoylamino-α-D-glucopyranoside (1): Compound **8** (0.05 g, 0.05 mmol) was dissolved in dry CH_2Cl_2/MeOH (1:2, 6 mL), and Pd on activated charcoal (catalytic amount) and AcOH were then added. The reaction mixture was stirred overnight at RT under H_2, with monitoring of the disappearance of starting material by TLC (toluene/AcOEt 7:3). Triethylamine (100 μL) was then added to the reaction mixture, and the suspension was filtered with a syringe filter in order to remove Pd/C catalyst and washed with CH_2Cl_2. The product was then passed over an Amberlite IR 120 Na⁺ exchange resin in order to remove triethylamine to give compound **1** as its sodium salt (0.04 g, quantitative).

¹H NMR (400 MHz, CD₃OD+3% D₂O, 25 °C, TMS): $\delta = 5.44$ (dd, $^3J_{H,P} = 6.8$ Hz, $^3J_{H,H} = 3.4$ Hz, 1H; H-1), 5.20 (dd, $^3J_{H,H} = 10.6$, 9.4 Hz, 1H; H-3), 4.15 (dt, $^3J_{H,H} = 5.7$, 3.2 Hz, 1H; H-2), 3.95 (m, 1H; H-5), 3.85 (dd, $^3J_{H,H} = 11.8$, 2.0 Hz, 1H; H-6a), 3.72 (dd, $^3J_{H,H} = 11.8$, 5.2 Hz, 1H; H-6b), 3.63–3.54 (m, 1H; H-4), 2.42–2.27 (m, 2H; $CH_2\alpha$ chains), 2.27–2.14 (m, 2H; $CH_2\alpha$ chains), 1.56 (m, 4H; $CH_2\beta$ chains), 1.37–1.20 (m, 40H; CH_2 bulk), 0.89 ppm (t, $^3J_{H,H} = 6.8$ Hz, 6H; CH_3); ¹³C NMR (101 MHz, CD₃OD+3% D₂O, 25 °C, TMS): $\delta = 175.23$, 174.18, 93.77, 73.33, 72.91, 68.06, 60.60, 51.83, 35.80, 33.81, 33.31, 31.67, 29.47, 29.42, 29.38, 29.29, 29.19, 29.14, 29.08, 28.95, 25.69, 25.31, 24.60, 24.56, 22.35, 13.16, 7.88 ppm; MS (ESI): *m/z* calcd: 679.44; found: 678.6, 339.4.

2-Deoxy-4-O-phosphoryl-3-O-tetradecanoyl-2-tetradecanoylamino-α,β-D-glucopyranose (2): Compound **11** (0.14 g, 0.15 mmol) was dissolved in dry CH_2Cl_2/MeOH (1:2, 6 mL), and Pd on activated charcoal was then added in catalytic amounts. The reaction mixture was stirred at RT under H_2 overnight, with monitoring of the disappearance of starting material by TLC (ETP/AcOEt 7:3). Triethylamine (100 μL) was added to the reaction mixture, and the suspension was filtered with a syringe filter in order to remove Pd/C catalyst. The pure triethylammonium salt was then passed over an Amberlite IR 120 Na⁺ exchange resin in order to remove triethylamine, giving compound **2** as its sodium salt (mixture of α- and β-anomers, 5:1) in quantitative yield. ¹H NMR (400 MHz, CD₃OD+2.5% CDCl₃, 25 °C, TMS): $\delta = 7.66$ (d, $^3J_{H,H} = 9.6$ Hz, 1H; NH), 5.34 (t, $^3J_{H,H} = 9.8$ Hz, 1H; H-3α), 5.14 (t, $^3J_{H,H} = 9.7$ Hz, 1H; H-3β), 5.05 (d, $^3J_{H,H} = 3.6$ Hz, 1H; H-1α), 4.68 (d, $^3J_{H,H} = 8.4$ Hz, 1H; H-1β), 4.26–4.10 (m, 3H; H-2α, H-4α, H-4β), 3.98–3.90 (m, 3H; H-5α, H-6aα, H-6aβ), 3.85–3.75 (m, 2H; H-2b; H-6bβ), 3.68 (m, 1H; H-6bα), 3.40 (m, 1H; H-5β), 2.44–2.11 (m, 8H; $CH_2\alpha$ chains), 1.56 (m, 8H; $CH_2\beta$ chains), 1.45–1.17 (m, 80H; CH_2 bulk), 0.89 ppm (t, $^3J_{H,H} = 6.7$ Hz, 12H; CH_3); ¹³C NMR (101 MHz, CD₃OD+2.5% CDCl₃, 25 °C, TMS): $\delta = 78.97$, 178.15, 99.68, 95.74, 75.93, 75.44, 75.16, 64.65, 59.48, 56.55, 50.39, 46.21, 40.31, 39.87, 37.99, 35.90, 33.69, 33.63, 33.59, 33.55, 33.52, 33.33, 33.25, 29.98, 28.69, 26.55, 17.27, 11.93 ppm; MS (ESI): *m/z* calcd: 679.44; found: 678.52.

Phosphoryl 2-deoxy-4-O-phosphoryl-3-O-tetradecanoyl-2-tetradecanoylamino-α-D-glucopyranoside (3): Compound **13** (0.08 g, 0.06 mmol) was dissolved in dry CH_2Cl_2/MeOH 1:2 (5 mL), and Pd on activated charcoal was then added in catalytic amounts. The reaction mixture was stirred at RT under H_2 overnight (TLC AcOEt). Triethylamine (150 μL) was then added to the reaction mixture, and the suspension was filtered with a syringe filter. The triethylammonium salt was then passed over an Amberlite IR 120 Na⁺ exchange resin to remove triethylamine, giving compound **3** as its sodium salt in quantitative yield (61 mg). ¹H NMR (400 MHz, CD₃OD, 25 °C, TMS): $\delta = 5.45$ (dd, $^3J_{H,P} = 6.4$ Hz, $^3J_{H,H} = 3.5$ Hz, 1H; H-1), 5.37 (t, $^3J_{H,H} = 9.9$ Hz, 1H; H-3), 4.31–4.18 (m, 2H; H-2, H-4), 4.02–3.95 (m, 2H; H-5, H-6a), 3.72 (d, $^2J_{H,H} = 12.6$ Hz, 1H; H-6b), 2.46–2.14 (m, 4H; $CH_2\alpha$ chains), 1.56 (m, 4H; $CH_2\beta$ chains), 1.39–1.20 (m, 40H, CH_2 chains), 0.89 ppm (t, $^3J_{H,H} = 6.6$ Hz, 6H; CH_3 chains); ¹³C NMR (101 MHz, CD₃OD, 25 °C, TMS): $\delta = 174.60$, 173.29, 94.11, 72.22, 71.89, 70.86, 60.22, 53.41, 52.16, 46.14, 35.87, 33.77, 31.72, 29.51, 29.45, 29.42, 29.37, 29.35, 29.32, 29.28, 29.15, 29.09, 25.71, 24.87, 24.49, 22.37, 13.09, 7.74 ppm; MS (ESI): *m/z* calcd: 759.41; found: 758.5, 378.7.

Biology

HEK-Blue assay: HEK-Blue hTLR4 cells (HEK-Blue LPS Detection Kit, InvivoGen) were cultured according to the manufacturer's instructions. Cells were cultured in Dulbecco's modified Eagle's medium (DMEM) high-glucose medium supplemented with fetal bovine

serum (FBS, 10%), glutamine (2 mM), 1× Normocin (InvivoGen), and 1× HEK-Blue Selection (InvivoGen). Cells were detached by use of a cell scraper, and the cell concentration was estimated by use of a cell counter. Cells were then diluted in DMEM high-glucose medium supplemented with FBS (10%), glutamine (2 mM), 1× Normocin (InvivoGen), and cell suspension (200 μL, 20 000 cells) was added to each well. After overnight incubation (37 °C, 5% CO₂, 95% humidity), cells had reached 80% confluency. Supernatant was removed, and cell monolayers were washed with warm PBS without Ca²⁺ and Mg²⁺, preincubated for 30 min in 190 μL DMEM + 0.03% BSA, supplemented with compounds **1**, **2**, or **3** (different concentrations in different wells, from 0 to 50 μM). LPS (*E. coli* O55:B5 strain, Sigma–Aldrich) at a final concentration of 10, 100, or 1000 ng mL⁻¹ was then added as stimulus (10 μL per well), and cells were incubated overnight under the same conditions as above. After the incubation, supernatants were collected. Each sample (50 μL) was added to a pNPP solution in PBS (0.8 mM, 100 μL). Plates were incubated in the dark at room temperature and then analyzed spectrophotometrically (absorbance at 405 nm).

Murine-bone-marrow-derived macrophages (BMMΦs) assay: Murine BMMΦs were obtained from wild-type and CD14−/− mice and cultured by the published procedure.[30] Cells were washed with PBS and detached by treatment with EDTA in PBS (2 mM). The cellular suspension was then centrifuged at 188 *g* for 5 min, and the cellular pellet was resuspended in DMEM high-glucose + FBS 10% and plated in a 96-well plate (20 000 cells per well). After overnight incubation (37 °C, 5% CO₂, 95% humidity), supernatant was removed, and cell monolayers were washed with warm PBS without Ca²⁺ and Mg²⁺, preincubated for 30 min in 190 μL DMEM + 0.03% BSA, and supplemented with compounds **1**, **2**, or **3** (different concentrations in different wells, from 0 to 50 μM). LPS (*E. coli* O55:B5 strain, Sigma–Aldrich) at a final concentration of 10, 100, or 1000 ng mL⁻¹ was then added as stimulus (10 μL per well), and cells were incubated overnight under the same conditions as above. After the incubation, supernatants were collected, and TNF concentration was detected through an ELISA.

Flow cytometry analysis: BMMΦs were washed twice with PBS and detached by treatment with EDTA in PBS (2 mM). The cellular suspension was then centrifuged at 188 *g* for 5 min, and the cellular pellet was resuspended in DMEM high glucose + FBS 10% (100 μL) and incubated at 37 °C, 5% CO₂, and 95% humidity for 40 or 70 min with compound **1**, **2**, or **3** (10 μM) or LPS (1 μg mL⁻¹). Cellular suspensions were then centrifuged at 188 *g*, 4 °C, for 5 min, and the cellular pellet was resuspended with ice-cold PBS. The receptor-specific fluorescent antibodies were then added (aCD14: FITC rat anti-mouse CD14, clone SA2–8, eBIOSCIENCE; aTLR4: PE rat anti-mouse TLR4, clone SA15–21, Biolegend), at 1 μg mL⁻¹, for 20 min in ice in the dark. The cells were then washed twice with ice-cold PBS, and fluorescence was analyzed with a FaCSCalibur flow cytometer (BD Biosciences).

Production and isolation of MD-2: Recombinant MD-2 was produced in *E. coli* as described previously[31] with use of solubilization of inclusion bodies in Gdn·HCl (6 M) followed by purification and refolding on a C8 reversed-phase column. Eluted fractions were lyophilized and dialyzed against Milli-Q water. Biological activity of each batch of MD-2 has been assessed for the ability to support LPS induced TLR4 activation in HEK293 cells transfected with TLR4.

Determination of CMCs through pyrene fluorescence measurements:[29] For every sample, independently of the synthetic compound's concentration, a final pyrene concentration of 0.6 μM is desired. A mother solution of pyrene in THF (1 mM) was prepared

in a 25 mL volumetric flask, and diluted into a solution (237 mM, 6 mL of the concentrated solution, followed by addition of 19 mL of THF, to a final volume of 25 mL). An aliquot of this solution (252 μL) is then diluted with Milli-Q water to a final volume of 100 mL. Aqueous solutions of each compound (0.6 μM in pyrene) were prepared at concentrations from 1 mM to 0.05 μM, by two-fold serial dilutions. The 1 mM solutions were prepared by adding pyrene solution (0.6 μM) to each compound and sonicating for 1 h. The serial dilutions were incubated for 1 h at 37.0 °C. For fluorescence measurements, the solution (1.5 mL) was placed in a conventional 1 cm quartz cuvette; fluorescence spectra were recorded with a Varian Cary Eclipse spectrofluorophotometer at (37 ± 0.1) °C, with use of 5 mm excitation and emission slits. The onset of micelle formation can be observed in a shift of the fluorescence excitation spectra of the samples at an emission wavelength of 372 nm. In the concentration range of aqueous micellar solutions, a shift of the excitation band in the 335 nm region toward higher wavelengths confirms the incorporation of pyrene in the hydrophobic interiors of micelles. The ratio of the fluorescence intensities at 339 and 335 nm was used to quantify the shift of the broad excitation band. The critical micelle concentrations were determined from the crossover point in the low concentration range.

NMR binding experiments: NMR experiments were performed with a 600 MHz DRX spectrometer (Bruker) equipped with a cryoprobe. ¹H NMR spectra were recorded at 298 K, by acquisition of 120 scans. DOSY spectra were recorded at 311 K with the stebpgls19 Bruker pulse sequence by acquisition of 160 scans, with a diffusion time of 300 ms, a gradient length of 1.9 ms, and a gradient ramp from 2% to 95% in 32 linear steps. Protein samples were prepared by diluting the stock solution of MD-2 (0.11 mM in deuterated acetate buffer at pH 5) with the same buffer. Ligand samples were prepared by dissolving solid compound **3** in deuterated acetate buffer at pH 5. For ¹H NMR experiments the final concentrations reached for the analyzed samples were 30 μM MD-2 and 150 μM compound **3**, whereas for DOSY experiments final concentrations of 60 μM MD-2 and 300 μM compound **3** were needed.

Molecular modeling: 3D coordinates of compound **3** were built with the aid of Maestro (version 9.3, Schrödinger, LLC, New York, NY, 2012). Phosphate groups were considered to be monoprotonated. Molecular mechanics optimization (UFF force field), semiempirical calculations (AM1), and DFT (B3LYP/6–31G*) were subsequently applied by use of Gaussian03.[32] Final geometry was submitted to MD simulations with implicit water and MM3* as force field, by use of Schrödinger Maestro 9.3 Impact 5.8, [Maestro, v. 9.3, Schrödinger, LLC, New York, NY, 2012. Suite 2012: Impact v. 5.8, Schrödinger, LLC, New York, NY, 2012] and the MM3* force field, dielectric constant 80.0, number of MD steps 100, and time step of 0.001 ps. 3D coordinates of human MD-2 protein (from PDB ID: 2E59), and CD14 protein (from PDB ID: 1WWL) were refined and minimized by use of the Protein Preparation Wizard module of Maestro and the Amber force field.[33] In the case of CD14, only the sequence from Ala3 to Leu130 was considered for docking purposes. Compound **3** was docked into both MD-2 and CD14 proteins with the aid of AutoDock 4.2.,[25] and separately with the aid of AutoDock Vina 1.1.2.[26] Predicted binding energies ranged from −2 to −6 kcal mol⁻¹ in the AutoDock results and from −6 to −9 kcal mol⁻¹ in the AutoDock Vina results. For MD-2 the Autogrid grid point spacing was set at 0.375 Å, center coordinates of the grid box were −0.379, 17.201, 16.216 (*x*, *y*, *z*), and number of grid points in *xyz* was 58, 92, 82. For CD14 the Autogrid grid point spacing was set at 0.375 Å, center coordinates of the grid box were 13.500, 51.000, 56.500 (*x*, *y*, *z*), leading to 66, 72, 88 (*x*, *y*, *z*)

grid points. All allowed torsional bonds were considered rotatable. Docking calculations with AutoDock were performed by use of Genetic Algorithm (number of runs 250, number of individuals in population 150). Docking calculations with AutoDock Vina were also performed. Coordinates and dimensions of grid boxes, starting geometries, and general methodology were the same as for Auto-Dock. 3D structures of the docked complexes were optimized by performing MD simulations with Impact (implicit water, and AMBER* force field).

[1] a) A. Poltorak, X. He, I. Smirnova, M. Liu, C. Van Huffel, X. Du, D. Birdwell, E. Alejos, M. Silva, C. Galanos, M. Freudenberg, P. Ricciardi-Castagnoli, B. Layton, B. Beutler, *Science* **1998**, *282*, 2085–2088; b) B. Beutler, X. Du, A. Poltorak, *J. Endotoxin Res.* **2001**, *7*, 277–280; c) B. Beutler, *Curr. Top. Microbiol. Immunol.* **2002**, *270*, 109–120.
[2] a) B. Park, D. Song, H. Kim, B. Choi, H. Lee, J. Lee, *Nature* **2009**, *458*, 1191–1195; b) U. Ohto, K. Fukase, K. Miyake, T. Shimizu, *Proc. Natl. Acad. Sci. USA* **2012**, *109*, 7421–7426.
[3] S. Wright, R. Ramos, P. Tobias, R. Ulevitch, J. Mathison, *Science* **1990**, *249*, 1431–1433.
[4] a) J. da Silva Correia, K. Soldau, U. Christen, P. Tobias, R. Ulevitch, *J. Biol. Chem.* **2001**, *276*, 21129–21135; b) T. Gioannini, A. Teghanemt, D. Zhang, N. Coussens, W. Dockstader, S. Ramaswamy, J. Weiss, *Proc. Natl. Acad. Sci. USA* **2004**, *101*, 4186–4191; c) K. Moore, L. Andersson, R. Ingalls, B. Monks, R. Li, M. Arnaout, D. Golenbock, M. Freeman, *J. Immunol.* **2000**, *165*, 4272–4280.
[5] M. Triantafilou, K. Triantafilou, N. Fernandez, *Eur. J. Biochem.* **2000**, *267*, 2218–2226.
[6] I. Zanoni, R. Ostuni, L. R. Marek, S. Barresi, R. Barbalat, G. M. Barton, F. Granucci, J. C. Kagan, *Cell* **2011**, *147*, 868–880.
[7] K. A. Shirey, W. Lai, A. J. Scott, M. Lipsky, P. Mistry, L. M. Pletneva, C. L. Karp, J. McAlees, T. L. Gioannini, J. Weiss, W. H. Chen, R. K. Ernst, D. P. Rossignol, F. Gusovsky, J. C. Blanco, S. N. Vogel, *Nature* **2013**, *497*, 498–502.
[8] M. Piazza, L. Yu, A. Teghanemt, T. Gioannini, J. Weiss, F. Peri, *Biochemistry* **2009**, *48*, 12337–12344.
[9] M. S. Rangel-Frausto, *Arch. Med. Res.* **2005**, *36*, 672–681.
[10] M. Casula, A. M. Iyer, W. G. Spliet, J. J. Anink, K. Steentjes, M. Sta, D. Troost, E. Aronica, *Neuroscience* **2011**, *179*, 233–243.
[11] L. Cao, F. Tanga, J. Deleo, *Neuroscience* **2009**, *158*, 896–903.
[12] S. Rivest, *Nat. Rev. Immunol.* **2009**, *9*, 429–439.
[13] F. Peri, M. Piazza, *Biotechnol. Adv.* **2012**, *30*, 251–260.
[14] J. Schletter, H. Heine, A. J. Ulmer, E. T. Rietschel, *Arch. Microbiol.* **1995**, *164*, 383–389.
[15] C. Raetz, C. Whitfield, *Annu. Rev. Biochem.* **2002**, *71*, 635–700.
[16] R. L. Danner, K. A. Joiner, J. E. Parrillo, *J. Clin. Invest.* **1987**, *80*, 605–612.
[17] C. Lam, J. Hildebrandt, E. Schütze, B. Rosenwirth, R. A. Proctor, E. Liehl, P. Stütz, *Infect. Immun.* **1991**, *59*, 2351–2358.
[18] K. Funatogawa, M. Matsuura, M. Nakano, M. Kiso, A. Hasegawa, *Infect. Immun.* **1998**, *66*, 5792–5798.
[19] A. L. Van Dervort, M. E. Doerfler, P. Stuetz, R. L. Danner, *J. Immunol.* **1992**, *149*, 359–366.
[20] M. Matsuura, M. Kiso, A. Hasegawa, *Infect. Immun.* **1999**, *67*, 6286–6292.
[21] L. Brade, K. Brandenburg, H. M. Kuhn, S. Kusumoto, I. Macher, E. T. Rietschel, H. Brade, *Infect. Immun.* **1987**, *55*, 2636–2644.
[22] a) R. Tamai, Y. Asai, M. Hashimoto, K. Fukase, S. Kusumoto, H. Ishida, M. Kiso, T. Ogawa, *Immunology* **2003**, *110*, 66–72; b) H. M. Kuhn, L. Brade, B. J. Appelmelk, S. Kusumoto, E. T. Rietschel, H. Brade, *Infect. Immun.* **1992**, *60*, 2201–2210.
[23] R. L. Danner, A. L. Van Dervort, M. E. Doerfler, P. Stuetz, J. E. Parrillo, *Pharm. Res.* **1990**, *7*, 260–263.
[24] J. Chen, Y. Zhou, C. Chen, W. Xu, B. Yu, *Carbohydr. Res.* **2008**, *343*, 2853–2862.
[25] D. S. Goodsell, G. M. Morris, A. J. Olson, *J. Mol. Recognit.* **1996**, *9*, 1–5.
[26] O. Trott, A. J. Olson, *J. Comput. Chem.* **2010**, *31*, 455–461.
[27] U. Ohto, K. Fukase, K. Miyake, Y. Satow, *Science* **2007**, *316*, 1632–1634.
[28] M. Piazza, C. Rossini, S. Della Fiorentina, C. Pozzi, F. Comelli, I. Bettoni, P. Fusi, B. Costa, F. Peri, *J. Med. Chem.* **2009**, *52*, 1209–1213.
[29] A. M. Hofmann, F. Wurm, H. Frey, *Macromolecules* **2011**, *44*, 4648–4657.
[30] F. Granucci, C. Vizzardelli, N. Pavelka, S. Feau, M. Persico, E. Virzi, M. Rescigno, G. Moro, P. Ricciardi-Castagnoli, *Nat. Immunol.* **2001**, *2*, 882–888.
[31] M. Mancek-Keber, R. Jerala, *FASEB J.* **2006**, *20*, 1836–1842.
[32] Gaussian 03, Gaussian Inc., Wallingford, CT, USA, **2003**.
[33] a) Suite 2012: Schrödinger Suite **2012** Protein Preparation Wizard; b) Epik version 2.3, Schrödinger, LLC, New York, NY, **2012**; c) Impact version 5.8, Schrödinger, LLC, New York, NY, **2012**; d) Prime version 3.1, Schrödinger, LLC, New York, NY, **2012**.

Functional Characterization of *E. coli* LptC: Interaction with LPS and a Synthetic Ligand

Stefania E. Sestito,[a] Paola Sperandeo,[a] Carlo Santambrogio,[a] Carlotta Ciaramelli,[a] Valentina Calabrese,[a] G. Enrico Rovati,[b] Luca Zambelloni,[a] Rita Grandori,[a] Alessandra Polissi,*[a] and Francesco Peri*[a]

Lipopolysaccharide (LPS), the main cell-surface molecular constituent of Gram-negative bacteria, is synthesized in the inner membrane (IM) and transported to the outer membrane (OM) by the Lpt (lipopolysaccharide transport) machinery. Neosynthesized LPS is first flipped by MsbA across the IM, then transported to the OM by seven Lpt proteins located in the IM (LptBCFG), in the periplasm (LptA), and in the OM (LptDE). A functional OM is essential to bacterial viability and requires correct placement of LPS in the outer leaflet. Therefore, LPS biogenesis represents an ideal target for the development of novel antibiotics against Gram-negative bacteria. Although the structures of Lpt proteins have been elucidated, little is known about the mechanism of LPS transport, and few data are available on Lpt–LPS binding. We report here the first determination of the thermodynamic and kinetic parameters of the interaction between LptC and a fluorescent lipo-oligosaccharide (fLOS) in vitro. The apparent dissociation constant (K_d) of the

fLOS–LptC interaction was evaluated by two independent methods. The first was based on fLOS capture by resin-immobilized LptC; the second used quenching of LptC intrinsic fluorescence by fLOS in solution. The K_d values by the two methods (71.4 and 28.8 μM, respectively) are very similar, and are of the same order of magnitude as that of the affinity of LOS for the upstream transporter, MsbA. Interestingly, both methods showed that fLOS binding to LptC is mostly irreversible, thus reflecting the fact that LPS can be released from LptC only when energy is supplied by ATP or in the presence of a higher-affinity LptA protein. A fluorescent glycolipid was synthesized: this also interacted irreversibly with LptC, but with lower affinity (apparent $K_d = 221$ μM). This compound binds LptC at the LPS binding site and is a prototype for the development of new antibiotics targeting LPS transport in Gram-negative bacteria.

Introduction

Gram-negative bacteria are typically surrounded by two membranes, an inner membrane (IM) and an outer (OM) membrane, separated by an aqueous compartment, the periplasm, which contains a thin layer of peptidoglycan.[1] The OM is an asymmetric lipid bilayer with lipopolysaccharide (LPS), a complex glycolipid in the outer leaflet, and phospholipids in the inner leaflet.[2] The tightly packed, amphipathic LPS molecules in the outer leaflet prevent the entry of both large polar molecules and small hydrophobic molecules into the cell, thus protecting the bacterium from toxic chemicals and antibiotics.[1] The OM is essential for bacterial cell viability and represents the first

site of interaction with the host. The functionality of OM requires proper assembly of this structure and correct placement of LPS in the outer leaflet. Therefore LPS biogenesis represents an ideal target for development of novel chemicals with antibiotic action against Gram-negative bacteria.

Smooth LPS is formed of lipid A, the core oligosaccharide, and a long polysaccharide chain known as O-antigen[2] (Figure 1 A); rough LPS (or lipo-oligosaccharide, LOS) lacks the O-antigen. Lipid A, the most conserved portion of LPS is the pathogen-associated molecular pattern (PAMP) component that is sensed by the combined action of Toll-like receptor 4 (TLR4), MD-2, and CD14 co-receptors of the host innate immune system.[3] Although the steps along the LPS biosynthetic pathway have been clarified, the precise mechanism of transport and assembly at the cell surface are still poorly understood. The lipid A core moiety is synthesized in the cytoplasm, and its translocation across the IM is performed by the essential ABC transporter MsbA.[4] The final step of LPS biosynthesis takes place at the periplasmic face of the IM, where the lipid A core moiety is ligated to O-antigen.[2] Export of complete LPS to the cell surface is mediated by the lipopolysaccharide transport (Lpt) machinery, which is composed of seven essential proteins (LptABCDEFG),[5,6] located in the IM (LptBCFG), in the periplasm (LptA), and in the OM (LptDE; Fig-

[a] S. E. Sestito, Dr. P. Sperandeo, Dr. C. Santambrogio, C. Ciaramelli, Dr. V. Calabrese, L. Zambelloni, Prof. R. Grandori, Prof. A. Polissi, Prof. F. Peri
Department of Biotechnology and Biosciences
University of Milano–Bicocca
Piazza della Scienza 2, 20126 Milano (Italy)
E-mail: alessandra.polissi@unimib.it
        francesco.peri@unimib.it

[b] Prof. G. E. Rovati
Laboratory of Molecular Pharmacology
Department of Pharmacological and Biomolecular Sciences
Università di Milano
Via Balzaretti 6, 20124 Milano (Italy)

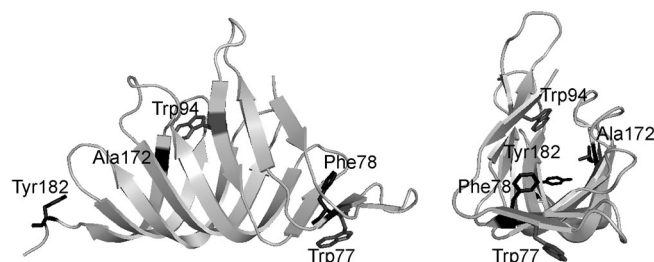Supporting information for this article is available on the WWW under http://dx.doi.org/10.1002/cbic.201300805.
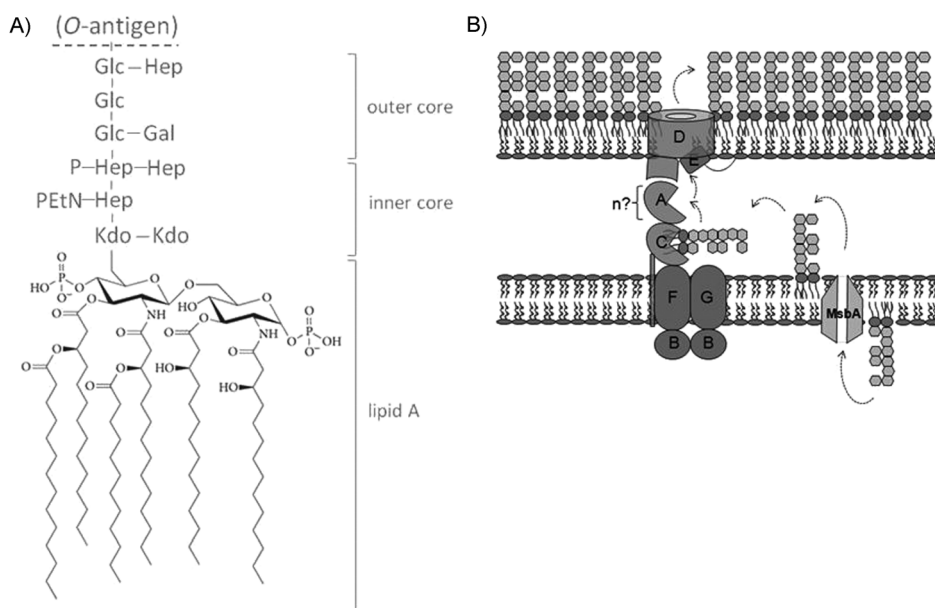
Figure 1. LPS structure and transport in *E. coli*. A) Molecular structure of *E. coli* K12 LPS. B) LPS transport from IM to OM. MsbA flips LPS across the IM, and seven Lpt proteins transport it to the cell surface.

Based on these results, it was proposed that LPS transport starts with LPS extraction from the IM by the LptBFG complex, which transfers the molecule to the periplasmic domain of membrane-bound LptC; LptC then transfers LPS to LptA. At least two energy-dependent steps are involved in LPS transport: extraction from the IM to the periplasmic domain of membrane-bound LptC, and transfer of LPS from LptC to LptA.[14] The in vitro reconstitution of LPS transport allowed dissection of LPS transport mechanism into discrete steps from IM to LptC and from LptC to LptA. These are representative of LPS transfer by the Lpt proteins in vivo.[14]

ure 1B). All seven proteins interact and form a transenvelope complex.[7] The IM ABC transporter LptBFG[8] interacts with the bitopic IM protein LptC.[9] Then, homologous domains mediate the interactions between the C-terminal region of LptC and the N-terminal region of LptA, and between the C terminus of LptA and the N-terminal periplasmic region of LptD.[6,10] The oligomeric structure formed by LptC, LptA, and LptD constitutes the protein bridge that connects the IM and OM.[7] Although the overall architecture of the transenvelope bridge has been defined,[6] the mechanism of LPS transport across the periplasm to the outer leaflet of the OM is not yet understood.

Qualitative in vitro assays have shown that both LptA[11] and LptC[12] bind to LPS. The crystal structures of LptA[13] and the periplasmic domain of LptC[12] revealed that the two proteins present a very similar β-jellyroll fold, although they do not share significant sequence similarity. Both LptA and LptC possess hydrophobic residues; these form a hydrophobic core along the proteins that potentially serve as an LPS-binding site.[12,13] Interestingly, LptA can displace LPS from LptC in vitro (but not vice versa), consistent with their location in the protein bridge and the (unidirectional) LPS export pathway.[12] However, despite the increasing information obtained on LptC–LPS and LptA–LPS interactions, no quantitative measurements of binding have been performed. Very recently the mechanism of transport of the LPS molecule has been dissected both in vivo and in vitro, by crosslinking the LPS ligand to the different components of the Lpt machinery.[14] Specifically, four residues in LptC and five in LptA were found to interact with LPS in vivo.[14] LptC residues directly involved in LPS binding are Thr47, Phe78, Ala172, and Tyr182 (Figure 2), located almost exclusively inside the β-jellyroll structure, thus suggesting that LPS binds inside these proteins and transits through the periplasm bound to the cavity of the conserved β-jellyroll fold.[14]

Figure 2. Cartoon representation of the LptC crystal structure (PDB ID: 3MY2).[12] Putative LPS binding residues[13] are labeled.

We report here the first determination of thermodynamic and kinetic parameters of the in vitro interaction between a heterologously expressed, truncated version of LptC and fluorescently conjugated LOS (fLOS), by two independent methods. Such studies represent a necessary step to understanding the LPS transport mechanism by Lpt proteins. We also describe the rational design, synthesis, and binding properties of a synthetic fluorescent ligand that competes with LPS for LptC binding.

Results and Discussion

Preparation of fluorescent lipo-oligosaccharide (fLOS) and sH-LptC

Radiolabeled LPS is generally used for LPS binding studies. We replaced radioactivity with the safer fluorescence labeling. The main issues with fluorescent LPS are 1) low sensitivity with commercial fluorescein isothiocyanate (FITC)-LPS because of the low level of fluorescence incorporation, and 2) the risk of altering LPS activity and binding properties by introducing the fluorescent moiety. The LPS in this work was Ra-LPS (a rough

type LPS from *Escherichia coli* MG1655); this was extracted from cells by the phenol/chloroform/ petroleum ether (PCP) method,[15] then labeled with FITC by a procedure modified from Troelstra et al.[16] The purity and the chemical identity of fLOS were assessed by NMR and SDS-PAGE analysis. The labeling ratio was determined to be 1:1 (LOS/FITC), higher than for commercial FITC-LPS from Sigma–Aldrich (~50:1 LPS/FITC). High levels of fluorescein incorporation are essential to obtain reliable signals in binding experiments.

LptC is a bitopic protein, composed of a single transmembrane (TM) helix (Trp7–Asp29) near the N terminus and a large periplasmic domain that is able to bind LPS in vitro.[12] We used a truncated version of LptC (lacking the first 23 amino acids of the transmembrane helix) fused to a N-terminal His$_6$ tag (sH-LptC)[10] as a model to characterize the binding of LPS to the periplasmic C-terminal domain of LptC. Deletion of the LptC TM region yields a stable, soluble, functional protein.[9, 10] sH-LptC was purified to near homogeneity by nickel-nitrilotri-acetic acid (Ni-NTA) affinity chromatography, and the overall protein structure (secondary and tertiary) was verified by circular dichroism analysis (data not shown).
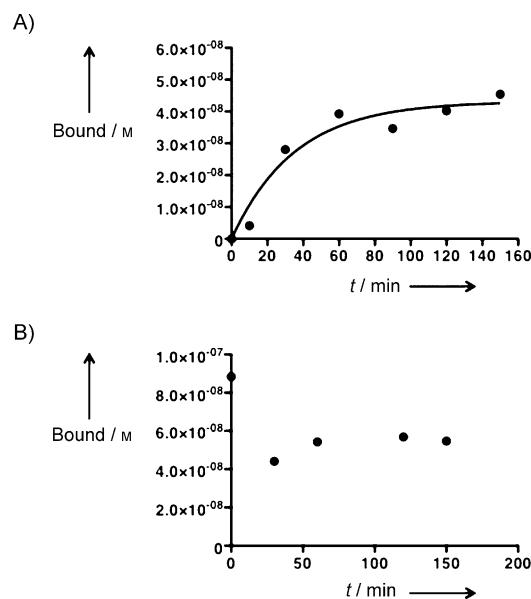
fLOS binding to resin-immobilized sH-LptC

Our first objective was to develop a sensitive and reliable test for detecting and quantifying LPS binding to LptC in vitro. We first investigated the time-dependence of LptC–LPS association. sH-LptC was immobilized on Ni-NTA resin, then fLOS (500 nM) was added and incubated for various periods (10–150 min). The resin was then washed, the LptC–fLOS complex was eluted from resin with imidazole, and fluorescence emission was quantified in the eluate. Nonspecific binding (binding of the same concentration of fLOS to Ni-NTA resin in the absence of absorbed sH-LptC) was calculated in different experiments to be less than 15% of the amount of absorbed fLOS in the presence of the protein. It is clear that LPS specifically binds to LptC with a one-phase association rate constant ($k =$ 0.028 min^{-1} ± 29% coefficient of variation (CV); Figure 3 A); it reached maximum saturation with a half-time of 24.4 min.

Interestingly, fLOS binding proved to be mostly irreversible, and the addition of increasing concentrations of unlabeled LPS did not result in displacement of fLOS from the protein (Figure 3 B). Consequently, it was not possible to calculate the true equilibrium constant, thus we report values for "apparent" K_d. An incubation time of 90 min was used for all subsequent equilibrium binding experiments.

Saturation curves of fLOS binding to resin-immobilized sH-LptC, and competition by unlabeled LPS

In order to calculate the affinity of LPS for its transporter, sH-LptC was immobilized on Ni-NTA resin, and equilibrium binding experiments were performed with fLOS as the ligand. We first carried out a series of saturation experiments (90 min incubation) with sH-LptC protein and increasing fLOS concentrations (0.1–50 μM). The quantity of fLOS captured by resin-bound sH-LptC was determined by the method described

Figure 3. Association and dissociation time-courses of fLOS binding to sH-LptC immobilized on Ni-NTA resin. A) For association kinetics, 500 nM fLOS was incubated with 50 mM sH-LptC at room temperature. B) Dissociation was induced by perturbing the equilibrium with addition of 50 μM unlabeled LOS. The curve represents the fit to the appropriate equation (see the Experimental Section), and is derived from analysis of three independent experiments, each in triplicate.
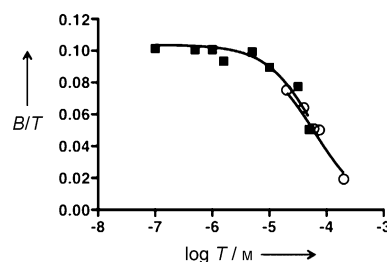
Figure 4. Saturation (■) and competition (○) curves of fLOS binding to resin-absorbed sH-LptC under pseudo-equilibrium conditions. Saturation (0.1–50 μM fLOS) and competition (10 μM fLOS (tracer) competing with different concentrations of unlabeled LPS) experiments were performed at room temperature, with 90 min incubation. Binding is expressed as the concentration ratio of bound to total ligand (B/T), versus the logarithm of total unlabeled ligand concentration (log T). Curves represent the fit to the appropriate equation (see the Experimental Section) and are derived from analysis of three independent experiments, each in triplicate.

above. Nonspecific binding of fLOS to the resin was always determined in the absence of absorbed sH-LptC. In these experiments (Figure 4) the calculated affinity K_a was 1.4 × 10^4 M^{-1} ± 27 % CV, corresponding to an apparent K_d of 71.4 μM. To assess whether fLOS has the same affinity as unlabeled LPS, we also plotted competition curves with increasing amounts of unlabeled LOS as a competitor at a fixed concentration of fLOS (Figure 4). Despite the fact that binding of fLOS to sH-LptC is essentially irreversible, it is possible to perform competition experiments, as long as the competing ligands are added simultaneously to the reaction mixture containing the binding target. The obtained competition curve follows the simple "mass-action law" under "pseudo-equilibrium" conditions.

These experiments revealed similar affinities for unlabeled LOS ($IC_{50} = 62.3$ μM $\pm 49\%$ CV; apparent $K_i = 35$ μM) and for fLOS, thus confirming that the presence of the fluorescent moiety does not affect LOS binding properties, so allowing pooling of data to calculate binding parameters.[17] Therefore, simultaneous analysis of saturation and competition curves allowed us to calculate the affinity of LOS for its transporter sH-LptC as $K_a = 1.91 \times 10^4$ M^{-1} $\pm 21\%$ CV (apparent $K_d = 52.4$ μM).

### sH-LptC-fLOS binding in solution by tryptophanfluorescence quenching

sH-LptC–fLOS affinity was also estimated in solution, in order to rule out any bias arising from resin capture. Binding was monitored as quenching of LptC intrinsic fluorescence. LptC has two tryptophan residues: Trp94 buried in the hydrophobic cavity of the protein and Trp77 exposed to the solvent at the edge of the β-jellyroll (Figure 2). Tryptophan fluorescence emission reduced progressively upon incubation with increasing fLOS concentration (Figure 5 A, insert), thus indicating that fLOS is an efficient quencher of sH-LptC fluorescence. The Stern–Volmer plot of the data (Figure 5 A) reveals an upward curve at high fLOS concentrations, consistent with two distinct quenching mechanisms: de-excitation of the fluorophore by

random collisions with fLOS molecules (dynamic quenching) and formation of a sH-LptC–fLOS nonfluorescent complex (static quenching). Based on their position in the sH-LptC structure, we ascribe dynamic and static quenching to Trp77 and Trp94, respectively. The constant for dynamic quenching (K_{dyn}) was estimated from titration of free tryptophan by fLOS (see Figure S1 in the Supporting Information); the influence of the protein structure on the quenching of the exposed Trp77 side chain was neglected. The resulting K_{dyn} value (14.7×10^3 M^{-1}) was then employed to calculate the apparent dissociation constant of the sH-LptC–fLOS complex by the combined equation for static and dynamic quenching. The obtained value ($K_d = 28.8$ μM) is similar to that obtained by the capture method ($K_d = 71.4$ μM).

In order to test the reversibility of binding, samples containing 40.7 μM sH-LptC and 45 μM fLOS were treated as above to allow complex formation. Aliquots were mixed to solutions of 45 μM fLOS, in order to dilute the protein while keeping the ligand concentration constant; the mixtures were incubated for a further 120 min before fluorescence measurement. The fluorescence values were normalized for protein concentration (as a function of the protein dilution factor), and compared to the expected values for reversible binding, by using the above-estimated K_d and K_{dyn} values (Figure 5 B). The experimental data deviate drastically from the theoretical trend (reversible binding); rather, they are consistent with simple progressive dilution of a fixed amount of fluorophore (this would be expected to yield a horizontal line in the plot). This result confirms that sH-LptC–fLOS binding is irreversible, at least on the timescales tested here.

Design and synthesis of an artificial LptC ligand

Our group recently developed small molecules that interact with the LPS-binding protein CD14 with high affinity and specificity (compounds iaxo-101 and iaxo-102, Scheme 1), thereby inhibiting TLR4 activation and signaling in cells[18] and in
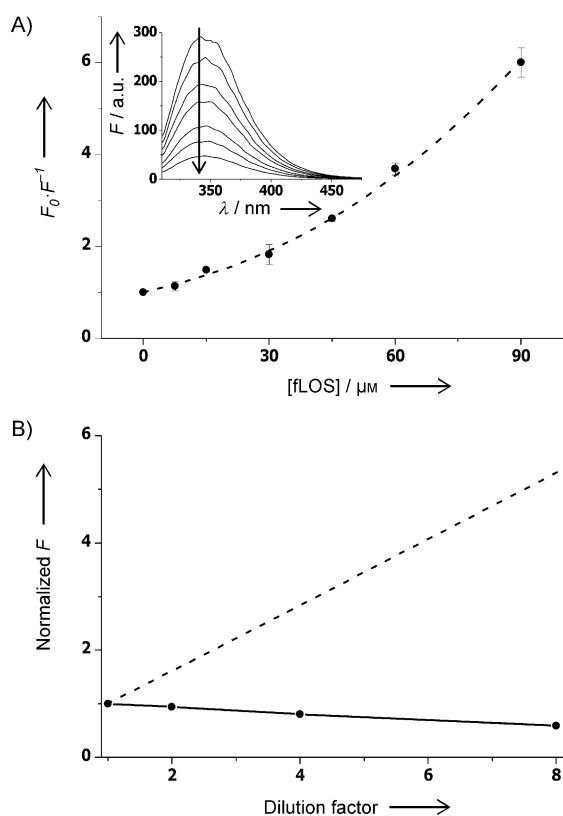
Figure 5. LptC fluorescence quenching by fLOS. A) Relative fluorescence is plotted against total fLOS concentration. The dashed line was obtained fitting data to Equation (6). Inset: fluorescence spectra (the arrow indicates the direction of spectral changes with increasing fLOS concentration). B) Normalized fluorescence upon dilution of LptC–fLOS complex. The dashed line indicates the expected trend for reversible binding with $K_d = 28.8$ μM.
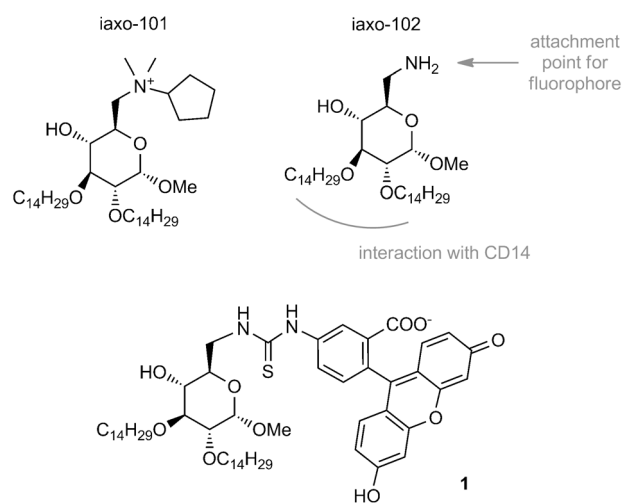

Scheme 1. Rational design of 1. The C-6 amine group of iaxo-102 was conjugated to FITC by a thiourea linker.

mice.[19] Structure–activity studies showed that the pharmacophore is composed of a cyclic sugar core, a protonated (positively charged) nitrogen on C-6, and two C_{14} linear aliphatic ether chains. Like CD14,[20] LptA and LptC proteins have been demonstrated to bind LPS within the interior of the hydrophobic cavities formed by their β-sheets.[14] We thus reasoned that new Lpt ligands could be designed, based on the high-affinity CD14 ligand iaxo-102[19] (Scheme 1). NMR data showed that the hydrophobic linear ether chains of iaxo-102 directly interact with the CD14 binding site,[21] thus suggesting that conjugation of a fluorophore at the C-6 primary amine should preserve the interaction with CD14 (Scheme 1). In compound **1**, iaxo-102 is chemically linked to fluorescein by a three-atom thiourea linker.

Binding of fluorescent probe 1 to sH-LptC and association kinetics

The in vitro binding of **1** to sH-LptC was investigated by using the resin-capture procedure described above. Nonspecific binding was also determined as above, by quantitating fLOS adsorbed on the resin in the absence of the protein, and found to be less than 30% of the signal in the presence of adsorbed protein. Association time course of fluorescent probe **1** binding to sH-LptC was performed by incubating 50 μM of **1** at room temperature for different times (10–150 min).

Compound **1** rather rapidly and specifically bound to LptC, again with a one-phase association rate constant ($k = 0.058$ min^{-1} ± 40% CV), and reached maximum saturation with a half-time of 12 min (Figure 6 A). As observed with LPS, binding of **1** proved to be essentially irreversible (Figure 6 B).
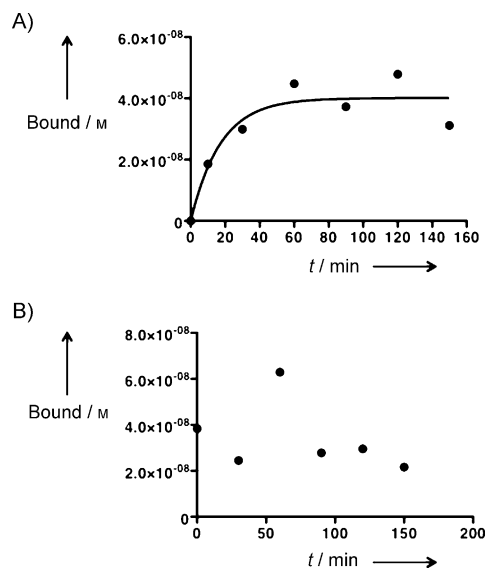

Figure 6. Association and dissociation time-courses of **1** binding to sH-LptC immobilized on Ni-NTA resin. A) For association kinetics, 50 μM **1** was incubated with sH-LptC at room temperature for up to 150 min. B) Dissociation was induced by perturbing the equilibrium with addition of 500 μM corresponding unlabeled ligand. Curves represent the fit to the appropriate equation (see the Experimental Section) and are derived from analysis of three independent experiments, each in triplicate.

Saturation experiment for compound 1 binding to sH-LptC, and competition curves with unlabeled precursors iaxo-102 or LOS

In order to calculate affinity of iaxo-102 for sH-LptC, a series of binding experiments were performed with **1** as the tracer. The amount of **1** captured by resin-bound sH-LptC was determined by the method described above for kinetics experiments. For each concentration of **1**, nonspecific binding was determined as binding to Ni-NTA resin in the absence of absorbed sH-LptC.

Saturation experiments were performed by incubation for 90 min with increasing concentrations of **1** (10–500 μM; Figure 7 A, saturation curve); heterologous competition experi-
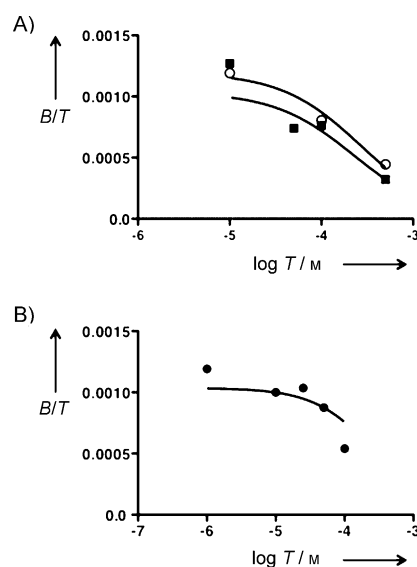
Figure 7. Saturation (■) and competition (○) curves of **1** binding to resin-absorbed sH-LptC under pseudo-equilibrium conditions. A) Saturation (10–500 μM **1**) and competition (50 μM **1** (tracer) competing with increasing concentrations of iaxo-102) binding experiments were performed at room temperature for 90 min. B) Binding curves for 50 μM **1** competing with increasing concentrations of LPS (●). Binding is expressed as the concentration ratio of bound to total ligand (B/T) against the logarithm of total unlabeled ligand concentration (log T). Curves represent the fit to the appropriate equation (see the Experimental Section) and are derived from analysis of three independent experiments, each in triplicate.

ments were performed by incubating 50 μM **1** with increasing concentrations of iaxo-102 (Figure 7 B, competition curve). These experiments revealed affinities similar for iaxo-102 and **1**, thus allowing pooling of the data and simultaneous analysis of saturation and competition curves (as performed above for fLOS and unlabeled LOS). Computer-assisted analysis yields affinity $K_a = 4.52 \times 10^3$ M^{-1} ± 36% CV (apparent $K_d = 221$ μM) for iaxo-102; this is statistically different ($p < 0.01$), but still in the range of affinity for LOS.

Finally, we performed heterologous competition experiments with 50 μM **1** (tracer) and increasing concentrations of LOS. LOS was indeed able to compete for the site occupied by **1** (Figure 7 B), with a calculated affinity, as expected, not signifi-

cantly different from that calculated when using fLOS as a tracer ($K_a = 1.15 \times 10^4 \, \text{M}^{-1} \pm 31\%$ CV, apparent $K_i = 87.2 \, \mu\text{M}$).

The antibacterial activities of iaxo-102 and **1** were evaluated in vivo by the micro-broth dilution method[22] against wild-type *E. coli* strains MG1655[23] and AS19 (permeable mutant).[24] No antibacterial activity was observed against either strain (up to 1 mM ; data not shown).

Conclusions

The development of fluorescent LOS (fLOS) with high levels of fluorescein incorporation allowed us to calculate, for the first time, the thermodynamic parameters of LOS–LptC interaction. Experiments based on resin-captured sH-LptC–fLOS complex yielded reliable association/dissociation and saturation/competition curves. In saturation and competition experiments (Figure 4), fLOS and unlabeled LOS precursor showed similar affinities towards LptC (apparent calculated dissociation constant $K_d = 71.4$ and $52.4 \, \mu\text{M}$, respectively). The very similar affinity values found for fLOS and LOS suggest that fLOS interacts with LptC similarly to unlabeled LOS. The introduction of the fluorescent moiety did not significantly alter the binding properties or biological activity of LOS; this demonstrates that fLOS can be used as a tracer in quantitative analysis. In kinetic experiments, we observed that binding of LOS to LptC is mostly irreversible, as dissociation time-course experiments with unlabeled LOS failed to displace the bound ligand. Binding experiments in solution based on LptC tryptophan quenching corroborated the results obtained by the resin-capture method, thus giving an apparent dissociation constant of the same order of magnitude ($K_d = 28.8 \, \mu\text{M}$) and confirming the apparent irreversibility of fLOS binding.

In vitro transfer of LPS from LptC to LptA—but not vice versa—occurs in the absence of ATP, possibly implying different affinities for LPS by the two proteins, and consistent with a unidirectional export pathway.[12] LptC function in vivo requires energy from the LptBFG ABC transporter, and a round of ATP hydrolysis is necessary to extract LPS from the IM. A second round of ATP hydrolysis is then required in vivo for LPS delivery from LptC to LptA.[14] Our data indicate that LPS bound to LptC cannot be released in the absence of either energy or the higher-affinity LptA protein. Indeed, it has been recently shown that release of LPS into the periplasm (caused by defective transport) triggers the extracytoplasmic stress response.[25] Overall these data are consistent with the idea that binding and release of LPS by the Lpt proteins is tightly controlled, to avoid LPS mistargeting and its release into the periplasm.

The Lpt machinery operates downstream of MsbA-mediated flipping of LPS across the IM, so LptC could be the first protein of the machinery to interact in the periplasm with newly translocated LPS. MsbA is a member of the ATP-binding cassette (ABC) superfamily of transporters; it alternates between inward-facing and outward-facing conformations, thereby presenting the substrate-binding pocket to the cytoplasmic and periplasmic faces of the IM, respectively. These conformational changes are guided by binding to and hydrolysis of ATP.[26] The

MsbA interaction with lipid A and Ra- and deep rough LPS (Re LPS) has been studied by ligand-induced quenching of MsbA intrinsic tryptophan fluorescence.[27] Interestingly, lipid A and the Ra- and Re-LPS variants quenched MsbA Trp fluorescence, with K_d between 2 and 6 μM.[27] We calculated here an apparent K_d of 52.4 μM for the LPS–LptC interaction, typical for the affinity of a transporter, and of the same order of magnitude as K_d for the MsbA–LPS interaction. The similar K_d values for LPS–MsbA and LPS-LptC interactions are consistent with a model of LPS shuttling from MsbA to LptC; irreversible binding between LptC and LPS (observed in this study) reflects the peculiar nature of LPS transport across the periplasm. LPS needs to be properly transferred through the Lpt chain and not released into the aqueous periplasm.

In this study, new compounds were identified to interact with LptC at the LPS-binding site. Two compounds, iaxo-102 and its fluorescent analogue **1**, were identified as good candidates to compete with LOS for binding to LptC. We have previously shown that iaxo compounds interact with the LPS-binding protein CD14, with high affinity and specificity, thereby leading to TLR4 signaling inhibition in cells and in mice.[18,19] As CD14 and LptC share the same ligand, we explored the possibility that compounds interfering with CD14 activity (e.g., iaxo) can be used as scaffolds to generate compounds able to bind to, and interfere with, LptC activity. Compared to LPS, **1** displayed faster association kinetics to LptC, but with fourfold lower affinity for the protein (apparent $K_d = 221 \, \mu\text{M}$). As in the case of LPS, the presence of the fluorophore did not profoundly affect LptC binding affinity, as iaxo-102 presented an apparent K_i of 129 μM.

Interestingly, **1** and LPS appear to bind to the LptC protein at the same site, as demonstrated in competition experiments. As noted for LPS, binding by **1** is mostly irreversible, thus suggesting a common mechanism of interaction with LptC.

The dissection into single steps of LPS binding and release through the Lpt machinery provides important information on the molecular mechanisms underlying LPS transport. Moreover, the ability to block LPS transport to the cell surface by small molecules suggests an appealing strategy for a new generation of antibiotics targeting multiresistant Gram-negative bacteria. Rational optimization of the molecular structures of these compounds (with the aim of improving bioavailability, cell penetration, and LptC affinity) could afford the first generation of Gram-negative bacteria-specific antibiotics targeting the LPS transport mechanism.

Experimental Section

LOS extraction and labeling with fluorescein: For rough LPS (LOS, Ra-LPS) extraction, *E. coli* strain MG1655 (laboratory collection)[23] was grown at 37 °C in LD medium (tryptone (1%), yeast extract (0.5%), NaCl (0.5%))[28] for 16 h. This culture was diluted 1:100 in fresh medium and grown to mid-logarithmic phase (OD$_{600}$ = 0.6). Cells were then harvested by centrifugation (5000 g, 20 min), washed in NaH$_2$PO$_4$ (50 mM, pH 8.0), and stored at −20 °C before extraction. LOS was selectively extracted from dry cells by the PCP method.[15] Briefly, a solution of phenol (90%)/chloroform/light petroleum (2:5:8, v/v/v) was prepared; to this was added solid

phenol until the solution went clear. Dry cells (9.73 g) were suspended in PCP solution (2.5%, (w/v)), stirred for 30 min, and extracted three times. Then, the light solvents were removed under vacuum, and LOS was precipitated from the remaining phenol solution by adding water. The solid was centrifuged, collected, suspended in water and dialysed (cut-off 1000 Da) against distilled water for three days. Finally, it was lyophilized, and 85 mg of pure LOS was recovered (yield: 0.9% (w_{LOS}/w_{cells})). The sample obtained from this procedure was screened by ^{1}H NMR spectroscopy and discontinuous SDS-PAGE for contaminants.[29] The gel was prepared with a 15% separating gel (lower gel) and a 5% stacking gel (upper gel). The gel was silver stained for lipopolysaccharide;[30] this has a sensitivity limit of 1 μg for S-type LPS and 10 μg for of R-type LPS.

LOS conjugation to FITC: LOS obtained from *E. coli* MG1655 (see above) was labeled with fluorescein by the following procedure. FITC was conjugated to LOS by using an optimized protocol of a published procedure.[16] LOS (20 mg) was treated with triethylamine (0.5%, 10 mL) and sonicated on ice for 15 min, then EDTA (100 mM, 1 mL) was added, followed by HCl (1 M) addition to pH 5. FITC (100 mg) in borate buffer (0.25 M, pH 10.5, 4 mL) was added, and the mixture was sonicated for 5 min. After addition of sodium deoxycholate (1.6%, 5 mL), the solution was stirred at 37 °C for 30 h. The reaction mixture was centrifuged (10 000 g, 30 min) to eliminate aggregates, and the supernatant was dialyzed (cut-off 1000 Da) against NaCl (137 mM). The sample was concentrated and purified with Sephadex G-25 in a PD-10 desalting column (GE Healthcare), and eluted in water. Fractions containing fLOS were collected and lyophilized (16 mg). To evaluate labeling efficiency, the ratio between LOS and FITC concentrations in the sample was calculated. The concentration of FITC was determined spectrophotometrically ($\varepsilon_{492\,nm} = 85\,000$ M^{-1} cm^{-1}); the concentration of LOS was determined by a thiobarbiturate assay,[31] which evaluates the level of KDO (2-keto-3-deoxyoctulosonic acid), a marker sugar for LPS. In these measurements, a sample of commercial LPS-FITC (Sigma–Aldrich) was used as the reference. A LOS/FITC labeling ratio of 1.02:1 was calculated for the sample; the reference showed a ratio of about 50:1 (LPS/FITC).

Purification of sH-LptC: *E. coli* M15[pREP4] (Qiagen) harboring plasmid pQEsH-lptC,[10] which expresses N-terminal His$_6$-tagged LptC lacking the first 23 residues (sH-LptC), was grown at 30 °C in LD medium[28] containing kanamycin (25 μg mL^{-1}) and ampicillin (100 μg mL^{-1}) for 16 h. The culture was diluted (1:100) in fresh LD medium and grown to mid-logarithmic phase ($OD_{600} = 0.6$). Expression of sH-LptC was induced by addition of isopropyl-β-D-thiogalactopyranoside (IPTG; 0.5 mM; Sigma–Aldrich) and further incubated for 16–18 h at 20 °C. Cells were then harvested by centrifugation (5000 g, 20 min). The cell pellet was resuspended in buffer A (NaH$_2$PO$_4$ (50 mM, pH 8.0), NaCl (300 mM), imidazole (10 mM), glycerol (10%)), followed by incubation for 30 min at 4 °C with shaking in the presence of lysozyme (0.2 mg mL^{-1}), DNAse I (100 μg mL^{-1}), MgCl$_2$ (10 mM), and phenylmethylsulfonyl fluoride (PMSF, 1 mM; Sigma–Aldrich). Cells were disrupted by a single pass through a One Shot model French press (Constant Systems, Daventry, UK) at 25 000 psi. Unbroken cells and cell debris were removed by centrifugation (39 000 g, 30 min, 4 °C). The soluble protein was purified from the supernatant on Ni-NTA agarose columns (Qiagen). The column was washed with 10 column volumes of 4% buffer B (NaH$_2$PO$_4$ (50 mM, pH 8.0) NaCl (300 mM), imidazole (500 mM), glycerol (10%)) with buffer A. The protein was eluted by using a stepwise gradient of buffer B (10, 20, 50, 70, and 100%) with buffer A. At each step, one column volume was passed through the column. Elution fractions were monitored by 12.5% polyacrylamide SDS-PAGE. The pooled fractions containing purified protein (> 90%) were dialyzed twice against 100 volumes of buffer C (NaH$_2$PO$_4$ (50 mM, pH 8.0), NaCl (150 mM)) in cellulose tubing (12 000 Da cut-off; Thermo Scientific), and finally concentrated in a Vivaspin 15R column (10 000 molecular weight cut-off; Sartorius, Göttingen, Germany). Protein concentration was determined by a Coomassie (Bradford) assay kit (Thermo Scientific), with bovine serum albumin as the standard.

Ligand binding studies by the resin-capture method

Saturation experiments: The in vitro LPS binding assay was based on a previous protocol with modifications.[12] Briefly, purified sH-LptC (50 μM) was incubated in buffer C (1 mL) with HisLink protein purification resin (100 μL; Promega) for 90 min on a rotary shaker at room temperature, to allow absorption of protein to the resin. Unbound protein was removed by decanting the resin-bound sH-LptC and eliminating the supernatant. Resin-bound sH-LptC was incubated in buffer C (1 mL) at room temperature in the dark on a rotary shaking in the presence of different concentrations of fLOS (0.1–50 μM) or **1** (10–500 μM) for a further 90 min to allow binding of ligand to the resin-bound sH-LptC. The supernatant (unbound ligand) was discarded, and the resin was washed three times with buffer C. The protein–LPS complex was eluted in four steps, each with buffer C (1 mL) containing imidazole (500 mM). Nonspecific binding was determined as the binding of the same concentration of fLOS to Ni-NTA resin in the absence of absorbed sH-LptC. Each fraction (100 μL) was placed in a Costar white flat-bottomed microtiter plate (Corning, NY), and fluorescence was measured in a Cary Eclipse spectrophotometer ($\lambda_{ex} = 490$ nm, $\lambda_{em} = 510$ nm, slit = 5 nm; Varian). The concentration of tracer present in each sample was determined by interpolation with a standard curve (fLOS or **1**) and corrected by subtraction of the nonspecific-binding value. The amount of sH-LptC bound to the resin and eluted with imidazole was evaluated for the pooled elution fractions with a Coomassie (Bradford) assay kit (Thermo Scientific), with bovine serum albumin as the standard.

Association and dissociation time courses: For the association experiments, labeled ligand (fLOS (500 nM) or **1** (50 μM)) was added at room temperature, in the dark, to sH-LptC (50 μM) adsorbed to the resin in buffer C (1 mL); the mixture was incubated with shaking for different times (10–150 min). For each time, the supernatant was removed and samples were washed and eluted as described above. Dissociation kinetics experiments were performed with the same tracer concentrations, and incubation with immobilized sH-LptC for 150 min (volume of reaction = 800 μL). Then, LOS (50 μM) and iaxo-102 (500 μM) in buffer C (1 mL) were added for different times (10–150 min). For each time, the sample was treated as above.

Competition experiments: Competition experiments were performed for sH-LptC binding to fLOS and **1**. For fLOS, resin-bound sH-LptC (50 μM) was incubated (90 min) with a mixture of fLOS (10 μM) and different concentrations of unlabeled LOS (20, 40, 60 and 75 μM) in buffer C. After wash and elution steps, the concentration of fLOS bound to sH-LptC was quantified as described above. For **1**, resin-bound sH-LptC (50 μM) was incubated with **1** (50 μM) in buffer C (800 μL) for 90 min. Homologous and heterologous competition experiments were performed by adding iaxo-102 (200 μL, 100 or 500 μM) or LOS (200 μL, 10–100 μM) and incubated for a further 90 min. Wash and elution steps were performed; concentrations of tracer bound to resin were determined as described above.

Data and statistical analysis: Data from fluorescent ligand binding assays were evaluated by a nonlinear, least-squares curve-fitting procedure in Prism (version 4,GraphPad Software, La Jolla, CA). Association and dissociation time courses were analyzed by one-phase association and one-phase dissociation exponential decay curves, respectively. Equilibrium binding data were analyzed in Prism by using the *n*-ligand *m*-binding site model in the Ligand[32] and DESIGN[33] computer programs. Parameter errors are expressed as percentage CV and were calculated by simultaneous analysis of at least three independent experiments performed in duplicate or triplicate. Parameter comparisons were performed based on the F-test for extra sum of square principle. All curves are computer generated.

LptC intrinsic fluorescence quenching: Samples containing sH-LptC (40.7 μM) and fLOS (0–90 μM) were prepared in sodium phosphate (50 mM, pH 8) with NaCl (50 mM), incubated (22 °C, 90 min) with agitation (300 rpm), then transferred into a quartz cuvette (1 cm path length). Fluorescence emission spectra (310–475 nm) were recorded at 22 °C with an Eclipse spectrofluorimeter (Varian; excitation 295 nm, excitation/emission slits 5 nm). To test binding reversibility, aliquots of the 45 μM fLOS sample were diluted (up to 1:8) at fixed fLOS concentration, and incubated for a further 120 min before fluorescence measurements.

Data analysis for quenching experiments: In the presence of dynamic quenching, the fraction of fluorescence intensities in the absence (F_0) and presence (F) of the quencher (fLOS) is given by the ratio of the decay rate in the presence ($\gamma + k_q[\text{fLOS}]$) and absence ($\gamma$) of the quencher (Equation (1)):

$$\frac{F_0}{F} = \frac{\gamma + k_q[\text{fLOS}]}{\gamma} = 1 + K_{dyn}[\text{fLOS}] \tag{1}$$

When static quenching also occurs due to binding, Equation (1) applies only for fluorophores that are not involved in a complex. The contribution of this fraction can be expressed by Equation (2):

$$\frac{F_0}{F} = \frac{[\text{LptC}]_{tot}}{[\text{LptC}]}(1 + K_{dyn}[\text{fLOS}]) \tag{2}$$

The equations that define the dissociation constant (K_d) and the conservation of total protein and ligand are as follows [Eqs (3), (4), and (5)]:

$$K_d = \frac{[\text{LptC}][\text{fLOS}]}{[\text{complex}]} \tag{3}$$

$$[\text{complex}] = [\text{LptC}]_{tot} - [\text{LptC}] \tag{4}$$

$$[\text{fLOS}] = [\text{fLOS}]_{tot} - [\text{complex}] = [\text{fLOS}]_{tot} - [\text{LptC}]_{tot} + [\text{LptC}] \tag{5}$$

Combining Equations (1)–(5) it is possible to express F_0/F as a function of total protein and total ligand concentrations, K_{dyn} and K [Eq. (6)]

$$\frac{F_0}{F} = \frac{[\text{LptC}]_{tot}\left(2 + K_{dyn}\left([\text{fLOS}]_{tot} - [\text{LptC}]_{tot} - K_d + \sqrt{([\text{LptC}]_{tot} - [\text{fLOS}]_{tot} - K_d)^2 + 4K_d[\text{LptC}]_{tot}}\right)\right)}{[\text{LptC}]_{tot} - [\text{fLOS}]_{tot} - K_d + \sqrt{([\text{LptC}]_{tot} - [\text{fLOS}]_{tot} - K_d)^2 + 4K_d[\text{LptC}]_{tot}}} \tag{6}$$

The K_d value was determined by a nonlinear, least-squares curve-fitting procedure of fluorescence data by Equation (6), by using the

K_{dyn} value obtained from free tryptophan experiments (see the Supporting Information).

Acknowledgements

[1] H. Nikaido, *Microbiol. Mol. Biol. Rev.* **2003**, *67*, 593–656.

[2] C. R. H. Raetz, C. Whitfield, *Annu. Rev. Biochem.* **2002**, *71*, 635–700.

[3] S. Akira, S. Uematsu, O. Takeuchi, *Cell* **2006**, *124*, 783–801.

[4] A. Polissi, C. Georgopoulos, *Mol. Microbiol.* **1996**, *20*, 1221–1233.

[5] a) P. Sperandeo, R. Cescutti, R. Villa, C. Di Benedetto, D. Candia, G. Dehò, A. Polissi, *J. Bacteriol.* **2007**, *189*, 244–253; b) P. Sperandeo, F. K. Lau, A. Carpentieri, C. De Castro, A. Molinaro, G. Dehò, T. J. Silhavy, A. Polissi, *J. Bacteriol.* **2008**, *190*, 4460–4469; c) N. Ruiz, L. S. Gronenberg, D. Kahne, T. J. Silhavy, *Proc. Natl. Acad. Sci. USA* **2008**, *105*, 5537–5542; d) S.-S. Chng, N. Ruiz, G. Chimalakonda, T. J. Silhavy, D. Kahne, *Proc. Natl. Acad. Sci. USA* **2010**, *107*, 5363–5368.

[6] a) E. Freinkman, S. Okuda, N. Ruiz, D. Kahne, *Biochemistry* **2012**, *51*, 4800–4806; b) C. Santambrogio, P. Sperandeo, R. Villa, F. Sobott, A. Polissi, R. Grandori, *J. Am. Soc. Mass Spectrom.* **2013**, *24*, 1593–1602.

[7] S.-S. Chng, L. S. Gronenberg, D. Kahne, *Biochemistry* **2010**, *49*, 4565–4567.

[8] S. Narita, H. Tokuda, *FEBS Lett.* **2009**, *583*, 2160–2164.

[9] R. Villa, A. M. Martorana, S. Okuda, L. J. Gourlay, M. Nardini, P. Sperandeo, G. Dehò, M. Bolognesi, D. Kahne, A. Polissi, *J. Bacteriol.* **2013**, *195*, 1100–1108.

[10] P. Sperandeo, R. Villa, A. M. Martorana, M. Samalikova, R. Grandori, G. Dehò, A. Polissi, *J. Bacteriol.* **2011**, *193*, 1042–1053.

[11] A. X. Tran, M. S. Trent, C. Whitfield, *J. Biol. Chem.* **2008**, *283*, 20342–20349.

[12] A. X. Tran, C. Dong, C. Whitfield, *J. Biol. Chem.* **2010**, *285*, 33529–33539.

[13] M. D. L. Suits, P. Sperandeo, G. Dehò, A. Polissi, Z. Jia, *J. Mol. Biol.* **2008**, *380*, 476–488.

[14] S. Okuda, E. Freinkman, D. Kahne, *Science* **2012**, *338*, 1214–1217.

[15] C. Galanos, O. Lüderitz, O. Westphal, *Eur. J. Biochem.* **1969**, *9*, 245–249.

[16] A. Troelstra, P. Antal-Szalmas, L. A. de Graaf-Miltenburg, A. J. Weersink, J. Verhoef, K. P. Van Kessel, J. A. Van Strijp, *Infect. Immun.* **1997**, *65*, 2272–2277.

[17] G. E. Rovati, *Trends Pharmacol. Sci.* **1998**, *19*, 365–369.

[18] a) F. Peri, F. Granucci, B. Costa, I. Zanoni, C. Marinzi, F. Nicotra, *Angew. Chem. Int. Ed.* **2007**, *46*, 3308–3312; *Angew. Chem.* **2007**, *119*, 3372–3376; b) M. Piazza, V. Calabrese, C. Baruffa, T. Gioannini, J. Weiss, F. Peri, *Biochem. Pharmacol.* **2010**, *80*, 2050–2056.

[19] a) I. Bettoni, F. Comelli, C. Rossini, F. Granucci, G. Giagnoni, F. Peri, B. Costa, *Glia* **2008**, *56*, 1312–1319; b) M. Piazza, C. Rossini, S. Della Fiorentina, C. Pozzi, F. Comelli, I. Bettoni, P. Fusi, B. Costa, F. Peri, *J. Med. Chem.* **2009**, *52*, 1209–1213.

[20] a) J.-I. Kim, C. J. Lee, M. S. Jin, C.-H. Lee, S.-G. Paik, H. Lee, J.-O. Lee, *J. Biol. Chem.* **2005**, *280*, 11347–11351; b) S. L. Kelley, T. Lukk, S. K. Nair, R. I. Tapping, *J. Immunol.* **2013**, *190*, 1304–1311.

[21] M. Piazza, L. Yu, A. Teghanemt, T. Gioannini, J. Weiss, F. Peri, *Biochemistry* **2009**, *48*, 12337–12344.

[22] I. Wiegand, K. Hilpert, R. E. Hancock, *Nat. Protoc.* **2008**, *3*, 163–175.

[23] F. R. Blattner, G. Plunkett III, C. A. Bloch, N. T. Perna, V. Burland, M. Riley, J. Collado-Vides, J. D. Glasner, C. K. Rode, G. F. Mayhew, J. Gregor, N. W. Davis, H. A. Kirkpatrick, M. A. Goeden, D. J. Rose, B. Mau, Y. Shao, *Science* **1997**, *277*, 1453–1462.

[24] M. Sekiguchi, S. Iida, *Proc. Natl. Acad. Sci. USA* **1967**, *58*, 2315–2320.

[25] S. Lima, M. S. Guo, R. Chaba, C. A. Gross, R. T. Sauer, *Science* **2013**, *340*, 837–841.

[26] D. A. P. Gutmann, A. Ward, I. L. Urbatsch, G. Chang, H. W. van Veen, *Trends Biochem. Sci.* **2010**, *35*, 36–42.

[27] P. D. W. Eckford, F. J. Sharom, *J. Biol. Chem.* **2008**, *283*, 12840–12850.

[28] P. Sabbattini, F. Forti, D. Ghisotti, G. Dehò, *J. Bacteriol.* **1995**, *177*, 1425–1434.

[29] U. K. Laemmli, *Nature* **1970**, *227*, 680–685.

[30] R. Kittelberger, F. Hilbink, *J. Biochem. Biophys. Methods* **1993**, *26*, 81–86.

[31] H. Brade, C. Galanos, *Anal. Biochem.* **1983**, *132*, 158–159.

[32] P. J. Munson, D. Rodbard, *Anal. Biochem.* **1980**, *107*, 220–239.

[33] G. E. Rovati, D. Rodbard, P. J. Munson, *Anal. Biochem.* **1988**, *174*, 636–649.

Acknowledgments

In questi anni di PhD ho imparato tanto, sia dal punto di vista scientifico che personale e, soprattutto negli ultimi mesi, ho capito che ho tanto di cui essere grata: per questo voglio ringraziare la persone che mi hanno accompagnata, sostenuta e incoraggiata.

Grazie al prof. Peri che mi ha insegnato a far volare sempre più in alto la curiosità scientifica, senza dimenticare di valorizzare i traguardi raggiunti.

Grazie a tutto il lab 4048: a chi c'è sempre stato e a chi è stato solo di passaggio, rendendo unica questa avventura. In particolare, grazie a Vale, perché è stata la mia guida nella giungla della sintesi, ma anche confidente e vera amica, permettendomi di condividere con lei momenti indimenticabili; grazie a Sere, perché tutto è cominciato insieme e oggi so che il 4048 mi ha lasciato un dono prezioso: la sua amicizia; grazie a Roby, per la sua grande disponibilità e i "raptus" di infantilità incontrollabile; grazie a Ste, insieme abbiamo condiviso l'intero percorso, tra esperimenti e corse al Niguarda: con lei ho capito che l'amicizia conquistata può essere sorprendentemente bella.

Grazie al lab 4054 e, in particolare, grazie a Cristina, che ha sempre creduto in me: la sua onestà scientifica mi è stata d'ispirazione e la fiducia che ha mostrato nei miei confronti mi ha incoraggiata nei momenti difficili. E grazie a Cinzia, per le nostre chiacchierate e i giri in macchina: essere la sua "tutor milanese" mi ha dato grandi soddisfazioni!

Grazie a Barbara e Geppo, che con i loro consigli chimici, tra le altre cose, mi hanno salvata dall'Osmio!

Grazie al gruppo di Madrid, Prof. Jimenez-Barbero, Ana, Luca, Angeles, Pilar, Anita e Alvaro, perché in quei mesi mi sono sentita più che a casa.

Grazie al gruppo di Napoli, perché non bisogna mai dimenticare da dove veniamo. Grazie alla prof.ssa Rosa Lanzetta, perché continua ad essere la mia mentore, anche a distanza. E grazie a Cristina, per il sostegno e i consigli indispensabili nei momenti più bui: senza di lei non ce l'avrei fatta.

Grazie alla mia famiglia: alla mia mamma, che per me ha fatto più di quello che si possa immaginare, non come solo le mamme sanno fare, ma come solo le donne coraggiose e piene d'amore possono fare; al mio papà, che mi ha sempre protetta e sa come incoraggiarmi, perché in fondo siamo uguali, e che mi ha insegnato a combattere per i propri sogni; al mio fratellino, il mio english reviewer, perché mi è sempre accanto con il suo modo unico ed insostituibile, raccontandomi una vita incredibile attraverso i suoi occhi; ai nonni, che devono star dietro alle incomprensibili idee scientifiche della nipote; e a te.. tu sai bene perché.

Grazie alle mie migliori amiche, Cate, per le sue folli sorprese, e Marty, perché è la mia forza, che all'occorrenza sono state anche le mie baby-sitter e infermiere, ma soprattutto le mie sorelle, perché trovano sempre il modo di starmi vicine, anche se lontane.

Grazie ad Anto, il mio graphic designer, per l'amore, la comprensione, la fiducia e il sostegno infiniti di ogni singolo giorno, di ogni singolo istante… perché da soli possiamo essere speciali, ma insieme siamo straordinari.

Grazie al "elbow team", Prof. Russo, Dott. Della Rotonda, Dott.ssa Foglia, Angelo, Fulvio, Alberto, che mi ha fisicamente rimessa in condizioni di scriverla questa tesi!